I: Isotopic Systematics in Archean Rocks, West Greenland

II: Mineralogic and Petrologic Investigations of Lunar Rock Samples

Thesis by

Alexander John Gancarz Jr.

In Partial Fulfillment of the Requirements

for the Degree of

Doctor of Philosophy

California Institute of Technology

Pasadena, California

1976

(Submitted May 26, 1976)

ACKNOWLEDGEMENTS

I would like to thank Professor G. J. Wasserburg for his persistent encouragement and contaminating enthusiasm. I would like to thank Professor A. L. Albee for his continued interest in not only petrologic studies, but also isotopic systematics as applied to petrologic problems. Dr. F. Tera generously volunteered the secrets of chemical separation and has been actively interested in the work. Dr. D. A. Papanastassiou efficiently supervised the maintenance of the Lunatic Asylum and has always been willing to discuss the operation of mass spectrometers. A. Chodos kept the electron microprobe in top shape.

I would like to thank my co-authors for allowing me to include unmodified published papers in the thesis.

This work was supported by the National Science Foundation (DES-75-03417) and the National Aeronautics and Space Administration (NGL-05-002-188 and NGL-05-002-338). The expedition to Greenland was supported by a grant from the National Science Foundation (GA-31729). I received a three-year graduate fellowship from the National Science Foundation.

ABSTRACT

Pb isotopic abundances and U-Th-Pb concentrations are reported for feldspar megacrysts from the 3.59 AE old Amîtsoq Gneiss, Godthaab District, West Greenland. The distinctive Pb in the feldspars is the most primitive terrestrial Pb so far observed. It is observed in feldspars which are from different geographic localities and which exhibit varying degrees of deformation and recrystallization. This appears to be either the initial Pb in the Amîtsoq Gneiss or the initial Pb only slightly modified by subsequent metamorphism in a low $^{238}U/^{204}Pb$ environment. $^{238}U/^{204}Pb$ in the feldspars is low and the corrections for *in situ* produced Pb are only 0.4 per cent for $^{207}Pb/^{206}Pb$ and 0.6 per cent for $^{204}Pb/^{206}Pb$. The mean corrected isotopic abundances are $^{204}Pb/^{206}Pb = 0.08720$, $^{207}Pb/^{206}Pb = 1.1513$, and $^{208}Pb/^{206}Pb = 2.7309$. The feldspars contain a very small amount of easily leachable radiogenic Pb which is strongly correlated with U and which indicates the formation of U-rich phases at about 2.7 AE. The matrix surrounding the feldspar megacrysts contains Pb which is much evolved relative to the megacrysts and this matrix does not appear to have behaved as a simple closed system. Element redistribution and open system behavior at about 2.7 AE is also suggested by Pb in feldspar from a dyke cutting across the gneiss. Assuming that the Amîtsoq Gneiss feldspar Pb corrected for *in situ* U decay was the initial Pb in the gneiss at 3.59 AE (Baadsgaard, 1973), a single-stage "age of the earth" is determined as 4.47 ± 0.05 AE and μ is 8.5. This is indistinguishable from the single-stage age for modern rocks and is distinctly younger than the age of some meteorites. If we assume that the earth originally formed at

4.6 AE and assume that it underwent major, large-scale differentiation at a time T_D, we use the same observed data to calculate that the time of differentiation is approximately 4.4 AE and that μ for the total earth is approximately 1.6 while μ for the mantle and crustal rocks is approximately 9.5.

Pb and Sr isotopic data and K-Rb-Sr-U-Th-Pb concentration data are presented for three anorthosite complexes in West Greenland. The three complexes are the Majorqap Qâva outcrop of the Fiskenaesset Anorthosite Complex, the Storø Anorthosite Complex, Godthaab District, and the Ivnajaugtoq Anorthosite Complex, Godthaab District. The Pb isotopic data yield an age of 2.8 AE for the Majorqap Qâva Anorthosite and Storø Anorthosite. The Ivnajaugtoq data are consistent with a 2.8 AE age. We interpret this as the time of igneous crystallization and metamorphic recrystallization. U-Pb data indicate substantial U redistribution within the last ~100 m.y. These three complexes have very different initial Sr isotopic abundances. These differences indicate that either the anorthosites crystallized at 2.8 AE from melts with different μ's which were derived and fractionated at ~3.6 AE from "normal" (i.e. $\mu \sim 9$) mantle material and remained isolated until 2.8 AE or the anorthosites crystallized at 2.8 AE from melts derived at 2.8 AE from "normal" mantle material and which were variably contaminated during emplacement with Pb like that in the Amîtsoq Gneiss.

Included are a series of published articles which are primarily concerned with the mineralogic and petrographic characterization of lunar highland samples.

TABLE OF CONTENTS

BRIEF OUTLINE OF THE THESIS

The thesis is divided into two parts. The first part is a summary of U-Th-Pb isotopic studies on Precambrian rocks from Greenland. The purpose of these studies was to determine the initial Pb isotopic composition of a granitic gneiss which is the oldest known terrestrial rock and to determine the age and initial Pb of some anorthositic rocks. The second part of the thesis is composed of a series of petrologic studies on rocks from the lunar highlands. The purpose of these studies was to characterize mineralogically and petrographically samples of rocks from the moon and to relate the observations to isotopic data on the rocks.

A brief outline of part I follows. In section 1 we report the initial Pb and U and Th data for the granitic gneiss, the Amîtsoq Gneiss, and discuss the implications on the age and differentiation time of the earth. Section 2 is a summary of our age and initial Pb determinations on anorthositic rocks from Greenland. Section 3 is a summary of expedition "Oldstone" to Greenland to collect the samples studied in sections 1 and 2. Field descriptions and locations of the samples are included in this section.

Part II consists of unmodified versions of published articles or articles in press.

Part I: Section 1

Initial Pb of the Amîtsoq Gneiss and a 4.47AE "Age of the Earth"

1.1 Introduction

Determination of the isotopic composition of Pb in igneous rocks at the time of their formation, the initial Pb, provides information on the U-Th-Pb fractionation history of the source regions from which these rocks were derived. Studies of the Pb isotopic composition in ancient igneous rocks are thus a key in deciphering the early chemical history of the earth. In principal, the most ancient rocks should provide the best record of early differentiation processes if the initial Pb isotopic abundances have survived unaltered. Ancient cratonic blocks, however, are typically characterized by complicated polymetamorphic histories and the rocks usually show evidence of significant modification of the primary isotopic abundances.

Black et al. (1971) recently discovered very ancient rocks in West Greenland and demonstrated that Pb with very primitive isotopic abundances is preserved. This is the first sample distinctly more primitive than the previously known most primitive terrestrial Pb from the Rosetta mine in South Africa measured by Collins et al. (1953). The primitive nature of this Pb is illustrated on figure 1. Black et al. (1971) did not measure U abundances and did not determine an initial Pb.

These ancient rocks are from what appears to be the oldest lithologic unit in the Precambrian craton of West Greenland, the Amîtsoq Gneiss, and have been shown to be 3.75±0.09 AE old by Moorbath et al. (1972) and 3.65±0.05 AE old by Baadsgaard (1973). The original field relationships which precipitated these isotopic studies were delineated by McGregor (1973) who interprets them to indicate that the Amîtsoq Gneiss was originally a series of igneous rocks. This information suggested that a search for a well-defined ancient initial Pb be fruitful and could possibly

lead to the determination of the characteristics of the magma sources which produced crustal rocks very early in the history of the earth.

The initial Pb is the Pb common to all phases of a rock at the time of most recent isotopic homogenization. The constituent mineral phases of a rock which were in Pb isotopic equilibrium at time T and which have remained undisturbed until today behave according to the relationships:

$$\left(^{206}Pb/^{204}Pb\right)^{j}_{today} = \left(^{206}Pb/^{204}Pb\right)_{initial} + \left(^{238}U/^{204}Pb\right)^{j}_{today}\left(e^{\lambda T}-1\right)$$

$$\left(^{207}Pb/^{204}Pb\right)^{j}_{today} = \left(^{207}Pb/^{204}Pb\right)_{initial} + \left(^{235}U/^{204}Pb\right)^{j}_{today}\left(e^{\lambda' T}-1\right)$$

$$\left(^{208}Pb/^{204}Pb\right)^{j}_{today} = \left(^{208}Pb/^{204}Pb\right)_{initial} + \left(^{232}Th/^{204}Pb\right)^{j}_{today}\left(e^{\lambda'' T}-1\right)$$

where the superscript j indicates the j^{th} phase and λ, λ', λ'' are the decay constants for ^{238}U, ^{235}U, and ^{232}Th, respectively. In this case U and Pb isotopic data for the phases form a straight line or mineral isochron on a plot of $^{206}Pb/^{204}Pb$ versus $^{238}U/^{204}Pb$ and the intercept, corresponding to a phase with no U, defines the initial $^{206}Pb/^{204}Pb$ value. Similarly on plots of $^{207}Pb/^{204}Pb$ versus $^{235}U/^{204}Pb$ and $^{208}Pb/^{204}Pb$ versus $^{232}Th/^{204}Pb$ the data form isochrons and the intercepts define the initial values of $^{207}Pb/^{204}Pb$ and $^{208}Pb/^{204}Pb$, respectively. The slopes of the lines correspond to the age which should be the same by all three methods.

Because of the mobility of U, Th, and Pb and the intermediate decay products of U and Th most terrestrial rocks do not behave as

simple systems and few isochrons have been determined. However, in typical igneous and metamorphic rocks, the feldspar minerals are generally very strongly enriched in Pb relative to U and Th. Thus, the relative amount of Pb produced by in situ decay of U and Th is small and the Pb in the feldspar may be close to the initial Pb. "Initial" Pb isotopic abundances in terrestrial rocks most frequently have been determined this way.

In igneous rocks with complicated polymetamorphic histories determining the initial Pb at the time of primary formation of the rocks is very difficult, since the metamorphic effects modifying the primary isotopic characteristics must be understood quantitatively. For example, consider a suite of igneous rocks which at the time of their formation have the same initial Pb isotopic abundances, but different values of Th/Pb and U/Pb. Subsequent metamorphism with local isotopic rehomogenization results in rocks with different local "initial" Pb isotopic abundances. The extent to which the new "initial" Pb subsequent to metamorphism is evolved from the original initial Pb depends on the time between primary formation and metamorphism and the U/Pb and Th/Pb values. In polymetamorphic areas one way of demonstrating that an initial Pb is an original igneous Pb and not a product of subsequent metamorphism is, therefore, to show that rocks with different U/Pb and Th/Pb values preserve the same initial Pb isotopic abundances.

In the search for the initial Pb in the ancient rocks from West Greenland we have measured Pb in Pb-rich, U-poor phases. We report in this paper U, Th, and Pb measurements on potassium and plagioclase

feldspar separated from the Amîtsoq Gneiss. These include samples from different geographic localities and samples from a restricted locality which exhibit a wide range of deformation and recrystallization. It will be shown that the Pb isotopic composition of all these samples is nearly identical and is very primitive.

To understand the nature and extent of U, Th, and Pb redistribution in the rocks and the effects on the feldspar Pb, we report data on biotite-rich chips of the gneiss and an estimate of $^{238}U/^{204}Pb$ for the total rocks. To see if an isotopically well-defined Pb was added to the feldspar samples, samples of feldspar were leached with different reagents. Data for these experiments are presented. We also present Pb and U data for feldspar in a dyke which cuts the Amîtsoq Gneiss.

1.2 General Geology

The geology of the West Greenland Precambrian craton is very complex due to intense deformation and multiple episodes of metamorphism. In the Godthaab District, however, the lithostratigraphic relationships have been studied in detail and four major units are recognized. The units (see also the map by McGregor, 1973) are the Amîtsoq Gneiss, the Nûk Gneiss, the Malene supracrustals, and the Qôrqut Granite.

Stratigraphically the oldest of the four units is the Amîtsoq Gneiss, which is defined by the presence of mafic, salt and pepper textured dykes, the Ameralik Dykes. It is these dykes which distinguish the Amîtsoq Gneiss from the otherwise similar appearing Nûk Gneiss. The Ameralik Dykes exhibit a wide range in the degree of deformation

from occasional, undeformed dykes which clearly cut across the gneiss to common, strongly deformed and broken up dykes which exhibit nearly concordant relationships with the foliation of the gneiss. The degree of deformation of the Ameralik Dykes is not always commensurate with the degree of deformation of the Amîtsoq Gneiss indicating pre-Ameralik Dyke deformation.

In a few localities there are areas (~10 m^2) of moderately deformed gneiss. The gneiss is well-foliated, is characterized by large (~5 cm) euhedral, potassium feldspar megacrysts, and is a potassium feldspar porphyroblastic granodiorite. It is from these types of exposures that McGregor (1973) has inferred that the Amîtsoq Gneiss is an orthogneiss. In general, however, the gneiss is much more intensely deformed and ranges from homogeneous, finely banded gneiss to heavily pegmatite-banded gneiss.

The samples used in this study were collected by us with the guidance of V. R. McGregor and were taken from localities where the cross cutting relationships of the Ameralik Dykes were quite obvious, clearly identifying the gneiss as Amîtsoq Gneiss. It is from similar localities in the same general region where we collected our samples that the rocks from which zircons were separated by Baadsgaard (1973) were collected.

Stratigraphically younger than the Amîtsoq Gneiss is the Nûk Gneiss. The rocks which comprise this unit range in composition from tonalitic to granodioritic, and are the most abundant lithology in the Godthaab District. A Rb-Sr whole-rock isochron of samples collected

from a restricted area yields an age of 3.04 ± 0.05 AE (Pankhurst et al., 1973a).

The Malene Supracrustal unit, composed of metavolcanic and metasedimentary rocks, is from the field relationships older than the Nûk Gneiss (McGregor, 1973), although there is apparently some ambiguity in the field relationships (Chadwick and Coe, 1975; McGregor, 1975) and the precise stratigraphic position of the unit is not well established. Hawkesworth et al. (1975) have suggested from preliminary, unpublished data, that the "Malene Supracrustals are probably not much older than ca. 3000 m.y."

Stratigraphically, the youngest major unit in the Godthaab District is the Qôrqut Granite. It is a fine-grained, biotite granite dated by Rb-Sr at 2.85 ± 0.03 AE (Pankhurst et al., 1973b).

1.3 Analytical Techniques

The method of separation of U, Th, and Pb are basically those described by Tera and Wasserburg (1972 a,b). We have modified the procedure in extracting U, Th, and Pb from the sample and now use approximately 1 ml of concentrated HNO_3 rather than a 3:1 mixture of CCl_4 and 94% CH_3OH + 6% concentrated HNO_3. The blank levels for large (~100 mg) samples are generally 3 to 6 picomoles of Pb and 0.1 picomole of U. More precise estimates are tabulated for each sample (see table 2). For the Amîtsoq Gneiss potassium feldspar samples, the blank is generally about 0.02% of the total Pb and has a small effect on the Pb isotopic composition.

For the leaching experiments on the Amîtsoq Gneiss potassium feldspar, the leachates using 0.1N and 1N HCl and 2N HNO_3 were not

processed through ion exchange chemistry. Pb was measured by directly loading 1% to 3% aliquots of the leachate onto the filament. The spectra in the mass region 194-210 contain besides Pb, Bi and $BaPO_2$. As observed by Tera and Wasserburg (1975) the ion beam emitted by samples run without chemical separation tend to develop severe instabilities at high temperatures (~1400°C). In leaching potassium feldspar with more concentrated acids too much material was leached to run the sample without chemical separation of Pb. All aliquots of leachates which were analyzed for U were processed through ion exchange chemistry. However, instead of loading the U samples on Ta filaments with Ta powder and H_3PO_4 we used Re "V" filaments with silica gel and H_3PO_4. The emitted ion beam using this method is more stable and lasts for a much longer time than by using the previous method. 10^{-9} g of ^{235}U provided a stable ion beam ($\sim 10^{-13}$A) for four hours between temperatures of 1400°C to 1550°C.

The Pb isotopic data obtained using our normal mass spectrometric procedures have been checked by 1) calculating ratios from analog data, 2) measuring ratios with different background settings, 3) running Pb standards of known isotopic composition immediately prior to and after a sample run, and 4) measuring ratios over temperatures ranging from 1250°C to 1450°C. In none of these cases do we note isotopic ratios different from those obtained with normal operating procedures.

All of the Pb data presented in the tables and plotted on the figures are normalized to absolute values. 10^{-9} moles of C.I.T. lead standard are run regularly. Fractionation factors for the data relative to the absolute values determined by Catanzaro (1967) are given in

table 1. The Pb isotopic data reported in this paper are all corrected by 1.1 per mil per mass unit. We have also run the National Bureau of Standard's SRM 982 (Catanzaro et al, 1968). The values (unnormalized) are $^{207}Pb/^{208}Pb = 0.46744 \pm 3$; $^{206}Pb/^{208}Pb = 1.0018 \pm 1$; $^{204}Pb/^{208}Pb = 0.02730 \pm 1$.

1.4 Analytical Results

1.4.1 Amîtsoq Gneiss Feldspar

At the few localities where the Amîtsoq Gneiss is moderately deformed the gneiss is homogeneous. The transition zone from this moderately deformed gneiss to intensely deformed gneiss is quite narrow (~10m). The intensely deformed gneiss is strongly laminated and banded. The whole spectrum of deformation is exhibited in the rock samples used in this study. The precise locations of the samples are shown on figure 2. Rock A was collected from one of the areas with the least deformation and Rock C was collected approximately 10 m away and shows strong deformation. Rock B is from another area of relatively weak deformation, but is slightly more deformed than Rock A. Sample B locality is approximately 2 km from the locality of samples A and C. In no case were exposures of undeformed Amîtsoq Gneiss observed.

There are two compositionally distinct types of Amîtsoq Gneiss. One is granodioritic in composition and the other is tonalitic. Rocks A, B, and C are the granodioritic variety and are composed of 0 to 20% hornblende, 10 to 20% biotite, 15 to 35% potassium feldspar, 25 to 35% plagioclase, 15 to 25% quartz, ~5% epidote, 1 to 3% sphene, 1 to 3% apatite and trace amounts of zircon and opaque minerals. Rock D

is a tonalitic gneiss. It is a sample of very intensely deformed gneiss and is composed of ~20% hornblende, ~8% biotite, ~35% plagioclase, ~30% quartz, ~3% sphene, and ~3% apatite. This sample was collected about 5 km from Rock A.

Samples of the moderately deformed gneiss contain large (~5 cm) single crystals of potassium feldspar surrounded by thin (1 to 2 mm) polygranular aggregates of potassium feldspar. We refer to the large single crystals as cores and the polycrystalline aggregates surrounding them as rims. With progressively more intense deformation the potassium feldspar megacrysts are flattened and recrystallized. When the flattening ratio is ~2:1, cores of feldspar are ~1 to 3 cm in diameter and the rims are ~1 cm thick. For flattening ratios of approximately 10:1 the feldspars are totally recrystallized and occur as lenses composed completely of granular aggregates of potassium feldspar. In the extreme case the original megacrysts are so strongly deformed that it is difficult to differentiate original megacrysts from products of metamorphic segregation.

The feldspar is microcline and is microperthitic. As shown on the histogram of feldspar compositions (figure 3) the core and rim samples are indistinguishable. In general, the feldspar cores are composed of large, angular fragments of an original crystal which have been rotated very slightly with respect to one another. There does not appear to be any systematic crystallographic orientation of the feldspar crystals composing the rims. One important problem is determining when in the history of the gneiss this partial recrystallization occurred and what the attendant isotopic and element redistribution effects were.

Core samples 1, 2, and 3 from Rock A are from large single crystals of potassium feldspar. Of all the rock samples collected the potassium feldspars in Rock A have the thinnest rims (~1 to 2mm). All of these samples were taken as closely as possible to the center of single crystals except core 2 which was taken from the edge of a single crystal, but was carefully selected so as not to include any of the polycrystalline rim material. The purpose of this experiment was to see if different crystals from the same hand-specimen size sample have the same or different Pb isotopic compositions. For comparison with the Pb isotopic composition of the core sample, a sample of biotite-rich material surrounding core sample 2 was analyzed.

To observe the effects of recrystallization on the Pb isotopic composition, a core and rim sample from Rock B were analyzed. The potassium feldspar in Rock B from which the samples were taken consists of a core ~3 cm in diameter and a 1 cm thick rim. We also analyzed a sample of the biotite-rich material surrounding the feldspar samples.

Rock C is a sample in which the feldspar megacrysts are intensely deformed and occur as lenses ~2 mm thick of totally recrystallized aggregates of potassium feldspar.

Plagioclase is also present in the Amîtsoq Gneiss and occurs as small grains ~1 mm in diameter intimately associated with quartz, hornblende and biotite. One sample of plagioclase feldspar was analyzed. The sample is from Rock D which is intensely deformed and which was collected about 5 km from Rock A. The sample was selected by crushing the rock and handpicking plagioclase crystals. The sample

analyzed was approximately 75% plagioclase ($An_{24}Ab_{76}$) and 25% quartz with minor amounts of biotite and phosphate.

The analytical data corrected for laboratory blank for the Pb isotopic composition and the U, Th, and Pb concentrations for the Amîtsoq Gneiss are presented in tables 2 and 3. The mean value and 2σ deviation of the mean of nine samples of α, β, and γ are $\alpha = 11.531 \pm 0.013$, $\beta = 13.224 \pm 0.008$ and $\gamma = 31.430 \pm 0.014$. The data are also plotted on figure 4 as the open polygons. These error polygons include not only uncertainty associated with the mass spectrometry and with fluctuation in the chemistry blank, but also uncertainty in the magnitude of the mass discrimination factor. We have chosen to represent the data on this β/α versus $1/\alpha$ diagram rather than the more conventional β versus α diagram for two reasons, both of which concern the size of the error envelopes. First, on the ordinate is plotted $^{207}Pb/^{206}Pb$ which has a smaller error than ratios involving ^{204}Pb which are plotted on both axes in the β versus α representation. Second, the mass fractionation errors are smaller in the adopted representation since the errors are proportional to the difference in mass of the isotopes used in an isotopic ratio which are 1 and 2 mass units on the ordinate and abscissa of the β/α versus $1/\alpha$ diagram and 3 and 2 mass units in the β versus α representation.

The most obvious feature of these data is the extreme similarity of the Pb isotopic composition not only in β/α and $1/\alpha$ for both of which the spread is 0.5%, but also γ/α for which the spread is 0.3%. This tight clustering is quite remarkable considering that the samples come from different geographic localities, exhibit wide degrees of

deformation, and include both potassium and plagioclase feldspar. However, despite the similarity of the Pb isotopic abundances, the spread in the values as shown on figure 4, is much larger than the analytical uncertainty. Also shown on figure 4 are the data corrected for in situ U decay for 3.59 AE. The mean corrected values are: $\alpha = 11.468 \pm 0.027$, $\beta = 13.203 \pm 0.017$, and $\gamma = 31.36$. The correction is small (0.5% for α and 0.2% for β), but still quite significant. The correction also somewhat increases rather than decreases the dispersion in the data.

These data confirm the original reconnaissance observations by Black et al. (1971) of the primitive nature of the Pb isotopic abundances in the gneiss. There is, however, some discrepancy in the values reported here and the minimum value reported by Black et al. (1971) (whole-rock sample - 125519). An instrumental mass fractionation of approximately 0.25%/mass unit shifts their datum to lie on a 3.6 AE isochron using as an initial Pb the Pb isotopic abundances measured in the feldspar samples.

1.4.2 Characteristic Pb and Metamorphic Effects

Considering the structurally complex, polymetamorphic evolutionary history of the Amîtsoq Gneiss, it is not a priori obvious that there should exist a characteristic Pb throughout these rocks on a large variety of scales. The striking uniformity of the Pb isotopic abundances, however, occurs on a ~1 cm scale as seen in the analysis of the core and rim potassium feldspar, on a ~10 cm scale as seen in the analysis of potassium feldspar crystals from a single hand-specimen of the gneiss, to a

km scale as seen in the analysis of feldspar samples from different geographic localities.

Recurrent metamorphic episodes have clearly affected the Amîtsoq Gneiss. Rb-Sr and $^{40}Ar/^{39}Ar$ data on minerals separated from the gneiss (Pankhurst et al., 1973b) demonstrate the open-system behavior of the gneiss. The extreme scatter in the Pb whole-rock data reported by Black et al. (1971) also indicates significant open-system behavior. In contrast the whole-rock, Rb-Sr data (Moorbath et al., 1972) indicate that on approximately a 10 cm scale, samples of the Amîtsoq Gneiss appear to have behaved as reasonably well-closed systems since 3.7 AE. The small scatter which we observe in the Pb isotopic abundances in the feldspar samples may be a metamorphic effect or may be true variations in initial Pb. In this subsection we present data on the feldspar leads bearing on the extent to which they were affected by metamorphism and on the nature of the metamorphic processes.

Two experiments indicate quite clearly the open-system behavior of the Amîtsoq Gneiss feldspar. In Rock B, U and Pb were analyzed in a potassium feldspar core and recrystallized rim (analyses 6 and 7 on figure 4). The Pb isotopic composition of the core is approximately 0.3% more radiogenic than the rim. This difference is not simply due to differing amounts of U since it persists when the data are corrected for in situ U decay. The Pb and U concentrations are about 12% lower in the rim sample than in the core and suggest that the rim feldspar may have been open to Pb and U exchange during recrystallization.

As noted previously, there exists dispersion in the isotopic composition of Pb in the feldspar which is greater than analytical uncertainties

in both the data uncorrected and corrected for in situ decay. This dispersion could be accounted for by the presence of small amounts of labile Pb added to the feldspar. In addition, U is known to be quite mobile under the physical-chemical conditions prevalent in the terrestrial environment (Rosholt et al., 1973) and the dispersion may be because the feldspar crystals have been open to both U loss and gain. In principal, labile Pb added to the feldspar and Pb produced by in situ decay of U should be preferentially leachable from the feldspar. Therefore, to see if the feldspar contains leachable Pb three leaching experiments were done and the data are presented on figures 4 and 5 and in table 4.

In the first experiment a split of Rock A, core 2 sample, crushed to -40 + 100 mesh, was sequentially leached with progressively stronger acids and the leachate from each step was analyzed. In the leaches about 2% of the total Pb in the feldspar was removed. The first leach was with cold 1N HCl for 15 minutes and ~50% of the total leached Pb was removed. This indicates the presence of a very easily leachable component. The fourth leach (see table 4, footnote) was with boiling concentrated HNO_3. We infer that the Pb remaining in the residue which comprises 98% of the total Pb is really intrinsic to the feldspar.

In the second experiment another split of core 2 feldspar from Rock A was crushed (-40 + 100 mesh) and leached twice: first with cold 0.1N HCl for 15 minutes and second with boiling concentrated HNO_3 for several hours. The amount of Pb removed by the first leach is similar to that removed by the first leach of the first leaching experiment, confirming the presence of easily leachable Pb in this sample.

The isotopic composition of the Pb leached in these two experiments is quite radiogenic compared to the Pb in the untreated samples. $^{206}Pb/^{204}Pb$ values range from 14.40 to 17.29. As is shown on figure 5 the data define a linear array and suggest that a unique Pb is added to the feldspar. To examine for the ubiquity of an isotopically well-defined, easily leachable component the core sample of Rock B was crushed and leached. This particular sample was selected since the Pb in the untreated sample is the most radiogenic Pb in all the feldspars analyzed, suggesting that it has been most strongly affected by the addition of a radiogenic component. The feldspar was first leached for 15 minutes in cold 0.1N HCl. Less than 0.05% of the Pb in the feldspar was removed, which is proportionately about 20 times less than removed by the same type of leach on Rock A core 2. However, the Pb is apparently part of the linear array defined by the leaches on core 2 of Rock A, indicating the addition of the same component to the feldspars of Rocks A and B. The linear array intersects the ordinate (figure 5) at $^{207}Pb/^{206}Pb = 0.185$ and yields an age of 2.7 ± 0.1 AE. From these data alone it is not possible to distinguish if the linear array is a simple two-component mixing line without temporal significance or if the array defines a meaningful time.

We have also measured U in some of the leaches. In contrast to the Pb where only ~2% was removed by leaching, from 60% to 70% of the U was removed. Unlike the Pb isotopic data alone, there does not appear to be any precise systematic relationships between the U and Pb removed by individual leaches. However, in the two leaching experiments on Rock A-core 2 there appears to be a semi-quantitative

relationship between the amounts of U and Pb removed. In the first leaching experiment, the amount of radiogenic 2.7 AE old Pb removed is only 6% more than that produced in 2.7 AE *in situ* decay as calculated from the amount of leached U. For the second experiment the leached radiogenic Pb is about 30% more than that calculated from the U leached. This suggests that the leaching process is dissolving a phase formed at 2.7 AE which is rich in U and is associated with the feldspar. This is fundamentally different from leaching from the feldspar Pb which was produced in the interval from 2.7 AE to today and was recently incorporated with the feldspar. This "phase" dissolved by the leaching process is apparently soluble in HCl and HNO_3 and, therefore, is probably phosphate or a metamict phase. No Th concentrations were determined, but the Pb isotopic data on the second leach of the second leaching experiment, assuming an age of 2.7 AE, indicate that a Th/U of 3.7 is necessary to produce the labile Pb. Thus, the "phase" cannot be a Th-rich mineral.

These leaching experiments clearly indicate that there has been significant element migration in the Amîtsoq Gneiss and furthermore, indicate that it occurred at 2.7 AE. This is the time of rather intense igneous and metamorphic activity in and around the Godthaab district. The Qôrqut Granite has been dated at 2.85 ± 0.03 AE by Rb-Sr (Pankhurst *et al.*, 1972b), the granulite facies metamorphic event just to the north of the Godthaab area has been dated at 2.89 ± 0.07 AE (Black *et al.*, 1973), and the revised Rb-Sr isochron on whole-rock samples of the Nûk Gneiss yields an age of 2.75 AE (Moorbath, 1976 personal communication). The most reasonable interpretation of these data is that

at 2.7 AE thermal activity associated with the igneous and metamorphic events resulted in the redistribution of elements in the Amîtsoq Gneiss with the formation of phases enriched in Th and U relative to Pb which were incorporated as discrete phases into the Amîtsoq Gneiss feldspar.

The isotopic abundances of Pb in the residual feldspar are shown on figure 4 (analyses 10 to 12). All of these feldspar samples were boiled in concentrated HNO_3 in an effort to remove all Pb not intrinsic to the feldspar and dissolve soluble U-rich phases. In all cases the leaching resulted in a distinct shift in isotopic composition relative to the untreated samples. The shifts are small, ranging from 0.2% to 0.6% in α, and are less than the in situ Pb corrections made on the respective untreated samples. U was also measured on the residue samples and the data corrected for in situ U decay are also shown on figure 4. In neither the residues uncorrected for in situ U decay nor corrected for in situ U decay, is the dispersion noted in the data on untreated samples decreased. It therefore appears that there exists small, but real differences in the isotopic composition of Pb in the feldspar samples. To what extent these differences represent real differences in the initial Pb in the Amîtsoq Gneiss versus differences produced by subsequent metamorphic events is not apparent and clearly remains a significant problem to which we will return.

1.4.3 Pb in the Matrix Adjacent to the Feldspar Megacrysts

To further assess the effects of metamorphism on U and Pb redistribution and identify Pb which might be available for redistribution during metamorphism we analyzed U and Pb in two samples of biotite-rich material surrounding the potassium feldspar.

The biotite-rich margin samples were obtained by removing small (~75 mg) chips from around a potassium feldspar to be analyzed until 200 to 500 mg of material was collected. The analyses of these materials are tabulated in table 2 and illustrated on figure 6. The isotopic composition of the Pb in these two biotite-rich margin samples is quite different between the two samples and much more radiogenic than the Pb in the associated feldspar. In neither case does the isotopic composition of Pb in these materials lie along a 3.6 AE isochron with the initial Pb for the Amîtsoq Gneiss as determined in this work. This clearly indicates the open system behavior of the rocks subsequent to 3.6 AE. As shown on figure 6, the data points lie below the 3.6 AE reference isochron indicating that the samples were enriched in U subsequent to 3.6 AE. However, because of the relatively small differences in isotopic composition between these data and the Amîtsoq Gneiss initial Pb, the time of post-3.6 AE disturbance(s) is not defined. We cannot ascertain from these data if the time of element redistribution in these samples coincides with that in the Amîtsoq Gneiss feldspar.

1.4.4 Pb in Dyke Feldspar

An experiment to characterize Pb in rock associated with the Amîtsoq Gneiss was to analyze U, Th, and Pb in potassium feldspar selected from a small, relatively undeformed, biotite-quartz-potassium feldspar, pegmatite dyke cutting across the Amîtsoq Gneiss. The major element composition of this feldspar is the same as the potassium feldspar separated from the Amîtsoq Gneiss (see figure 3). This feldspar sample was soaked in acid and both the supernate and residue were

analyzed. The Pb isotopic abundances are quite different from the abundances in the feldspar of the gneiss and the leached Pb is much more radiogenic than the Pb in the residue. The results are presented in table 2 illustrated on figure 6. The line defined by the leach and residue corresponds to an age of 2.4 AE.

The Pb leached from the dyke feldspar lies on the $^{207}Pb/^{206}Pb$ versus $^{204}Pb/^{206}Pb$ linear array defined by the leaches of the Amîtsoq Gneiss potassium feldspar. A similar relationship is not observed between $^{208}Pb/^{204}Pb$ and either $^{207}Pb/^{204}Pb$ or $^{206}Pb/^{204}Pb$. This precludes that the Pb leached from the Amîtsoq Gneiss feldspar and Pb leached from this dyke feldspar represent a unique, labile Pb added to all feldspar. These leach data indicate that associated with the dyke feldspar are 2.4 AE old, readily soluble phases. This element redistribution at 2.4 AE recorded by these soluble phases is apparently not recorded in the Amîtsoq Gneiss feldspar.

The leaching process removed only a small amount of Pb and approximately 98 per cent is in the residue. The Pb in this residue has a single-stage model age of 3.3 AE and single-stage parameters of $\mu = 7.6$ and Th/U = 3.6. There is, however, no obvious indication from the other data reported here or by other worker of igneous activity at this time.

It is interesting to note that the residual dyke feldspar Pb could be a mixture of Amîtsoq Gneiss feldspar Pb and Pb produced in the interval from 3.6 AE to 2.7 AE. The latter is the time of U redistribution as indicated by the Amîtsoq Gneiss feldspar leaching experiment. The μ in this interval, 3.6 AE to 2.7 AE, needed to produce the dyke

feldspar Pb is ~2, which is similar to the μ inferred for the Amîtsoq Gneiss. The data strongly suggest that at 2.7 AE U and Pb in the Amîtsoq Gneiss were mobilized. The Pb was removed and incorporated as the dyke feldspar Pb, and U-rich phases formed and were added to the Amîtsoq Gneiss feldspar.

If the Pb in the dyke feldspar is indeed like that in the Amîtsoq Gneiss at 2.7 AE and which was redistributed, then the Amîtsoq Gneiss feldspar did not isotopically equilibrate with this Pb. Consequently, the feldspars preserve older, more primitive isotopic abundances. The degree to which the pre-2.7 AE feldspar Pb was effected by partial isotopic equilibration with the 2.7 AE Pb is not evident from these data, but is of serious consequence to subsequent calculations and will be discussed in more detail.

1.4.5 Initial Pb

The analyses of the biotite-rich matrix samples, the dyke feldspar, and leaches of the Amîtsoq Gneiss feldspar do not explain the dispersion which we observe in the Pb isotopic abundances of the Amîtsoq Gneiss feldspar. One possible explanation is that the dispersion indicates real differences in the initial Pb of the gneiss. Alternatively, Pb could have been added to the feldspar. The addition of phases which are rich in U which decays to Pb does not explain the dispersion since in the leach experiments it persists even after extremely harsh leaching processes.

In general, the trends shown by the Pb data on figure 4 are not sufficiently well defined to indicate precisely the time and/or composition of Pb addition. However, they do show that an admixture of

either Pb like that in the dyke feldspar or Pb like that in the biotite-rich matrix samples could not account for the dispersion.

If Pb addition is responsible for the dispersion, then do any of the samples represent pristine material with unmodified isotopic characteristics? The relatively small dispersion suggests only limited modification since it is difficult to arrive at a relatively uniform isotopic compositions by mixing processes whereby Pb is added and mixed with Pb preexisting in the feldspar. This process requires that the amount of Pb added be proportional to the amount of Pb preexisting in the feldspar. This seems unlikely since the feldspar has Pb concentrations from 10 to 55 ppm.

Despite effects which modify the Pb isotopic characteristics of the gneiss, there are apparently small and the feldspar data indicate that there exists a reasonably well-defined characteristic Pb in the Amîtsoq Gneiss. The best estimate of the initial Pb isotopic composition from these data is $\alpha = 11.468$, $\beta = 13.203$, and $\gamma = 31.429$. Two critical questions whose answers are prerequisites to interpreting the significance of this Pb are 1) at what time in history of the Amîtsoq Gneiss was this characteristic Pb acquired, and 2) does this Pb represent isotopic homogenization during large scale metamorphic reequilibration?

1.5 Age of Initial Pb

For the initial Pb of the Amîtsoq Gneiss to have significance relating to the early chemical evolution of the earth, a time must associated with the Pb. A variety of isotopic age determinations have been done on the Amîtsoq Gneiss (Black et al., 1971; Moorbath et al., 1972; Baadsgaard,

1973) and are generally consistent with an age of 3.6 AE to 3.8 AE. The most precise data are reported by Baadsgaard (1973) who separated zircons from samples of Amîtsoq Gneiss most of which were collected in the vicinity of Rock B. The U, Th, and Pb data define a precise linear array and yield an age of 3.65 ± 0.05 AE. This is the age we will associate with the initial Pb.

Assuming that the isotopic composition of Pb in the feldspar is the initial Pb in the rocks at 3.7 AE, understanding whether 3.7 AE represents an igneous or metamorphic event is paramount to subsequent interpretation. Moorbath et al. (1972) have addressed the problem using their Rb-Sr data and found the data inconclusive. The zircon data of Baadsgaard (1973) suggest that 3.7 AE represents an igneous event. U, Th, and Pb analyses of zircons from complex polymetamorphic gneisses typically display complicated patterns (c.f. Pidgeon and Hopgood, 1975). The pattern of zircons from the Amîtsoq Gneiss is remarkably simple and similar to those in unmetamorphosed igneous rocks (c.f. Naylor et al., 1970). These simple relationships appear not only in the U-Pb systematics, but also the Th-U-Pb systematics. There is no indication from the zircon data of events prior to 3.7 AE.

McGregor (1973) has suggested on the basis of field relationships that the Amîtsoq Gneiss is a metaigneous gneiss. One interpretation reconciling both the variety of isotopic data and field observations is that ~3.7 AE is the time of igneous intrusion and penecontemporaneous deformation and recrystallization. In this case the initial Pb is a mixture of the initial Pb at the time of crystallization of the rocks from a melt plus Pb produced during the interval between the igneous event and

metamorphic event. The degree to which the Pb isotopic composition changed during this interval depends on the U/Pb ratio in the rocks and duration of the interval.

Assuming that the characteristic Pb in these rocks reflects rather accurately the Pb in the rocks at the time of crystallization from a melt, critical questions are: 1) is the Pb in the silicate melt at 3.7 AE characteristic of large scale reservoirs from which crustal rocks were derived, 2) does this Pb reflect a mixture of the Pb in the melt plus Pb of a different isotopic composition assimilated during intrusion and crystallization ?

In the following discussion we will examine the consequences for the early evolution and differentiation of the earth assuming that the initial Pb isotopic composition in the Amîtsoq Gneiss is the isotopic composition of Pb in global reservoirs from which rocks at 3.7 AE were derived. We will also examine the effect on these consequences if the composition of this Pb is the product of large scale metamorphic reequilibration at 3.7 AE and if the Pb isotopic composition has been altered by metamorphic events subsequent to 3.7 AE.

1.6 Discussion

1.6.1 Comparison with Initial Pb in Other Rocks

The measured Pb isotopic composition of Pb in the feldspar samples of Amîtsoq Gneiss is the most primitive terrestrial Pb known, and is much less radiogenic than other primitive terrestrial Pb samples. The two most primitive Pb isotopic compositions previously known in feldspar samples occurs in feldspar from the Barberton Region of South Africa with α = 12.75, β = 14.07, and γ = 32.22 (Sinha and Tilton, 1973) and in

feldspar from the Peninsular Gneiss, Mysore, India with $\alpha = 13.16$, $\beta = 14.50$, and $\gamma = 35.08$ (Sinha and Tilton, 1973). There are also galena samples with primitive isotopic compositions of Pb which are from the Barberton Region of South Africa with $\alpha = 12.461$, $\beta = 14.077$, and $\gamma = 32.285$ (Stacey et al., 1969) and from Manitouwadge, Ontario $\alpha = 13.211$, $\beta = 14.401$, and $\gamma = 33.069$ (Stacey et al., 1969).

In a gross analysis the Pb in the feldspar from the Amîtsoq Gneiss plot quite close to, but not precisely on the "normal" Pb evolution curve with T = 4.5 AE and $\mu = 9.5$.

Despite the primitive nature of the Pb reported here, it is still significantly evolved from the most primitive Pb in meteorite samples, and a search for more primitive terrestrial Pb is of merit.

1.6.2 Single-Stage Model Age of the Earth

For a simple single-stage model for the evolution of Pb the equation coupling time and α and β is

$$\frac{\beta_t - \beta_T}{\alpha_t - \alpha_T} = \frac{^{235}U}{^{238}U} \left(\frac{e^{\lambda' T} - e^{\lambda' t}}{e^{\lambda T} - e^{\lambda t}} \right)$$

where

α_t and β_t are the values of the initial Pb at t

α_T and β_T are the values at time T.

λ and λ' are the decay constants of ^{238}U and ^{235}U, respectively

$\lambda = 0.155125 \times 10^{-9}\ yr^{-1}$ and $\lambda' = 0.98485 \times 10^{-9}\ yr^{-1}$

$^{235}U/^{238}U = 1/137.8$

If α_T and β_T are the values when the earth formed, then T is the age of the earth. Patterson (1956) first measured the isotopic composition of Pb in the troilite from Canyon Diablo meteorite and assigned these values to α_T and β_T. Using the Pb isotopic composition of modern (i.e. t = 0) pelagic sediments and assuming a single-stage model Patterson (1956) calculated the age of the earth as 4.55 AE. Subsequently, Tilton and Steiger (1965) measured Pb in galena from 2.8 AE old rock and calculated the age of the earth as 4.75 AE. Their calculation has been the subject of extensive discussion since the validity of assigning 2.8 AE as the age of Pb mineralization is difficult to establish firmly. Using the decay constants recently measured by Jaffey et al. (1971) the age calculated by Patterson (1956) is recalculated as 4.48 AE. Using α_T = 9.307 and β_T = 10.294 as measured by Tatsumoto et al. (1973) and the new determinations of the decay constants, the age of the earth from the data of Tilton and Steiger (1965) is 4.53 AE. All subsequent age calculations use these recent determinations of α_T, β_T, λ, and λ'. The new values of the decay constants reduce the age of the Amîtsoq Gneiss determined from the zircon data (Baadsgaard, 1973) to 3.59 AE.

Using the initial Pb isotopic composition determined for the Amîtsoq Gneiss (α = 11.468 and β = 13.203) and t = 3.59 $\pm$ 0.05 AE, the single-stage model age of the earth is 4.47 $\pm$ 0.05 AE. The μ value in the internal 4.47 AE to 3.59 AE is 8.5. The errors on T include errors on t and on α_t and β_t. T is very sensitive to t (dT/dt = 0.8) since at 3.6 AE the ratio $^{207}Pb/^{206}Pb$ changes rapidly. For all the feldspar data, both corrected and uncorrected for in situ U decay, the

total range in the single-stage model age of the earth is from 4.4 AE to 4.5 AE.

This age of ~4.45 is remarkably similar to the age of the earth calculated from average modern terrestrial Pb and from the initial Pb in terrestrial rocks ranging in age from 0 to 3.2 AE. In addition, μ of 8.5 is similar, although somewhat less than the value calculated for the source reservoirs of rocks younger than 3.2 AE. The other planet for which some detailed chemical and isotopic data are available is the moon. For this planet the Pb and U isotopic data on rock samples ranging in age from 3.9 to 3.2 AE consistently indicate that the single-stage model age of the moon is 4.42 AE (Tera and Wasserburg, 1974). This is strikingly similar to the age ~4.47 AE for the earth. In neither the case of the earth nor the moon are there any indications that the age of these planets is ~4.55 AE which are the ages of some meteorites. This apparent ~100 m.y. difference between the age of meteorites and the earth and moon may have fundamental implications for the evolution of the terrestrial planets.

The age of 4.45 AE is meaningful only if the following criteria are met: 1) the potassium feldspar in the Amîtsoq Gneiss crystallized at 3.59 AE and remained closed to gain or loss of U and Pb from 3.59 AE until the present, 2) the initial Pb in the gneiss evolved from T until 3.59 AE in an uranium equivalent system and started with $\alpha = 9.307$ and $\beta = 10.294$.

Considering the complex polymetamorphic history of the gneiss it is quite reasonable to consider that one or both of these criterion are not satisfied. Indeed, the leach data on the Amîtsoq Gneiss feldspar

samples indicate open-system behavior at 2.7 AE. If the rocks formed at 3.6 AE and reequilibrated at 2.7 AE at which time the feldspar acquired its characteristic Pb, then the initial Pb at 3.6 AE depends on μ of the whole-rock systems in the interval 3.6 AE to 2.7 AE. We have measured by gamma-ray counting the U in a 2.5 kg sample of Rock A. The U abundance is 0.5 ppm, and we estimate μ of ~1. Using μ of 1 for the interval 3.6 AE to 2.7 AE to calculate the isotopic composition of Pb in the rock at 3.6 AE results in an initial Pb at 3.6 AE which yields a single-stage model age of the earth of 4.57 AE and μ of 6.8 in the interval 4.57 AE to 3.6 AE.

For the generalized case of metamorphic reequilibration subsequent to 3.6 AE, if we assume the age of the earth to be 4.6 AE and 3.6 AE an igneous crystallization age subsequent to which metamorphic equilibration imparted the characteristic Pb to the feldspar, then the single-stage μ of the magma reservoirs in the interval 4.6 AE to 3.6 AE from which the igneous protolith of the gneiss was derived must be between 6 and 7. The μ of the igneous protolith of the gneiss ranges from 0 to 6 for metamorphic equilibration between today and 3.4 AE. The value of μ between 6 and 7 for the source of the igneous protolith of the gneiss is significantly less than the inferred μ of the source material from which igneous rocks younger than 3.2 AE are derived. The range of μ values for the igneous protolith are peculiar in that the values are less than the μ of the material from which the igneous protolith of the gneiss is derived. In general the production of granitic melts results in an increase in μ in the melt relative to the bulk source material. The low values are

consistent, however, with the range of values inferred from the isotopic data on total-rock samples of the gneiss (Black et al., 1971) and measured by us.

The second criterion necessary for a meaningful single-stage model age is more difficult to evaluate. From the present data we cannot distinguish if the rocks formed in a single or multiple stages with concomitant U-Pb fractionation. However, if the age of the earth is 4.6 AE and 3.6 AE reflects metamorphic equilibration at which time the Amîtsoq Gneiss acquired its characteristic Pb as recorded by the feldspar samples, then to account for the igneous nature of the gneiss requires production of an igneous protolith prior to 3.6 AE. An igneous protolith produced prior to 3.6 AE from an uranium equivalent source in the interval 4.6 AE to the time of production must be derived from a source with μ less than 6. This value is considerably less than the μ of ~9.5 typical of source reservoirs from which igneous rocks are derived. Derivation of the igneous protolith of the Amîtsoq Gneiss prior to 3.6 AE also requires that μ of this protolith range from ~9 for production at 4.45 AE to 15 for production at 3.8 AE. Production subsequent to 3.8 AE requires μ in excess of ~20.

As observed by Black et al. (1971) the Amîtsoq Gneiss appears from the Pb isotopic data to be severely depleted in U relative to Pb. The calculated μ values of the total-rock samples are generally less than ~2. This depletion from μ greater than 9 in the protolith prior to 3.6 AE to μ of less than 2 subsequent to 3.6 AE then must have accompanied the metamorphism at 3.6 AE. Such extensive U loss postulated

by this model appears to be a characteristic of very high-grade metamorphic regimes. (Moorbath et al., 1969; Lambert and Heier, 1967).

1.6.3 Two-Stage Model

The significance of the single-stage model age of the earth of 4.47 AE is complicated by the lack of knowledge of events which occurred during the first aeon of earth's history. Simple single-stage models and two-stage models invented to account for the isotopic evolution of Pb for this time period are probably oversimplifications and not totally realistic. Similarly, however, more complicated models are probably just as unrealistic and their manufacture does not seem warranted with the present state of prejudice and misunderstanding. In the following discussion we examine a two-stage model describing Pb isotopic evolution.

The impetus for pursuing this model is that the age of the earth of 4.47 AE appears to be too young by 100 to possibly 200 m.y. This conclusion is based on the older ages of other planetary objects and the short time estimated to chemically isolate these bodies. The ages of old lunar samples range from 4.55 AE to 4.60 AE (Papanastassiou and Wasserburg, 1975, 1976) and Rb-Sr internal isochron ages on meteorites are 4.56 AE (Gray et al., 1973) to 4.61 AE (Sanz et al., 1970). These Rb-Sr data on meteorites also indicate formation at ~4.65 AE (Gray et al., 1973). In addition U, Th, and Pb data on a meteorite indicate a formation age of 4.55 AE (Adorables F. T., 1976). The time estimated theoretically by Goldreich and Ward (1973) to isolate planetary materials is $\sim 10^3$ yr and estimated empirically by both Gray et al. (1973) using Sr isotopic data and by Podosek et al. (1970)

using Xe isotopic data is $\sim 10^7$ years. These time estimates are much less than the ~100 m.y. between the single-stage model age of the earth and ages of other solar system objects.

We attribute the loss of ~0.1 AE in the early history of the earth to extensive chemical differentiation of the planet resulting in the formation of homogeneous source reservoirs with their characteristic μ from which crustal rocks subsequently are derived. This interpretation is similar to the early history of the moon as inferred from Pb isotopic data (Tera and Wasserburg, 1974).

Two-stage models with a planetary accretion time T_A and a differentiation time T_D are illustrated on figures 7a and 7b. Stage 1 is from T_A to T_D and stage 2 is from T_D to today. The values of T_A, T_D, and μ_1, are solutions to the equations

$$\alpha_t = \alpha_{T_A} + \mu_1 \left(e^{\lambda T_A} - e^{\lambda T_D} \right) + \mu_2 \left(e^{\lambda T_D} - e^{\lambda t} \right)$$

$$\beta_t = \beta_{T_A} + \nu_1 \left(e^{\lambda' T_A} - e^{\lambda' T_D} \right) + \nu_2 \left(e^{\lambda' T_D} - e^{\lambda' t} \right)$$

where α_{T_A} and β_{T_A} are the values of primordial Pb (Tatsumoto et al., 1973) and α_t and β_t are the values of the Amîtsoq Gneiss initial Pb. The values of t and μ_2 are determined from α_t, β_t, and the isotopic composition of modern terrestrial Pb (α_{MT} and β_{MT}) according to the equations

$$\alpha_{MT} = \alpha_t + \mu_2 \left(e^{\lambda t} - 1 \right)$$

$$\beta_{MT} = \beta_t + \nu_2 \left(e^{\lambda' t} - 1 \right).$$

Therefore, two-stage Pb evolution curves pass through primordial Pb (α_{T_A} β_{T_A}), the initial Pb of the Amîtsoq Gneiss (α_t, β_t) and modern terrestrial Pb (α_{MT}, β_{MT}). For the range of values of the isotopic composition of modern terrestrial Pb samples t and μ_2 are anticorrelated. For the two-stage model calculations we have chosen t and μ_2 calculated from the mean value of modern terrestrial Pb (i.e. α = 18.700 and β= 15.628, Stacey and Kramers, 1975). t is calculated as 3.64 AE which is close to the value to 3.59 AE determined from the zircon data (Baadsgaard, 1973), and μ_2 is 9.53.

As is shown on figure 7a an assumed accretion time, T_A, of ~4.6 AE corresponds to an instantaneous differentiation time of ~4.4 AE. The μ, in the interval T_A to T_D is, as illustrated on figure 7b, approximately 1.6. These parameters are radically different from the two-stage model parameters recently presented by Stacey and Kramers (1975), who using T_A = 4.57 AE calculated μ_1 = 7.19 and μ_2 = 9.76. Stacey and Kramers (1975) evaluated the quality of their model by comparing absolute and model ages for initial Pb as measured in feldspar and galena samples of a variety of ages. Using our model parameters (i.e. T_A = 4.62 AE, T_D = 4.38 AE, t = 3.64 AE, μ_1 = 1.63, and μ_2 = 9.53) the agreement between the calculated model ages and absolute ages for the same feldspar and galena samples used by Stacey and Kramers (1975) is as good as obtained by these authors.

Doe and Stacey (1974) also compared model and absolute ages of these initial Pb samples using a single-stage model and varying T. The best fit was with T= 4.43 AE and μ= 9.58. The two-stage model

which we described fits the initial Pb data much better than the model of Doe and Stacey (1974). Another model, recently proposed by Sinha and Tilton (1973), to describe the isotopic evolution of Pb starts at T = 4.66 AE and μ increases linearly with time. This model predicts an initial Pb isotopic composition at 3.6 AE significantly different from the Pb isotopic abundances measured in the Amîtsoq Gneiss feldspar. The model predicts α = 11.69 and β = 13.80 compared to the measured values of α = 11.47 and β = 13.20. In addition, their model requires a mean μ of 7.7 in the interval 4.66 AE to 3.6 AE, which is much lower than the single-stage μ of 8.5.

The large change in μ indicated by the two-stage model requires the isolation of substantial amounts of either Pb or U. One possible process which could change μ significantly is to form a core at T_D and bury the Pb in this core. For $\mu_2/\mu_1 \sim 6$ approximately 85% of the Pb needs to be removed. This percentage is not inconsistent with the partition coefficients of Pb between a silicate melt and immiscible metal melt measured by Oversby and Ringwood (1971). For a core composed of 85% wt Fe-Ni metal and 15% wt Fe-sulfide, the equilibrium partitioning of Pb simultaneously between the total masses of sulfide and silicate in the earth requires that 65% of the Pb be buried into the core. For a core composed of 89% wt Fe-Ni metal and 11% wt. Si, 60% of the Pb is partitioned into the core. In either of these cases the calculations indicate that substantial amounts of Pb can be extracted from silicate material in equilibrium with materials of appropriate core compositions. These amounts, however, are considerably less than the 85% indicated by the two-stage model calculations.

The assumption in the above calculations for partitioning Pb is that the silicate and metal melts are simultaneously in total equilibrium. Possibly a more realistic model for the earth is multistage extraction of Pb by the core material as it settles through the earth. In this case up to 92% of the Pb can be extracted into the core.

There are two significant consequences to burial of a large percentage of Pb in the core. First, there must exist at present Pb in the core with an extremely primitive isotopic composition and this Pb is totally isolated from the rock reservoirs from which crustal rocks are derived. Secondly, the earth is generally regarded to be severely depleted in volatile elements such as Pb relative to solar abundances. This depletion is in part inferred from the generally assumed terrestrial μ value of ~10 as compared to the solar system estimate of ~0.3. Therefore, the μ_1 of ~2 implied by the two-stage model indicates that the earth is much less depleted in Pb. By analogy, other volatile elements such as Tl, Bi, Cd, Zn, Hg, and In are also less depleted than generally believed. Similarly the volatile, alkalis K, Rb, and Cs should be less depleted. Lewis (1971) on the basis of thermodynamic calculations suggested that these alkali elements should form very stable sulfide compounds and be selectively partitioned into the core of the earth.

An alternative to changing μ with differentiation is redistributing U. If for example 90% of the U in the earth is concentrated into the upper 400 km of the earth during differentiation and subsequently rocks are only derived from this upper 400 km, then it appears that μ changes by ~6, the value indicated by our two-stage model calculation.

Clearly these models for fractionating Pb and not redistributing U and *vice versa* are not realistic and U and Pb must be concomitantly fractionated and redistributed. However, they do indicate that very sizeable proportions of these elements are moved during planetary differentiation.

References

Adorables F.T. (1976) Progress by the consorts of Angra Dos Reis (abstract). In Lunar Science VII, p. 443-445, The Lunar Science Institute, Houston, Texas.

Baadsgaard H. (1973) U-Th-Pb dates on zircons from the early Precambrian Amîtsoq Gneiss, Godthaab District, West Greenland. Earth Planet. Sci. Letters, 19, 22-28.

Black L. P., Gale N. H., Moorbath S., Pankhurst R. J., and McGregor V. R. (1971) Isotopic dating of very early Precambrian Amphibolite Facies gneisses from the Godthaab District, West Greenland. Earth Planet. Sci. Letters, 12, 245-259.

Black L. P., Moorbath S., Pankhurst R. J., and Windley B. F. (1973) $^{207}Pb/^{206}Pb$ whole rock age of the Archaean Granulite Facies Metamorphic Event in West Greenland. Nature, Phys. Sci., 244, 50-53.

Catanzaro E. J. (1967) Absolute isotopic abundance ratios of three common lead reference samples. Earth Planet. Sci. Letters, 3, 343-346.

Catanzaro E. J., Murphy T. J., Shields W.R., and Garner E. L. (1968) Absolute isotopic abundance ratios of common, equal atom, and radiogenic lead isotopic standards. Jour. Res. Nat. Bureau Stds. -A, 72A, 261-267.

Chadwick B. and Coe K. (1975) A horizontal tectonic regime in the Archaean of Greenland and its implications for early crustal thickening - a comment. Precambrian Res., 2, 397-400.

Collins C.B., Russell R.D., and Farquhar R.M. (1953) The maximum age of the elements and the age of the earth's crust. Canadian Jour. Phys. 31, 402-418.

Doe B. R. and Stacey J. S. (1974) The application of lead isotopes to the problem of ore genesis and ore prospect evaluation: A review. Econ. Geol., 69, 757-776.

Goldreich P. and Ward W. (1973) The formation of planetesimals. Astrphys. J., 183, 1051-1061.

Gray C. M., Papanastassiou D. A., and Wasserburg G. J. (1973) The identification of early condensates from the solar nebula. Icarus, 20, 213-239.

Hawkesworth C. J., Moorbath S., O'Nions R. K., and Wilson J. F. (1975) Age relationships between greenstone belts and "granites" in the Rhodesian Archaean craton. Earth Planet. Sci. Letters, 25, 251-262.

Jaffey A. H., Flynn K. F., Glendenin L. E., Bently W. C., and Essling A. M. (1971) Precision measurements of half-lives and specific activities of ^{235}U and ^{238}U. Phys. Rev. C, 4, 1889-1906.

Lambert I. B. and Heier K. S. (1967) The vertical distribution of uranium, thorium, and potassium in the Continental Crust. Geochim. Cosmochem. Acta, 31, 377-390.

Lewis J. S. (1971) Consequences of the presence of sulphur in the core of the earth. Earth Planet. Sci. Letters, 11, 130-134.

McGregor V. R. (1973) The early Precambrian gneiss of the Godthåb district, West Greenland. Phil. Trans. Roy. Soc. London A, 273, 343-358.

McGregor V. R. (1975) A horizontal tectonic regime in the Archaean of Greenland and its implications for early crustal thickening - a reply. Precambrian Res., 2, 400-404.

Moorbath S., Welke H., and Gale N. H. (1969) The significance of lead isotope studies in ancient, high-grade, metamorphic basement complexes, as exemplified by the Lewisian rocks of Northwest Scotland. Earth Planet. Sci. Letters, 6, 245-

Moorbath S., O'Nions R. K., Pankhurst R. J., Gale N. H., and McGregor V. R. (1972) Further rubidium-strontium age determinations of very early Precambrian rocks of the Godthaab District, West Greenland. Nature, Phys. Sci., 240, 78-82.

Naylor R. S., Steiger R. H., and Wasserburg G. J. (1970) U-Th-Pb and Rb-Sr systematics in 2700 x 10^6 year old plutons from the southern Wind River Range, Wyoming. Geochim. Cosmochim. Acta, 34, 1133-1159.

Oversby V. M. and Ringwood A. E. (1971) Time of formation of the earth's core. Nature, 234, 463-465.

Pankhurst R. J.,Moorbath S., and McGregor V. R. (1973a) Late event in the geological evolution of the Godthaab District, West Greenland. Nature, Phys. Sci., 243, 24-27.

Pankhurst R. J., Moorbath S., Rex D. C., and Turner G. (1973b) Mineral age patterns in ca. 3700 m.y. old rocks from West Greenland. Earth Planet. Sci. Letters, 20, 157-170.

Papanastassiou D. A. and Wasserburg G. J. (1975) Rb-Sr study of a lunar dunite and evidence for early lunar differentiates. Geochim. Cosmochim. Acta, Suppl. 6, 1467-1490.

Papanastassiou D. A. and Wasserburg G. J. (1976) Early lunar differentiates and lunar initial $^{87}Sr/^{86}Sr$ (abstract). In Lunar Science VII, p. 665-667. The Lunar Science Institute, Houston, Texas.

Patterson C. (1956) Age of meteorites and the earth. Geochim. Cosmochim. Acta, 10, 230-237.

Pidgeon R. T. and Hopgood A. M. (1975) Geochronology of Archaean gneisses and tonalites from north of Frederikshabs isblink. S. W. Greenland. Geochim. Cosmochim. Acta. 39, 1333-1346.

Podosek F. A. (1970) Dating of meteorites by high-temperature release of iodine-correlated Xe^{129}. Geochim. Cosmochim. Acta, 34, 341-365.

Rosholt J. N., Zartman R. E., and Knomo I. T. (1973) Lead isotope systematics and uranium depletion in the Granite Mountains, Wyoming. Geol. Soc. Amer. Bull., 84, 989-1002.

Sanz H. G., Burnett D. S., and Wasserburg G. J. (1970) A precise $^{87}Rb/^{87}Sr$ age and initial $^{87}Sr/^{86}Sr$ for the Colomera iron meteorite. Geochim. Cosmochim. Acta, 34, 1227-1239.

Sinha A. K. and Tilton G. R. (1973) Isotopic evolution of common lead. Geochim. Cosmochim. Acta, 37, 1823-1849.

Stacey J. S., Delevaux M. H., and Ulrych T. J. (1969) Some triple filament lead ratio measurements and absolute growth curve for single stage leads. Earth Planet. Sci. Letters, 6, 16-25.

Stacey J. S. and Kramers J. D. (1975) Approximation of terrestrial lead isotope evolution by a two-stage model. Earth Planet. Sci. Letters, 26, 207-221.

Tatsumoto M., Knight R. J., and Allegre C. J. (1973) Time differences in the formation of meteorites as determined from the ratio of lead 207 to lead 206. Science, 180, 1279-1283.

Tera F. and Wasserburg G. J. (1972a) U-Th-Pb analyses of soil from the Sea of Fertility. Earth Planet. Sci. Letters, 13, 457-466.

Tera F. and Wasserburg G. J. (1972b) U-Th-Pb systematics in lunar highland samples from the Luna 20 and Apollo 16 missions. Earth Planet. Sci. Letters, 17, 36-51.

Tera F. and Wasserburg G. J. (1974) U-Th-Pb systematics on lunar rocks and inferences about lunar evolution and the age of the moon. Goechim. Cosmochim. Acta, Suppl. 5, 1971-1599.

Tera F. and Wasserburg G. J. (1975) Precise isotopic analysis of lead in picomole and subpicomole quantities. Anal. Chem., 47, 2214-2220.

Tilton G. R. and Steiger R. H. (1965) Lead isotopes and the age of the earth. Science 150, 1805-1807.

Figure 1:

Pb evolution diagram, $^{207}Pb/^{204}Pb$ versus $^{206}Pb/^{204}Pb$, showing initial leads from a wide variety of rocks. The isotopic composition of the leads was determined by analyzing feldspars, galenas, and whole-rock samples of modern rock. The Amîtsoq Gneiss initial Pb as determined from the analysis of Pb in feldspars is shown. The extremely primitive nature of this Pb as compared to all other known terrestrial Pb samples is apparent as is the highly evolved nature of the Pb as compared to primordial Pb ($\alpha_{PAT}, \beta_{PAT}$).

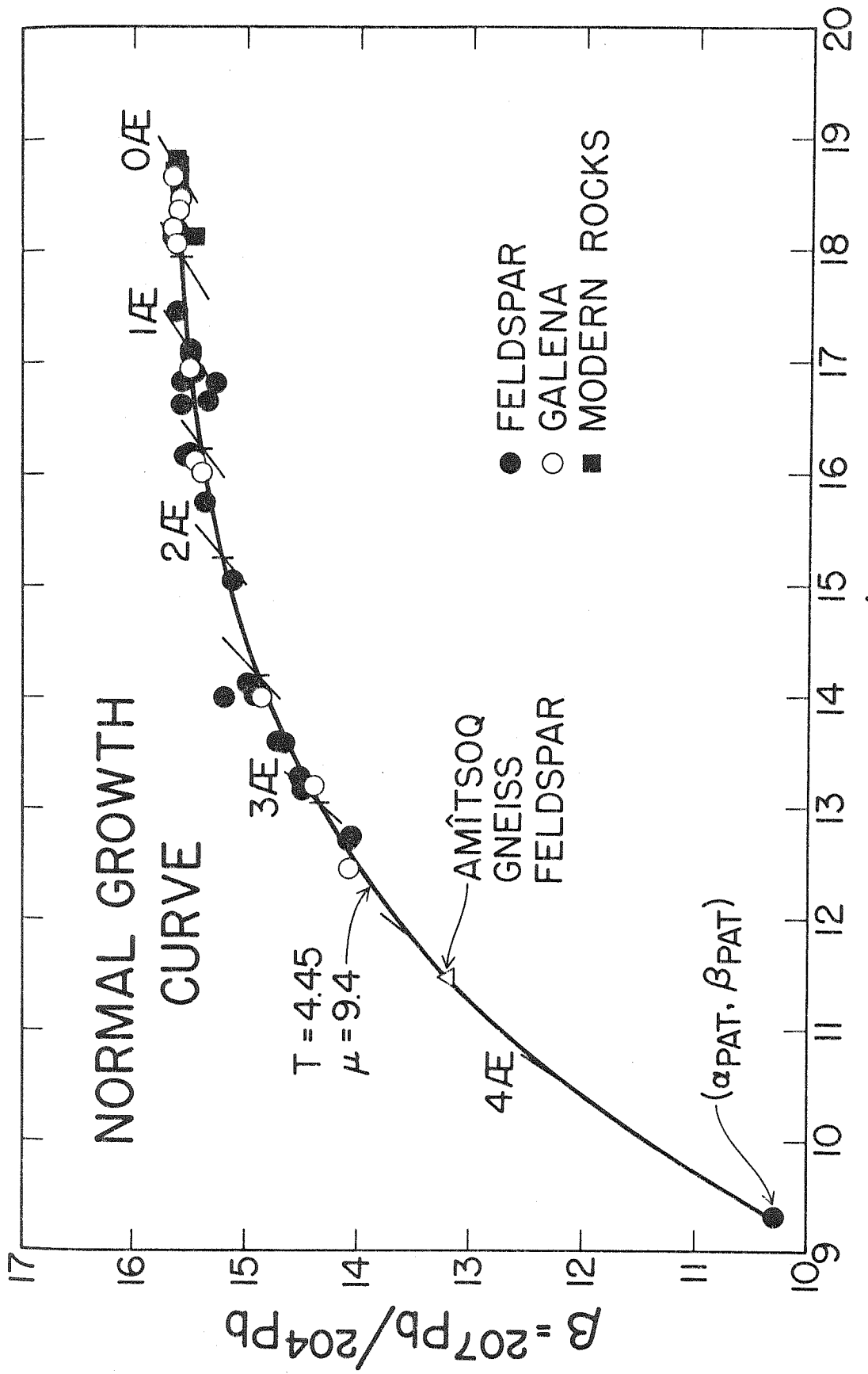
NORMAL GROWTH CURVE
0Æ
1Æ
2Æ
3Æ
4Æ
T = 4.45
μ = 9.4
AMÎTSOQ GNEISS FELDSPAR
(αPAT, βPAT)
FELDSPAR
GALENA
MODERN ROCKS
β = 207Pb/204Pb
α = 206Pb/204Pb
17
16
15
14
13
12
11
10
9
10
11
12
13
14
15
16
17
18
19
20

Figure 2:

Sketch map of the area south of Godthaab where the samples used in this study were collected.

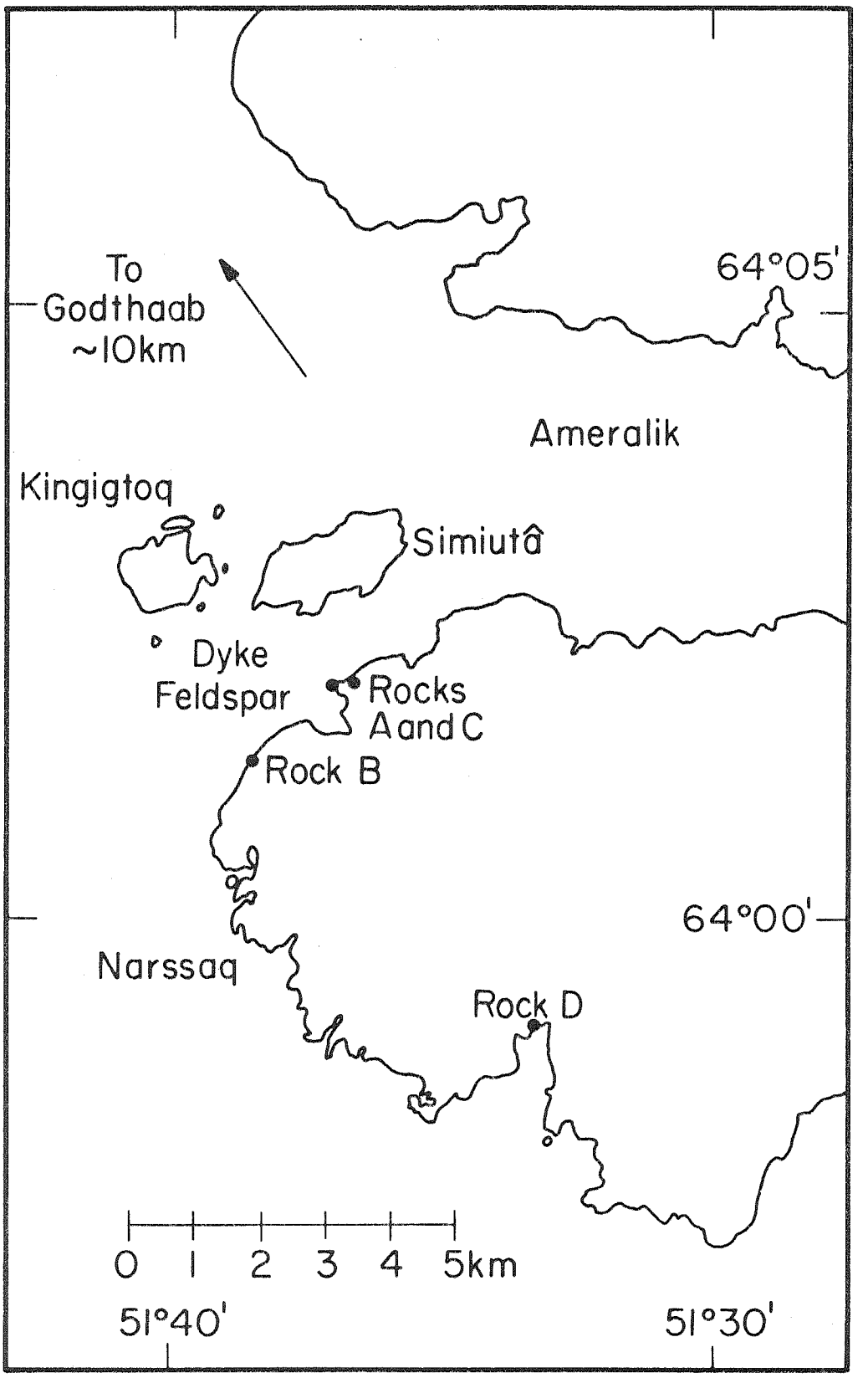
To
Godthaab
~10km
64°05'
Ameralik
Kingigtoq
Simiutâ
Dyke
Feldspar
Rocks
A and C
Rock B
64°00'
Narssaq
Rock D
0 1 2 3 4 5km
51°40'
51°30'

Figure 3:

Major element composition of the potassium feldspar samples which were analyzed for U and Pb.

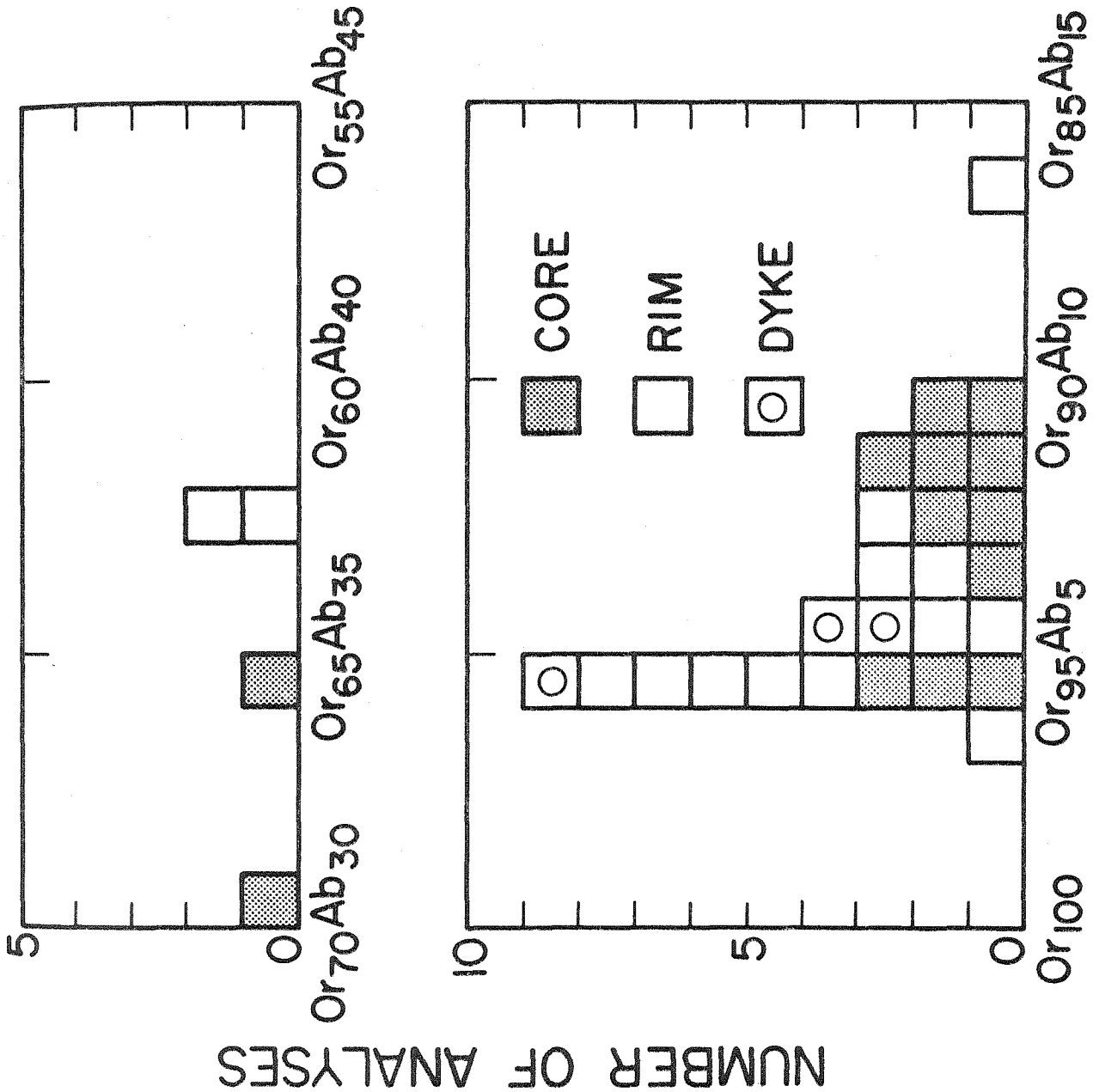
NUMBER OF ANALYSES
10
5
0
5
0
CORE
RIM
DYKE
Or100
Or95Ab5
Or90Ab10
Or85Ab15
Or70Ab30
Or65Ab35
Or60Ab40
Or55Ab45

Figure 4: Pb isotopic data on the Amîtsoq Gneiss Feldspar.

The open polygons are the Pb isotopic data on feldspar separated from the Amîtsoq Gneiss. The data have been corrected for laboratory contamination and mass discrimination. The size of the polygons reflects both mass-spectrometric error and mass-discrimination error. The numbers in the polygons correspond to numbered data in table 3. Analyses 10 and 11 are the residue points for the leaching experiment on Rock A-core 2, and analysis 12 is the residue point for the leaching experiment on Rock B-core. The patterned polygons on the data corrected for in situ U decay for 3.59 AE. The solid polygons are the residue points corrected for in situ U decay for 3.59 AE for the amount of U in the residues.

The isochrons shown on the figure for T = 4.40 AE, 4.45 AE and 4.50 AE are constructed assuming T = 3.59 AE and $\beta/\alpha)_{PAT}$=1.1060 and $1/\alpha)_{PAT}$ = 0.10745. The best estimate of T from the data corrected for in situ U decay is 4.47 ± 0.05 AE. The corresponding μ in the interval is 8.5.

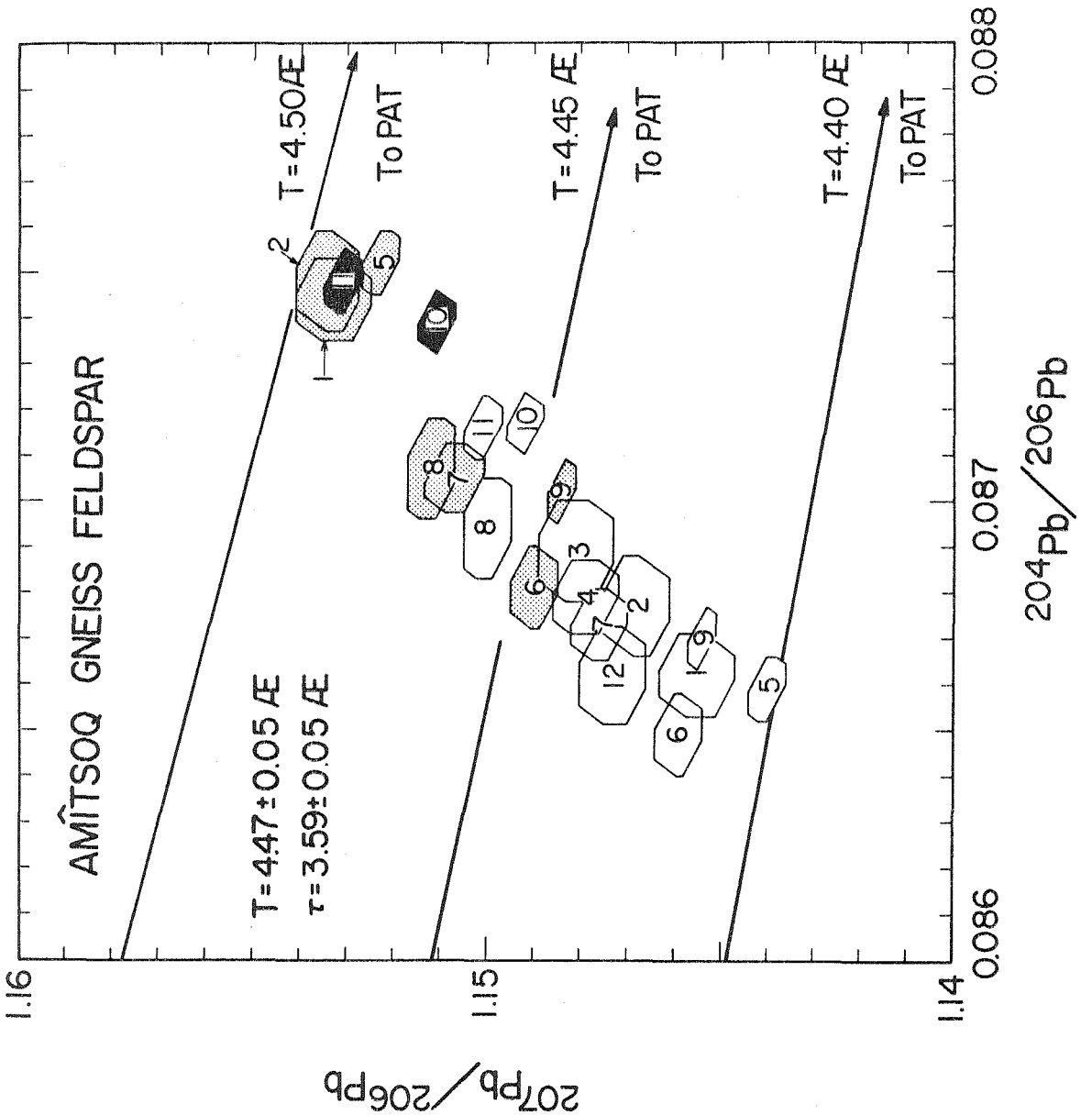
AMÎTSOQ GNEISS FELDSPAR
T=4.47±0.05 AE
τ=3.59±0.05 AE
T=4.50 AE
To PAT
T=4.45 AE
To PAT
T=4.40 AE
To PAT
1.16
1.15
1.14
0.086
0.087
0.088
207Pb/206Pb
204Pb/206Pb

Figure 5:

β/α versus $1/\alpha$ diagram showing data for the Amîtsoq Gneiss potassium feldspar leaching experiments. The symbols are ⊙ for Rock A-core 2; ◊ Rock A-core 2 repeat and ⬡ Rock B-core. The leaches are all enriched in radiogenic Pb relative to the total samples and to the residue samples. The data define a linear array corresponding to T = 2.7 AE. Deviations of the data from the line are shown on the inset where Θ is the fractional deviation of $^{204}Pb/^{206}Pb$ from the line in parts in 10^3.

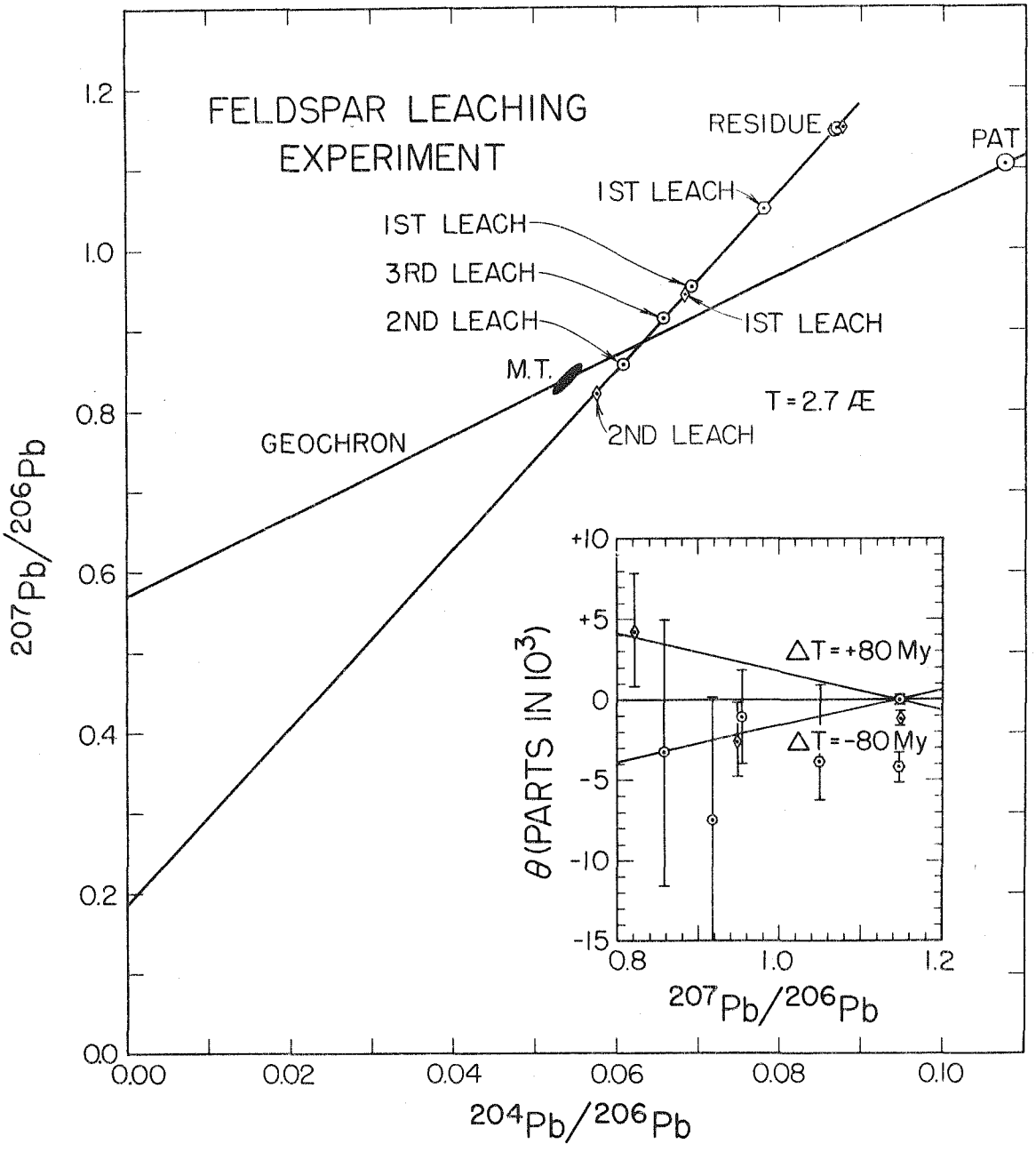
FELDSPAR LEACHING
EXPERIMENT
RESIDUE
PAT
1ST LEACH
1ST LEACH
3RD LEACH
2ND LEACH
1ST LEACH
M.T.
T = 2.7 Æ
GEOCHRON
2ND LEACH
ΔT = +80 My
ΔT = -80 My
θ (PARTS IN 10³)
207Pb/206Pb
204Pb/206Pb
0.0
0.2
0.4
0.6
0.8
1.0
1.2
0.00
0.02
0.04
0.06
0.08
0.10
+10
+5
0
-5
-10
-15
0.8
1.0
1.2

Figure 6: Pb isotopic data on rock associated with the Amîtsoq Gneiss feldspar samples.

The Pb in the biotite-rich chips of Amîtsoq Gneiss surrounding the feldspar and in the feldspar from the dyke cutting across the Amîtsoq Gneiss has very different isotopic compositions from that in the feldspar. These types of Pb are possible contaminants and could account for the small dispersion in the Amîtsoq Gneiss feldspar data. The biotite-rich chip samples lie distinctly of the 3.6 AE reference isochron indicating the open-system behavior of these samples subsequent to 3.6 AE.

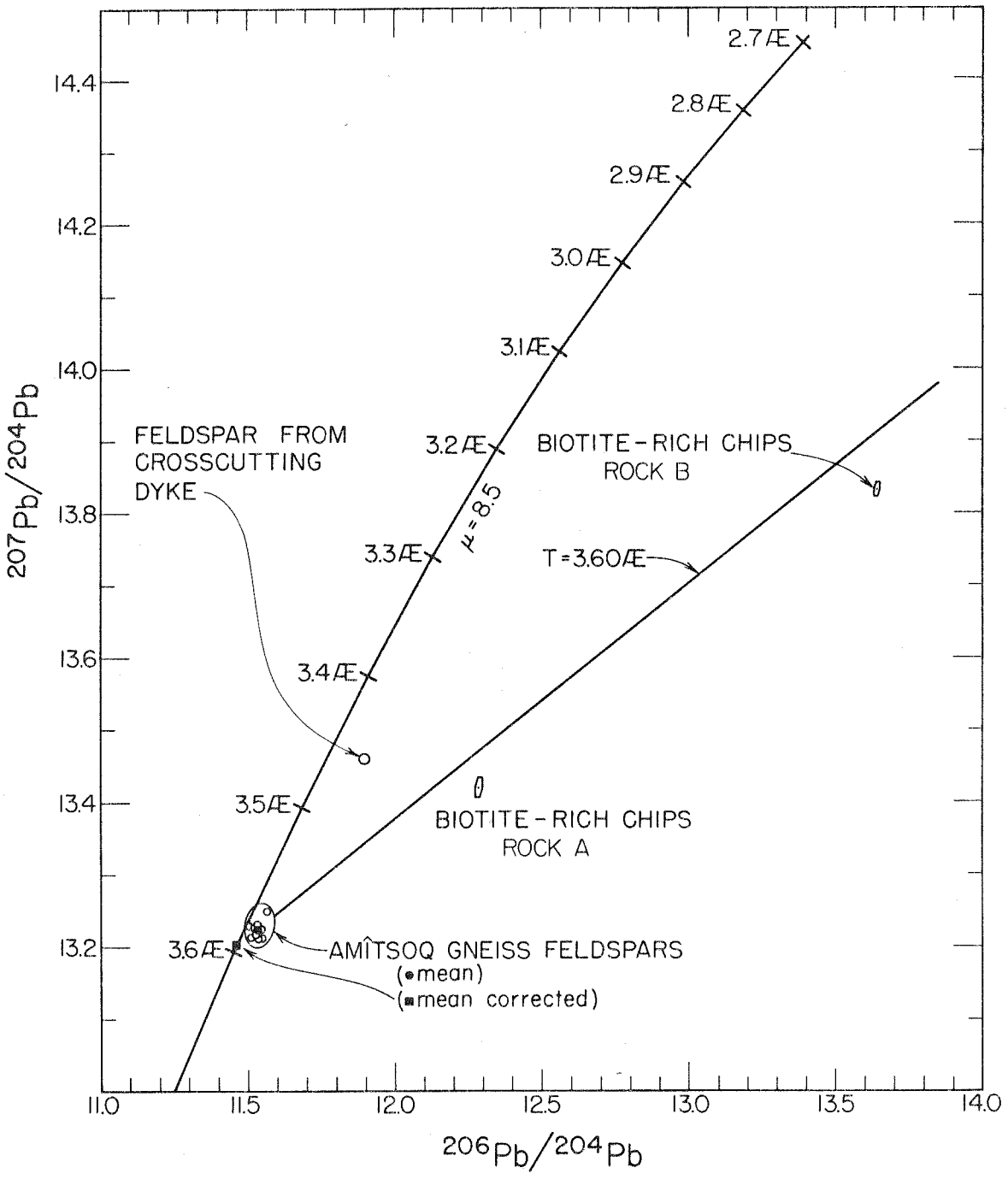
2.7Æ
2.8Æ
2.9Æ
3.0Æ
3.1Æ
3.2Æ
3.3Æ
3.4Æ
3.5Æ
3.6Æ
μ=8.5
T=3.60Æ
FELDSPAR FROM CROSSCUTTING DYKE
BIOTITE-RICH CHIPS ROCK B
BIOTITE-RICH CHIPS ROCK A
AMÎTSOQ GNEISS FELDSPARS
(•mean)
(▪mean corrected)
14.4
14.2
14.0
13.8
13.6
13.4
13.2
11.0
11.5
12.0
12.5
13.0
13.5
14.0
207Pb/204Pb
206Pb/204Pb

Figure 7:

Figure 7A is a plot of the time of accretion (T_A) versus the time of differentiation (T_D) which is the solution to the two-stage Pb evolution model. Stage 1 is from T_A to T_D and stage 2 is from T_D to today. The model is constrained so that the initial Pb in the Amîtsoq Gneiss and modern terrestrial Pb be derived from source rocks U equivalent for all of stage 2. This constraint also defines the age of the initial Pb in the Amîtsoq Gneiss assuming a zero age for modern terrestrial Pb. For the time of accretion of the earth ~4.55 to 4.65 AE, T_D is well-defined at ~4.37 AE.

Figure 7B is a plot of μ during stage 1, μ_1, versus T_D. For T_D ~4.37 AE, μ_1 is ~2. Thus μ changes at T_D by about a factor of 5. This change in μ requires either extensive loss of Pb in the source materials of subsequently derived rocks and/or enrichment of U in these source materials.

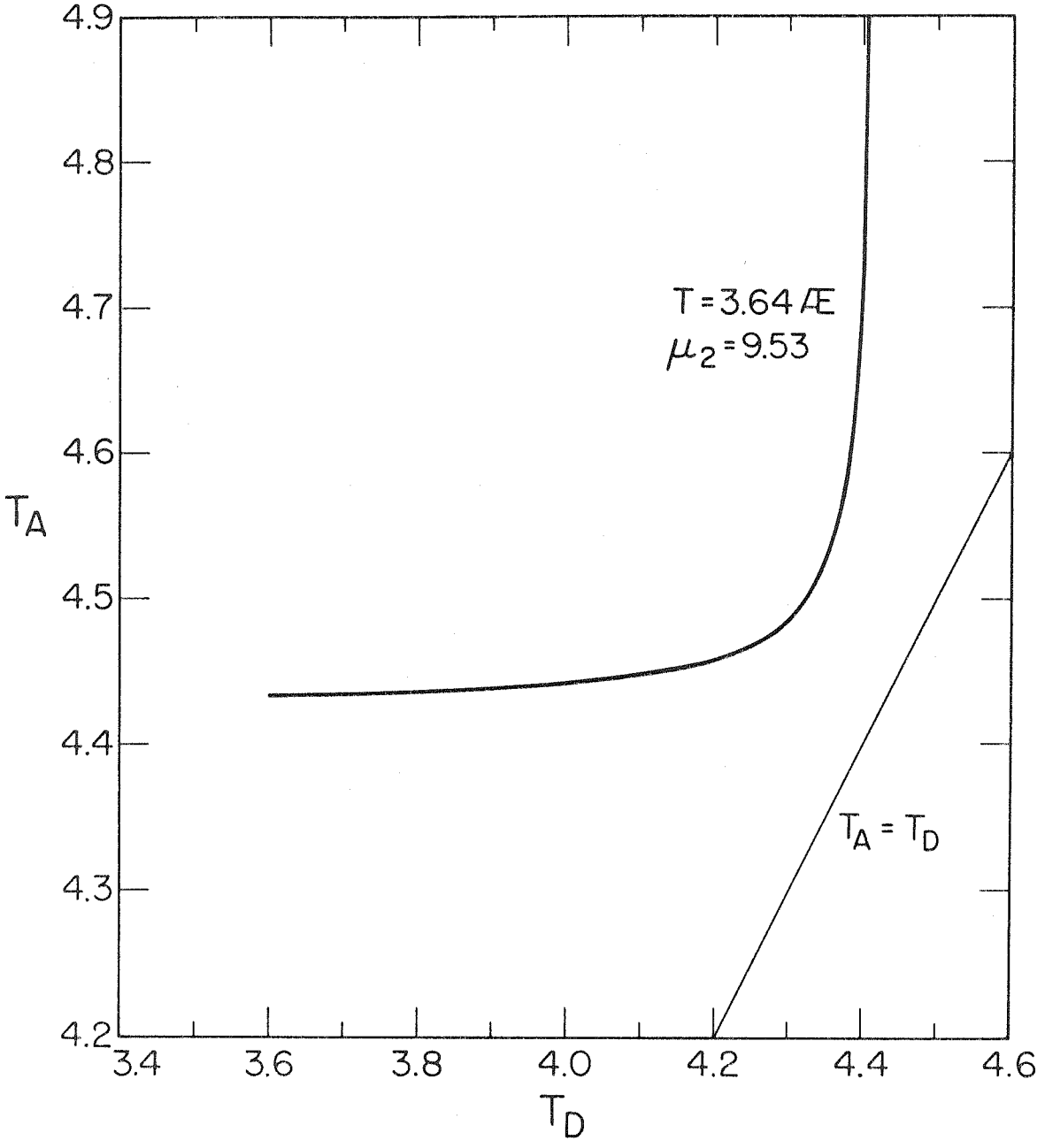
4.9
4.8
4.7
4.6
4.5
4.4
4.3
4.2
T_A
3.4
3.6
3.8
4.0
4.2
4.4
4.6
T_D
T = 3.64 Æ
μ_2 = 9.53
$T_A = T_D$

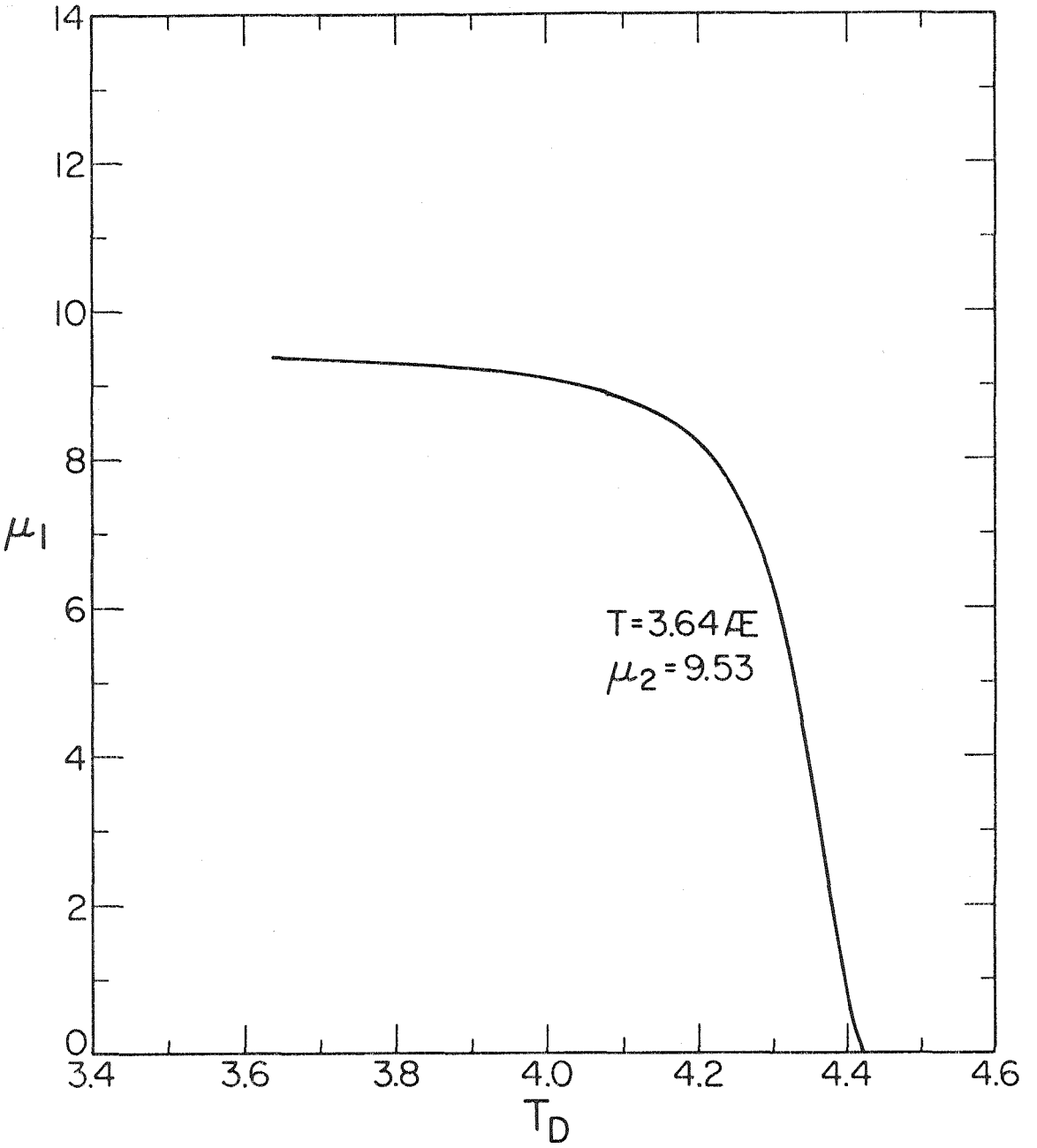
14
12
10
8
6
4
2
0
μ_1
T=3.64 Æ
μ_2=9.53
3.4
3.6
3.8
4.0
4.2
4.4
4.6
T_D

Table 1

FRACTIONATION FACTORS FOR C.I.T. STANDARD*

$^{207}Pb/^{208}Pb$	$^{206}Pb/^{208}Pb$	$^{204}Pb/^{208}Pb$
-1.1 ± 0.6	-1.2 ± 0.3	-0.9 ± 0.3
-1.4 ± 0.6	-1.5 ± 0.2	-1.3 ± 0.4
-0.9 ± 0.6	-0.9 ± 0.3	-0.7 ± 0.3
-1.1 ± 0.6	-1.1 ± 0.2	-1.0 ± 0.3
-2.2 ± 0.7	-1.3 ± 0.2	-0.8 ± 0.3

$$*\text{fractionation factor} = \left[\left(\frac{R_a}{R_m} - 1\right) \times 1000\right] / \Delta m$$

R_a = absolute ratio

R_m = measured ratio

Δm = mass difference

Table 2: U-Th-Pb Data

	$^{204}Pb/^{206}Pb$	$^{207}Pb/^{206}Pb$	$^{208}Pb/^{206}Pb$	^{206}Pb pm/mg	^{238}U pm/mg	^{232}Th pm/mg	sample weight mg	^{206}Pb blank pm
Rock A (Sample OGG 128)								
1 core #1 (OGG 128,6)	0.08662±5	1.1455±6	2.7237±7	48.43±0.08	0.604±0.004	-	29.9	6.0
2 core #2 (OGG 128,7A)	0.08677±7	1.1468±5	2.7289±20	48.16±0.09	0.528±0.006	-	29.4	1.3
3 core #2 (OGG 128,7B)	0.08689±7	1.1481±6	2.7275±10	48.78±0.10	-	-	12.5	1.2
4 Repeat	0.08679±4	1.1479±5	2.7273±6	-	-	-	-	-
5 core #3 (OGG 128,9A)	0.08659±3	1.1440±2	2.7219±5	49.42±0.07	0.704±0.005	-	41.7	1.6
Biotite-rich margin (OGG 128,10)	0.08138±8	1.0921±3	2.5878±40	12.19±0.01	1.219±0.008	-	158.6	4.4
Rock B (Sample OGG 225)								
6 core (OGG 225,3)	0.08649±6	1.1459±3	2.7193±6	33.76±0.05	0.167±0.001	-	46.0	1.0
7 rim (OGG 225,1)	0.08673±4	1.1476±4	2.7251±7	29.05±0.04	0.146±0.002	-	39.1	0.9
Biotite-rich margin (OGG 225,5)	0.07332±5	1.0142±2	2.3679±4	19.28±0.03	4.87±0.02	-	100.8	1.0
Rock C (Sample OGG 129)								
8 most deformed feldspar (OGG 129,1)	0.08694±7	1.1500±3	2.7308±5	52.75±0.07	0.103±0.002	1.05±0.01	67.8	0.8
Rock D (Sample OGG 233)								
9 plagioclase (OGG 233,1)	0.08670±3	1.1454±1	2.7269±3	11.74±0.01	0.057±0.01		59.6	0.8
Potassium feldspar crosscutting dyke (Sample OGG 134,1)								
leach	0.05121±5	0.7491±3	1.7015±5	0.806±0.001			-	0.4
residue	0.08456±4	1.1373±2	2.6858±3	52.70±0.06	0.098±0.001			0.8
total	0.08406±14	1.1315±19	2.6710±43	53.51±0.06			64.7	

Table 3:

Amîtsoq Gneiss Feldspar Data

	$^{206}Pb/^{204}Pb$	$^{207}Pb/^{204}Pb$	$^{208}Pb/^{204}Pb$
Rock A (Sample OGG 128)			
1 core #1 (OGG 128,6)	11.545±7*	13.224±8	31.444±20
2 core #2 (OGG 128,7A)	11.525±9	13.217±9	31.450±34
3 core #2 (OGG 128,7B)	11.509±9	13.213±11	31.390±28
4 repeat	11.522±5	13.226±8	31.424±16
5 core #3 (OGG 128,9A)	11.549±4	13.212±5	31.434±12
Rock B (Sample OGG 225)			
6 core (OGG 225,3)	11.562±8	13.249±6	31.441±23
7 rim (OGG 225,1)	11.530±5	13.232±6	31.421±17
Rock C (Sample OGG 129)			
8 most deformed feldspar (OGG 129,1)	11.502±9	13.228±11	31.410±26
Rock D (Sample OGG 233)			
9 plagioclase (OGG 233,1)	11.534±4	13.211±4	31.452±11
mean $\pm 2\sigma$ mean	11.531±13	13.224±8	31.439±14

*2σ errors; not included within the quoted error limits are errors due to uncertainty in the mass discrimination factor.

Table 4:

Amîtsoq Gneiss Feldspar Leaching Data

Rock A - core 2[a]	$^{204}Pb/^{206}Pb$	$^{207}Pb/^{206}Pb$	^{206}Pb/pm/mg	^{238}U pm/mg
1st leach	0.06943±20	0.9539±10	0.481±0.002	-
2nd leach	0.06065±50	0.8582±15	0.210±0.001	-
3rd leach	0.06546±50	0.9146±24	0.161±0.001	-
Residue	0.08717±3	1.1492±2	47.62[c]	0.161±1
Total	-	-	48.47[d]	0.528[d]
Rock A - core 2 repeat				
1st leach	0.06853±16	0.9450±12	0.449±0.002	0.0660±0.0004
2nd leach	0.05783±20	0.8220±10[b]	0.412±0.002	0.278±0.002
Residue	0.08716±3	1.1501±2	47.61[c]	0.238±0.002
Total	-	-	48.47[d]	0.582
Rock B - core				
1st leach	0.07792±40	1.0508±25	0.0134±0.0002	0.0037±0.0001
2nd leach				
Residue	.08663±8	1.1473±5		
Total	-	-	33.76[d]	0.167[d]

[a] Four leaches were done on this sample. The fourth leach was with boiling concentrated HNO_3 for 1 hour. The isotopic composition is quite different from points along the linear array defined by all the other leach data and suggests that the leachate was contaminated within the laboratory. The repeat experiment of boiling in concentrated HNO_3 resulted in Pb which lies along the linear array (see 2nd leach Rock A - core 2 - Repeat).

[b] $^{208}Pb/^{204}Pb = 37.32$ versus 31.41 is the residue

[c] Calculated from average Pb concentrations in table 2 and measured concentrations in leaches

[d] Measured - see table 2.

Part I: Section 2

2.8 AE Old Anorthosites from West Greenland

2.1 Introduction

The characterization of the magma from which anorthosite and anorthositic rocks crystallize and of the nature of the source rocks from which these silicate melts are derived remains an unsolved petrologic problem, although hypotheses are numerous and varied. This characterization has received renewed attention (c.f. Windley, 1970) following suggestions inferred from data on lunar rock samples that anorthosite is a major rock type produced during early planetary differentiation (Wood et al., 1970). Consequently, the extensive separation of plagioclase is critical in establishing geochemical signatures of crustal and mantle rocks formed during this differentiation.

Anorthosite and associated rocks are widespread throughout old Precambrian cratons. Although their total volume is not large, their ubiquity suggests that they are fundamentally related to the evolution of these early crustal blocks. One particular area where anorthositic rocks are common is in the Precambrian terrain of West Greenland from Fiskenaesset to Sukkertoppen. We report in this paper the results of our study of these anorthosites: determination of the crystallization and/or metamorphic ages, and determination of the initial Pb and Sr isotopic compositions, which in principle characterize the reservoirs from which the anorthositic magmas were derived.

2.2 Analytical Techniques

The methods of sample dissolution and chemical separation of U, Th, and Pb used in this study are those described by Tera and Wasserburg (1972a, b). The scheme of Tera and Wasserburg (1972 a,b)

is useful only for elements in common, rock-forming minerals. Therefore, a different technique was used for the extraction of Pb and U from the sample of molybdenite analyzed. The sample was attacked with boiling concentrated HNO_3. The resulting white precipitate was dissolved in aqua regia diluted with water so that the solution was ~1N. After aliquoting and spiking, the sample was dried and redried several times in the presence of excess HNO_3 to eliminate all Cl. The sample was mixed with 100 μl of 0.1N HNO_3, allowed to sit for 15 minutes, centrifuged, the supernate containing Pb and U removed and loaded onto an ion exchange column.

The ion exchange column (0.2Ø x 8 cm) was prepared by filling to a height of 2cm with cation exchange resin (AG 50W-X8), washing with 1 ml of H_2O to remove all HCl and conditioning with 500 μl of 0.1N HNO_3. The supernate was loaded onto the prepared column. Mo was eluted with 250 μl 0.5 N HNO_3 followed by elution of Pb with 150 μl 1.5 N HCl and finally U was eluted with 300 μl 4N HCl.

The Pb isotopic data reported in this paper are normalized to absolute values. We have repeatedly measured the isotopic composition of 10^{-9} mole of C.I.T. standard Pb. These data indicate a 1.1 ± 0.2 per mil per mass unit mass fractionation (Catanzaro, 1967). All the data reported here have been corrected using this discrimination factor.

2.3 Analytical Results

We have selected to study three anorthosite bodies which are 1) The Majorqap Qâva outcrop of the Fiskenaesset Anorthosite Complex,

located near Fiskenaesset, 2) the Storø Anorthosite Complex located in the Godthåbsfjord Area, and 3) the Ivnajaugtoq Anorthosite Complex also located in the Godthåbsfjord Area. One feature common to all of these bodies is the complex nature of their contacts with the country rocks. As a consequence, the relative time-stratigraphic position of these bodies is difficult to establish convincingly, as is their precise mode of emplacement.

Of the three complexes, the one at Fiskenaesset has been studied in the greatest detail (Windley et al. 1973; Windley and Smith, in press; Myers, 1973). The Majorqap Qâva outcrop covers approximately 40 km^2. The body is complexly folded and in contact with the gneiss and amphibolite of the Kangeq gneiss complex. Myers (personal communication 1973), has mapped this part of the anorthosite complex in great detail and established a stratigraphy consisting of a tripart layered series and an anorthosite unit. Within the layered series original igneous features are well preserved. These include undeformed cumulate textures and graded layering. The three units in the layered series are 1) the lower leucogabbro unit (20-40 m thick), 2) the gabbro unit (40-80 m thick), and 3) the upper leucogabbro unit (200-1000 m thick). The anorthosite unit occurs as a concordant sheet up to 600 m thick within the upper leucogabbro unit. Kalsbeek and Myers (1973) estimate from sand samples that approximately 85% by volume of the Majorqap Qâva outcrop is plagioclase.

We have analyzed minerals from three rocks from the Majorqap Qâva outcrop. Two samples are from the anorthosite unit and the third

sample is from the upper leucogabbro unit of the layered series. The two rocks from the anorthosite unit, Rocks A and B, are both true anorthosites. These two samples contain in excess of 97% plagioclase. In general, the plagioclase throughout the Fiskenaesset Anorthosite Complex occurs as equant grains (~1 to 2 mm in diameter) which form polygranular aggregates. In a few cases large, single crystals up to 7 cm in diameter are present. Characteristically these single crystals are zoned from dark grey at the center to light grey on the margin. The single crystals, cores, are surrounded by rims of very white, polygranular plagioclase. These cores are interpreted to be relict igneous megacrysts which have survived, unaffected by subsequent metamorphism. One of the interesting problems associated with the anorthosite complex is, was the recrystallization event temporally associated or quite discrete from the igneous crystallization of the body? Both plagioclase core and rim samples were analyzed to see if isotopic differences are preserved which bear on this question.

Rock A contained the largest plagioclase cores of all rocks which we observed in the Majorqap Qâva outcrop. The core plagioclase selected for analysis is about 7 cm in diameter and a piece of the dark grey center was removed and analyzed. For comparison with the core a sample of the recrystallized rim plagioclase was analyzed. This sample was prepared by crushing large pieces (~1 cm) of rim material to less than 250 μm and then handpicking plagioclase grains free of biotite flakes and metal smeared onto the grains during crushing.

Not only are there textural and color differences between the core and rim plagioclase, but there are also differences in the major element

chemical composition. Quantitative electron microprobe data on these core and rim samples from Rock A show the core composition to be $Ab_{13}An_{87}$ in contrast to the rim sample with the composition $Ab_{19}An_{81}$.

Disseminated throughout Rock A are large molybdenite crystals. To try to understand if this molybdenum mineralization was temporally associated with the igneous crystallization and/or recrystallization of of the anorthositic rocks a sample was analyzed. The sample was selected by splitting a piece of Rock A (~20 cm in diameter) and removing with tungsten tweezers large (~1 cm) molybdenite crystals from the freshly exposed surface of the rock.

Like Rock A, Rock B is also from the anorthosite unit. This rock was collected several km from Rock A, but because of the complex folding of the Majorqap Qâva outcrop its stratigraphic position relative to Rock A is uncertain. Rock B also contains plagioclase core crystals (~3 to 4 cm in diameter), but they are smaller than those in Rock A. Also in contrast to Rock A, where the recrystallized plagioclase is uniform in grain size, in Rock B surrounding the core is a zone of coarse-grained (2 to 3 mm) partially recrystallized plagioclase which grades into the finer-grained, more uniformly sized (1 to 2 mm) plagioclase. Samples of both this fine- and coarse-grained rim plagioclase were analyzed. The two samples were prepared by crushing chunks of material to +30 - 20 mesh and handpicking grains devoid of biotite, epidote, and smear metal. About 5% of Rock B is composed of 1 to 2 mm clots of biotite surrounded by epidote. The biotite and epidote associated with the fine-grained rim sample was analyzed.

The third sample, Rock C, was from the upper leucogabbro unit of the layered series. This rather unique rock is composed of masses about 10 to 15 cm in diameter of 99% pure plagioclase and of amoeboid masses about 10 cm in diameter of 99% pure hornblende. The plagioclase masses are generally composed of polygranular aggregates of plagioclase. However, at the center of some of the masses are single crystals (1 to 2 cm in diameter) of plagioclase. Samples of both core and rim plagioclase were analyzed as was a sample of the hornblende.

The Storø Anorthosite Complex located in Godthåbsfjord is the second body studied. The complex is a sheet of anorthosite which, in places, is heavily agmatized by Nûk Gneiss. Samples of the Nûk Gneiss which crop out approximately 5 km west of the anorthosite complex yield a Rb-Sr whole-rock age of 3.04 AE (Pankhurst et al., 1973). The anorthosite sample which we selected for analysis was from an area where the effects of agmatization appear minimal. The sample contains cores (~2 cm in diameter) of plagioclase with the composition Ab_{16} An_{84} surrounded by fine-grained rims of polygonalized aggregates of plagioclase with the composition Ab_{19} An_{81}. In addition to plagioclase, the sample contains approximately 5% hornblende which occurs in 1 to 2 cm clots. We have analyzed a sample of a single crystal core plagioclase and sample of the rim plagioclase. A core sample was also leached to see if there exists a labile Pb component added to the feldspar.

The third anorthosite body, samples from which we studied occurs at Ivnajaugtoq in Godthåbsfjord. The samples were collected from large

talus blocks and consequently, the structural and stratigraphic position of the samples is not known. The talus material, if representative of the whole body, indicates that this complex is composed of greater than ~90% plagioclase. Texturally these samples of anorthosite are quite different from those described from the Majorqap Qâva outcrop or the Storø Anorthosite complex. In contrast to the polygonalized grains which texturally characterize the anorthosite from these later two localities, the anorthosite samples from Ivnajaugtoq are characterized texturally by clear, subequant (to 5 mm), interlocking plagioclase grains. In Rock A, which is one of the two rocks studied from this complex, the plagioclase is uniform in composition which is $Ab_{17}An_{83}$. The other sample, Rock B, is similar to Rock A. Both of these samples are composed of ~95% plagioclase with about 5% of biotite plus hornblende. The plagioclase occurs as very pure (greater than 99%) aggregates approximately 10 cm in diameter surrounded by a zone about 1 cm thick of plagioclase + biotite + hornblende. The rocks also contain minor amounts of epidote and carbonate associated with fractures.

The U and Pb data for the samples from the three anorthosite bodies are presented in tables 1 and 2 and are shown on figure 1. The data for the Majorqap Qâva outcrop samples are also shown on figure 2.

In both Rocks A and C from Majorqap Qâva outcrop plagioclase core and rim samples were analyzed. In both cases the isotopic composition of the Pb in the core samples is less radiogenic than that in the rim samples. In Rock A α of the core is ~0.5% less than the rim and in Rock B α of the core is ~6% less than the rim. This relationship persists

in the plagioclase core and rim samples from the Storø Anorthosite Complex, where α of the core is ~4% less than in the rim. Although there are small differences in the Pb isotopic abundances in core and rim samples of plagioclase, in general the plagioclase is enriched in Pb relative to U and preserves Pb with primitive isotopic abundances. In contrast the samples of hornblende and epidote plus biotite contain very radiogenic Pb. The hornblende sample from Rock C from the Majorqap Qâva outcrop is extremely pure (greater than 99% hornblende) and contains much more radiogenic Pb than the sample of biotite and epidote rich material from Rock B which is composed of almost equal proportions of plagioclase and biotite plus epidote (see figure 2). The plagioclase and hornblende data define a linear array which yields an age of 2.75 ± 0.02 AE. The molybdenite sample from Rock A does not form part of this linear array and its temporal and petrogenetic relationships with the rock remain uncertain. The sample of biotite- and epidote-rich material from Rock B is almost, but not precisely, part of the array. We attribute this deviation to recent enrichment of U in this sample.

The colinearity of the minerals from the different rocks suggests that total rock samples are also part of the array. This is corroborated by Black et al. (1973). These workers analyzed Pb in whole-rock samples samples of the Anorthosite Complex on Qeqertarssuatsiaq near Fiskenaesset, which has been described by Windley et al. (1973) and Windley and Smith (in press). The petrologic similarity and spacial proximity of this complex with the Majorqap Qâva outcrop suggest that

that they are cogenetic. The samples analyzed by Black et al. (1973) lie along the line defined by the minerals analyzed by us from the Majorqap Qâva outcrop samples. Whether 2.75 AE, the time defined by the linear array, dates igneous crystallization, metamorphic recrystallization, or igneous crystallization and autometamorphism associated with the late stages of igneous crystallization is not specified by these isotopic data and remains an important question which we will subsequently address.

The U-Pb data for the Majorqap Qâva outcrop samples are in table 1. There does not appear to be any systematic relationship among these data and clearly indicates that the rocks have been open to U and/or Pb exchange. The generally systematic behavior of the Pb isotopic data suggest that the disparate behavior of the U-Pb data is a result of recent U redistribution. The magnitude of this redistribution is apparently quite different between different samples. In table 3 are presented K, U, and Th abundances determined from γ-ray data on Rocks A and C. The amount of U measured in the total sample of Rock C is the same as calculated from the isotope dilution abundance data for the minerals in Rock C (table 1), indicating that all the U in this sample is contained in the plagioclase and hornblende. However, the plagioclase appears to have lost between 75% and 85% of the U commensurate with the measured Pb isotopic composition and the age of 2.75 AE. The hornblende appears to have lost 25% of its U.

In Rock A the U in the molybdenite sample plus the U assumed to be in the plagioclase (i.e. ^{238}U not more than 0.1 pm ^{238}U/mg)

accounts for less than 20% of the U measured in a 2 kg sample of the rock (table 3). The only other phases in the rock are small amounts of hornblende, biotite, and epidote. These may contain substantial amounts of U as is observed in Rock B where epidote- and biotite-rich material appears from the comparison of the μ necessary to account for the Pb isotopic abundances with the μ measured to be enriched in U by about 500%. As we noted previously the Pb in the epidote and biotite mixture falls slightly off the 2.75 AE isochron. Assuming that they were previously part of the array and that the divergence is due to the five fold increase in U abundance, we calculate that the U redistribution occurred ca. 100 m.y. ago.

The Storø Anorthosite Complex data are shown on figure 1. Like the Majorqap Qâva outcrop samples plagioclase cores contain less radiogenic Pb than the rim plagioclase. We have only measured feldspar samples from this complex and the difference in isotopic compositions of only 3% in α is not sufficient to precisely determine an age. The data, however, suggest the same age as the Majorqap Qâva outcrop which is 2.75 AE. Similarly, for the Ivnajaugtoq Anorthosite Complex samples, the differences in Pb isotopic composition between the samples is not large enough to determine an age, but the data are consistent with an age of circa 2.8 AE.

The most striking feature about the data on these three sets of anorthosite samples is that they have extremely different initial Pb isotopic abundances. As is shown on figure 1, and assuming the Ivnajaugtoq Anorthosite Complex is indeed 2.8 AE old, the three

isochrons are offset from one another. Therefore, the differences in initial Pb isotopic composition exist regardless of whether the initial Pb is that in the feldspar samples with the least radiogenic Pb or is less radiogenic. From these observations on the initial Pb, these anorthosite complexes cannot be cogenetic and represent pristine, uncontaminated samples of magma derived from the same rock reservoirs at ~2.8 AE. To invoke a cogenetic relationship between the anorthosites necessarily requires that they have multi-stage histories or have been variably contaminated with Pb at the time of their crystallization or recrystallization. We will discuss both of these possibilities and implications for the geochemical characteristics of the reservoirs from which the rocks were derived. We will also discuss the petrogenetic consequences assuming that the rocks are totally unrelated.

2.4 Recrystallization

There is abundant evidence that the single crystal cores of plagioclase were not in equilibrium with the polygranular rim material. The plagioclase grains composing the rim aggregates are clear grains, uniform in size, and exhibit well-developed 120° junctions, both indicative of approach to textural equilibrium. These aggregates are in direct contact with the large single crystals of plagioclase which frequently exhibit strain features manifest in undulatory extinction. This juxtaposition indicates disequilibrium. More compelling is the difference in chemical composition between core and rim material. The core samples of all rocks have a greater amount of anorthite component than the rim plagioclase. The lack of equilibrium is also

manifest in the oxygen isotopic measurements. δO^{18}SMOW of the core plagioclase from Rock A from the Majorqap Qâva outcrop is $+6.5 \pm 0.1$ and δO^{18} of the rim plagioclase is $+6.2 \pm 0.1$. In the sample from the Storø Anorthosite Complex δO^{18} of the feldspar core is $+6.6 \pm 0.1$ and the rim feldspar is 5.9 ± 0.1 (M. Daily, oral communication). These differences are larger than analytical uncertainties and are not due to differences in bulk chemical composition of the feldspar core and rim samples.

The feldspar core samples from the Majorqap Qâva Complex are part of the linear array defined by the Pb data on associated plagioclase rim and hornblende samples. Thus all these phases contain initial Pb of the same isotopic composition. Therefore, in contrast to the textural patterns, the bulk chemical data, and oxygen isotopic data, which indicate incomplete equilibrium between core and rim plagioclase, these data suggest total Pb isotopic equilibrium. This discrepancy could develop if the rocks partially recrystallized without complete core-rim equilibrium and the isotopic composition of the Pb in the rock did not evolve more than analytical error in the interval between crystallization and partial recrystallization. This can occur if the time interval is short or if μ of the rocks is low or both. Both Rocks A and C from Majorqap Qâva outcrop have from the mineral abundance data and the abundances of U and Pb given in tables 1 and 3 estimated μ values of about 6. With these values the time interval between crystallization and recrystallization is ~20 m.y. at 2.75 AE.

Windley and Smith (in press) recently suggested that the hornblende in the Fiskenaesset Anorthosite Complex is a primary igneous

phase, in contrast to the interpretation of hornblende in other anorthosite complexes as a product of uralitization (Carter and Silver, 1972; Boulanger, 1959) or of metamorphism (Subramaniam, 1956). In the Majorqap Qâva samples, there are no obvious reaction relationships between hornblende and olivine, hypersthene, and plagioclase. If the hornblende is primary then we interpret it to have formed at 2.75 AE. If it is secondary, then like the recrystallization of the plagioclase, it must have formed less than about 20 m.y. after the igneous crystallization of the complex.

2.5 Initial Pb of the Anorthosite Complexes.

As we noted previously the different anorthosite bodies have very different initial Pb isotopic compositions. Since the isochrons are offset these differences persist regardless of whether or not the initial Pb isotopic composition is known. Large differences in initial isotopic compositions are not restricted to Pb, but also appear to exist for Sr. Preliminary Sr data (table 4) show that feldspar from different anorthosite bodies are not part of a 2.8 AE linear array with the same initial Sr isotopic abundances. For the Majorqap Qâva feldspar the calculated $(^{87}Sr/^{86}Sr)_I$ at 2.8 AE is 0.70188±6 and for the Ivnajaugtoq feldspar the corresponding value is 0.70116±5.

In principle, since the U-Pb systematics are incoherent, it is not possible to determine the initial Pb of the anorthosite complexes. However, the feldspar is generally enriched in Pb relative to U and preserve a Pb with an isotopic composition close to the initial. To argue more cogently that the least radiogenic Pb in the feldspar samples

corrected for a small amount of in situ U decay is precisely the initial Pb requires additional experiments indicating the uniqueness of this Pb.

To see if a significant amount of either easily leachable in situ decay produced Pb or easily leachable extraneous contaminant Pb is mixed with the initial Pb in the feldspar a piece of the core feldspar from the Storø Anorthosite sample was crushed and leached. The data are given in tables 1 and 2. The leach lies along the ~2.8 AE isochron defined by the rim sample and untreated core sample, and is more radiogenic than the untreated core sample. Approximately 10% of the Pb was removed in the leaching process. The calculated shift in the Pb isotopic composition of the core Pb due to the leaching is approximately 0.5% for α. This is small but clearly resolvable, and is 50% of the shift in Pb isotopic composition for the in situ U decay correction on the untreated core sample. Although the leaching process removes radiogenic Pb and produces a shift in isotopic composition of the core Pb, the shift is relatively small and there does not appear to be Pb easily removable from the core samples which has significantly altered the intrinsic Pb isotopic composition.

Assuming that the least radiogenic Pb in the anorthosite samples is close to the true initial, then as is apparent on figure 1, there is a gross linear trend of these initial Pb's toward the initial Pb which we have identified for the Amîtsoq Gneiss. If the three anorthosite bodies are related, then these differences in initial Pb imply multi-stage histories or contamination histories.

To explain the trend by a multi-stage process requires that the magmatic materials from which the anorthosites formed were separated and fractionated from a common reservoir at ca. 3.6 AE, and evolved without element fractionation until 2.8 AE at which time they crystallized and recrystallized. The μ of the common reservoir at ~3.6 AE is ~8 to 9. The μ of the magmatic materials derived from this reservoir range from ~4 for the Storø Anorthosite to ~8 to 9 for the Majorqap Qâva Anorthosite. This history requires that these secondary magma reservoirs formed at ~3.6 AE are preserved and maintain their isotopic and element abundances for ~1 AE.

A possible evolutionary history resulting in the observed differences in the initial Pb isotopic composition of the anorthosites is primary generation of the anorthositic magmas at ~2.8 AE from normal (ca. $\mu = 9$) μ reservoirs and contaminating the magmas during emplacement. The Pb contaminating these magmas is like the Amîtsoq Gneiss initial Pb, which for reference is shown on figure 1. It is interesting to note that the Majorqap Qâva outcrop of the Fiskenaesset Anorthosite Complex and the outcrop of this complex at Qeqertarssuatsiaq which are over 100 km from the closest known outcrop of Amîtsoq Gneiss appear least contaminated whereas the most heavily contaminated body, the one on Storø is only a km from terrain composed predominantly of Amîtsoq Gneiss. There is of course the very formidable problem with this history in that it requires the assimilation of large amounts of relatively felsic material, the Amîtsoq Gneiss, by a relatively basic

silicate melt, the magma from which the anorthosites crystallized. Not only is this difficult thermodynamically, but also there is no field evidence of large partially reacted blocks of granitic material in the anorthosite bodies.

In both of these two cases for describing the formation of the trend observed for the initial Pb's, if either the magmas were formed at ~ 3.6 AE for the first case or if they were formed at 2.8 AE for the contamination case, the primary source reservoirs appear to have μ ranging from 8 to 9. These values are similar to, although as much as 15% less than, values normally considered to be those of the mantle. Consequently, the anorthosites appear to be derived from normal mantle material.

We cannot exclude the possibility that the anorthosite complexes are not related and the different initial Pb isotopic abundances record unique evolutionary histories. These histories must, however, indeed be quite distinct as is reflected in the single-stage model ages and corresponding μ values determined from the different initial Pb isotopic compositions. These values are as follows: 1) Majorqap Qâva outcrop T_{model} = 2.75 AE, μ = 8.2; 2) Ivnajaugtoq Anorthosite T_{model} = 3.0 AE, μ = 7.6 and 3) Storø Anorthosite T_{model} 2.97, μ = 5.4. The μ values for the later two complexes are much less than "normal" μ values and in general there is no evidence for the existence of such low μ source reservoirs.

Despite the variety of possible evolutionary schemes presented for these anorthosite complexes, there is no compelling evidence from these data to support the suggestion of Windley (1970) that they "are fragments

of (primordial?) layered differentiates formed early in the evolution of the earth" and that "both planetary bodies [the moon and the earth] went through parallel stages of development as far as the anorthosite event is concerned."

References

Black L. P., Moorbath S., Pankhurst R. J., and Windley B. F. (1973) $^{207}Pb/^{206}Pb$ whole rock age of the Archaean Granulite Facies Metamorphic Event in West Greenland. Nature, Phys. Sci. 244, 50-53.

Boulanger J. (1959) Les Anorthosites de Madagascar. Ann. Géol. Madagascar, xxvi.

Carter B. and Silver L. T. (1972) Structure and petrology of the San Gabriel Anorthosite, California, U.S.A. (abstract). Proc. 24th Intl. Geol. Congress, sect. 2, 303-311.

Catanzaro E. J. (1967) Absolute isotopic abundance ratios of three common lead reference samples. Earth Planet. Sci. Letters, 3, 343-346.

Kalsbeek F. and Myers J. S. (1973) The geology of the Fiskenaesset region. In: Progress report on the geology of the Fiskenaesset region, South-West Greenland, Geol. Survey Greenland Report 51, 6-18.

Myers J.S. (1973) Igneous structures and textures in the Majorqap Qâva outcrop of the Fiskenaesset Anorthosite Complex. In: Progress report on the geology of the Fiskenaesset region, South-West Greenland, Geol. Survey Greenland Report 51, 47-53.

Pankhurst R. J., Moorbath S., and McGregor V. R. (1973) Late event in the geological evolution of the Godthaab District, West Greenland. Nature, Phys. Sci., 243, 24-27.

Subramaniam A. P. (1956) Minerology and petrology of the Sittampundi Complex, Salem District, Madras State, India. Bull. Geol. Soc. Amer., 67, 317-390.

Tera F. and Wasserburg G. J. (1972a) U-Th-Pb analyses of soil from the Sea of Fertility. Earth Planet. Sci. Letters, 13, 457-466.

Tera F. and Wasserburg G. J. (1972b) U-Th-Pb systematics in lunar highland samples from the Luna 20 and Apollo 16 missions. Earth Planet. Sci. Letters, 17, 36-51.

Windley B. F. (1970) Anorthosites in the crust of the earth and on the moon. Nature, 226, 333-335.

Windley B. F., Herd R. K., and Bowden A. A. (1973) The Fiskenaesset Complex, West Greenland, Part I. A preliminary study of the stratigraphy, petrology, and whole rock chemistry from Qeqertarssuatsiaq. Meddelelser om Grønland, 196, 1-80.

Windley B. F. and Smith J. V. (in press) The Fiskenaesset Complex, West Greenland. Part 2, General mineral chemistry. Meddelelser om Grønland.

Wood J. A., Dickey J. S. Jr., Marvin U. B., and Powell B. N. (1970) Lunar anorthosites and a geophysical model of the moon. Geochim. Cosmochim. Acta, Suppl. 1, 965-988.

Figure 1. Pb isotopic data for minerals separated from Greenland anorthosite samples. The open circles are the measured values corrected for laboratory blank and mass discrimination. The filled circle is the Pb isotopic composition corrected for *in situ* U decay. The Majorqap Qâva anorthosite and Storø anorthosite have ages of 2.8 AE and the Ivnajaugtoq data are consistent with a ~2.8 AE age. The three isochrons are offset and, therefore, the complexes have distinctly different initial Pb isotopic abundances. There is a general trend for the initial Pb towards the initial Pb of the Amîtsoq Gneiss as is indicated on the figure by a solid square. If the complexes are cogenetic, these differences in initial Pb isotopic abundances indicate either multi-stage histories prior to ~2.8 AE or contamination of the individual anorthosite magmas at ~2.8 AE.

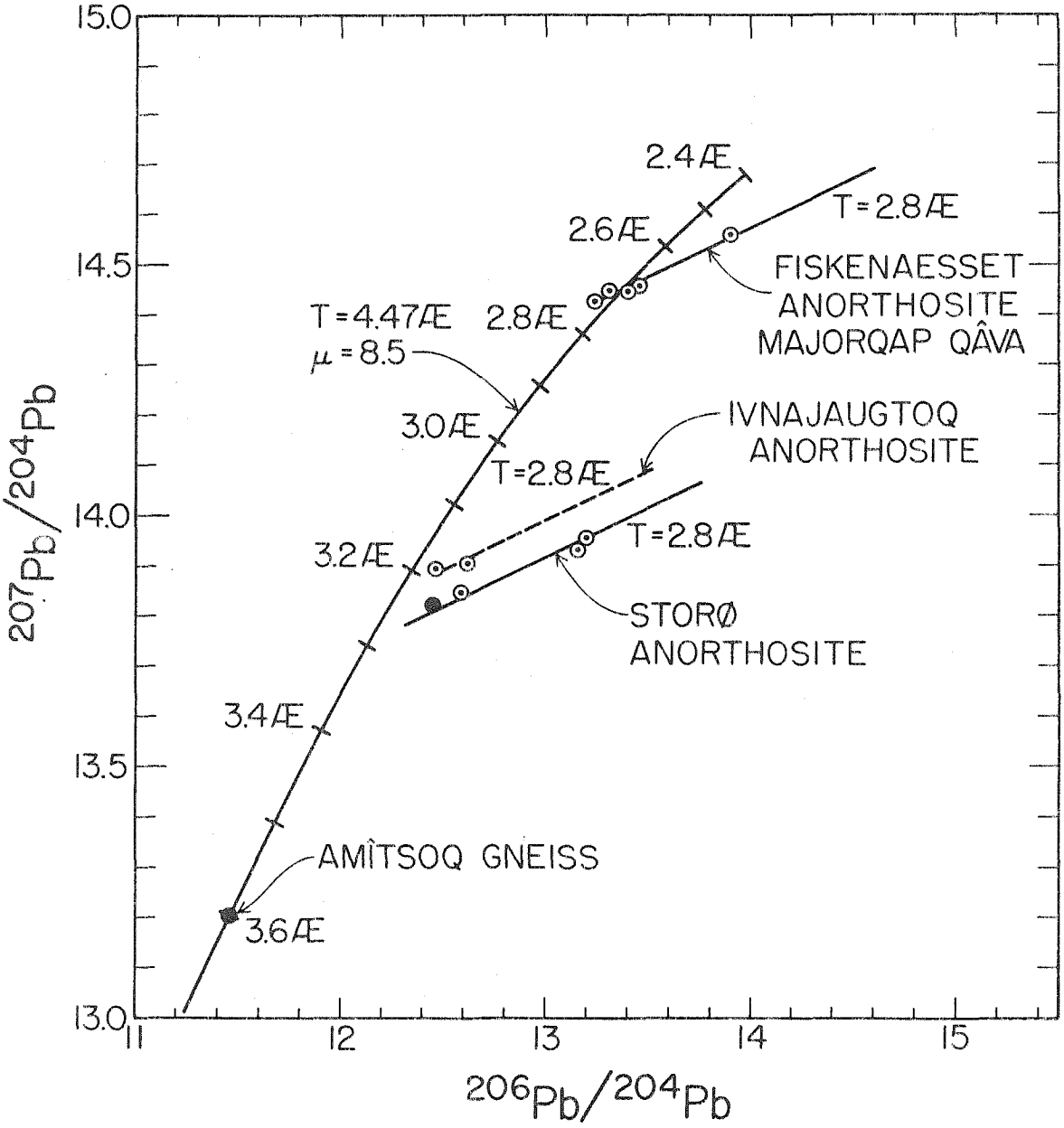
15.0
14.5
14.0
13.5
13.0
11
12
13
14
15
$^{207}Pb/^{204}Pb$
$^{206}Pb/^{204}Pb$
2.4Æ
2.6Æ
T=2.8Æ
FISKENAESSET
ANORTHOSITE
MAJORQAP QÂVA
T=4.47Æ
μ=8.5
2.8Æ
3.0Æ
IVNAJAUGTOQ
ANORTHOSITE
T=2.8Æ
3.2Æ
T=2.8Æ
STORØ
ANORTHOSITE
3.4Æ
AMÎTSOQ GNEISS
3.6Æ

Figure 2. Pb isotopic data for minerals from Majorqap Qâva anorthosite at Fiskenaesset. The samples of plagioclase and hornblende lie on a 2.75 AE isochron. The biotite plus epidote datum lies distinctly off the isochron. This shift is attributed to a factor of 5 enrichment of U in this sample ca. 100 m.y. age. The molybdenite datum also lies off the isochron and its petrologic and temporal relationship to the anorthosite remain uncertain. The inset shows deviations

$$\theta = \frac{\left(^{206}Pb/^{204}Pb\right)_{\text{Best fit}} - \left(^{206}Pb/^{204}Pb\right)}{\left(^{206}Pb/^{204}Pb\right)_{\text{Best fit}}}$$ measured in parts in 10^4.

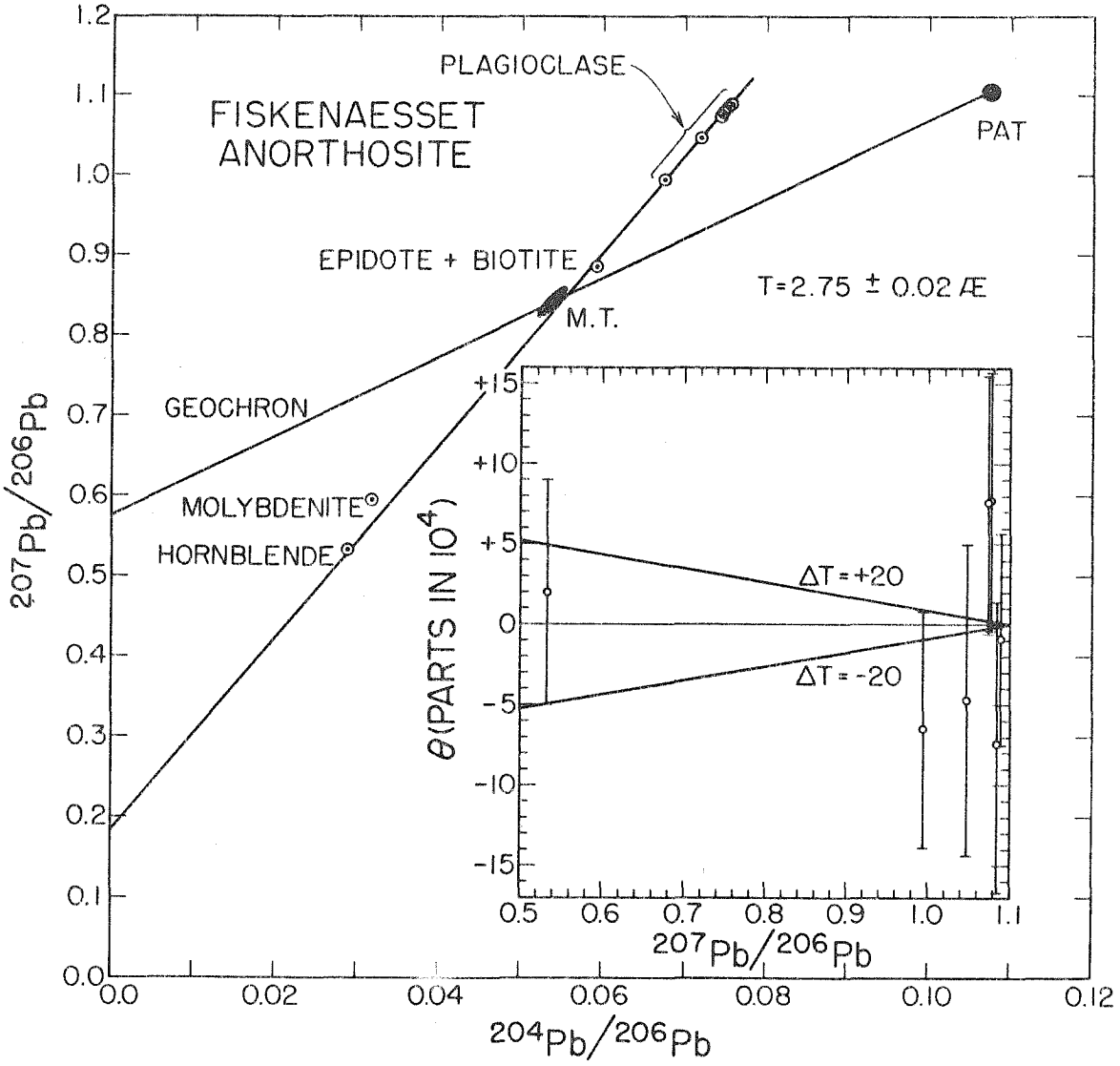
FISKENAESSET
ANORTHOSITE
PLAGIOCLASE
PAT
EPIDOTE + BIOTITE
M.T.
T=2.75 ± 0.02 Æ
GEOCHRON
MOLYBDENITE
HORNBLENDE
ΔT=+20
ΔT=-20
θ(PARTS IN 10⁴)
207Pb/206Pb
204Pb/206Pb

Table 1: U-Pb Data

		$^{204}Pb/^{206}Pb$	$^{207}Pb/^{206}Pb$	$^{208}Pb/^{206}Pb$	^{206}Pb pm/mg	^{238}U pm/mg	wt mg	blank pm
I Majorqap Qâva								
Rock A (OGG 215)								
plagioclase core	(,2)	0.07552±10	1.0893±7	2.490±1	5.72±1	--	155.1	6.5
plagioclase core	(,5)	0.07513±7	1.0852±6	2.475±1	7.54±2	--	154.8	6.0
molybdenite	(,9)	0.03177±20	0.5942±6	1.295±1	5.62±6	1.08±1	4.9	2.2
Rock B (OGG 210)								
plagioclase rim coarse	(,2)	0.07425±7	1.0733±5	2.543±1	4.75±1	0.074±1	178.9	3.5
plagioclase rim fine	(,3)	0.07460±3	1.0776±2	2.485±1	4.90±1		67.7	3.1
biotite + epidote	(,4)	0.05909±4	0.8857±4	2.256±1	5.49±1	10.65±6	123.7	3.4
Rock C (OGG 196)								
plagioclase core	(,2A)	0.07196±8	1.0458±8	2.445±1	1.042±4	0.0168±2	76.6	7.4
plagioclase rim	(,1A)	0.06746±5	0.9919±3	2.428±1	0.774±8	0.0411±6	67.5	7.4
hornblende	(,3A)	0.02869±3	0.5324±4	1.483±1	0.891±6	0.826±5	81.3	7.6
II Storø Anorthosite								
Rock A (OGG 74)								
plagioclase core	(,2)	0.07950±11	1.0998±14	2.574±2	9.74±3	0.192±2	41.4	3.9
plagioclase rim	(,5)	0.07600±3	1.0593±3	2.469±1	12.51±4	--	24.0	6.5
plagioclase core leach	(,6)	0.07556±3	1.0552±3	2.463±1	1.1±1**	--	54.8	1.0
III Ivnajaugtoq Anorthosite								
Rock A	(108)							
plagioclase	(,2)	0.08008±3	1.1127±4	2.593±1	2.9±3*	--	78.7	6.6
Rock B	(110)							
plagioclase	(,3)	0.07939±9	1.1032±6	2.580±1	3.4±3*	--	145.9	9.5

* from yield concentration

** conc. in leach per mg of sample

Table 2: Anorthosite Pb Data

		α	β	γ
I Majorqap Qâva				
Rock A (OGG 215)				
plagioclase core	(,2)	13.242±17	14.424±18	32.98±4
plagioclase rim	(,5)	13.310±13	14.444±13	32.94±3
molybdenite	(,9)	31.476±97	18.703±58	40.76±13
Rock B (OGG 210)				
plagioclase rim coarse	(,2)	13.469±13	14.456±13	34.25±3
plagioclase rim fine	(,3)	13.404±5	14.444±5	33.31±1
biotite + epidote	(,4)	16.922±11	14.988±7	38.18±2
Rock C (OGG 196)				
plagioclase core	(,2A)	13.897±13	14.534±14	33.98±3
plagioclase rim	(,1A)	14.823±11	14.703±11	35.98±3
hornblende	(,3A)	34.851±30	18.556±17	51.67±4
II Storø Anorthosite				
Rock A (OGG 74)				
plagioclase core	(,2)	12.578±18	13.834±19	32.37±3
plagioclase rim	(,5)	13.156±6	13.936±6	32.48±1
plagioclase core leach	(,6)	13.234±6	13.965±6	32.60±1
III Ivnajaugtoq Anorthosite				
Rock A (OGG 108)				
plagioclase	(,2)	12.488±5	13.895±5	32.38±1
Rock B (OGG 110)				
plagioclase	(,3)	12.597±13	13.896±6	32.50±3

Table 3: Majorqap Qâva Anorthosite Data

	Th pm/mg	U pm/mg	K nm/mg
Rock A (OGG 215)	4.7±0.9	2.5±0.5	61±12
Rock C (OGG 196)	0.66±0.13	0.32±0.06	46±9

Table 4: Rb-Sr Data

	Rb 10^{-8} m/g (a)	^{88}Sr 10^{-8} m/g (a)	$^{87}Rb/^{86}Sr$	$^{87}Sr/^{86}Sr$ (b)
Majorqap Qava				
Rock A plag. core (OGG 215,21)	4.98	102.6	0.113	.70630±6
Ivnajaugtoq				
Rock A plagioclase (OGG 108,11)	1.79	130.8	0.032	.70241±5

(a) Rb concentrations are calculated for $^{85}Rb/^{87}Rb = 2.591$, Sr concentrations are calculated assuming normal abundances $^{86}Sr/^{88}Sr = 0.1194$ and $^{84}Sr/^{88}Sr = 0.006748$.

(b) Errors correspond to the last figures given and represent $\pm 2\sigma$ mean.

Part I: Section 3

Project Oldstone

3.1 Introduction

Through the use of careful field work (McGregor, 1973) and corroborative isotopic investigations a suite of very ancient rocks (~3.7 AE old) were discovered in West Greenland. This discovery has been important in rejuvenating interest in older Precambrian rocks. The study of ancient rocks is critical to delimiting the time scale and physiochemical processes of large-scale differentiation early in the earth's history and of the growth of the earth's crust. The rocks found in West Greenland for two reasons are particularly valuable in deciphering this early evolution. First, they are ~0.5 AE older than any previously known terrestrial rocks and bridge for the first time the heretofore distinct time gap between ~3.3 AE and ~4.5 AE. Second, the rocks preserve very primitive isotopic characteristics.

Because of their importance and our interest in such rocks permission to go to Greenland and collect specimens of these and associated rocks was requested on June 6, 1972. Following protracted negotiations with the Ministry for Greenland and the Greenland Geological Survey, permission was finally granted on June 7, 1973. Expedition "Project Oldstone" under the aegis of California Institute of Technology and the National Science Foundation went to Greenland during the summer of 1973. Collection of the samples started on June 15 and continued to August 20. There were nine members of the expedition, seven of whom were from California Institute of Technology and were, Professors A. L. Albee and G. J. Wasserburg, graduate students R. F. Dymek and A. J. Gancarz, undergraduate student R. M. Kieckhefer, and two field assistants J. Albee and C. Wasserburg. There were also two Danish

members of the party who were responsible for navigation and maintenance of the 33-foot boat which housed and transported the expedition.

Through the cooperation of the Greenland Geological Survey (Grønlands Geologiske Undersøgelse), the expedition was frequently accompanied and assisted by members of the survey who have done extensive mapping in the area. Dr. V. R. McGregor, the geologist who first recognized the possibility of the very ancient rocks and Dr. David Bridgwater, director of the Greenland Geological Survey's study of the Precambrian rocks in West Greenland, both accompanied the expedition in the Godthaab District. Dr. McGregor also accompanied the group in the Nordland region and in the area around Tovqussap Nuna. In the Fiskenaesset region, the Greenland Geological Survey provided logistical and helicopter support to areas otherwise inaccessible. In this area we were accompanied by geologists Dr. Feiko Kalsbeek, and Dr. John Myers.

The majority of samples for isotopic studies were collected by drilling and blasting to insure fresh and unweathered as possible material. Drilling was done with a gasoline powered Atlas Cobra drill and blasting with ammonium nitrate plus a nitrated organic liquid detonated with commercial blasting caps. Generally, $\sim$1000 lb of material was blasted from the outcrop and $\sim$200 lbs of totally interior pieces were selected as the sample. These samples were and are stored in steel barrels especially coated with Pb free paint to insure minimal contamination.

A total of approximately 20 tons of rock samples were collected and are now at the California Institute of Technology. There are two groups of samples. One group of approximately 250 samples consists of material primarily for isotopic and corroborative studies. The second group consists of approximately 600 samples collected specifically for petrologic and electron microprobe studies. These include metasedimentary, metavolcanic and ultramafic rocks. The study of these materials is being done by R. F. Dymek under the supervision of professor A. L. Albee and further detailed information on these samples will not be presented.

The samples were collected from throughout the terrain between Fiskenaesset on the south and Sukkertoppen on the north. In general, the rocks in this region are comprised of quartzofeldspathic gneisses, anorthosite, anorthositic gabbro and associated mafic rock, metasedimentary and metavolcanic rock, and minor pods of ultramafic rock. All of the rocks have been very extensively deformed and have undergone multiple episodes of metamorphism ranging from amphibolite facies to granulite facies. The tectonic and metamorphic events have resulted in extremely complex structural and stratigraphic relations.

In the Godthaab District, which comprises the peninsula and islands east and south of Godthaab, McGregor (1973) has recognized distinct lithologic units. The oldest unit is the Amîtsoq Gneiss, the antiquity of which was first recognized by McGregor (1973) and confirmed by Black et al. (1971), who reported that a suite of total-rock samples yielded a Rb-Sr age of 3.98 AE and a Pb-Pb age of 3.62 AE.

Subsequently, Moorbath et al. (1972) reanalyzed the suite of rocks analyzed by Black et al. (1971) and reported that this suite and three additional suites of samples from a much larger area yield total-rock ages ranging from 3.69 AE to 3.74 AE. Baadsgaard (1973) showed that zircons separated from the Amîtsoq Gneiss preserve U-Th-Pb isotopic systematics and define an age of 3.65 AE.

Complexly associated with the Amîtsoq Gneiss is the quartso-feldspathic Nûk Gneiss, which has been dated locally by Rb-Sr whole-rock techniques at 3.04 AE by Pankhurst et al. (1973a).

These two gneiss units in the Godthaab District were sampled extensively and represent a substantial proportion of the material collected by us. Detailed descriptions of specific sampling sites, local geologic relationships, and locations of the sites are in section 3.2.

The Nordland Complex extends approximately 200 km north of Godthaab. It includes the large peninsula of Nordlandet proper and the country north of Fiskefjord to Uivfaq. The complex is a well-defined structural unit and all the rocks in the complex were once subjected to granulite facies metamorphic conditions (Berthelsen and Noe-Nygaard, 1965). We collected granulite facies gneisses and associated agmatized anorthositic rocks from central Nordlandet. More extensive collecting of rocks in the Nordland complex was done at Tovqussap Nunâ which lies between Fiskefjord and Uivfaq. The Tovqussap area was mapped in detail by Berthelsen (1960). The major rock types which comprise the area and which we collected are hypersthene-bearing and hornblende bearing gneisses. Although not quantitatively important, anorthosites occur at Tovqussap and were collected.

North of the Nordland Complex is a region composed of generally homogeneous gneiss named the Finnefjeld Gneiss. The gneiss is quartz-dioritic in composition (Berthelsen and Noe-Nygaard, 1965) and is of unknown age. We collected a suite of samples of this gneiss for isotopic studies.

Anorthosites and associated rocks occur throughout the region from Sukkertoppen to Fiskenaesset as either agmatitic lenses in the gneisses or as layered complexes grading from ultramafic to anorthositic rocks. Only locally were more massive bodies of pure anorthosite encountered. Volumetrically, these rocks are of minor importance, but they are ubiquitous. In the Nordland Complex anorthosite samples were collected from Tovqussap Nunâ and in central Nordland. In the Godthaab District samples were collected from the anorthosite body on Storø and at Ivnajaugtoq. South of Godthaab District anorthosite samples were collected in Ameralik, at the mouth of Buksefjord, at Tre Brøde, and extensively from the large, layered complexes at Fiskenaesset and Majorqap Qâva.

3.2 Project Oldstone Field Notes and Maps

OLDSTONE GREENLAND GANCARZ

FIELD NOTES

SUMMER 1973

24 June, 1973

Looked at the Nûk Gneiss northeast of Godthåb, especially the "pale-gray gneiss" and the "basic gneiss" as noted by V.R. McGregor in The early Precambrian gneisses of the Godthåb district, West Greenland (1973) Philosophical Transactions of the Royal Society of London, A, 273, p. 343-358. The distinction between the two phases is subtle, but this is the first day looking at the gneiss.

SAMPLE OGG 1: Map 3 (collected with sledge hammer)
Medium-grained, biotite, quartzofeldspathic gneiss. The rock is homogeneous on an outcrop scale of approximately 15 m. There are, however, inclusions of biotite-rich gneiss. The sample is from the headland at the east end of the tunnel at Nordhavn, Godthåb.

SAMPLE OGG 2: Map 3 (collected with sledge hammer)
At the west end of the tunnel on the headland above Nordhavn, Godthåb is darker gneiss with coarse quartz+biotite+plagioclase inclusions on a meter scale. These may be the "enclaves" of darker gneiss including the Amîtsoq Gneiss as noted by McGregor (1973). The sample has three parts a,b, and c, all of which are for the most part the inclusion material.

SAMPLE OGG 3: Map 3 (collected with sledge hammer)
This is a sample of the darker gneiss.

3 July, 1973

Worked along Godthåbsfjord to Qôrqut. Samples OGG 4 to OGG 8 were collected west of the inlet at Qôrqut. The Qôrqut Granite is generally rather massive, but in places it is filled with large, angular inclusions of gneiss some of which are biotite and hornblende (?) rich. The Qôrqut Granite also contains biotite+quartz+feldspar pegmatites and thin (1 to 25 cm), aplitic dykes. At the locality for samples OGG 4 and OGG 5 there are gneiss inclusions. At the locality for samples OGG 6 to OGG 8 the granite is more homogeneous, but still has some inclusions.

SAMPLE OGG 4: Map 3 (collected with sledge hammer)
This is a sample of one of the gneiss inclusions in the Qôrqut Granite.

SAMPLE OGG 5: Map 3 (collected with sledge hammer)
This is a sample of one of the biotite-rich gneiss inclusions in the Qôrqut Granite.

SAMPLE OGG 6: Map 3 (collected with sledge hammer)
This is a sample of an aplitic dyke which cuts across the Qôrqut Granite.

SAMPLE OGG 7: Map 3 (blasted sample)
This is a sample of the homogeneous, massive Qôrqut Granite.

SAMPLE OGG 8: Map 3 (collected with sledge hammer)

This is a sample of one of the biotite+hornblende inclusions in the Qôrqut Granite.

In the Godthåbsfjord region on Storø across from Qeqertarssûp nûa Qôrqut Granite crops out. At this locality samples OGG 9 and OGG 10 were collected. Here the granite contains numerous gneissose inclusions on a 10 to 20 m scale which are filled with quartz+microcline+biotite pegmatites. The pegmatites do not appear to cut the granite.

SAMPLE OGG 9: Map 3 (collected with sledge hammer)

This is a sample of the massive Qôrqut Granite.

SAMPLE OGG 10: Map 3 (collected with sledge hammer)

This is a sample of one of the pegmatites.

4 July, 1973

Traveled with V. R. McGregor to look at the Amîtsoq Gneiss and the Ameralik Dykes. The locality at Kanajorssuit shows the deformational transition of the Amîtsoq Gneiss from the porphyritic potassium feldspar granite to the fine-grained gneiss. The Ameralik Dykes show little deformation in this area.

5-6 July, 1973

Sailed along the north side of Ameralik (Lysefjord) to look at the Qôrqut Granite and at the contact between the Amîtsoq Gneiss and the Qôrqut Granite.

SAMPLE OGG 11: Map 3 (collected with sledge hammer)
This is a sample of the Qôrqut Granite which shows pervasive staining features. The sample was collected from a large talus slope.

SAMPLE OGG 12: Map 3 (collected with sledge hammer)
This is a sample of Qôrqut Granite, but it is different from sample OGG 11 in that it is paler in color and contains less biotite.

SAMPLE OGG 13: Map 3 (collected with sledge hammer)
This is a sample of Amîtsoq Gneiss included within the Qôrqut Granite.

After collecting these samples we sailed east along Ameralik to look at the gabbro-leucogabbro and Nûk Gneiss. The leucogabbro has very nice graded layers and is clearly of igneous origin.

SAMPLE OGG 14: Map 3 (collected with sledge hammer)
There are three parts to this sample: a, b, and c. Sample OGG 14a and OGG 14b are both anorthositic gabbro. Sample OGG 14c is a sample of gabbro. All were collected from a single block and the contact between the gabbro and leucogabbro is between samples OGG 14b and OGG 14c.

SAMPLE OGG 15: Map 3 (collected with sledge hammer)
This is a sample of a pegmatite cutting the leucogabbro.

SAMPLE OGG 16: Map 3 (blasted sample)
This is a sample of the homogeneous leucogabbro.

SAMPLE OGG 17: Map 3 (blasted sample)

This is a sample of the homogeneous gabbro.

SAMPLE OGG 18: Map 3 (collected with sledge hammer)

This is a sample of a veinlet, presumably Nûk Gneiss, cutting across the outcrop from which sample OGG 17 was collected.

Just east of the locality from which samples OGG 16 to OGG 18 were collected Nûk Gneiss crops out. About 1 km east of the locality from which samples OGG 16 to OGG 18 were collected is a pegmatite dyke approximately 1 m wide and about 150 m long. We could not find the end of the pegmatite dyke as the area is covered with vegetation. There is a strong cross-cutting relationship between this pegmatite dyke and the Nûk Gneiss. The pegmatite dyke cuts at approximately 90° the schistosity of the Nûk Gneiss. The pegmatite dyke is moderately zoned with a muscovite and quartz rim, grading inwards to a two feldspar plus quartz zone and finally to a bull-quartz core.

SAMPLE OGG 19: Map 3 (blasted sample)

This is a sample of the muscovite-containing portion of the pegmatite.

SAMPLE OGG 20: Map 3 (collected with sledge hammer)

This is a sample of the coarse-grained feldspar at the approximate center of the pegmatite.

SAMPLE OGG 20A: Map 3 (collected with sledge hammer)
This sample is a large feldspar crystal from near the locality of sample OGG 19.

In the Nûk Gneiss in the area between sample locality for samples OGG 16 to OGG 18 and for samples OGG 19 and OGG 20 there are two types of gneiss: one is a medium-grey gneiss and the other is a dark-grey gneiss. Neither type is particularly homogeneous. The area is near the contact between the leucogabbro and the Nûk Gneiss and there are many large rounded inclusions of leucogabbro. These inclusions are in some cases 10 to 15 m in diameter, but the size of the inclusions decreases rapidly from the agamatitic contact zone. In addition the Nûk Gneiss contains many pre-Nûk Gneiss deformation pegmatites which are now parallel to the foliation of the gneiss.

SAMPLE OGG 21: Map 3 (blasted sample)
This is a sample of the medium-grey, relatively homogeneous Nûk Gneiss. One of the pieces contains part of a "coarse" (i.e. relatively coarse with respect to the deformed pegmatites in the Nûk Gneiss) pegmatite.

SAMPLE OGG 22: Map 3 (blasted sample)
This is a sample of leucogabbro collected from an inclusion of leucogabbro approximately 2 m in diameter in the Nûk Gneiss.

SAMPLE OGG 23: Map 3 (collected with sledge hammer)
This is a small sample of leucogabbro collected approximately 0.5 m from sample OGG 22.

Just west of the locality from which samples OGG 21 to OGG 23 were collected is the Nûk Gneiss-leucogabbro contact. The contact between the gneiss and the massive leucogabbro is very sharp (approximately 1 to 2 cm). Here the Nûk Gneiss is strongly foliated and banded. Possibly the gneiss contains granulated and sheared leucogabbro.

SAMPLE OGG 24A: Map 3 (collected with sledge hammer)
This is a sample of leucogabbro. (see sketch #1 below)

SAMPLE OGG 24B: Map 3 (collected with sledge hammer)
This is a sample of leucogabbro. (see sketch #1 below)

SAMPLE OGG 25A: Map 3 (collected with sledge hammer)
This is a sample of leucogabbro. (see sketches #1 and #2 below)

SAMPLE OGG 25B: Map 3 (collected with sledge hammer)
This is a sample of leucogabbro. (see sketches #1 and #2 below)

SAMPLE OGG 26: Map 3 (collected with sledge hammer)
This is a sample of the banded Nûk Gneiss at the gneiss-leucogabbro contact. (see sketch #1 below)

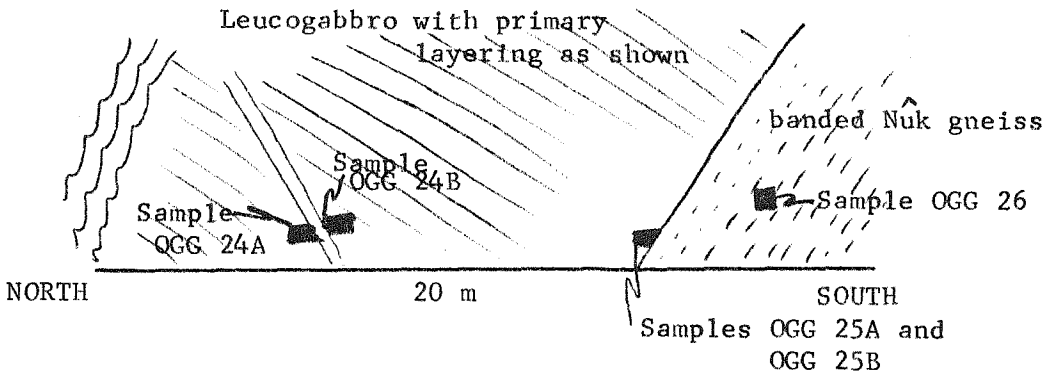

SKETCH 1

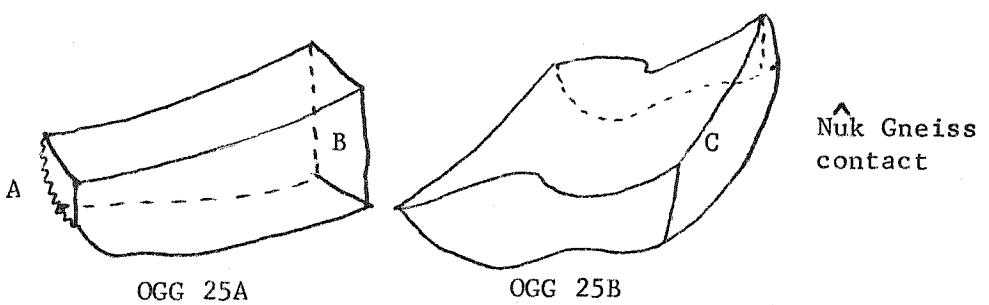

SKETCH 2

SAMPLE OGG 27: Map 3 (collected with sledge hammer)

This is a sample from a large block of leucogabbro which occurs between the sites of samples OGG 20 to OGG 23 and OGG 24 to OGG 26.

9 July, 1973

Sailed to Tovqussap Nunâ. The reference for this area is Berthelsen, Asger (1960) Structural studies in the Pre-Cambrian of Western Greenland: II Geology of Tovqussap Nunâ. Meddelelser om Grønland, Bd. 123, Nr. 1, pp. 1-223. Samples OGG 28 and OGG 29 were collected from the Navlen area which is near the center on the gneiss dome. The "purple gneiss" is a quartzofeldspathic gneiss with less than approximately 20% mafic minerals. The gneiss is fine grained and very homogeneous on a scale of 100 m. It weathers to patchy purple brown. There are a few pods of ultramafic rocks with reactions rims, contorted veins of blue quartz, and apparently undeformed (probably late-stage), pegmatite dykes.

SAMPLE OGG 28: Map 3 (blasted sample)
This is a sample of the "purple gneiss". Despite the drilling and blasting, the completely interior pieces still look weathered (i.e. have purple and brownish blotches).

SAMPLE OGG 29: Map 3 (collected with sledge hammer)
This is a sample of the "purple gneiss". The sample is much fresher looking than sample OGG 28 and also has some small, blue-quartz podlets.

After collecting in the Navlen area we sailed to Kangeq (see map by Berthelsen (1960)) to sample the anorthositic rocks.

The sample area of the "anorthosites" is characterized by sub-angular inclusions of leucogabbro to gabbroic anorthosite (to 2 or 3 m) agmatized by some "granitic" material. However, many of the inclusions are separated by cataclastic "anorthosite". The inclusions illustrate a wide variety of deformation. The least deformed samples are characterized by polygranular aggregates of plagioclase (to approximately 10 cm) surrounded by hypersthene, hornblende, and some biotite. The most deformed inclusions are highly streaked and sheared leucogabbro. The local area also contains dolerite dykes.

G.J. Wasserburg comment "Anorthosite body is composed of pods of this rock commonly 1 to 2 m sheathed in thin approximately 20 cm "granitic" or pegmatitic material. Sometimes the sheath is sheared anorthosite. The individual pods are sort of like superaugen, which on their margins frequently show increased degree of cataclasis. Some faults are present with a thickness of "healed, recrystallized" gouge of up to 25 cm. This looks like an aplite. No anorthosite pods were found free of granitic material on a 1 m scale. Larger anorthosite areas on the outcrop (approximately 5 - 10 m) were always cut by shear zones and granitic material, on a scale of less than 1 m. There does not appear to be any migmitization of the pods. The separation of these bodies is rather sharp, although smaller sharply defined veins of pegmatite may cross them. The general appearance is of what was originally a sizeable (approximately 1/2 km) body of anorthosite (which included some ultrabasics) were then deformed into a superaugen gneiss and that subsequently they were injected by granitic material which was then cut by several small faults while still "hot" and then the faults rewelded."

SAMPLE OGG 30: Map 3 (collected with sledge hammer)

This is a sample of sheared, fractured, and stretched out leuco-gabbro. The sample was collected from a float block which seems to have fallen from a spall zone about 3 m from an ultramafic inclusion.

SAMPLE OGG 31: Map 3 (collected with sledge hammer)
This is a sample of gabbroic anorthosite. The sample has large polygranular aggregates of plagioclase. The inclusion from which this sample was collected is surrounded by granitic material, and one corner of the sample has some of this material attached to it. The sample was collected from a float block.

SAMPLE OGG 32: Map 3 (collected with sledge hammer)
This is a prime sample of gabbroic anorthosite with large polygranular aggregates of plagioclase.

G. J. Wasserburg comment. "This came from a typical pod sheathed in granitic or pegmatitic material. It was taken from a much larger block with the sledge hammer. No blasting. The size of the plagioclase aggregates is typical although they were seen to range up to 30 cm and then ground down to 0."

SAMPLE OGG 33: Map 3 (collected with sledge hammer)
This is a sample of the "pink" aplitic or granitic material which cuts and separates the anorthosite inclusions. The sample was collected about 5 m from sample OGG 32.

SAMPLE OGG 34: Map 3 (collected with sledge hammer)
This is a sample of a polygranular-plagioclase aggregate from an inclusion of gabbroic anorthosite. The sample was collected in the immediate vicinity of samples OGG 31 and OGG 32.

Sailed up to Eqaluk and anchored overnight next to a waterfall in the small bay at the east end of Eqaluk.

10 July, 1973

The area around the east end of Eqaluk is characterized by inclusions of a variety of lithic types agmatized by what is now quartzofeldspathic gneiss and which was later cut by salt and pepper textured dykes. The dykes are clearly transgressive to the foliation of the gneiss.

SAMPLE OGG 35: Map 3 (collected with sledge hammer)

This is a sample of the medium-grained gneiss from the area at the east end of Eqaluk. The sample was collected from a rather homogeneous block.

G. J. Wasserburg comment: "Sample is typical of the uniform material exposed for some distance (approximately 1 km) in the inner harbour periphery as seen in both talus and outcrop."

SAMPLE OGG 36: Map 3 (collected with sledge hammer)

This is a sample of the gneiss which is similar to OGG 35, but somewhat coarser grained.

G. J. Wasserburg comment: "This sample is of a type common (but not most typical) in the talus and possibly outcrop."

10 July, 1973

Sailed to the north end of Tovqussap Nunâ to collect gneiss in the area mapped by Berthelsen (1960).

The gneisses at the northern end of Tovqussap Nunâ are massive and appear very homogeneous on a scale of 1/2 km. Undeformed pegmatites, aplites and granitic stringers are relatively rare in the gneiss. The gneiss is highly deformed and many very tight folds, whose amplitude ranges from 25 cm to 2 m are present.

In addition, there are ghosts of pods of biotite-rich material and ghosts of pegmatites, particularly at the site where samples OGG 37 and OGG 41 were collected. Samples OGG 38, OGG 39, and OGG 40 were all collected within 50 m of one another. This locality is near (approximately 100 m) the contact between the gneiss and the pyribolite unit. About 100 m from the contact and towards the contact blocks of the pyribolite become more and more common. The blocks at this contact are moderately folded and slightly stretched out. However, on the east side of the pyribolite and at the contact of the next pyribolite layer to the east, the blocks of pyribolite in the gneiss are blocky, angular fragments which exhibit little deformation. In general the blocks are not injected with granitic material.

SAMPLE OGG 37: Map 3 (collected with sledge hammer)
This is a sample of homogeneous gneiss which Berthelsen (1960) calls "quartz-dioritic to granodioritic biotite gneiss (the purple gneiss)". The sample was collected with V. R. McGregor and A. L. Albee.

SAMPLE OGG 38: May 3 (blasted sample)
This is a sample of homogeneous gneiss which Berthelsen (1960) calls " homogeneous granodioritic to granitic biotite gneiss".

SAMPLE OGG 39: May 3 (blasted sample)
This is another sample of homogeneous gneiss which Berthelsen (1960) calls "homogeneous granodioritic to granitic biotite gneiss".

SAMPLE OGG 40: Map 3 (blasted sample ?)

This is a sample of one of the pyribolite inclusions which occur at the contact between the granodioritic to granitic biotite gneiss and the pyribolite. This particular inclusion is only moderately deformed. There is some gneiss attached to this sample.

SAMPLE OGG 41: Map 3 (blasted sample)

This is a sample of homogeneous gneiss which Berthelsen (1960) calls "quartz-dioritic to granddioritic biotite gneiss (the purple gneiss)".

SAMPLE OGG 42: Map 3

This is a sample of one of the numerous, less than 1 m thick, pegmatites composed of quartz, biotite, and microcline which occur in the pyribolite unit adjacent to the locality where samples OGG 38, OGG 39, and OGG 40 were collected. The sample includes the contact and some pieces of the pyribolite.

11 July, 1973

After collecting the samples at the north end of Tovqussap Nunâ we sailed to Napassoq for food and fuel. For the next three days we collected gneisses of the Finnefjeld Gneiss Complex. As described in The Geologic Systems, The Precambrian; volume 2: Ed. K. Rankama p. 176, the gneiss complex is composed of "rather homogeneous hornblende- and biotite-bearing gneisses of more or less quartz-dioritic composition."

Samples OGG 43, OGG 44, and OGG 45 were collected on Qeqertasugssuk. The rock is a very dense, banded and somewhat foliate gneiss. The same lithologic types occur for 1/2 km. In a few places the foliation is well developed, but this is not a common occurrence. There are also some highly deformed pegmatites. Some of the gneiss is almost cataclastic. The float is composed of rocks like the purple gneiss in the central dome at Tovqussap Nunâ and of rock which is coarse-grained, equigranular material and looks like it could be the protolith of samples OGG 46, OGG 47, and OGG 48. In general blocks about 1/2 m are homogeneous.

SAMPLE OGG 43: Map 5 (collected with sledge hammer)
This is a sample of the homogeneous gneiss with little of the prominent banding.

SAMPLE OGG 44: Map 5 (collected with sledge hammer)
This is a sample of the banded gneiss.

SAMPLE OGG 45: Map 5 (collected with sledge hammer)
This is a sample of gneiss and includes part of a plagioclase-bearing pegmatite.

We then sailed to Napassup timâ and collected samples OGG 46, OGG 47, and OGG 48. The rocks at this locality are composed of massive, homogeneous gneiss which appears to have originally been igneous. The rocks are homogeneous for at least 1/2 km. The gneiss is deformed with large (10 to 20 m) crenulate folds.

These folds also include thin (10 to 25 cm), quartzofeldspathic layers. The gneiss is cut by a few late-stage, undeformed, zoned pegmatites. The pegmatites have quartz cores with perthite and biotite+magnetite+garnet rims. The pegmatites are up to 1 m wide and 50 to 100 m long. The gneiss contains what appears to be streaked out feldspar crystals.

SAMPLE OGG 46: Map 5 (collected with sledge hammer)
This is a sample of the homogeneous gneiss typical of the lithology at this locality.

SAMPLE OGG 47: Map 5 (collected with sledge hammer)
This is a sample of the typical homogeneous gneiss which is cut by 5 cm pegmatites. The pegmatites are undeformed.

SAMPLE OGG 48: Map 5 (collected with sledge hammer)
This is a sample of a core of a fold with 10 to 15 cm quartzo-feldspathic layer surrounded by the typical homogeneous gneiss.

G. J. Wasserburg comment: "The lithology at Napassup timâ is distinctive lithology. Distinct from sample location of samples OGG 43, OGG 44, and OGG 45. The location of samples OGG 43, OGG 44, and OGG 45 is more of a banded gneiss, although still not as banded as the gneiss seen at Napassoq."

Sailed up to Akia near the abandoned town of Ikerasak. Here the rocks are banded, massive gneisses which are not as uniform as those at the locality of samples OGG 46, OGG 47, and OGG 48. There is moderately well-developed foliation in the gneiss. The gneiss includes a variety of deformed lithic inclusions which include amphibolite and ultramafic. This locality is close to

the contact of the Alángua supracrustals (V.R. McGregor). There are also "granitic sheets" (G. J. Wasserburg calls them "pegmatites") 5 to 10 m thick which are slightly deformed (i.e. large open folds with some local shearing). Contact of the gneiss with the "granitic" material is extremely sharp. Berthelsen in : The Geologic Systems: The Precambrian, volume 2 Ed. K. Rankama says that the gneiss is uniform because of cataclastic deformation. Some of the gneiss is almost porphyritic (plagioclase feldspar clots: A. L. Albee comment). G. J. Wasserburg thinks that these clots may reflect the original igneous texture.

SAMPLE OGG 49: Map 5 (collected with sledge hammer)
This is a sample of the banded homogeneous gneiss. These bands are alternately feldspathic and mafic material.

SAMPLE OGG 50: Map 5 (collected with sledge hammer)
This sample was collected to get the contact between the gneiss and the "granitic sheet". The contact is extremely sharp (5 mm) and the granite is clearly intruded into the gneiss since it truncates folds in the gneiss.

SAMPLE OGG 51: Map 5 (collected with sledge hammer)
This is a sample of the Finnefjeld Gneiss with "porphyroblastic" plagioclase.

One final comment about the Akia locality. G. J. Wasserburg finds sheets 3 to 4 m wide of hornblende "gabbro" which cut the

gneiss. This rock sounds similar to the "diorite" described by Berthelsen in The Geologic Systems: The Precambrian, volume 2, Ed. K. Rankama.

12 July, 1973

Sailed to Upperniviup qeqertâ in Kangia to collect Finnefjeld Gneiss. The rock at this locality is a rather highly deformed, hornblende + biotite + quartz + feldspar gneiss. The layer from which sample OGG 52 was collected is homogeneous for 1/2 to 3/4 km. There are a few thin, biotite-and/or hornblende-rich layers which are highly segmented. The sample layer is not strongly banded, but adjacent layers are strongly banded with layers of more mafic and more feldspathic rock (bands are up to 1/2 m thick). About 2 km from the sample site there is a thick aplite. However, in general there are very few pegmatites in the area, and the ones that are present contain large (up to 5 cm) black plagioclase crystals. Near the sample locality there is a zone of highly foliated gneiss which may be reflecting a zone of fracturing associated with a possible fault. This falut (?) was recognized by a 1/2 km linear rock face. However, there are cataclastic zones and the foliation may be associated with one of these zones.

SAMPLE OGG 52: Map 5 (blasted sample)

This is a sample of the homogeneous Finnefjeld Gneiss. The locality is described above.

13 July, 1973

Sailed to Amitsuarssuk to collect more Finnefjeld Gneiss. The samples collected at this locality are OGG 53, OGG 54, OGG 55, OGG 56, OGG 57, and OGG 58. A variety of lithic types are present at the locality. These include the following: 1) relatively coarse-grained, well-foliated, mafic, hornblende gneiss, 2) a variety of finer-grained gneisses which grade from rock like type #1, but finer-grained to biotite-hornblende gneiss to biotite gneiss (In general, all of rocks of this type are much finer grained and more felsic than type #1), and 3) a few late-stage, cross cutting pegmatites and/or aplites (1 to 10 cm) which contain dark-grey plagioclase crystals. The rocks are all strongly deformed and no clear examples of transgressive relationships were seen, except for the late-stage, black-plagioclase, pegmatite dykes. In all cases the finer-grained, leucocratic to mesocratic biotite gneisses appear concordant with the coarser-grained, melanocratic, hornblende-biotite gneisses. The deformation features include 1 m shear folds, stretching and shearing of inclusions, and thin cataclastic zones.

SAMPLE OGG 53: Map 5 (blasted sample)

The outcrop from which the different parts of sample OGG 53 were collected was selected since it contains the contact between the medium-grained, moderately banded and foliated, mafic, biotite-hornblende gneiss and the finer-grained, massive, leucocratic, biotite gneiss. There are also a few small aplite dykes.

SAMPLE OGG 53A:

This is a sample of the mafic, hornblende-biotite gneiss collected exactly at the contact between the mafic, hornblende-biotite gneiss and the leucocratic, biotite gneiss. A is written on the contact face of the sample.

SAMPLE OGG 53B:

This is a sample of the homogeneous, mesocratic to leucocratic, biotite gneiss. This sample was taken farthest from the contact described above.

SAMPLE OGG 53C:

This is a sample of the mafic, hornblende-biotite gneiss collected farthest from the contact described above.

SAMPLE OGG 53D:

This is a hand specimen of the contact.

SAMPLE OGG 53E:

This is a sample of the homogeneous, mesocratic to leucocratic, biotite gneiss collected about one-half way between the contact and sample OGG 53B.

SAMPLE OGG 54: Map 5 (blasted sample)

This is a sample of the mafic, hornblende-biotite gneiss which is in contact with one of the black-plagioclase-bearing pegmatites.

SAMPLE OGG 55: Map 5 (blasted sample)

This is a sample of the foliated, fine-grained, leucocratic biotite gneiss.

SAMPLE OGG 56: Map 5 (blasted sample)

This is a sample of the coarse-grained, hornblende-biotite gneiss. It was collected about 20 m from the site where sample OGG 53 was collected.

SAMPLE OGG 57: Map 5 (blasted sample)

This is a sample of the medium-grained biotite gneiss. It was collected about 50 m from the site where sample OGG 55 was collected.

SAMPLE OGG 58: Map 5 (collected with sledge hammer)

This is a sample of the hornblende-biotite gneiss. The sample is well foliated. It was collected at the north end of the bay from a large talus block.

Sailed to a small island just north of the north end of Tovqussap Nunâ.

At this locality the rocks consist of highly deformed gneiss with inclusions of broken amphibolite. There is one thin zone with coarse-grained anorthosite. Throughout this zone there are many cataclastic zones.

SAMPLE OGG 59: Map 3 (blasted sample)

This is a sample of recrystallized anorthosite. It was taken from a large boulder (3 m diameter) found by V.R. McGregor and A. L. Albee. This sample also includes some of the country rock.

SAMPLE OGG 60: Map 3 (blasted sample)

This is a sample of mixed anorthosite and country rock.

SAMPLE OGG 61: Map 3 (collected with sledge hammer)

This sample is composed of a number of hand specimens which were collected to illustrate the variety of types of "anorthosite" found in the immediate vicinity of the sites where samples OGG 59 and OGG 60 were collected.

14 July, 1973

Sailed to Ankerbugt on the western edge of Tovqussap Nunâ. At this locality samples OGG 62, OGG 63, OGG 64, and OGG 65 were collected. In the area where samples OGG 62 and OGG 63 were collected the geology is characterized by agmatized blocks of biotite-rich and hornblende-rich rocks in a matrix of leucocratic to predominantly mesocratic gneiss. Agmatized gneiss is about 85% of the rock. The agmatized blocks show little to moderate deformation. In general, the inclusions are broken, angular fragments to slightly stretched and flattened fragments. The fragments rarely show extensive folding. The gneiss is part of the "frame layer" described by Berthelsen (1960) and belongs to the unit of "quartz-dioritic to granodioritic biotite gneiss (the purple gneiss)". In a few spots the gneiss is homogeneous,

massive, and relatively undeformed. Sample OGG 62 was from one of the blocks of the homogeneous massive gneiss. There are virtually no deformed pegmatites (i.e. pegmatites deformed during the period of agmatization). There are a few thin, late-stage pegmatites and very small aplite dykes.

SAMPLE OGG 62: Map 3 (blasted sample)

This is a sample of the homogeneous purple gneiss collected in an area characterized by much deformed gneisses and broken inclusions of amphibolite-and biotite-rich rocks.

G. J. Wasserburg comment: The basic inclusions are deeply weathered and the inclusion-rich gneiss also (crumbly brown to 4 cm of the surfaces.)

SAMPLE OGG 62A: Map 3 (collected with sledge hammer)

This sample was collected between 150 and 200 m north of the site where sample OGG 62 was collected. It is an inclusion in the gneiss.

SAMPLE OGG 63: Map 3 (collected with sledge hammer)

This is a sample of the "quartz-dioritic to granodioritic biotite gneiss (the purple gneiss)" (Berthelsen (1960)). It was collected from a very large slab (3 m x 2 m x 1 m) of very fresh looking gneiss on a large talus pile.

G.J. Wasserburg comment: "very uniform with very few small pegmatite bands in it."

SAMPLE OGG 64: Map 3 (collected with sledge hammer)

The spot where this sample was collected is mapped by Berthelsen

(1960) as "quartz-dioritic to granodioritic biotite gneiss (the purple gneiss)". In general there are a variety of lithologies all of which are intruded by "granitic material". The "granitic" material constitutes about 50% of the rock. G. J. Wasserburg collected 15 to 20 samples of the various lithic types.

G. J. Wasserburg comment: "These include a dark inclusion labeled I and two fragments of the more massive pegmatitic material which is intrusive here."

In the Ankerbugt area not only does the purple gneiss crop out, but also the "homogeneous granodioritic to granitic biotite gneiss" Berthelsen (1960). Sample OGG 65 was collected where the later unit is exposed.

SAMPLE OGG 65: Map 3 (collected with sledge hammer)

There are a variety of lithologies at the sample site, but the most common type is a highly foliated gneiss. Two typical samples were collected by G. J. Wasserburg.

15 July, 1973

Sailed south to Nordland.

The locality from which samples OGG 66, OGG 67, OGG 68, and OGG 69 were collected is granulite facies terrain. In general the area is composed of "brown-weathering" hypersthene gneisses, moderately foliated to massive. Areas 25 to 150 m in diameter are composed predominantly of "anorthosite". The "anorthosite" occurs as rounded, generally undeformed blocks to 1.5 m in diameter. The gneiss surrounding these blocks (approximately

15 to 25% of the outcrop) is much more mafic than the "anorthosite" and therefore is not simply sheared and granulated "anorthosite". The anorthosite is composed of plagioclase as polygranular aggregates to 10 cm. The plagioclase is both white and grey. Some biotite and hornblende is present, and there may be some hypersthene. There are patches of biotite-rich material in the anorthosite as clots up to 15-20 cm in diameter.

G. J. Wasserburg comment: "On other unnamed island visited by G. J. Wasserburg and R. F. Dymek large anorthosite masses on the island. The anorthosite appears to be of two types on this island. The predominant one is massive equigranular, white-gray anorthosite with low mafic content. This has been intimately dissected by quartzofeldspathic (black) dykes which are more resistant to weathering. A small fragment taken from the outcrop is in R. F. Dymek's collection. (sample OGD-71504). The other type is of the anti-plum pudding variety-pods of plagioclase (several cm) white in a matrix of mafics. One large outcrop of this was found. The dykes are commonly undeformed and cross cut and surround the anorthosites."

SAMPLE OGG 66: Map 3 (blasted sample)

This is a sample of anorthosite and some of the gneiss surrounding the block of anorthosite. The block of anorthosite from which the sample was taken is about 1.5 m in diameter.

SAMPLE OGG 67: Map 3 (blasted sample)

This is a sample of the homogeneous, massive hypersthene gneiss. The sample was collected about 50 m north of the site where sample OGG 66 was collected.

SAMPLE OGG 68: Map 3 (collected with sledge hammer)

This sample was collected about 200 m south of where samples

OGG 66 and OGG 67 were collected. The sample is part of a late-stage biotite + plagioclase pegmatite which cuts the anorthosite.

SAMPLE OGG 69: Map 3 (collected with sledge hammer)
This is a sample of anorthosite. It was taken from a fresh block (block not in place) next to sample OGG 68.

16 July, 1973

Took dinghy into the eastern part of the Nordland area. The rocks in this area are composed of hypersthene gneiss and anorthosite. The anorthosite is agmatized in a fashion very similar to that described for the site from which samples OGG 66 and OGG 67 were collected. Two samples were collected and they are OGG 70 and OGG 71.

SAMPLE OGG 70: Map 3 (collected with sledge hammer)
This is a sample of anorthosite.

SAMPLE OGG 71: Map 3 (collected with sledge hammer)
This is a sample of anorthosite. The rocks in this area weather very deeply and so the rocks are very sugary textured.

18 July, 1973

Sailed with V. R. McGregor and D. Bridgwater to Storø. In the third bay on the west side of Storø four samples were collected (OGG 72, OGG 73, OGG 74, and OGG 75). Anorthosite crops out in this bay. The anorthosite is rather massive, but is strongly cut by coarse-grained pegmatites and gneiss. The pegmatites constitute about 30% of the outcrop and the biotite gneiss

(Nûk (?)) about 10%. The anorthosite is generally extensively recrystallized, but a few samples appear to have original plagioclase preserved. About 10 m from the locality is a 2 m wide dolerite dyke which is undeformed.

SAMPLE OGG 72: Map 3 (collected with sledge hammer)
This is a sample of the dolerite from the undeformed dolerite dyke.

SAMPLE OGG 73: Map 3 (collected with sledge hammer)
This is a sample of the gneiss "injected" into the anorthosite. There may be clots of plagioclase in this sample.

SAMPLE OGG 74: Map 3 (blasted sample)
This is the prime sample of anorthosite. It contains what appear to be original plagioclase crystals.

SAMPLE OGG 74A: Map 3 (blasted sample)
This is another prime sample of anorthosite. It was collected about 1/2 m away from sample OGG 74.

SAMPLE OGG 75: Map 3 (blasted sample)
This is a sample of the very strongly recrystallized anorthosite.

Anchored overnight in the second bay on the west side or Storø.

19 July, 1973

On the north side of the second bay on the west side of Storø anorthositic rocks crop out. It is in this area that samples OGG 76, OGG 77, OGG 78, OGG 79, OGG 80, OGG 81, OGG 82, OGG 83, and OGG 84 were collected. This anorthosite locality

was chosen by D. Bridgwater and V. R. McGregor. Pure massive anorthosite per se is not present. In general the anorthosite is migmatized by grey, salt and pepper textured gneiss, and is cut by pegmatites (up to 2 m wide) which appear to be associated with the Qôrqut Granite. The anorthosite is strongly recrystallized. The migmatization is very extensive and homogeneous blocks only 1 to 2 m in diameter are present. The gneiss which cuts the anorthosite ranges from approximately 10% of the outcrop where sample OGG 76 was collected to as much as 90% of the outcrop where samples OGG 83 and OGG 84 were collected. The pegmatites do not appear to exhibit this range of density.

SAMPLE OGG 76: Map 3 (plug and feather sample)
This is a sample of granulated and recrystallized anorthosite.

SAMPLE OGG 77: Map 3 (collected with sledge hammer)
About 2 m southeast of the site where sample OGG 76 was collected is a pegmatite probably associated with the emplacement of the Qôrqut Granite. This is a sample of the pegmatite.

SAMPLE OGG 78: Map 3 (collected with sledge hammer)
About 75 m northwest of where samples OGG 76 and OGG 77 were collected is an undeformed dolerite dyke. This is a sample of the dolerite dyke.

SAMPLE OGG 79: Map 3 (collected with sledge hammer)
This is a sample of the Qôrqut Granite which cuts both the anorthosite and the gneiss which cuts the anorthosite. The

sample was collected about 30 m southeast of where sample OGG 76 was collected.

SAMPLE OGG 80: Map 3 (collected with sledge hammer)
This sample was collected about 20 m southeast of where sample OGG 76 was collected. This is a sample of anorthosite "breccia". The matrix of the breccia is mostly Qôrqut Granite, but there is some gneiss.

SAMPLE OGG 81: Map 3 (collected with sledge hammer)
This sample was collected about 15 m southeast of where sample OGG 76 was collected. This sample is from a talus block and is anorthosite with crosscutting gneiss, both of which are cut by a late pegmatite.

SAMPLE OGG 82: Map 3 (collected with sledge hammer)
This is a sample of anorthosite. It is somewhat coarser-grained than anorthosite sample OGG 76. The sample also displays a relict cumulus texture. This sample was collected about 10 m southeast of where sample OGG 76 was collected.

SAMPLE OGG 83: Map 3 (collected with sledge hammer)
About 250 to 300 m northwest of where sample OGG 76 was collected is an outcrop of predominantly a melanocratic gneiss which cuts the anorthosite. This is a sample of the gneiss. It contains a few small bands of "anorthosite"(?) about 2 to 3 cm thick.

SAMPLE OGG 84: Map 3 (collected with sledge hammer)
This sample was collected at the same place as sample OGG 83.

It is a sample of the melanocratic gneiss with anorthosite bands. In this sample however, the bands are 5 to 10 cm thick as opposed to 2 to 3 cm thick in sample OGG 83.

Sailed to the south side of the second bay on the west side of Storø to collect the Amîtsoq Gneiss marked out by A. L. Albee, V. R. McGregor, and D. Bridgwater. The samples have R. F. Dymek numbers and will be described in the transcription of his field notes.

Sailed to the northeast side of the second bay on the west side of Storø with A. L. Albee to collect Amîtsoq Gneiss. At this locality an Ameralik Dyke cuts across both the Amîtsoq Gneiss and a pegmatite. Sample OGG 85 was collected here.

SAMPLE OGG 85: Map 3 (collected with sledge hammer)
This is a sample of the Amîtsoq Gneiss and the pegmatite, both of which are cut by an Ameralik Dyke.

20 July, 1973

There is some confusion about the location of samples OGG 85, and OGG 89-96. All of these samples are labeled on air photograph 281J-207. My comment on the back of the air photograph as of November 28, 1973 is as follows: "This location (that labeled OGG 89 to OGG 96) for OGG 89 to OGG 96 is incorrect as they were collected from a talus found by G. J. Wasserburg, D. Bridgwater, and V. R. McGregor while A. L. Albee and I were finishing with samples OGG 72 to OGG 75 of anorthosite. This should be the site for OGG 85 collected by A. L. Albee and me one evening. Similarly the point labeled OGG 85 on this photograph is labeled wrong and is one of R. F. Dymek's samples OGD-71904. Here (referring to point with this note) is where we lost the plugs and feathers. This can't be one of my samples, because the sketch of the outcrop by G. J. Wasserburg is in R. F. Dymek's notebook. Sample localities for OGG 89 to OGG 96 are on air photograph 281K-090." These corrections have been made on map 3.

Sailed to the southeast corner of Bjørneøen to Sitdlisit nûat to collect Nûk Gneiss. G. J. Wasserburg went off and collected sample OGG 86 while the rest of us collected samples OGG 87 and OGG 88, and samples OGD 71905, OGD 71906, OGD 71907, OGD 72001 to OGD 72006.

SAMPLE OGG 86: Map 3 (collected with sledge hammer)
This is a sample of grey Nûk Gneiss.

SAMPLE OGG 87: Map 3 (plug and feather sample)
This is a sample of coarse-grained, homogeneous, undeformed, medium-grey Nûk Gneiss. The sample was collected from a loose block of talus.

SAMPLE OGG 88: Map 3 (collected with sledge hammer)
This is a sample of Nûk Gneiss. It is finer grained and darker than Nûk Gneiss sample OGG 87. The sample was collected from a talus block.

Sailed to the north side of the third bay on the west side of Storø to collect samples OGG 89, OGG 90, OGG 91, OGG 92, OGG 93, OGG 94, OGG 95, and OGG 96. These samples may be Amîtsoq Gneiss. The locality was chosen by G. J. Wasserburg, D. Bridgwater, and V. R. McGregor on 18 July. The samples are all collected from talus material, but the blocks are very large (up to 25 m). The rocks are characterized by strongly banded and deformed gneiss cut by mafic dykes which may be Ameralik Dykes and the gneiss may therefore be Amîtsoq Gneiss. The outcrop is

about 1/2 km long and has banded gneiss. The bands outline folds with amplitudes to several meters. The scale of layering is from cm to m range. The gneiss per se composes approximately 80% of the outcrop. The remainder is pegmatitic material. The pegmatites are generally concordant with the banded gneiss and range from about 100 cm to 1 m thick. Although most of the pegmatites appear concordant with the gneissosity, this may be due to rotation associated with deformation. Thin pegmatites are also seen to cut some of the massive gneiss and one block was seen with a 15 cm pegmatite cutting at a high angle to the schistosity.

SAMPLE OGG 89: Map 3 (collected with sledge hammer)
This is a sample of banded gneiss taken immediately adjacent to one of the Ameralik Dykes (?). The banding scale is 1 to 3 cm.

SAMPLE OGG 90: Map 3 (collected with sledge hammer)
This sample was collected about 10 m east of where sample OGG 89 was collected. This is another sample of banded gneiss collected immediately adjacent to an Ameralik Dyke (?). The side adjacent to the dyke has the sample number on it.

SAMPLE OGG 91: Map 3 (collected with sledge hammer)
The Ameralik Dyke (?) adjacent to sample OGG 90 is about 1.5 m wide. This is a sample of the dyke collected in the center of the dyke.

SAMPLE OGG 92: Map 3 (collected with sledge hammer)
This is a sample of medium-grey, more massive gneiss with discordant 2 to 5 cm pegmatites. The sample was collected about 5 m west of where sample OGG 89 was collected.

SAMPLE OGG 93: Map 3 (collected with sledge hammer)
This is a sample of banded gneiss collected as far away as possible from any Ameralik Dykes (?). The sample was collected about 15 m west of where sample OGG 89 was collected.

SAMPLE OGG 94: Map 3 (collected with sledge hammer)
This sample is the same as sample OGG 93, but was collected from a banded gneiss with a 20 cm band of more massive gneiss.

SAMPLE OGG 95: Map 3 (collected with sledge hammer)
This is a sample of a mafic band in the banded gneiss. The sample was collected 15 to 20 m west of where sample OGG 89 was collected.

SAMPLE OGG 96: Map 3 (collected with sledge hammer)
This is a sample of what appears to be a concordant pegmatite. The pegmatite is about 2 m thick and was collected about 20 m west of where sample OGG 89 was collected.

21 July, 1973

Sailed up to Ivnajaugtoq to collect anorthosite. This is a massive block of anorthosite about 1.5 km in diameter and 1200 m high. All of the samples OGG 97 to OGG 121 are from float blocks except samples OGG 100, OGG 101, OGG 102, OGG 103, and OGG 104.

The rocks in this area are generally massive anorthosite which weather to buff white. There are a very few pods and lenses of leucogabbro. No layering is visible in the anorthosite and the leucogabbro pods are scattered throughout the rocks suggesting that they may have been originally inclusions, or that if they were once distinct layers, then the anorthosite has been intensely deformed. Towards the eastern margin of the anorthosite body as mapped by Noe-Nygaard A. and Ramberg H. (1961) Geological Reconaissance Map of the Country Between Latitudes 69° N and 63° 45′ N, West Greenland, Meddelelser om Grønland, Bd. 123, Nr. 5., inclusions of gneiss and possibly pods of leucogabbro become more abundant grading into migmatized anorthosite and finally into homogeneous gneiss.

SAMPLE OGG 97: Map 4 (collected with sledge hammer)
This is a sample of leucogabbro.

SAMPLE OGG 98: Map 4 (collected with sledge hammer)
This is a sample of leucogabbro.

SAMPLE OGG 99: Map 4 (collected with sledge hammer)
This is a sample of very coarse leucogabbro with 2 to 5 cm plagioclase crystals.

SAMPLE OGG 100: Map 4 (collected with sledge hammer)
This is a sample of medium-grained, blue-grey anorthosite.

SAMPLE OGG 101: Map 4 (collected with sledge hammer)

This is a sample of white anorthosite.

SAMPLE OGG 102: Map 4 (collected with sledge hammer)

This is a sample of the grey anorthosite.

SAMPLE OGG 103: Map 4 (collected with sledge hammer)

This is a sample of anorthosite collected east of where samples OGG 97 to OGG 102 were collected.

SAMPLE OGG 104: Map 4 (collected with sledge hammer)

This is a sample of what is either anorthosite or a broken up pegmatite.

SAMPLE OGG 105: Map 4 (collected with sledge hammer)

This is a sample of leucogabbro.

SAMPLE OGG 106: Map 4 (collected with sledge hammer)

This is a sample of leucogabbro with large hornblende crystals.

SAMPLE OGG 107: Map 4 (collected with sledge hammer)

This is a sample of white anorthosite.

SAMPLE OGG 108: Map 4 (plug and feather sample)

This is a prime sample of blue-grey anorthosite.

SAMPLE OGG 109: Map 4 (plug and feather sample)

This is a sample of white anorthosite. It is a prime sample.

SAMPLE OGG 110: Map 4 (collected with sledge hammer)

This is a sample of anorthosite collected by A. L. Albee. It is a

prime sample because it has what appears to be original igneous (i.e. unrecrystallized) plagioclase crystals.

SAMPLE OGG 111: Map 4 (collected with sledge hammer)
This is a sample of white anorthosite.

SAMPLE OGG 112: Map 4 (collected with sledge hammer)
This is a sample of white anorthosite.

SAMPLE OGG 113: Map 4 (collected with sledge hammer)
This is a sample of white anorthosite.

SAMPLE OGG 114: Map 4 (collected with sledge hammer)
This is a sample of white anorthosite.

SAMPLE OGG 115: Map 4 (collected with sledge hammer)
This is a sample of blue-grey anorthosite.

SAMPLE OGG 116: Map 4 (collected with sledge hammer)
This is a sample of blue-grey anorthosite.

SAMPLE OGG 117: Map 4 (collected with sledge hammer)
This is a sample of blue-grey anorthosite.

SAMPLE OGG 118: Map 4 (collected with sledge hammer)
This is a sample of blue-grey anorthosite.

SAMPLE OGG 119: Map 4 (collected with sledge hammer)
This is a sample of "banded," blue-grey anorthosite.

SAMPLE OGG 120: Map 4 (collected with sledge hammer)

This is a sample of blue-grey anorthosite with large (up to 5 cm) hornblende crystals on one face of the sample.

SAMPLE OGG 121: Map 4 (collected with sledge hammer)

This is a sample of white anorthosite.

22 July, 1973

Sailed to the west side of Sadelø and stopped near the glacier and waterfalls. The area is composed of medium-grained metagabbro or metadiorite mapped by V. R. McGregor on northwest side of Sadelø. The massive metadiorite intruded into strongly sheeted grey gneiss. Three samples were collected here and are OGG 122, OGG 123, and OGG 124.

SAMPLE OGG 122: Map 3 (collected with sledge hammer)

This is a sample of the medium-to fine-grained metadiorite. It was collected from a talus block.

SAMPLE OGG 123: Map 3 (collected with sledge hammer)

This is a sample of the metadiorite. It is coarser grained than sample OGG 122 and contains somewhat more plagioclase.

SAMPLE OGG 124: Map 3 (collected with sledge hammer)

This is a large piece of metadiorite which was pried loose with the crowbar.

Sailed to unit D of McGregor (1973) and left A. L. Albee and R. F. Dymek off. The rest of us went to the locality of Amîtsoq Gneiss

selected by V. R. McGregor. The rocks at this locality contain strongly folded and broken up Ameralik Dykes. The amplitude of the folds in the Amîtsoq Gneiss is 1 to 2 m. There are a very few pegmatites which cut the gneiss. These pegmatites are 10 to 20 cm wide. To the east about 50 m is an Amîtsoq Gneiss outcrop with a 1/2 to 3/4 m cross-cutting vein of "aplite" which looks like "aplites" associated with the Qôrqut Granite, although G. J. Wasserburg disagrees with this. The Amîtsoq Gneiss here is very finely banded and is a biotite gneiss. The Ameralik Dykes are generally 20 to 30 cm thick. We collected two samples here OGG 126 and OGG 127.

SAMPLE OGG 125:

There is nothing in my notebook about sample OGG 125, but there is a sample in the collection with this number.

SAMPLE OGG 126: Map 3 (collected with sledge hammer)

This is a sample of the Amîtsoq Gneiss. It was collected from a spall sheet and is very close to one of the Ameralik Dykes.

SAMPLE OGG 127: Map 3 (collected with sledge hammer)

This is a sample of Amîtsoq Gneiss and includes a core of an Ameralik Dyke fold.

23 July, 1973

Sailed to Kanajorssuit to collect the prime samples of Amîtsoq Gneiss. We collected 10 samples here OGG 128 to OGG 137.

SAMPLE OGG 128: Map 3 (blasted sample)

This of all of the samples which were collected in Greenland is the most prime piece of Amîtsoq Gneiss. This is the large potassium-feldspar gneiss and according to McGregor is the least deformed of all the Amîtsoq Gneiss. This sample is about 10 m west of where the sample sent to Baadsgaard for zircon work was collected. This sample which we collected is somewhat better in that the recrystallized rims on the potassium feldspar are somewhat thinner.

SAMPLE OGG 129: Map 3 (blasted sample)

This is a sample of Amîtsoq Gneiss. It is somewhat more deformed and the feldspar somewhat more recrystallized than in sample OGG 128. The feldspar crystals are aligned parallel to the foliation, but are still relatively undeformed. The sample was collected about 2 m south of where sample OGG 128 was collected.

SAMPLE OGG 130: Map 3 (collected with sledge hammer)

This is a sample of strongly deformed Amîtsoq Gneiss. The potassium feldspar crystals are totally streaked out. This sample was collected about 5 m west of where sample OGG 128 was collected. All the samples OGG 128, OGG 129, and OGG 130 were collected along the strike of the foliation and in a sense are within stratigraphically about 1 m of one another.

SAMPLE OGG 131: Map 3 (collected with sledge hammer)

This is a sample of an aplite dyke located about 300 m east of the site where sample OGG 128 was collected. The dyke cuts across

the Amîtsoq Gneiss at an angle of about 80°. The dyke itself is about 1/2 m thick.

SAMPLE OGG 132: Map 3 (collected with sledge hammer)
Approximately 200 m west of the site where sample OGG 128 was collected is highly foliated Amîtsoq Gneiss with an Ameralik Dyke about 1 m to the north. About 4 m to the north of this highly foliated gneiss is another (ca.1 m) Ameralik Dyke which is undeformed. Sample OGG 132 is a sample of the highly foliated Amîtsoq Gneiss.

SAMPLE OGG 133: Map 3 (collected with sledge hammer)
This is a sample of the Ameralik Dyke described above and which cuts across the site where sample OGG 132 was collected.

About 250 m east of the site where sample OGG 128 was collected the large potassium feldspar Amîtsoq Gneiss crops out. The gneiss shows a variety of deformational features. It is cut by a pegmatite. This pegmatite also cuts the Ameralik Dykes and the late-stage "aplites".

SAMPLE OGG 134: Map 3 (blasted sample)
This is a sample of the pegmatite described above.

SAMPLE OGG 135: Map 3 (blasted sample)
This is a sample of foliated Amîtsoq Gneiss, but there are still some of the large potassium feldspar crystals present.

SAMPLE OGG 136: Map 3 (blasted sample)

This is a sample of Amîtsoq Gneiss. It is very highly deformed and banded with alternating bands 5 to 10 cm thick of very mafic and very felsic material.

SAMPLE OGG 137: Map 3 (blasted sample)

This is a sample of Amîtsoq Gneiss which shows little deformation and is similar in texture to sample OGG 128.

26 July, 1973

Sailed to Buksefjorden to collect anorthosite. The reference for this area is Windley, Brian F. (1972) Regional geology of early Precambrian high-grade metamorphic rocks in West Greenland--Part 1: Kananaitsoq to Ameralik. Grønlands Geologiske Undersøgelse Rapport Nr. 46.

The rocks composing the "anorthosite" body at the mouth of Buksefjorden are generally undeformed or little deformed anorthosite and gabbro. The variety of lithic types is extreme ranging from almost pure anorthosite (i.e. all plagioclase with a few 1 to 5 cm pods of hornblende) like sample OGG 145 to bands of pure hornblende (coarse-grained, grain size 1 to 2 cm) like sample OGG 140. In a few places "grey" often garnet bearing gneiss is "injected" into the "anorthosite" body and occurs either as bands or as the matrix material between blocks of anorthosite. In addition, there are some salt and pepper

textured hornblende gabbro dykes (1/2 m wide) which cut the anorthosite, but which were clearly involved in the deformation of the body. The dykes are deformed but still cross cut the "igneous layering". Finally, there are some late-stage (i.e. completely undeformed) very mafic dykes (about 2 m wide). Pegmatites are uncommon and generally cut at a high angle the layering in the anorthosite. Samples OGG 138 to OGG 147 were collected here.

SAMPLE OGG 138: Map 1 (collected with sledge hammer)
This is a sample of medium-grained gabbroic anorthosite. The sample is layered with mafic bands 2 to 3 cm wide composed of hornblende. The sample is from an outcrop of layered, gabbroic anorthosite which contains mafic bands 10 to 15 cm thick, which preserve original igneous graded layering.

SAMPLE OGG 139: Map 1 (collected with sledge hammer)
This is a sample of one of the very late-stage mafic dykes which cut the anorthosite body.

SAMPLE OGG 140: Map 1 (collected with sledge hammer)
This is a hand specimen sample from a loose block. It is from a core of a fold which contains very coarse-grained hornblende crystals.

SAMPLE OGG 141: Map 1 (collected with sledge hammer)
This is part of a fine-grained gabbroic band of rock which is adjacent to the core of the fold from which sample OGG 140 was collected.

SAMPLE OGG 142: Map 1 (plug and feather sample)
In one part of the body there is generally massive, medium-grained gabbroic anorthosite which exhibits little internal structure (i.e. no prominent layering and deformation). Sample OGG 142 is a piece of this massive material and was collected on the east side of the peninsula.

SAMPLE OGG 143: Map 1 (collected with sledge hammer)
This is a sample of coarse-grained pegmatite which cuts the igneous layering in the anorthosite. The pegmatite is about 1/2 m wide and contains quartz and biotite.

SAMPLE OGG 144: Map 1 (collected with sledge hammer)
This is a sample of gabbroic rock collected about 10 m northwest of sample OGG 145.

SAMPLE OGG 145: Map 1 (plug and feather sample)
This is a sample of anorthosite which contains small lenticular pods (1 to 10 cm) of hornblende. This particular sample is from a loose block, but nearby similar material is in place.

SAMPLE OGG 146: Map 1 (collected with sledge hammer)
Interlayered with the anorthosite like sample OGG 145 are 20 to 30 cm thick layers of gabbroic material. Sample OGG 146 is part of one of these gabbroic layers and was collected from a loose block.

SAMPLE OGG 147: Map 1 (collected with sledge hammer)
G. J. Wasserburg collected this sample and says "There are 1 to 3 m wide bands of gabbroic material which are massive and homogeneous. Sample OGG 147 is from a weathered block of this material."

Sailed to Tre Brødre to collect the anorthosite there.

22 July, 1973

G. J. Wasserburg and A. L. Albee went ashore at Tre Brødre and collected samples OGG 148 and OGG 149.

SAMPLE OGG 148: Map 1 (collected with sledge hammer)
A. L. Albee and G. J. Wasserburg went into the eastern part of Tre Brødre anorthosite body and found that it was a massive shear zone. This is a sample of strongly recrystallized anorthosite.

SAMPLE OGG 149: Map 1 (collected with sledge hammer)
This is a hand specimen of medium-grained anorthosite collected by A. L. Albee and G. J. Wasserburg.

Later we went ashore and visited the main part of the anorthosite body. Here the rocks are generally strongly recrystallized anorthosite (fine to medium grained). Much of what appears to be primary igneous layering is present. The anorthosite is in many places cataclastically deformed. Pegmatites are not uncommon and range to 1 m thick. The pegmatites are generally undeformed. The contact of the anorthosite body with gneiss and amphibolite runs through the island. Generally as the contact is approached angular blocks of anorthosite are observed grading into deformed blocks of anorthosite and the proportion of the gneiss increases. Samples OGG 150 to OGG 153 were collected here.

SAMPLE OGG 150: Map 1 (plug and feather sample)
This is a sample of massive, poorly-layered, fine-grained

anorthosite. Within 5 to 10 m of this site the lithology is very similar.

SAMPLE OGG 151: Map 1 (plug and feather sample)
This is a sample of medium-grained, quartz-bearing "anorthosite". The sample was collected about 5 m northwest of a shear zone about 2 m wide. Associated with this shear zone is a pegmatite about 1 m wide. About 5 m southeast is the contact. Sample was collected because of the coarse grain size, particularly the plagioclase which may be part of the original igneous mineralogy.

SAMPLE OGG 152: Map 1 (collected with sledge hammer)
This is a sample of the pegmatite near where sample OGG 151 was collected.

SAMPLE OGG 153: Map 1 (collected with sledge hammer)
This is a sample of the material in the shear zone which is near to where sample OGG 151 was collected.

28 July, 1973

Visited with F. Kalsbeek at Midgaard while Jens Jarl went to Fiskenaesset for supplies.

29 July, 1973

Collected anorthosite on the north side of Qeqertarssuatsiaq. The reference for this section is Windley B.F., Herd R.K., and Bowden A.A. (1973) The Fiskenaesset Complex, West Greenland: Part 1-A Preliminary study of the stratigraphy, petrology, and

whole rock chemistry from Qeqertarssuatsiaq. Grønlands Geologiske Undersøgelse, Bull. 106. Walked through the basal gneiss and amphibolite. The gneiss is well banded, foliated and rather leucocratic. Traversed units #2, #3, #5, #6, #7, and #8. Unit #7 (hornblende-chromite layer) is very thin and often faulted despite that it is mapped by Windley et al. (1973) as continuous. Samples OGG 154 to OGG 160 were collected here.

SAMPLE OGG 154: Map 2 (plug and feather sample)
This is a sample of ophitic gabbro from unit #5. The rock displays good intercumulus textures. About 1 m to the southeast is a small fault and to the northwest is a "shear zone". In this zone the layered series (unit #3) is present and there are many rotated blocks of layered material. This may be a primary igneous feature.

SAMPLE OGG 155: Map 2 (plug and feather sample)
In the layered series (unit #3) is massive, poorly-layered melanocratic rock. A. L. Albee thinks that this may be unit #4, but there is more layered rock above, so this may in fact still be unit #3. If unit #4 is lensoid in places then this may be that unit. This is a sample of material from either unit #3 or #4.

SAMPLE OGG 156: Map 2 (collected with sledge hammer)
This is a sample of rock stratigraphically below sample OGG 155. It is banded on a 1/2 to 1 cm scale.

SAMPLE OGG 157: Map 2 (plug and feather sample)
About 1.5 m down section from where samples OGG 155 and OGG

156 were collected is a massive, mesocratic rock belonging to unit #3. This is a sample of this rock.

SAMPLE OGG 158: Map 2 (plug and feather sample)

This is a sample of the leucocratic rock within unit #3.

SAMPLE OGG 159: Map 2 (plug and feather sample)

This is a sample of rock unit #5. The rock is an ophitic gabbro. It is a mesocratic rock with thin "laminae" of hornblende. This is a fairly mafic example of the types of rock found in unit #5. The divisions between the units are not always obvious. This rock may be from the very base of unit #6 as garnet is present in the sample.

SAMPLE OGG 160: Map 2 (plug and feather sample)

This is a sample of rock unit #6. The rock is a fine-grained layered anorthosite. The layers alternately mafic minerals and plagioclase are only a few mm thick. There is also some garnet in this sample.

30 July, 1973

Bad weather and the helicopter can't fly so we went to Fiskenaesset for supplies. Collected sample OGG 161 in the harbour at Fiskenaesset.

SAMPLE OGG 161: Map 2 (collected with sledge hammer)

This is a sample of the sapphirine rock.

31 July, 1973

G. J. Wasserburg and I went to Midgaard to get the helicopter into J. Myers area, but the weather was bad and the helicopter was not able to fly. The rest of the party went to Qeqertarssuatsiaq to collect more samples from the anorthosite complex.

The sample numbers OGG 162 to 169 are to be used later.

1 August, 1973

G. J. Wasserburg and I went with J. Myers to the Majorqap qâva outcrop of the Fiskenaesset anorthosite complex. The reference for this area is Myers J.S. (1973) Igneous structures and textures in the Majorqap qâva outcrop of the Fiskenaesset anorthosite complex; in Progress report on the geology of the Fiskenaesset region; South-West Greenland, Grønlands Geologiske Undersøgelse Rapport No. 51. In this area we collected samples OGG 170 to OGG 224.

SAMPLE OGG 170: Map 2 (collected with sledge hammer)
The outer gneiss around the Majorqap qâva anorthosite complex is generally well-foliated grey gneiss with or without potassium feldspar porphyroblasts. Potassium feldspar porphyroblasts become more common closer to the contact. There are amphibolite bands within the gneiss up to 10 to 15 m across and are also a few pods of ultramafic rock (1 to 2 m). Closer to the contact between the gneiss and the Majorqap qâva anorthosite complex, and starting about 15 m away, the gneiss becomes intensely deformed and

is most commonly a pegmatite-banded gneiss. This sample is part of one of the ultramafic bodies within the gneiss.

SAMPLE OGG 171: Map 2 (collected with sledge hammer)
This is a sample of the Lower Leucogabbro. The Majorqap qâva anorthosite complex is isoclinally folded and one limb of the fold where the deformation is most intense the section is only a few tens of meters thick. Most of the Lower Leucogabbro is highly deformed and the plagioclase is completely recrystallized into a polygranular aggregate. The plagioclase grains are equigranular and 2 to 3 mm in diameter. There are, however, a few small (to 1 mm) patches of the Lower Leucogabbro in which primary plagioclase is still present. This sample is a sample of such a small patch of the Lower Leucogabbro.

SAMPLE OGG 172: Map 2 (collected with sledge hammer)
Stratigraphically above the Lower Leucogabbro is a Gabbro followed by the Upper Leucogabbro and finally the Anorthosite Layer *sensu stricto*. However, within the Anorthosite Layer are lenses of more mafic-rich rock--gabbroic anorthosite and anorthositic gabbro. Within these lenses the plagioclase is often primary despite the fact that the anorthosite surrounding the lens is completely composed of recrystallized plagioclase. Sample OGG 172 is from one of the anorthositic gabbro pods with primary plagioclase.

SAMPLE OGG 173: Map 2 (collected with sledge hammer)
Within the Anorthosite Layer there are sometimes layers (1 to 2 m

thick) of biotite and hornblende. Sample OGG 173 is a sample of highly deformed and completely recrystallized anorthosite with these thin bands.

SAMPLE OGG 174: Map 2 (collected with sledge hammer)
This sample is a piece of typical deformed anorthosite with complete recrystallization of the plagioclase into a polygranular aggregate.

SAMPLE OGG 175: Map 2 (collected with sledge hammer)
At the base of the Anorthosite Layer there is a thin layer of anorthosite and "chromite-rich" bands. Both of these are only about 10 to 20 cm thick at maximum. The chromite-rich bands can be composed of almost pure chromite at one extreme to almost pure hornblende at the other extreme. This is a sample of one of these chromite-rich bands.

SAMPLE OGG 176: Map 2 (collected with sledge hammer)
This is a sample of the hornblende-rich, chromite-rich band. It differs from sample OGG 175 in that it appears to contain diopside.

SAMPLE OGG 177: Map 2 (collected with sledge hammer)
In the top few meters of the Upper Leucogabbro Unit there are interstitial (intercumulus (?)) chromite patches which are often 2 to 4 cm in diameter. Here the aggregates of polygranular plagioclase are up to 10 cm in diameter. These aggregates must represent recrystallized plagioclase crystals. This sample is a piece of the recrystallized Upper Leucogabbro with interstitial chromite, hornblende and biotite.

SAMPLE OGG 178: Map 2 (collected with sledge hammer)
This sample is the same as sample OGG 177, but it was collected about 10 m lower in the section.

SAMPLE OGG 179: Map 2 (collected with sledge hammer)
In the Upper Leucogabbro Unit there are a very few thin layers (2-3 m) with alternating bands of plagioclase, chromite, and diopside. This is a sample of one of these layers.

SAMPLE OGG 180: Map 2 (collected with sledge hammer)
The Upper Leucogabbro Unit contains primary plagioclase crystals which range in size from 1 cm to 10 cm. Remarkably, however, within any given outcrop all crystals are the same size and at the base of the unit the primary plagioclase is about 1 cm in diameter, whereas at the top of the unit all of the plagioclase crystals are 9 to 10 cm in diameter. This sample is of the large plagioclase crystals which were collected from an outcrop where the large, unrecrystallized plagioclase crystals weather less strongly than the recrystallized plagioclase surrounding them.

SAMPLE OGG 181: Map 2 (collected with sledge hammer)
This is a sample of the Upper Leucogabbro Unit with primary plagioclase crystals about 2 to 5 cm in diameter. The sample was collected about 1/3 of the way up from the bottom of the Upper Leucogabbro Unit.

SAMPLE OGG 182: Map 2 (collected with sledge hammer)
At the top of the Gabbro Unit there is commonly a thin granite sheet

only a meter or two thick. The common presence of this sheet at the contact of the Gabbro Unit and Upper Leucogabbro Unit has led J. Myers to suspect that this may be in fact two layered sequences. Sample OGG 182 is a piece of the granite sheet.

SAMPLE OGG 183: Map 2 (collected with sledge hammer)
The Gabbro Unit corresponds to the "layered sequence" in the anorthosite body. Generally it is a homogeneous, medium-grained gabbro composed of recrystallized plagioclase and secondary hornblende. In places there are lenses of gabbro with unrecrystallized plagioclase laths and primary hypersthene with hornblende overgrowths. In places there are graded units which are about the only "up" indicators within the body. Within the Gabbro Unit there are also lenses of ultramafic rock, mostly olivine, which are layered, but the layering is at an angle to the layering of primary olivine in the gabbro. Two other rock units are present in the Gabbro Unit which J. Myers associates with the magma forming the body. First, there are lenses 1 to 10m in size which show excellent graded bedding at an angle to the bedding in the gabbro and show well-developed harrisitic textured hornblende. J. Myers interprets these as late-stage "pipes" in the gabbro through which late-stage fluids passed and thus concludes that the harrisitic hornblende in these pipes is primary. Secondly, there are dykes of spinel-hornblende-hypersthene rock. Sample OGG 183 is a piece of the typical recrystallized gabbro.

SAMPLE OGG 184: Map 2 (collected with sledge hammer)
This is a sample of one of the late-stage, spinel-hornblende-hypersthene dykes. There is also magnetite which J. Myers thinks is secondary.

SAMPLE OGG 185: Map 2 (collected with sledge hammer)
This is a sample of moderately recrystallized gabbro. The sample was collected near a lens of unrecrystallized gabbro. Most of the hypersthene in this sample has reacted to form hornblende and much of the plagioclase appears to have been recrystallized.

SAMPLE OGG 186: Map 2 (collected with sledge hammer)
See sample description for sample OGG 183 where the "ultramafic lenses" are described. This is a sample of one of the "ultramafic lenses". It contains primary olivine, with some pyroxene, magnetite, biotite, and hornblende. Generally in these lenses olivine is concentrated in the center with progressively more pyroxene towards the rims.

SAMPLE OGG 187: Map 2 (collected with sledge hammer)
This is a sample of the finer-grained Upper Leucogabbro which contains much primary plagioclase.

SAMPLE OGG 188: Map 2 (collected with sledge hammer)
This is a sample of gabbro with primary plagioclase laths and hypersthene with hornblende rims.

SAMPLE OGG 189: Map 2 (collected with sledge hammer)
At the base of the scree slope there is a low ridge of gabbro about

500 m long most of which contains primary plagioclase and hypersthene. In one place the gabbro is much coarser grained (grain size up to 1 cm) and shows little effect of recrystallization. Sample OGG 189 is a piece of the unrecrystallized, coarse-grained gabbro.

SAMPLE OGG 190: Map 2 (collected with sledge hammer)
See sample OGG 183 for a description of the "pipes" which show graded bedding. This is a sample from the largest such "pipe" in J. Myers' area and is one complete graded unit.

SAMPLE OGG 191: Map 2 (collected with sledge hammer)
There are a very few "pegmatites" cutting the Majorqap qâva anorthosite complex. One of these cuts the "pipe" from which sample OGG 190 was collected. This is a piece of the "pegmatite".

SAMPLE OGG 192: Map 2 (collected with sledge hammer)
This is a sample of gabbro collected by G. J. Wasserburg which contains two amphiboles and primary (?) plagioclase.

SAMPLE OGG 193: Map 2 (collected with sledge hammer)
This is a sample which contains the contact between the Upper Leucogabbro Unit and the "granite" sheet. The sample was collected by G. J. Wasserburg.

SAMPLE OGG 194: Map 2 (collected with sledge hammer)
There are not uncommonly pegmatites which cut the gabbro and are relatively undeformed. This is a sample of one of these pegmatites.

2 August, 1973

G. J. Wasserburg and I went to Midgaard early, while the rest of the party sailed to a small island where the equipment can be picked up by the helicopter. G. J. Wasserburg, J. Myers, and I were helicoptered from Midgaard to the "scree slope" on the south-east side of the valley to mark sample locations. After the rest of the group and equipment was helicoptered in G. J. Wasserburg and J. Myers were taken to the northwest side of the valley.

The "scree slope" contains blocks of predominantly leucogabbro (Upper Leucogabbro Unit) with lesser amounts of anorthosite with lenses of mafic material, and a few blocks of gabbro, mostly recrystallized. Here we collected samples OGG 195 to OGG 209. Samples OGG 195, OGG 196, OGG 197, OGG 198, OGG 199, OGG 200, and OGG 202 were collected from the "scree slope", but all of these must be close to their original locations, since the cliff above the slope contains most of the stratigraphic section.

SAMPLE OGG 195: Map 2 (plug and feather sample)
This is a sample of medium-grained leucogabbro, with primary plagioclase crystals (crystals 4-5cm in diameter). The sample belongs to the Upper Leucogabbro Unit. This sample may not be the most typical type in that it appears to have more plagioclase than the typical material in the Upper Leucogabbro Unit.

SAMPLE OGG 196: Map 2 (whole block in scree slope)
This is a sample of completely recrystallized, medium-grained

rock from the Upper Leucogabbro Unit. There is some slight deformation with stretching of the hornblende clots.

SAMPLE OGG 197: Map 2 (plug and feather sample)
This is a sample of the medium-grained Upper Leucogabbro. There is biotite in this sample and it does not look exceptionally fresh.

SAMPLE OGG 198: Map 2 (plug and feather sample)
This is a sample of the fine-grained Upper Leucogabbro with abundant primary plagioclase (plagioclase crystals are 1 to 2 cm in diameter).

SAMPLE OGG 199: Map 2 (plug and feather sample)
There are "granite" sheets which cut the Majorqap qâva anorthosite complex. This is a sample of massive, pegmatite-banded, biotite-anorthosite. There is also some garnet in this sample.

SAMPLE OGG 200: Map 2 (blasted sample)
This is a sample of the Upper Leucogabbro. The sample has large (about 10 cm) crystals of primary plagioclase and therefore, probably comes from near the top of the Upper Leucogabbro Unit.

SAMPLE OGG 201: Map 2 (plug and feather sample)
This sample is the same as sample OGG 189, but was collected about 10 m to the southwest.

SAMPLE OGG 202: Map 2 (plug and feather sample)
The Anorthosite Unit of the Majorqap qâva anorthosite complex is

divided into two parts. The upper part is relatively pure anorthosite with uncommon blocks of medium-grained leucogabbro with primary plagioclase (plagioclase crystals 3 to 5 cm in diameter) and the lower part of the Anorthosite Unit which is anorthosite with small, elongate pods (20 to 40 cm) of mafic-rock material, mostly hornblende. This lower part is the "Leopard Rock". Sample OGG 202 is a piece of this lower part of the Anorthosite Unit. There are in this sample pervasive, somewhat altered sulfides, mostly pyrrhotite.

SAMPLE OGG 203: Map 2 (plug and feather sample)
This is a sample of recrystallized gabbro with a small mafic dyke which contains thin needles of a blue mineral, possibly apatite. The sample was collected on the north side of the stream.

SAMPLE OGG 204: Map 2 (plug and feather sample)
This is a sample of "mostly recrystallized" gabbro collected on the south side of the stream. Just below the site where this sample was collected is a small pegmatite about 1/3 m thick. This pegmatite cuts across the layering in the gabbro.

SAMPLE OGG 205: Map 2 (collected with sledge hammer)
This is a sample of the pegmatite which cuts across the gabbro near the site where sample OGG 204 was collected.

SAMPLE OGG 206: Map 2 (plug and feather sample)
This is a sample of unrecrystallized gabbro with primary plagioclase laths and primary hypersthene with hornblende rims.

It is similar to sample OGG 201, but is finer grained than OGG 201.

SAMPLE OGG 207: Map 2 (plug and feather sample)
This is a sample of relatively unrecrystallized gabbro. The plagioclase still appears primary, but there is no hypersthene and it has all apparently reacted to form hornblende.

SAMPLE OGG 208: Map 2 (plug and feather sample)
There are a very few "granite" sheets 1 to 1.5 m thick which cut the gabbro and the layering in the Gabbro Unit. The "granite" contains blocks (20 to 40 cm) of the gabbro. The gabbro in contact with the "granite" sheet is completely recrystallized. This is a sample of the recrystallized gabbro in contact with the "granite" sheet. The sample number is written on the contact side of the block.

SAMPLE OGG 209: Map 2 (plug and feather sample)
This is a piece of the granite sheet in contact with sample OGG 207. The sample number is written on the contact side of the block.

Helicoptered to the top of the cliff on the southeast side of the valley to collect the samples marked by G. J. Wasserburg, J. Myers and me on August 1st. Collected samples OGG 210 to OGG 213.

SAMPLE OGG 210: Map 2 (blasted sample)

This is a sample of anorthosite about 25 m stratigraphically above the contact between the anorthosite sensu stricto (upper part of the Anorthosite Unit) and the anorthosite with pods of hornblende ("Leopard Rock" lower part of the Anorthosite Unit). This sample has large (to about 10 cm) single crystals of primary plagioclase. Nearby are inclusions of recrystallized, medium-grained leuco-gabbro. The anorthosite is also cut by small (1 to 2 m) sheets of "granite". This is the site visited by G. J. Wasserburg, J. Myers and me on the first of August and where we left one of the orange markers.

SAMPLE OGG 211: Map 2 (plug and feather sample)

This is a sample of mostly recrystallized anorthosite with some primary plagioclase (up to 2 cm). There are also elongate layers of more mafic material in the sample and about 2 m upstream is a thin (about 8 cm) pegmatite of quartz + feldspar plus minor amounts of biotite. J. Myers and G. J. Wasserburg left a marker on the spot.

SAMPLE OGG 212: Map 2 (collected with sledge hammer)

This is a sample of the quartz + feldspar + minor biotite pegmatite described above.

SAMPLE OGG 213: Map 2 (plug and feather sample)

This is a sample of a granite sheet about 5 m thick which cuts the anorthosite. It was collected on the opposite side of the stream from where samples OGG 211 and OGG 212 were collected.

A. L. Albee and I moved from the southeast side of the valley to the northwest side of the valley to help G. J. Wasserburg collect samples. This is the area visited by J. Myers and G. J. Wasserburg during the snow storm on the second of August. We collected samples OGG 214 to OGG 224 here.

SAMPLE OGG 214: Map 2 (blasted sample)

In the area there are large (4 to 5 m), semi-angular blocks of leucogabbro, with a "matrix" of recrystallized plagioclase. J. Myers interprets the anorthosite "matrix" as a product of remobilization during metamorphism and deformation. This is a sample from a 3 m block of relatively coarse-grained leucogabbro.

SAMPLE OGG 215: Map 2 (blasted sample)

This sample is from a boulder of anorthosite with the highest density of primary plagioclase crystals that we saw in the Majorqap qâva area. There are also veins of molybdenite in the sample. Some of the molybdenite crystals are 5 cm in diameter.

SAMPLE OGG 216: Map 2 (collected with sledge hammer)

Late diorite dykes cut the Majorqap qâva anorthosite complex. These dykes are relatively undeformed. This is a sample of the contact between the diorite dyke and relatively undeformed and recrystallized leucogabbro. The sample was collected by G. J. Wasserburg.

SAMPLE OGG 217: Map 2 (collected with sledge hammer)

This is a sample of recrystallized anorthosite with garnet-rich

layers. The block from which the sample was collected is heterogeneous and hand specimens may not be representative as the garnet-rich layers are not uniformly distributed throughout the outcrop. This sample was collected by G. J. Wasserburg.

SAMPLE OGG 218: Map 2 (collected with sledge hammer)
This sample was collected from the same outcrop as sample OGG 217. The sample is more deeply weathered, but is generally richer in garnet than sample OGG 217. This sample was collected by G. J. Wasserburg.

SAMPLE OGG 219: Map 2 (collected with sledge hammer)
Within the anorthosite outcrop from which samples OGG 217 and OGG 218 were collected are deformed leucogabbro layers which are recrystallized. Sample OGG 219 is deformed and recrystallized leucogabbro. This sample was collected by G. J. Wasserburg.

SAMPLE OGG 220: Map 2 (collected with sledge hammer)
This is a sample of recrystallized chromite-rich layer with fuchsite. J. Myers interprets the fuchsite as a product of metamorphism. G. J. Wasserburg collected this sample.

SAMPLE OGG 221: Map 2 (collected with sledge hammer)
Below the cliff from where samples OGG 214 and OGG 215 were collected the rocks grade from sheared anorthosite to less deformed anorthosite. There are white pods to 20 cm across of recrystallized

single plagioclase crystals. There are also fewer pods of leucogabbro here. This sample is one of the anorthosite pods. The sample was collected by G. J. Wasserburg.

SAMPLE OGG 222: Map 2 (collected with sledge hammer)
This sample was collected from the same outcrop as sample OGG 221. It is a pod of leucogabbro with large primary plagioclase crystals. The sample was collected by G. J. Wasserburg.

SAMPLE OGG 223: Map 2 (collected with sledge hammer)
This sample consists of plagioclase cobbles from the area where samples OGG 216 to OGG 224 were collected. The sample was collected by G. J. Wasserburg.

SAMPLE OGG 224: Map 2 (collected with sledge hammer)
This is a sample of a quartz + feldspar + biotite pegmatite collected near to where sample OGG 214 was collected. This sample was collected by G. J. Wasserburg.

4 August, 1973

Sailed from Midgaard to Graedefjordenhavn

5 August, 1973

Sailed from Graedefjordenhavn to Godthåb.

6 August, 1973

Put A. L. Albee and G. J. Wasserburg on Disko to Søndre Strømfjord.

7 August, 1973

Packed rocks in barrels and prepared to sail to Narssaq.

8 August, 1973

Sailed to Narssaq area to collect Amîtsoq Gneiss.

We first stopped at Baadsgaard's locality #155817 to look and collect Amîtsoq Gneiss. Walked along the coast for about 1 km and found the locality which had been recently drilled and blasted. Here we collected samples OGG 225 to OGG 228. The Amîtsoq Gneiss is moderately deformed porphyritic potassium feldspar granite much like sample OGG 129. Along strike (i.e. along the coast) there is a large, thick Ameralik Dyke (?) (salt and pepper textured). The dyke is about 2m thick. Essentially along the contact between the Amîtsoq Gneiss and the Ameralik Dyke is a 1 to 2 m thick sheet of granite and associated pegmatites. These are in knife-sharp contact with the Amîtsoq Gneiss. The pegmatites cut through the granite, but were not observed cutting the Amîtsoq Gneiss or Ameralik Dyke. This granite sheet may be Nûk Gneiss. There are some late black-plagioclase pegmatites which cut through the Amîtsoq Gneiss.

SAMPLE OGG 225: Map 3 (plug and feather sample)
This is a sample of the potassium feldspar Amîtsoq Gneiss.

SAMPLE OGG 226: Map 3 (plug and feather sample)
This is a sample of the granite. It was collected about 5 m south, along strike, from where sample OGG 225 was collected.

SAMPLE OGG 227: Map 3 (plug and feather sample)
This is a sample of relatively fresh, although somewhat fractured

granite. At the contact of the granite and the Amîtsoq Gneiss is a highly deformed pegmatite. This is one of the pegmatites associated with the granite and not one of the crosscutting, big black feldspar pegmatites.

SAMPLE OGG 228: Map 3 (plug and feather sample)
This is a sample of the granite with the highly deformed pegmatite described under sample OGG 227.

Anchored overnight at Kanajorssuit.

9 August, 1973

Sailed south to Kangerdluk to collect Amîtsoq Gneiss.

This is a very complex and intensely deformed terrain. The gneiss is unrecognizable as Amîtsoq Gneiss compared to what we have seen previously. We walked for about 2 km along the coast and the rocks are extremely heterogeneous. There are many inclusions of amphibolite (inclusions to 10 m in diameter) and of green ultramafic rocks (the bodies are up to 3 m in diameter). The gneisses range from highly foliated, relatively biotite-rich rocks to more massive, quartzofeldspathic types. There are also many late aplites and pegmatites. One pegmatite is about 10 cm thick and continuous for several hundred meters. This pegmatite cuts the gneiss. Ameralik Dykes (?) are present, although generally deformed and more often broken up so that there are bands of Ameralik Dyke inclusions.

SAMPLE OGG 229: Map 1 (collected with sledge hammer)

This is a sample of an ultramafic inclusion broken up by pegmatitic material. The individual blocks of ultramafic rocks are up to 1/2 m in diameter.

SAMPLE OGG 230: Map 1 (blasted sample)

This is a sample of quartzofeldspathic gneiss (Amîtsoq Gneiss (?)) with parts of broken up Ameralik Dykes (?). This gneiss has an extremely sharp contact with the more biotite-rich gneiss. The quartzofeldspathic band is about 3 m wide and in all places appears conformable with the more mafic, more strongly foliated gneiss. The gneiss is highly deformed internally, but there is a sharp, uncontorted contact with the mafic gneiss.

SAMPLE OGG 231: Map 1 (blasted sample)

This is a sample of a highly contorted gneiss, somewhat more mafic than sample OGG 230. No Ameralik Dykes were seen cutting the sample outcrop. The layering and extreme deformation suggest that it is, however, Amîtsoq Gneiss.

SAMPLE OGG 232: Map 1 (blasted sample)

This is the sample of the most mafic gneiss seen so far in this area. The sample contains large (up to 1 cm) feldspar megacrysts. Broken up Ameralik Dykes cut across the outcrop from which this sample was taken. The sample site is about 15-20 m from the very large pegmatite described in the description of the general locality.

10 August, 1973

Went to the far east end of the harbour at Kangerdluk and collected two samples OGG 233 and OGG 234. This area is much more homogeneous than the locality where samples OGG 229 to OGG 232 were collected. There are rather uniform mafic gneisses, similar in texture to those seen at sample locality OGG 129, but the feldspar appears to be completely recrystallized. Inclusions of amphibolite and ultramafic rock (up to several meters in diameter) are not uncommon. Pegmatites are heterogeneously distributed. Large (1 to 2 m) pegmatites were not present near the locality where sample OGG 233 was collected, but small (10 to 20 cm) pegmatites cut the entire area. The gneiss is probably Amîtsoq Gneiss, but no really good Ameralik Dykes were seen. Despite the presence of Ameralik Dykes at the locality where samples OGG 229 to OGG 232 were collected, and their absence here, this material looks much more like some of the Amîtsoq Gneiss which we have seen previously.

SAMPLE OGG 233: Map 1 (blasted sample)
This is a sample of the dark, mafic gneiss. It is very homogeneous, moderately deformed, and strongly recrystallized.

SAMPLE OGG 234: Map 1 (collected with sledge hammer)
This is a sample of ultramafic rock collected from the core of an inclusion about 2.5 m in diameter.

Went to the big island east of Qagississagdlit and collected samples OGG 235 and OGG 236. There are two lithologically

distinct types of Amîtsoq Gneiss here. First is a highly foliated, relatively mafic gneiss with numerous inclusions of amphibolite. Second is almost a granite which occurs in sheets and appears to be interlayered with the first type. It is also in the granitic gneiss that broken and moderately deformed Ameralik Dykes occur.

SAMPLE OGG 235: Map 3 (plug and feather sample)
This is a sample of one of the granitic gneiss layers. The particular layer from which this sample was collected can be traced about 20 m north where Ameralik Dykes are present, therefore, this must be Amîtsoq Gneiss.

SAMPLE OGG 236: Map 3 (plug and feather sample)
There are in the area some granite sheets which cut across the highly foliated, biotite-rich gneiss. They cut across foliation and have blocks of the foliated gneiss incorporated into them. I could not trace this type of granitic material into the granitic material which is interlayered with the foliated, biotite-rich gneiss.

11 August, 1973

Sailed to Kigssavaussat to look at and collect Amîtsoq Gneiss. In general the gneiss here is highly contorted and deformed granitic gneiss, similar to sample OGG 231. Again this is very different from the Amîtsoq Gneiss seen with V. R. McGregor at Kanajorssuit. There are some large (up to 1 m thick) pegmatites which cut the gneiss and are relatively undeformed. In general, however, the more common type of pegmatite is thin bands or sheets, moderately deformed, but not conformable with the foliation in the gneiss.

The pegmatites conformable with the foliation of the gneiss are strongly boudinaged. We collected four samples here, OGG 162 to OGG 165.

SAMPLE OGG 162: Map 3 (collected with sledge hammer)
This is a hand-specimen sample of the typical gneiss from this locality.

SAMPLE OGG 163: Map 3 (collected with sledge hammer)
This is a hand-specimen sample of mafic gneiss not as typical of this site as is sample OGG 162.

SAMPLE OGG 164: Map 3 (collected with sledge hammer)
This sample is almost identical to sample OGG 163, but it was collected about 100 m to the west of where sample OGG 163 was collected.

SAMPLE OGG 165: Map 3 (plug and feather sample)
This is a sample of the typical, highly deformed granitic gneiss.

After lunch sail to Amîtsoq.

The rocks here are highly contorted gneisses. The constituents are however predominantly Ameralik Dykes (?) broken up by pegmatites and aplite sheets. These pegmatites and aplites constitute 40% to 50% of the rocks along the west coast of the harbour just east of Amîtsoq. We didn't collect any large samples because we weren't sure of the stratigraphic relationships. Whether this rock

is really Amîtsoq Gneiss I don't know, but after visiting Ugpik I think that it must be a massive Ameralik Dyke (?) swarm.

SAMPLE OGG 166: Map 3 (collected with sledge hammer)
This is a sample of one of the massive Ameralik Dykes (?) at Amîtsoq.

12 August, 1973

Sail to Ugpik. The rocks at Ugpik are much different from those at Amîtsoq which is close by. Here the rocks are generally intermediate-composition gneisses, strongly banded (pegmatite-banded gneisses) and often strongly folded and contorted. There are a few very wide, relatively undeformed Ameralik Dykes (up to about 10 m wide). Inclusions of amphibolite are generally small (less than 1 m in diameter) and are rare. Ultramafic inclusions were not observed. Late-stage, undeformed pegmatites (about 1 m thick) are present, but again they are not common. There are some layers, approximately 1 m thick, of more mafic gneiss which is similar to the Amîtsoq Gneiss samples OGG 129 and OGG 130. We collected five samples here.

SAMPLE OGG 167: Map 3 (collected with sledge hammer)
This is a sample of one of the thick Ameralik Dykes.

SAMPLE OGG 168: Map 3 (plug and feather sample)
This is a sample of the typical pegmatite-banded gneiss at Ugpik. There were no Ameralik Dykes observed nearby this sample. Small broken up Ameralik Dykes which are rather typical of the other

Amîtsoq Gneiss localities are absent in this area. This sample is a massive gneiss which is not strongly foliated. The strongly foliated gneiss is slightly more common in the immediate area.

SAMPLE OGG 169: Map 3 (plug and feather sample)
This is a sample of the more mafic gneiss in the area. It is rather rare at this site and is similar to gneiss samples OGG 129 and OGG 130.

SAMPLE OGG 237: Map 3 (plug and feather sample)
This is a sample of pegmatite-banded gneiss similar to sample OGG 169, but somewhat more biotite rich. This sample is also more strongly foliated than sample OGG 169. The sample is not very fresh.

SAMPLE OGG 238: Map 3 (collected with sledge hammer)
This is a sample of granitic or aplitic material from a layer adjacent to the layer from which sample OGG 169 was collected. The layer from which sample OGG 169 was collected is about 1 m thick and the layer from which this sample was collected is about 1/2 m thick. There are no apophyses of this material injected into the OGG 169 sample layer.

Sail to Godthåb and spend the night of 12 August in Godthåb.

13 August, 1973

Sent R. Kieckheffer with the Jens Jarl to Midgaard to bring back the rest of the samples from Majorqap qâva anorthosite complex.

R. F. Dymek and I worked in the quarries in Godthåb collecting Nûk Gneiss.

14 August, 1973

Collected nine samples in the Godthåb quarry.

SAMPLE OGG 239: Map 3 (blasted sample)

This is a sample of mafic Nûk Gneiss. It is a biotite-rich, relatively coarse-grained gneiss with weak foliation.

SAMPLE OGG 240: Map 3 (blasted sample)

This is a sample of quartzofeldspathic Nûk Gneiss. This is one of the most biotite-deficient rock types in the quarry.

SAMPLE OGG 241: Map 3 (blasted sample)

This is a sample of highly foliated, relatively biotite-rich Nûk Gneiss.

SAMPLE OGG 242: Map 3 (blasted sample)

This is a sample of the most mafic-rich Nûk Gneiss seen in the quarry. There is a small pegmatite on one corner of the approximately 1 m block from which the sample was collected.

SAMPLE OGG 243: Map 3 (blasted sample)

This sample is a hand-specimen sample of the pegmatite attached to sample OGG 242.

SAMPLE OGG 244: Map 3 (blasted sample)

This is a sample of the most biotite-poor Nûk Gneiss in the quarry.

SAMPLE OGG 245: Map 3 (blasted sample)

This is a sample of either allanite or zircon pegmatite cutting the Nûk Gneiss in the quarry. The pegmatite cuts the foliation in the gneiss and is itself little deformed.

SAMPLE OGG 246: Map 3 (blasted sample)

This is a sample of the contact between the pegmatite (sample OGG 245) and the Nûk Gneiss.

SAMPLE OGG 247: Map 3 (blasted sample)

This is a sample of a mafic inclusion in the Nûk Gneiss. This is a typical inclusion, but in general inclusions are rare in the quarry.

15 August, 1973

Bad weather. Stayed in Godthåb. Jens Jarl is returning from Fiskenaesset.

16 August, 1973

Unloaded and packed barrels all day.

17 August, 1973

Sailed at 9:30 a.m. for Praestefjord to collect Amîtsoq Gneiss.

This Amîtsoq Gneiss locality is very nearby the locality visited previously with V. R. McGregor. The rocks are generally homogeneous, moderately to highly deformed gneiss. Inclusions of amphibolite and ultramafic rock are rare. Undeformed sheets of "granitic material" are common. Collected two samples.

SAMPLE OGG 248: Map 3 (blasted sample)

This is a sample of Amîtsoq Gneiss. Nearby is an Ameralik Dyke which is broken up. The dyke contains anorthosite fragments.

SAMPLE OGG 249: Map 3 (blasted sample)

This is a sample of the "granite" sheet. The granite is often pegmatitic in places. The contact between the "granite" sheet and the Amîtsoq Gneiss is very sharp. The sheet of granite is 2 to 3 m wide.

18 August, 1973

Sail to collect Amîtsog Gneiss along the north coast of Praestefjord.

Stopped and collected three samples.

SAMPLE OGG 250: Map 3 (plug and feather sample)

This is a sample of Amîtsoq Gneiss. It was collected from a block of rock not in place, but obviously from the slope just above. It is typical Amîtsoq Gneiss, although it is not as intensely deformed as sample OGG 248. It is also more quartzofeldspathic than sample OGG 248.

SAMPLE OGG 251: Map 3 (plug and feather sample)

This is a sample of Amîtsoq Gneiss. It is relatively undeformed (i.e. not convoluted). The sample was collected adjacent to a granite sheet intruded parallel to the foliation of the gneiss. The sheet is about 20 cm thick and follows the strike of the outcrop for about 25 m.

SAMPLE OGG 252: Map 3 (collected with sledge hammer)

This is a hand-specimen sample of a "gabbroic" inclusion in the Amîtsoq Gneiss. Inclusions of this material are rare and the few blocks seen are 1 to 2 m in diameter.

Sailed to the tip of the north coast of Praestefjord and collected a sample.

SAMPLE OGG 253: Map 3 (blasted sample)

This is a sample of highly convoluted Amîtsoq Gneiss which is cut by undeformed Ameralik Dykes.

19 August, 1973

Sailed across Ameralik to collect a sample of Amîtsoq Gneiss.

SAMPLE OGG 254: Map 3 (blasted sample)

This is a sample of highly convoluted, quartzofeldspathic, pegamtite-banded Amîtsoq Gneiss. The pegmatite bands are folded parallel to the foliation and contain large feldspar megacrysts. This is the site of V. R. McGregor's triply folded Ameralik Dyke.

22 August, 1973

Collected Nûk Gneiss in the area near the new tunnel, Nordhavn, Godthåb.

SAMPLE OGG 255: Map 3 (blasted sample)

This is a sample of Nûk Gneiss.

SAMPLE OGG 256: Map 3 (blasted sample)

This is a sample of Nûk Gneiss filled with pyrite.

Part II

EARTH AND PLANETARY SCIENCE LETTERS 12 (1971) 1–18. NORTH-HOLLAND PUBLISHING COMPANY

PETROLOGIC AND MINERALOGIC INVESTIGATION OF SOME CRYSTALLINE ROCKS RETURNED BY THE APOLLO 14 MISSION*

A.J.GANCARZ, A.L.ALBEE and A.A.CHODOS
The Lunatic Asylum of the Charles Arms Laboratory
Division of Geological and Planetary Sciences,
California Institute of Technology,
Pasadena, California 91109, USA

Received 4 August 1971
Revised version received 11 August 1971

Apollo 14 crystalline rocks (14053 and 14310) and crystalline rock fragments (14001,7,1; 14001,7,3; 14073; 14167,8,1 and 14321,191,X-1) on which Rb/Sr, ^{40}Ar-^{39}Ar, or cosmic ray exposure ages have been determined by our colleagues were studied with the electron microprobe and the petrographic microscope. Rock samples 14053 and 14310 are mineralogically and petrologically distinct from each other. On the basis of mineralogic and petrologic characteristics all of the fragments, except 14001,7,1, are correlative with rock 14310. Sample 14073 is an orthopyroxene basalt with chemical and mineralogic affinities to 'KREEP', the 'magic' and 'cryptic' components. Fragment 14001,7,1 is very similar to Luny Rock I.

1. Introduction

As described by the Apollo 14 Preliminary Examination Team, fragmental rocks with complex textural relationships predominate in the Apollo 14 samples [1]. Out of the total 43 kg sample returned the only crystalline rocks which weigh over 50 g are 14053 (251 g) and 14310 (3439 g). However, smaller samples of crystalline rock were returned and are also available as fragments in the soil samples and as clasts within the breccia samples.

In this study we describe the petrology and mineralogy of seven crystalline samples, on which Rb/Sr, ^{40}Ar-^{39}Ar, or cosmic ray exposure ages have been determined [2,3]. These isotopic investigations indicate the existence of two rock groups characterized by different crystallization and cosmic ray exposure ages. Data on the various samples are summarized in table 1. The purpose of this study is to characterize the dated samples petrographically and to identify any differences which might permit the correlation of other individual lithic fragments with the dated fragments.

* Contribution no. 2048.

2. Analytical techniques

The analyses were made with a Materials Analysis Corporation model 5-SA3 electron microprobe interfaced with a PDP-8/L computer. Peak and background counting for up to 15 elements, online data processing and examination of the data was done on each spot. Consequently, relocation of the spot was not required. Standard operating conditions were 15 kV with beam current integration and pulse height selection. Immediately prior to each quantitative analysis programmed peak searches for Si, Al and Mg were run on the spot to be analyzed. Silicates, oxides, and phosphates were analyzed for most elements relative to a set of simple silicates, oxides, and phosphates using the general technique of Bence and Albee [4] and the interelement correction factors of Albee and Ray [5].

Table 1
Summary of sample data from Apollo 14 Preliminary Science Report [1], Turner et al. [3], Papanastassiou and Wasserburg [2].

Sample	Subnumber	Nature	Location	Weight	^{38}Ar-^{37}Ar exposure age	^{40}Ar-^{39}Ar age	Rb/Sr age	$(^{87}Sr/^{86}Sr)_I$
14310	slide 6	basalt grab sample	'smooth region'	3439 g	300 my	3.89 AE	3.87 AE	0.70036
14053	slide 17	basalt grab sample	Cone Crater rim	251 g	≤30	3.93	3.96	0.69948
14073	slide 8	basalt pebble from trench	'smooth region'	10 g			3.88	0.70034
14001		coarse fines, contingency sample	'smooth region'					
	14001,7,1	vesicular clast		0.062 g	590	3.87	4.30(model age)	
	14001,7,3	basalt clast		0.088 g	260	3.90	3.89	0.70036
14167		coarse fines, comprehensive sample	'smooth region'					
	14167,8,1	basalt		0.067 g	29	3.94		
14321	191,X-1	breccia basalt clast	Cone crater rim	0.16 g			3.95	0.69942
	144,1	composite of light-colored basalt clasts		0.072 g	≤30	3.92		
	144,F	composite of dark-colored clasts			≤40	3.93		

However, pure metals were used as standards for analyzing U, Th and Pb and alloys were used as standards for the metal phase. The accuracy of the analyses is about 2 or 3% for oxides constituting more than 5 wt % of the sample.

Polished thin sections (14310,6; 14053,17;14073,8) were provided by the curator of the lunar samples. The other samples were studied in micro-thin sections prepared from portions of the fragments used for the isotopic investigations [2,3]. These sections had an area of less than 1 mm^2. In addition, grain mounts were made of the 'quintessence' separates prepared for the Rb/Sr measurements. Sample heterogeneity is a problem for all samples since it is possible that neither the large thin sections nor the micro-thin sections fully represent the entire sample used for isotopic work.

The sections were studied by both optical and electron microprobe techniques. All analyzed points were examined optically and use of the term glass for an analysis indicates that the analyzed point was isotopic and contained relatively few inclusions. However, identification of apatite and whitlockite is based on the composition [6,7].

3. Sample descriptions

All seven studied samples are basalts, but they exhibit marked differences in texture, composition, mineralogy, and shock features. As pointed out by the Preliminary Examination Team [1], the two largest samples (14310 and 14053) are distinctly different. Of the five other samples studied four are similar in many respects to sample 14310 and may be correlative, whereas one differs from both 14310 and 14053. Sys-

Table 2
Phases present in the analyzed samples.

	Sample						
	14001,7,1	14001,7,3	14053,17	14073,8	14167,8,1	14310,6	14321,191 X-1
Iron metal	x	x	x	x	x	x	x
Troilite	x	x	x	x	x	x	x
Zircon	?	–	–	–	–	x	–
Baddeleyite	–	–	–	–	–	x	–
Rutile	?	–	?	–	–	–	–
Ilmenite	2	x	(3)	(2)	x	(3)	x
Chromian ulvospinel	?	–	x	NO	–	NO	–
Apatite	NO	x	x	x	–	x	x
Whitlockite	(3)	x	x	x	–	x	NO
Cristobalite	NO	NO	(2)	NO	NO	NO	NO
Olivine	NO	NO	x	NO	(30)	x	NO
Clinopyroxene		(20)	(50)	(25)	(30)	(40)	(25)
Augite	x	x	x	x	x	x	x
Pigeonite	x (45)	x	x	x	x	x	?
Orthopyroxene	x	NO	NO	(20)	NO	NO	NO
Plagioclase	x	(75)	(40)	(50)	(35)	(50)	(70)
K-Ba feldspar	x (55)	–	?	–	–	–	–
Glass	?	x	x	x	x	x	x
U-Th-rich phase	–	x	NO	–	–	x	–
Fe-Ti-Zr silicate	–	x	NO	x	NO	x	NO
Vugs	x	–	x	–	–	x	–

( ) = estimated modal proportion.
x = present.
NO = not observed.
– = not observed, but looked for systematically.
? = identification not positive.

tematic descriptions of the samples are presented as a basis for comparison of the samples in a later section.

3.1. *Sample 14053*

Sample 14053 was collected as a grab sample near the rim of Cone Crater and weighed 251 g [8]. It was studied in polished thin section 14053,17, which has an area of about 50 mm^2.

This section is of an ophitic basalt composed predominantly of plagioclase (40%), clinopyroxene (50%) with minor ilmenite (3%), cristobalite (2%), troilite, Fe-metal, mesostasis and other minor phases (table 2). Vugs partially filled with plagioclase, pyroxene and ilmenite are present [9]. No olivine cores were found in the pyroxene, although such cores have been reported in this sample [1].

As is shown in plate Ia the texture is a true ophitic texture with interlocking stubby laths of plagioclase (~0.5 mm long) enclosed in pyroxene grains ranging in length to 2 mm. Ilmenite and cristobalite grains occur both enclosed by pyroxene grains and as large interstitial grains.

Plagioclase occurs as stubby laths exhibiting polysynthetic twinning and marked zoning. Analyses of one grain indicated a compositional variation from $An_{90}Ab_{10}$ in the core to $An_{77}Ab_{21}Or_2$ on the rim (table 3, #3–#4).

Clinopyroxene occurs as large crystals optically exhibiting pronounced compositional zoning, compositional and structural discontinuities, and mosaic structure. The mosaic structure is like that seen in pyroxene in the Apollo 11 rocks [6,10] and is probably not a shock effect. The compositional variation in the pyroxene is extreme and will surely excite the pyrox-

Table 3
Representative electron probe analyses of plagioclase feldspar.

wt %	14001,7,1 rep. #1	14001,7,3 av. 7 #2	14053,17 core #3	14053,17 rim #4	14073,8 av. 7 #5	14167,8,1 av. 5 #6	14310,6 av. 6 #7	14321,191, X-1 rep. #8
Na_2O	2.08	0.64	1.14	2.35	0.61	0.76	0.70	0.75
MgO	<0.01	0.14	0.24	0.08	0.13	0.14	0.10	0.24
Al_2O_3	32.14	34.97	35.13	31.74	34.92	34.17	35.53	33.97
SiO_2	49.58	44.61	46.08	49.70	44.75	45.18	44.87	45.28
K_2O	0.44	0.06	0.04	0.39	0.08	0.22	0.10	0.03
CaO	15.36	19.82	18.54	15.76	19.22	18.05	19.01	19.28
FeO	0.06	0.19	0.32	0.83	0.19	0.44	0.36	0.18
BaO	<0.01	0.04	<0.01	0.02	0.13	<0.06	0.01	<0.01
Total ≡	99.66	100.47	101.49	100.87	100.03	99.02	100.68	99.73
			Formula proportions					
Na	0.19	0.06	0.10	0.21	0.05	0.07	0.06	0.07
Mg	<0.01	0.01	0.02	<0.01	0.01	0.01	0.01	0.02
Al	1.74	1.90	1.88	1.70	1.90	1.88	1.92	1.85
Si	2.28	2.05	2.09	2.26	2.07	2.11	2.06	2.10
K	0.03	<0.01	<0.01	0.02	<0.01	0.01	0.01	<0.01
Ca	0.76	0.98	0.90	0.77	0.95	0.90	0.93	0.96
Fe	<0.01	0.01	0.01	0.03	0.01	0.02	0.01	0.01
Ba	<0.01	<0.01	<0.01	<0.01	<0.01	<0.01	<0.01	<0.01
	5.00*	5.00*	5.00*	5.00*	5.00*	5.00*	5.00*	5.00*

* Normalization factor for catatoms.

ene specialist to a highly energetic state. As shown on fig. 1 and table 4 (#3–#6) magnesium pigeonite cores ($Wo_{10}Fs_{35}En_{55}$) are enclosed by augite ($Wo_{25}Fs_{45}En_{30}$), which grades to ferroaugite ($Wo_{25}Fs_{65}En_{10}$) and then to ferrohedenbergite ($Wo_{40}Fs_{55}En_5$). The ferrohedenbergite is on the rim of the grain adjacent to a mesostasis containing olivine ($Fa_{95}Fo_5$), cristobalite, troilite, Fe-metal, ilmenite, SiO_2-rich glass, and possibly fibers of K_2O-BaO-rich feldspar. Such marked Fe enrichment with progressive crystallization is more typical of the Apollo 11 pyroxenes than of the Apollo 12 pyroxenes.

Opaque minerals occur as large anhedral grains (up to 0.5 mm) throughout the rock as well as in the mesostasis. Analysis #20 in table 4 is of a typical anhedral grain of ilmenite. Ilmenite also occurs as smaller crystals enclosed within pyroxene, suggesting that entrapment occurred while growth continued.

Anhedral grains of chromian ulvöspinel contain exsolution lamellae of ilmenite to 2μ thick and plates of metallic iron parallel to the octahedral planes. The ulvöspinel and ilmenite lamellae are similar to the coexisting pairs observed in the Apollo 12 rocks [11] (table 4, #21–#22). The ilmenite lamellae are much higher in Cr and Mg than the anhedral ilmenite (table 4, #20–#21). Ilmenite grains also contain rare lamellae (<0.1μ) which electron beam scans indicate are rutile.

Fe-metal occurs as globules encased in troilite and as discrete grains. The Ni content of the Fe-metal ranges from 0.1 to 4 wt % (fig. 2).

The mesostasis in this sample is extremely complex.

Plate Ia. Photomicrograph of section 14053,17 (crossed nicols). 1 cm = 220 μm.

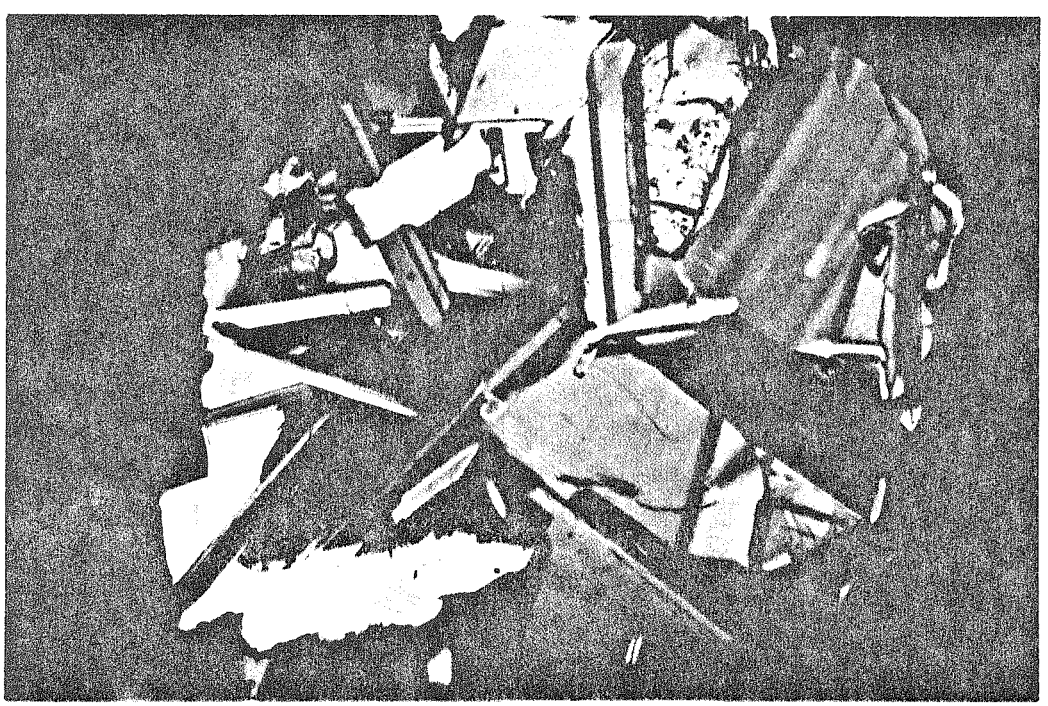

Plate Ib. Photomicrograph of section 14001, 7, 3 (crossed nicols). 1 cm = 110 μm.

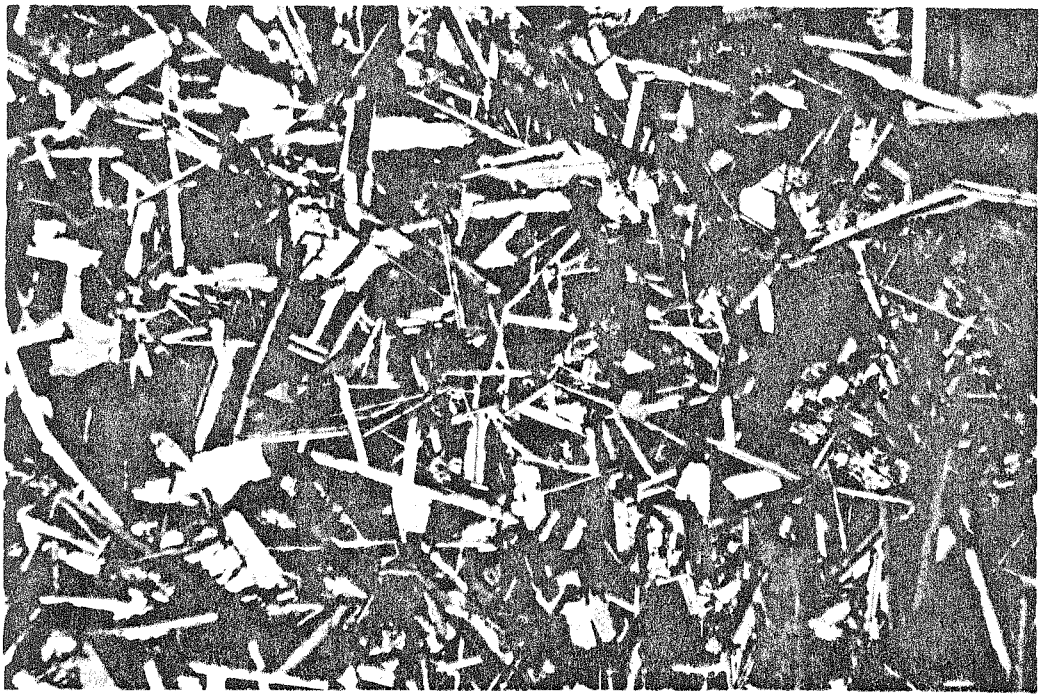

Plate IIa. Photomicrograph of section 14310,6 (crossed nicols). 1 cm = 220 μm.

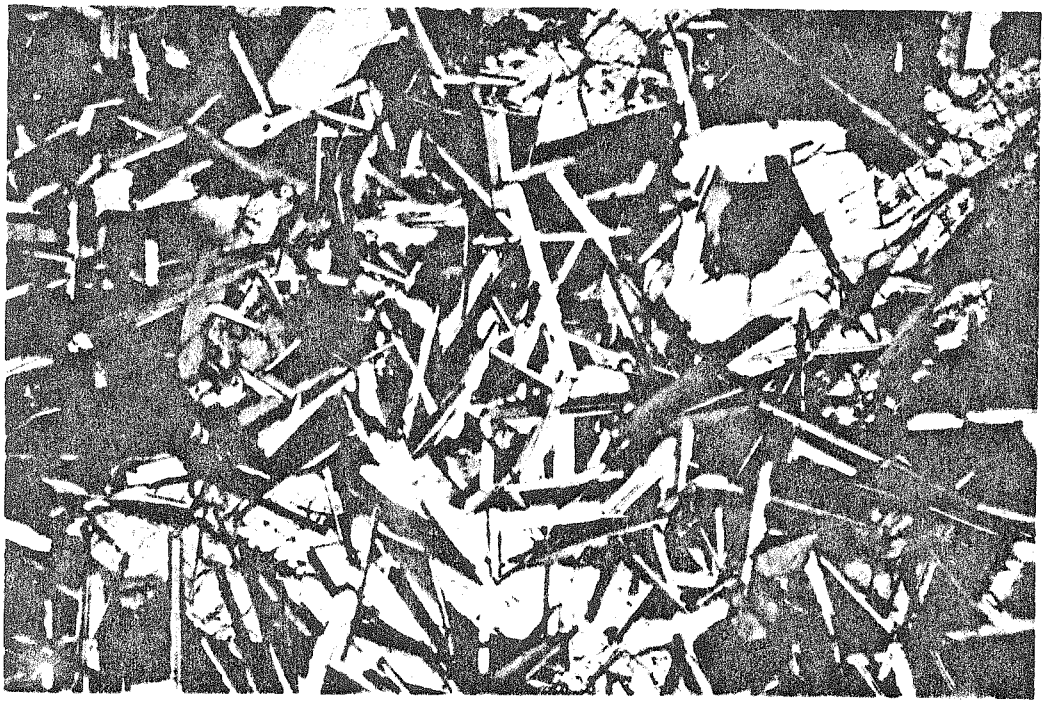

Plate IIb. Photomicrograph of section 14073,8 (crossed nicols). 1 cm = 110 μm.

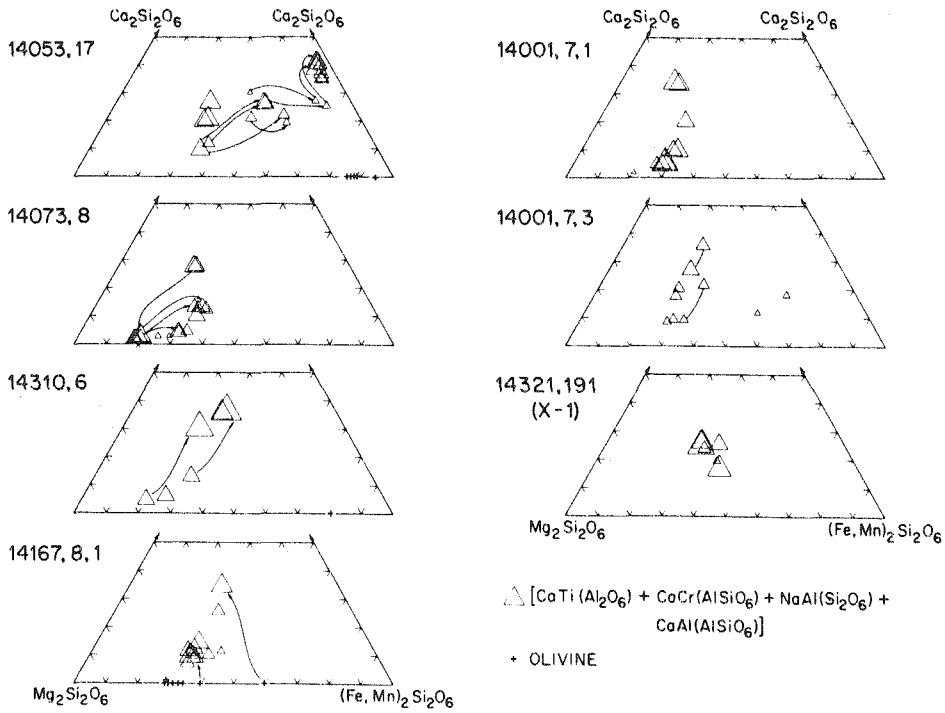

Fig. 1. Composition of pyroxenes from the studied samples. Solid lines indicate coexisting pairs of pyroxene and arrows indicate compositional variations from the core to the rim in a single grain. The size of the triangles is as indicated and discussed in the text (sect. 3.8). Note that only the pyroxenes from sample 14053,17 show extensive Fe enrichment.

It includes mosaic grains of cristobalite, phosphate minerals, SiO_2-rich glass, fayalite, ilmenite, troilite, Fe-metal, and possibly tiny fibers of K_2O-BaO feldspar. Troilite and Fe-metal commonly occur in peculiar spongy masses, not abundant in other lunar rocks (fig. 3). These complex mesostasis areas are also shown in plate Ia. Within one area of mesostasis is a 150μ single crystal of olivine ($Fa_{87}Fo_{13}$; table 4, #15) enclosing masses of the spongy troilite, Fe-metal and elongate globules ($<1\mu$) of SiO_2-rich glass (fig. 4; table 5). Furthermore, a small vesicle ($<0.1\mu$) is associated with each of the SiO_2-rich inclusions. These textural relationships strongly suggest late stage silicate melt immiscibility, as studied in detail by Roedder and Weiblen [12]. A colorless glass containing needles of phosphate minerals commonly occurs enclosed in ilmenite, but in sizes too small to analyze.

3.2. *Sample 14310*

Sample 14310 was a 3439 g grab sample collected from the 'smooth region' away from Cone Crater and was described by the Preliminary Examination Team [1]. It was studied in polished thin section 14310,6, which has an area of about 250 mm^2. The section is of a subophitic, intergranular to intersertal, basalt composed predominantly of plagioclase (50%) and clinopyroxene (40%), with minor ilmenite, troilite, Fe-metal, mesostasis, and other minor phases (table 2). Vugs or mesostasis lost during preparation of the thin section comprise nearly 5% of the slide. Although the volumetric percentage of vugs is uncertain, they are present and are partially filled with euhedral plagioclase, pyroxene and ilmenite crystals [9].

The texture is quite distinct from most of the Apollo 11 and 12 samples and distinct from thin sec-

Table 4
Representative electron probe analyses of pyroxene, olivine, and Fe-Ti-Cr oxides.

Pyroxene

wt%	14001,7,3 #1	14053,17 #2	#3 core	#4	#5	#6 rim	14073,8 #7	#8 core	#9	#10 rim	14167,8,1 #11
SiO_2	47.91	50.44	50.90	48.69	46.13	45.32	51.12	54.56	53.03	51.85	51.23
Al_2O_3	1.04	2.02	1.24	1.20	0.75	1.68	2.16	2.25	1.50	1.52	2.12
Cr_2O_3	0.10	0.65	0.56	0.32	0.11	0.02	0.66	0.48	0.40	0.36	0.84
TiO_2	0.80	1.34	0.93	1.09	0.98	1.62	1.25	0.47	0.85	0.85	0.72
CaO	8.73	13.31	5.98	12.71	11.28	18.24	14.52	1.82	2.42	6.70	5.40
MgO	6.98	14.70	17.85	8.62	2.20	0.57	16.68	29.15	23.41	19.35	20.14
FeO	34.71	16.62	21.48	26.54	36.60	30.32	14.12	11.93	18.83	18.42	19.79
MnO	0.47	0.27	0.37	0.43	0.50	0.30	0.28	0.27	0.27	0.39	0.36
Na_2O	0.12	0.11	0.05	0.07	0.03	0.07	0.14	0.01	0.02	0.07	0.03
K_2O	0.05	0.02	0.03	<0.01	0.03	0.04	<0.01	0.03	<0.01	<0.01	0.02
Total	100.91	99.48	99.39	99.67	98.61	98.18	100.93	100.97	100.73	99.51	100.65
Atomic proportions											
Si	1.93	1.92	1.94	1.94	1.96	1.91	1.90	1.92	1.94	1.94	1.90
Al	0.05	0.09	0.06	0.06	0.04	0.08	0.09	0.09	0.06	0.07	0.09
Cr	<0.01	0.02	0.02	0.01	<0.01	<0.01	0.02	0.01	0.01	0.01	0.02
Ti	0.02	0.04	0.03	0.03	0.03	0.05	0.03	0.01	0.02	0.02	0.02
Ca	0.38	0.54	0.24	0.54	0.51	0.83	0.58	0.07	0.09	0.27	0.21
Mg	0.42	0.84	1.01	0.51	0.14	0.04	0.92	1.53	1.28	1.09	1.11
Fe	1.17	0.53	0.69	0.89	1.30	1.07	0.44	0.35	0.58	0.58	0.62
Mn	0.02	0.01	0.01	0.01	0.02	0.01	0.01	0.01	<0.01	0.01	0.01
Na	0.01	0.01	<0.01	0.01	<0.01	0.01	0.01	<0.01	<0.01	<0.01	<0.01
	4.00*	4.00*	4.00*	4.00*	4.00*	4.00*	4.00*	4.00*	4.00*	4.00*	4.00*

* Normalization factor for catatoms.

wt%	pyroxene 14167,8,1 #12	14310,6 #13 core	#14 rim	olivine 14053,17 #15	14167,8,1 #16	#17	14310,6 #18	ilmenite 14310,6 #19	14053,17 #20	14053,17 #21 lamellae	chromian ulvöspinel 14053,17 #22 host
SiO_2	50.31	52.23	49.29	30.50	37.09	33.54	31.89	0.39	0.16	0.18	0.22
Al_2O_3	1.31	1.73	2.62	<0.01	0.01	<0.01	0.44	0.10	0.04	<0.01	6.39
Cr_2O_3	0.38	0.58	0.37	0.03	<0.01	0.08	0.02	0.38	0.29	1.14	23.06
TiO_2	1.35	0.90	2.48	0.09	0.08	0.17	0.22	52.66	50.75	52.48	20.46
CaO	16.41	6.72	17.46	0.39	0.23	0.23	0.30	0.12	0.03	0.11	0.02
MgO	11.78	19.76	11.63	5.13	35.29	17.96	8.39	0.83	0.29	3.85	3.17
FeO	15.95	17.86	15.87	60.42	28.05	47.60	58.26	44.62	46.27	42.42	46.32
MnO	0.37	0.26	0.28	1.78	0.32	0.55	0.56	0.32	0.62	0.41	0.59
Na_2O	0.18	0.06	0.13	0.01	0.01	0.01	0.03	<0.01	<0.01	<0.01	<0.01
K_2O	0.10	<0.01	0.02	<0.01	0.01	0.17	0.11	0.03	<0.01	<0.01	<0.01
Total	98.14	100.10	100.15	98.35	101.09	100.31	100.22	99.45	98.45	100.59	100.23

Table 4 (continued)

Atomic proportions

Si	1.96	1.95	1.89	1.01	0.98	0.99	1.01	0.01	<0.01	<0.01	<0.01
Al	0.06	0.08	0.12	<0.01	<0.01	<0.01	0.02	<0.01	<0.01	<0.01	0.18
Cr	0.01	0.02	0.01	<0.01	<0.01	<0.01	<0.01	0.01	0.01	0.02	0.43
Ti	0.04	0.03	0.07	<0.01	<0.01	<0.01	0.01	1.00	0.98	0.96	0.36
Ca	0.69	0.27	0.72	0.01	0.01	0.01	0.01	<0.01	<0.01	<0.01	<0.01
Mg	0.69	1.10	0.66	0.25	1.39	0.79	0.40	0.03	0.01	0.14	0.11
Fe	0.52	0.56	0.51	1.68	0.62	1.18	1.54	0.94	0.99	0.86	0.91
Mn	0.01	0.01	0.01	0.05	0.01	0.01	0.01	0.01	0.01	0.01	0.01
Na	0.02	<0.01	0.01	<0.01	<0.01	<0.01	<0.01	<0.01	<0.01	<0.01	<0.01
	4.00*	4.00*	4.00*	3.00*	3.00*	3.00*	3.00*	2.00*	2.00*	2.00*	2.00*

* Normalization factor for catatoms.

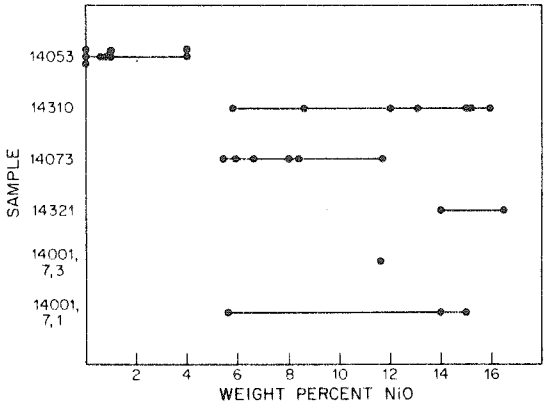

Fig. 2. Variation of the Ni content in Fe-metal grains from the studied samples. The Fe-metal in sample 14053 has a distinctly lower Ni content than in any of the other samples.

tion 14053,17 (compare plates Ia and IIa). Euhedral plagioclase laths (~0.5 mm long) form an interlocking or felted framework, the interstices of which contain anhedral pyroxene grains (~0.3 mm) and mesostasis. Locally the plagioclase laths are in radial aggregates or in finer-grained patches which may represent cognate inclusions [1]. In some areas the pyroxene grains are large, and an ophitic texture is developed.

The plagioclase grains are polysynthetically twinned parallel to the laths and less commonly normal to the laths. Zoning is not pronounced and the composition is typically $An_{93}Ab_6Or_1$ (table 3, #7).

Relatively little variation in clinopyroxene composition is evident optically, but some grains have pigeonite cores and augite rims. The compositions of pigeonite cores (table 4, #13) and their augite rims (table 4, #14) do not show extensive variation in Fe/Mg. The most Fe-rich core, shown on fig. 1, has a composition very close to that of orthopyroxene, but optical properties indicate that it is pigeonite.

Opaque phases include ilmenite, troilite, and Fe-metal. Although reported by the Preliminary Examination Team [1], neither chromian spinel nor ulvöspinel were found. Fe-metal has a Ni content ranging from 6 to 16 wt% (fig. 2) and occurs not only associated with troilite, but also independently.

The mesostasis is a complex of fine-grained material, including apatite, whitlockite, opaque phases, olivine and glass. An analysis of the whitlockite is included in table 6, and the composition of the fayalitic olivine is shown in table 4, #18. The glass has a wide range in composition (table 5; fig. 4) and will be discussed separately.

3.3. *Sample 14073*

Sample 14073 was a 10 g basalt pebble which was collected in the bottom of the trench dug in the 'smooth region' away from Cone Crater [8]. However, since part of the trench collapsed it is uncertain

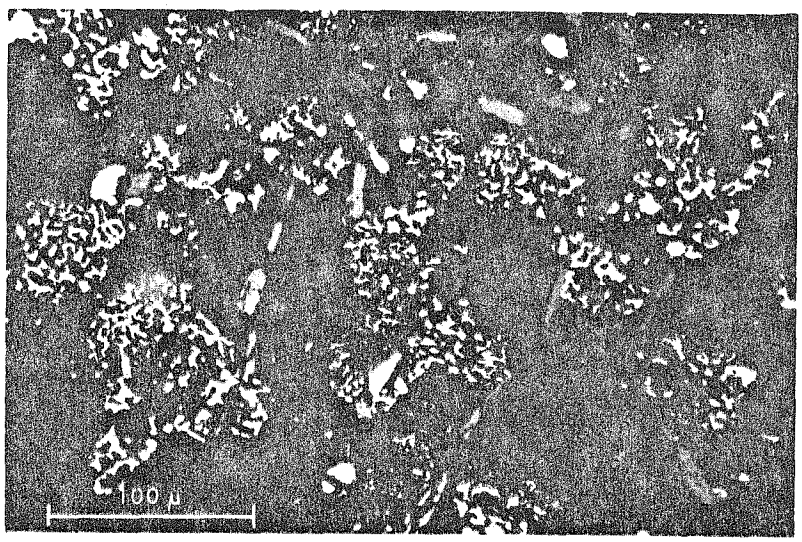

Fig. 3. Photomicrograph of the peculiar spongy masses of Fe-metal and troilite in sample 14053,17 (reflected light). The darker grey laths are ilmenite.

Table 5
Representative electron probe analyses of glass.

	14310,6 average of 5	14310,6 average of 2	14053,17 average of 3	14053,7 globule in olivine
Na_2O	1.00	0.60	0.32	0.06
MgO	0.01	0.05	0.02	0.04
Al_2O_3	19.82	13.94	11.82	11.88
SiO_2	61.32	77.02	75.87	82.85
K_2O	12.63	6.50	7.97	2.10
CaO	0.77	0.63	1.14	1.01
FeO	0.23	0.99	1.94	1.38
BaO	3.99	0.23	0.45	0.20
Total	99.77	99.96	99.53	99.52
	Normative minerals in catatom per cent			
or	76.50	39.65	49.05	13.10
ce*	7.40	0.45	0.85	0.40
ab	9.20	5.55	3.00	0.55
an	3.90	3.20	5.90	5.35
C	0.52	5.21	0.33	8.69
en	0.02	0.14	0.06	0.12
fs	0.36	1.58	3.14	2.26
Q	2.09	44.21	37.68	69.54
Total	100.00	100.00	100.00	100.00

* $BaAl_2Si_2O_8$.

Table 6
Electron probe analyses of phosphate minerals.

Apatite

	14053,17		14001,7,3		14321,191,X-1		14073,8	
	wt%	atom prop.*	wt%	atom prop.*	wt%	atom prop.*	wt%	atom prop.*
F	3.11	0.85	3.96	1.08	3.14	0.86	3.03	0.86
Cl	0.07	0.10	0.04	0.01	0.41	0.06	0.06	0.01
SiO_2	1.33	0.11	0.40	0.03	2.62	0.23	1.01	0.09
P_2O_5	39.79	2.90	40.56	2.96	37.66	2.78	37.90	2.86
Na_2O	<0.01	<0.01	<0.01	<0.01	<0.01	<0.01	<0.01	<0.01
MgO	<0.01	<0.01	<0.01	<0.01	<0.01	<0.01	<0.01	<0.01
CaO	53.79	4.96	53.95	4.99	52.70	4.92	52.45	5.01
FeO	0.15	0.01	0.01	0.01	0.54	0.04	0.11	0.01
Al_2O_3	<0.01	<0.01	<0.01	<0.01	<0.01	<0.01	0.03	<0.01
Y_2O_3	0.39	0.02	0.20	<0.01	0.64	0.03	0.50	0.03
La_2O_3	<0.01	<0.01	<0.01	<0.01	<0.01	<0.01	<0.01	<0.01
Ce_2O_3	<0.01	<0.01	<0.01	<0.01	0.12	<0.01	<0.01	<0.01
Nd_2O_3	<0.01	<0.01	<0.01	<0.01	<0.01	<0.01	<0.01	<0.01
Total	98.63		99.11		97.83		95.10	

* Cations normalized to 8.

Whitlockite

	14053,17		14001,7,3		14310.6		14001,7,1	
	wt%	atom prop.**	wt%	atom prop.**	wt%	atom prop.**	wt%	atom prop.**
F	<0.01	<0.01	<0.01	<0.01	<0.01	<0.01	0.03	0.01
Cl	<0.01	<0.01	<0.01	<0.01	<0.01	<0.01	0.01	<0.01
SiO_2	0.45	0.03	0.34	0.02	0.38	0.02	0.38	0.02
P_2O_5	41.45	2.01	41.96	2.07	41.78	2.04	43.65	2.01
Na_2O	<0.01	<0.01	0.18	0.02	<0.01	<0.01	0.24	0.03
MgO	1.47	0.13	0.83	0.07	1.27	0.11	2.98	0.24
CaO	40.33	2.48	41.26	2.57	40.77	2.52	42.83	2.49
FeO	2.89	0.14	3.51	0.17	3.46	0.17	1.43	0.06
Al_2O_3	<0.01	<0.01	<0.01	<0.01	<0.01	<0.01	0.04	<0.01
Y_2O_3	3.80	0.14	1.48	0.06	2.40	0.09	2.49	0.09
La_2O_3	0.43	0.01	<0.01	<0.01	0.11	<0.01	0.70	0.01
Ce_2O_3	2.53	0.05	1.47	0.03	2.37	0.05	2.27	0.04
Nd_2O_3	0.55	0.01	0.25	0.01	0.43	0.01	1.34	0.03
Total	93.90		91.28		92.97		98.39	

** Cations normalized to 5.

that it was actually buried [8]. It was studied in polished thin section 14073,8 which has an area of about 175 mm^2.

The section is of a subophitic, intergranular to intersertal, orthopyroxene basalt (plate IIb). It is composed predominantly of plagioclase (~50%) clinopyroxene (~25%) and orthopyroxene (~20%) with minor ilmenite (~2%), troilite, Fe-metal, mesostasis and other minor phases (table 2). The presence of orthopyroxene distinguishes this rock from the others studied and from the Apollo 11 and 12 samples. Despite the presence of orthopyroxene, the grain size and texture is nearly identical to that of 14310, characterized by a felted, plagioclase-lath framework and containing similar cognate inclusions (plates IIa and IIb). Locally, the pyroxene is coarser

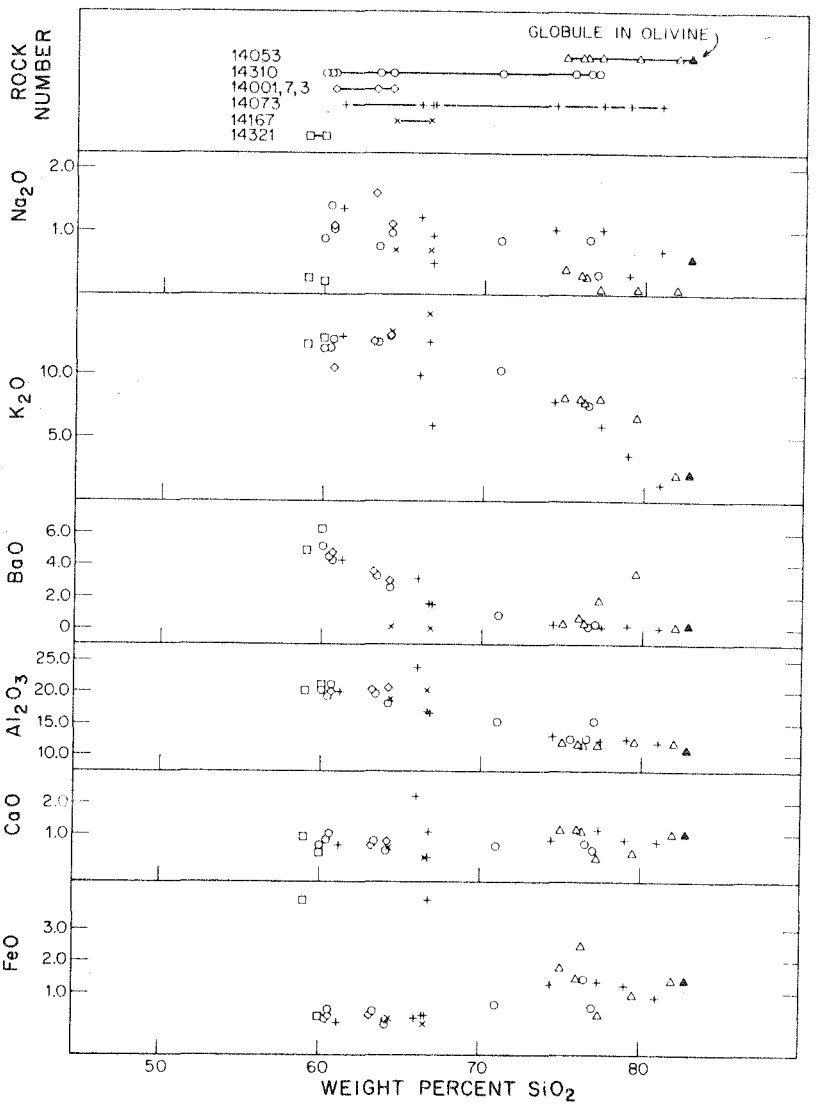

Fig. 4. Variation diagram of glass in the studied samples. Analyses are of both glass in the thin sections and glass from the 'quintessence' separates of samples 14053, 14073, and 14310.

grained enclosing the plagioclase and the texture becomes ophitic. The observed shock features are described in section 3.13.

Polysynthetic twinning parallel to the laths is common in the plagioclase. Zoning is not pronounced and the composition is typically $An_{94}Ab_5Or_1$ (table 3, #5). However, a few grains show zoning reversals at a distinct interface within the crystals.

Unlike 14310,6 nearly half the pyroxene in 14073,8 is orthopyroxene, but the compositional variation of

the pyroxene in 14310,6 and 14073,8 is grossly similar (fig. 1; table 4). Because the grains are irregular, it is difficult to discern the growth direction. However, both orthopyroxene and augite occur in some grains and in other grains orthopyroxene cores are rimmed by more Fe-rich orthopyroxene and by more Fe-rich pigeonite. As in thin section 14310,6 there does not appear to be extensive Fe/Mg variation in the clinopyroxene.

Opaque phases include ilmenite, troilite, and Fe-metal with a Ni content ranging from 5 to 12 wt% (fig. 2). The larger ilmenite grains commonly contain lensoidal inclusions of glass and associated minor phases.

The mesostasis contains opaque phases, apatite, whitlockite, and glass. The glass is predominantly brown and rich in K_2O and BaO. It exhibits a wider range in composition than in any of the other studied samples.

3.4. *Sample 14001,7,3*

Sample 7,3 was a 0.088 g fragment from the coarse fines of the contingency sample (14001,7) collected in the 'smooth region' away from Cone Crater [8]. It was studied in two micro-thin sections both with areas of about 0.25 mm^2. The fragment is an ophitic, intergranular basalt composed predominantly of plagioclase feldspar (~75%) and clinopyroxene (~20%) with minor Fe-metal, troilite, ilmenite, mesostasis and other minor phases (plate 1b; table 2). The texture is much like that of 14310, but such a fragment could be derived from selected portions of 14053,17. Mild shock features were observed both in the thin sections and in the fragment before thin section preparation. These features are discussed in sect. 3.13.

Pyroxene compositions are indicated on fig. 1 and in table 4, #1. Both augite and pigeonite are present, and substantial Fe-enrichment trends are evident (fig. 1). Plagioclase compositions are predominantly about $An_{95}Ab_5$ (table 3), but more sodic rims occur ($An_{82}Ab_{16}Or_2$).

Fe-metal is common, but only one grain was large enough for quantitative analysis and yielded a Ni content of 12 wt% (fig. 2).

Despite the small sample size, glass is so abundant as to permit its separation for isotopic investigation [2]. The glass is rich in K_2O and BaO. The chemical composition of the glass, Fe-metal, U-Th-rich phases and other minor phases is discussed in later sections.

3.5. *Sample 14321,191,X-1*

Sample X-1 is a 0.16 g fragment taken from "Big Bertha", a 8996 g breccia sample collected near Cone Crater rim [8]. It was studied in micro-thin sections with areas of 0.20 m^2 and 0.15 mm^2. The fragment is a subophitic, intergranular, basalt composed predominantly of plagioclase (~70%) and clinopyroxene (~25%) with minor Fe-metal, troilite, ilmenite, mesostasis and other minor phases (table 2). The texture more closely resembles the texture of 14310,6 than of 14053,17, but could be derived from portions of either (fig. 5). Mild shock features were observed and are discussed in sect. 3.13.

A limited number of pyroxene analyses are shown in fig. 1 and suggest a rather limited range of pyroxene composition, but only a few grains of pyroxene were present in the sections. Binocular microscope examination of the pyroxene separate used for Rb/Sr analysis show a greater range of color (pale yellow to dark brown) than is suggested by the electron probe analyses.

Plagioclase is polysynthetically twinned with compositions ranging from $An_{93}Ab_7$ to $An_{87}Ab_{12}Or_1$.

Fe-metal is common and analyses yielded a Ni content ranging from 14 to 17 wt% (fig. 2).

The chemical composition of glass is discussed later.

3.6. *Sample 14167,8,1*

Sample 8,1 was an 0.067 g fragment from the coarse fines of the comprehensive sample (14167,8) collected from the 'smooth region' away from Cone Crater [8]. It was studied in a microthin section with an area of about 1 mm^2.

The fragment is an ophitic, olivine basalt with laths (~0.1 mm) of plagioclase (~35%) enclosed in larger grains (~0.25 mm) of clinopyroxene (~30%) and olivine (~30%). Minor minerals include Fe-metal, troilite, ilmenite, mesostasis and other phases (table 2). Shock-induced features were observed and are discussed in sect. 3.13.

Plagioclase occurs in polysynthetically twinned laths with a composition of about $An_{90}Ab_{10}$.

The presence of abundant primary olivine distinguishes this fragment from the others studied. Most of the olivine has a composition of about $Fa_{30}Fo_{70}$, but much more Fe-rich olivine occurs as cores in pyroxene (fig. 1). Olivine occurs both as cores in pigeonite (table 4, #16, #11) and as cores in

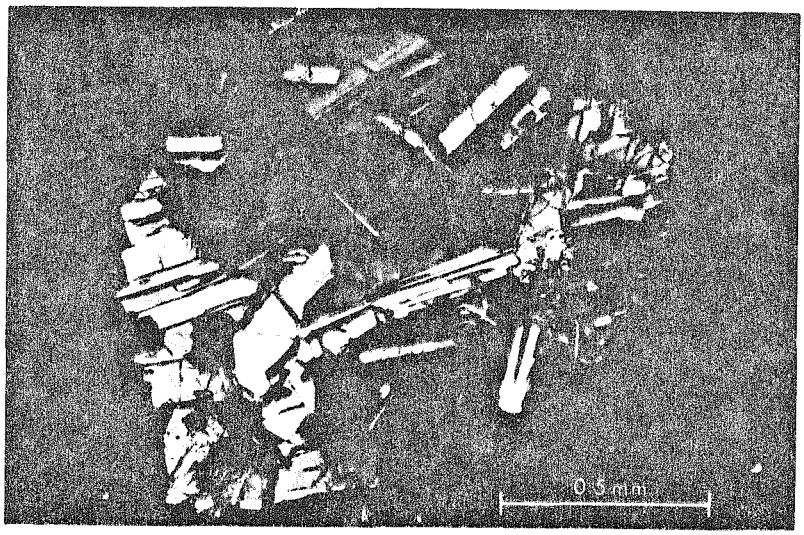

Fig. 5. Photomicrograph of section 14321,191,X-1 (crossed nicols).

augite (table 4, #17, #12). Neither the augite nor pigeonite show extensive variation in Fe/Mg.

The mesostasis in this sample is not well developed and only a small amount of glass is present (fig. 4).

3.7. *Sample 14001,7,1*

Sample 7,1 is an 0.062 g fragment from the coarse fines of the contingency sample (14001,7) collected in the 'smooth region' away from Cone Crater [8]. The fragment was examined and removed for study because it is the most distinctive lithic type in sample 14001,7 [9]. It is a dark-gray vesicular rock with a sugary texture [2]. Spherical vesicles and vugs are common and are lined with crystals of ilmenite, feldspar, and troilite [9].

The fragment was studied in two micro-thin sections with areas of about 0.6 mm^2 and 0.7 mm^2. It is a shocked rock with a very fine-grained texture which was shock induced. However, the preshocked character can be discerned by combining observations in reflected light with information from electron beam scans. The original rock was a subophitic, orthopyroxene basalt with an average grain size of about 0.03 mm and composed predominantly of pyroxene (~45%), feldspar and mesostasis (?) (together approximately 55%), and whitlockite (~3%) with minor amounts of ilmenite, Fe-metal, troilite, and other phases (table 2).

Pyroxene compositions are shown on fig. 1 and suggest the presence of augite, pigeonite, and orthopyroxene. Both orthopyroxene and clinopyroxene were identified optically, but no estimates of their relative abundances could be made.

Electron beam scan photographs indicate that many of the areas analysed are intimate mixtures of Ca-rich and K-rich feldspar. Consequently, the analyses are probably of mixtures of phases and were discarded. A plagioclase analysis was obtained with a composition of $An_{95}Ab_5$ and two were obtained with compositions of about $An_{80}Ab_{18}Or_2$.

Fe-metal has an Ni content ranging from 5 to 15 wt % (fig. 2). Other minor phases were not analyzed.

Fig. 6 illustrates the preshocked character of the rock. It was prepared by comparing reflected light photographs with electron beam scan photographs for Mg, K, Fe, Ti, Ca, Al, Na, Zr, S, Ba, P, Y and Cl. This particular area is believed to represent a shocked mesostasis area, because of the abundance of K-rich phase(s). These areas consist of low birefringent, somewhat fibrous appearing aggregates of K-rich and Ca-rich feldspar that possibly represent recrystallization after the shock event. The K-rich areas are not

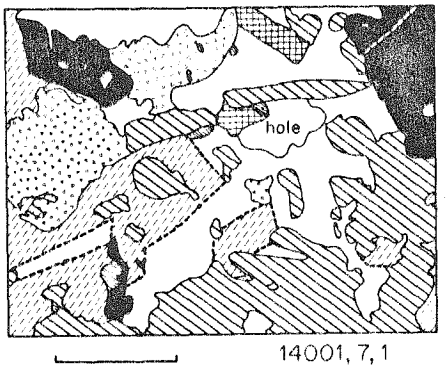

Fig. 6. A section of sample 14001,7,1 prepared by comparing reflected light photomicrographs and electron beam scan photographs.

completely isotropic. No large completely isotropic areas were observed in this sample.

Ilmenite shows no obvious shock effects, and preserves its lath shape and globular silicate inclusions. Pyroxene grains show undulose extinction, some polygonization, and rare lamellar structures. Although both plagioclase and pyroxene show shock-induced fractures, the original grain morphologies have not been seriously altered as are shown in fig. 6.

The mineralogy, the preshocked texture, and the shock effects in this rock are similar to those found in Luny Rock 1 from Apollo 11 [6]. However, the plagioclase grains in Luny Rock 1 are shock-isotropized (maskelynite), and the pyroxene and ilmenite crystals are fractured and somewhat granulated. These features suggest that Luny Rock 1 was subjected to greater shock pressure.

The presence of spherical vesicles lined with crystals presents a distinct problem in interpretation. Based on the visible shock features, the shock pressures were not sufficient to produce vesiculation [13]. However, if the vesicles were pre-shock features of the basalt it is difficult to understand their apparently undeformed survival.

3.8. *Pyroxene and olivine*

The pyroxene and olivine in some of the Apollo 14 samples display compositional and structural features very similar to those in Apollo 11 and 12 samples, but several of the samples have pyroxene and olivine which are quite distinctive.

Analytical data on the pyroxenes is summarized on fig. 1 and in table 4. Pyroxene in the Apollo 11 samples is predominantly augite which displays extensive Fe enrichment in single grains. The Apollo 12 samples contain both pigeonite and augite in complicated intergrowths, but generally limited Fe enrichment. Pyroxene in sample 14053,17 displays extensive Fe enrichment in single grains, similar to Apollo 11 pyroxene (fig. 1). Pyroxene in samples 14001,7,3; 14321,191,X-1 and 14310,6 do not display extensive Fe enrichment, but contain complicated intergrowths of pigeonite and augite.

Sample 14073,8 contains abundant orthopyroxene. Such rocks have been reported by many investigators as lithic fragments in the soils and breccias of both Apollo 11 and 12, and orthopyroxene grains are common in the soil samples [6,14–17]. However, sample 14073 is the first rock sample containing orthopyroxene. Sample 14001,7,1 also contains orthopyroxene, but is similar to Luny Rock 1 [6] and other lithic fragments (for example 17).

Sample 14167,8,1 contains Mg-rich olivine as an abundant primary phase and is somewhat like Apollo 11 sample 10020 [6]. The fayalitic olivine in sample 14053,17 is distinctive as it has a high MnO content (table 4, #15).

The size of the triangles on fig. 1 indicates the total $CaTi(Al_2O_6)$, $CaCr(AlSiO_6)$, $CaAl(AlSiO_6)$ and $NaAl(Si_2O_6)$ substitution in the pyroxenes. The principal substitution in the Apollo 11 pyroxenes was $CaTi(Al_2O_6)$ and $CaCr(AlSiO_6)$, but $CaAl(AlSiO_6)$ substitution was important in the pyroxene of the Apollo 12 samples. The analyses of pyroxene from these samples are most like the Apollo 12 samples and contain more Cr and Al than necessary to balance the Ti as $CaTi(Al_2O_6)$.

3.9. *Glass*

Glass occurs interstitial to the major phases and also trapped within the major phases. It was found in all the samples except 14001,7,1 in which material similar in composition to the glasses occurs but is anisotropic. Only of glass in the mesostasis of thin sections and in grain mounts of the 'quintessence' separates used for the Rb/Sr analyses of 14053, 14073 and 14310 was analyzed. The analyses are shown on the variation diagram (fig. 4) and averaged analyses from 14053 and 14310 are given in table 5.

Two chemically different, but optically similar glasses are present. The first type is rich in SiO_2 and poor in K_2O and BaO (SiO_2 70 to 82 wt%), and the second type is poor in SiO_2 and rich in K_2O and BaO (SiO_2 59 to 70 wt%) (table 5). All of the glass in 14053 is SiO_2-rich glass. This sample also contains glass globules enclosed in olivine within the mesostasis. These globules are the most SiO_2-rich glass analyzed (SiO_2 82.5 wt%), and are much higher in normative quartz and corundum than all the other glasses. Both SiO_2-rich and SiO_2-poor glass is present in sample 14310, but the SiO_2-poor glass predominates. Although sample 14310 contains both glass types, the overlap in the range of SiO_2 content of this sample and in 14053 is small. Sample 14073 exhibits a continuous range in SiO_2 content from 61 to 81 wt%. Samples 14001,7,3; 14167,8,1 and 14321,191,X-1 contain only SiO_2-poor glass and in this respect are similar to sample 14310.

Despite the complex mineral separation procedures in preparing samples for Rb/Sr analyses, the glass in the 'quintessence' grain mounts shows the same compositional range as the glass in the mesostasis of the respective thin sections.

3.10. *Fe-metal*

Metallic iron occurs in all the samples. As in the Apollo 12 samples and unlike the Apollo 11 samples metallic iron is not intimately associated with troilite and grains have a high and variable Ni content. A limited number of analyses (fig. 2) suggest that the Ni content of sample 14053 is lower than that of the other samples, in which the Ni content ranges from 5 to 17 wt%.

3.11. *Phosphate minerals*

Except for sample 14001,7,1 both apatite and whitlockite were found in those samples in which they were looked for systematically. Representative analyses are given in table 6. They typically occur as small needles or granules in the mesostasis except in sample 14001,7,1 where whitlockite crystals up to 0.2 mm are present. The compositions are like those found in other lunar samples [6,7,18]. The apatite is a chlorofluorapatite with a low content of rare earth elements. As in the analyses of whitlockite which we reported earlier [6], the summations are low and the substitution of Na^{+1} for Ca^{2+} and Si^{4+} for P^{5+} does not appear to balance the substitution of $(REE)^{3+}$ for Ca^{2+}. The low summations may be due in part to the presence of U and Th [19], Li [18], and other REE, or simply be an analytical error due to the small grain size [20]. Fission track work [21] indicates the presence of U and Th in phosphate grains from 14001,7,3, 14310 and 14053,17.

3.12. *Uranium and thorium rich phases*

Preliminary fission track work indicates that U-Th-rich phases are abundant in samples 14001,7,3 and 14310,6, but not in 14053,17 [21]. In samples 14001,7,3 and 14310,6 much of the U and Th is present in phosphate minerals and interstitial material. In addition, distributed throughout the rock are tight clusters of tracks which suggest the presence of a phase rich in U and Th. Analyses of this phase in sample 14001,7,3 are given in table 7. It is rich in Ti, Zr, and Fe and contains Si, Ca, Nb, U, Th, Pb, Y and REE. It occurs as small ($<5\mu$) opaque grains intimately associated with other opaque minerals. The summations are very low, presumably due to the very small, hard grains which developed curved surfaces when polished [20]. Furthermore, we did not analyze for elements in material surrounding the grains. The analyses, however, appear to represent two different compositions. In addition they appear to differ from both phase A of Frick et al. [22] and phase β of Haines et al. [19], analyses of which are also given in table 7. It is notable that the atomic Th/U in analyses 1 and 2 differs markedly from that of analyses 3 and 4. Assuming that all the Pb is radiogenic, ages have been calculated and are given in table 7. Because of the analytical error and lack of isotopic data, no precise age significance can be attached to these ages. The errors cited are simply those for the counting statistics.

Table 7
Electron probe analyses and calculated model ages for U and Th rich phases.

wt%	14001,7,3 #1	14001,7,3 #2	14001,7,3 #3	14001,7,3 #4	Phase β* #5	Phase A** #6
SiO_2	7.0	14.7	13.7	13.5	2.0	1.1
CaO	3.8	3.3	6.0	5.8	2.9	13.8
TiO_2	12.9	12.2	10.4	9.8	22.1	19.5
FeO	17.3	19.5	11.3	9.2	13.8	42.8
Y_2O_3	2.9	2.4	1.1	1.1	8.9	2.6
ZrO_2	23.5	16.1	34.4	34.1	17.2	17.4
Nb_2O_5	3.6	3.3	2.4	2.8	7.9	–
La_2O_3	0.2	0.3	<0.1	<0.1	0.2	–
Ce_2O_3	1.8	1.5	0.7	0.4	1.6	–
Nd_2O_3	1.3	1.2	0.4	0.6	0.9	–
Gd_2O_3	0.4	0.3	0.2	0.3	–	–
Er_2O_3	0.6	0.6	0.8	0.5	–	–
PbO	1.2	1.3	2.3	2.6	4.2	–
ThO_2	3.4	5.0	3.0	3.0	3.5	–
UO_2	0.6	0.9	2.3	2.4	3.6	–
Other	–	–	–	–	2.2	1.2
Total	80.5	82.6	89.0	86.1	91.0	98.4
Pb/U***	2.4 ± 0.6	1.8 ± 0.3	1.3 ± 0.3	1.3 ± 0.1	1.5 ± 0.8	
Th/U***	5.8 ± 1.3	5.7 ± 0.9	1.3 ± 0.3	1.3 ± 0.1	1.1 ± 0.4	
Age AE	4.0 ± 0.6	3.2 ± 0.5	3.6 ± 0.5	3.8 ± 0.2		

* Haines et al. [19].
** Frick et al. [22].
*** Atomic ratios.

In contrast to the above sample, sample 14053,17 has only a few weak clusters of tracks indicating a low U and Th content and suggesting that phases rich in these elements are absent.

With larger grains and more accurate analyses, the U and Th-rich phases in these crystalline rocks may be used to determine more accurate 'microprobe ages' [22]. The presence of these phases suggests that caution must be exercised in preparation of material for U-Th-Pb isotopic analysis and in interpretation of analytical results.

Another minor phase found in samples 14001,7,3, 14310,6 and 14073,8 is a transparent reddish-orange mineral which occurs as small platelets as large as $5 \times 5 \times 1\mu$. All the grains which we observed are oriented at an angle to the surface of the section and present too small a surface area for analysis. However, wavelength scans indicate that it is an Fe-Ti-Zr silicate without Nb and REE.

3.13. *Shock features*

In thin sections 14053,17 and 14310,6 the pyroxene grains exhibit irregular fractures. These, however, may have been induced during preparation of the thin sections. Distinctive features, observed in thin section 14073,8 which are suggestive of shock metamorphism, include extreme, irregularly fractured pyroxene, parallel-planar fractures in plagioclase, bent twin planes in plagioclase, and pressure-induced plagioclase twinning.

Fragments 14001,7,3; 14167,8,1 and 14321,191, X-1 were examined for shock-induced features prior to thin section preparation. In all cases they are surrounded by a very friable, milky-white aggregate of plagioclase which is distinct from the usual clear lunar plagioclase grains. This feature is probably shock induced and the fragments may represent the most weakly shocked kernels of the lithic fragments.

The most highly shocked fragment examined is

14001,7,1. As noted previously plagioclase grains have undulose extinction, show some polygonization and rare lamellar structures and pyroxene grains have undulose extinction and some polygonization.

4. Sample comparison and discussion

Isotopic investigations on these samples by our colleagues [2,3] indicate that they are distinctly older than the Apollo 11 and Apollo 12 basalts and slightly younger than rock 12013 [18]. Moreover, the analyzed Apollo 14 basaltic rocks fall into two groups with Rb/Sr crystallization ages of 3.88 and 3.95 AE and with distinct initial ($^{87}Sr/^{86}Sr$) values (table 1). The ^{40}Ar-^{39}Ar ages agree closely and there is a suggestion that the older age group has a younger ^{38}Ar-^{37}Ar cosmic ray exposure age.

Fortunately, each of these two groups contains one of the two large crystalline rock samples and these two rocks are petrologically distinct as discussed by the Preliminary Examination Team [1]. We shall attempt to define distinguishing petrologic features of these samples which might be determinable in the many lithic fragments on which isotopic investigations cannot be undertaken. It is important, however, to note that the fragments which we examined were probably biased toward the more coherent portions of the samples. Consequently, the fragments described may not represent the entire sample used for isotopic work.

Samples 14310 and 14053, as represented by the thin sections available to us, are distinguished by a number of following characteristics:

(1) Thin section 14310,6 has a subophitic texture with rather elongate plagioclase laths forming a randomly oriented framework to the interstitial pyroxene and mesostasis, whereas thin section 14053,17 has an ophitic texture more typical of Apollo 11 and 12 rocks. In addition the spongy masses of opaque minerals in 14053,17 are quite distinctive.

(2) Thin section 14310,6 has a higher plagioclase content than 14053,17.

(3) Thin section 14053,17 has a pronounced Fe-enrichment trend in the pyroxene (fig. 1), a more pronounced Na-enrichment trend in the plagioclase than 14310,6.

(4) The mesostasis glass in 14053,17 is distinctly richer in SiO_2 and poorer in K_2O and BaO than that in 14310,6 (fig. 3).

(5) The Ni content of the metal phase in 14053,17 is distinctly lower than that in 14310,6.

(6) Thin section 14310,6 contains more U and Th than thin section 14053,17 (as indicated by fission track studies), and contains both the unknown U-Th-rich phase and the unknown red Fe-Ti-Zr silicate, neither of which are found in thin section 14053.

Based on these criteria, samples 14001,7,3, and 14073,8, despite the presence of abundant orthopyroxene, can be correlated with 14310 on petrologic grounds in agreement with all the isotopic data. Similar glass composition and the restricted pyroxene compositions, suggest that sample 14167,8,1 can also be correlated with 14310 in agreement with the age assignment, but not the cosmic ray exposure age. However, the high olivine content and lack of other supporting evidence makes this correlation much less certain.

On the basis of its texture, its high plagioclase content, its lack of apparent Fe enrichment in the pyroxene, the high Ni content of its metal, and the glass composition, sample 14321,191,X-1 is more like 14310 than 14053, although it lacks the red Fe-Ti-Zr silicate. This correlation is neither in agreement with the age assignment nor the cosmic ray exposure age.

The distribution of lithologic types in the dated Apollo 14 samples, as well as cursory examination of thin sections of breccia samples 14321,218; 14305,13; 14083,7 and 8, and 14311 suggest that rock fragments that may be correlative with sample 14310 on the basis of mineralogic and petrologic similarities are important constituents of the soil and breccia at the Apollo 14 site. This is corroborated by the bulk chemical analysis [1] as both the major and minor element patterns of rock 14310 recur as the dominant pattern in the breccia and soil, and is distinctly different from the elemental abundances reported in sample 14053. Moreover, the Preliminary Examination Team reports that the three most abundant (non-fragmental) lithic clasts in the fragmental rocks are (1) clinopyroxene-plagioclase clasts with basaltic texture, (2) feldspathic clasts, and (3) plagioclase-orthopyroxene clasts with ophitic textures and minor clinopyroxene [1]. The first two types could be derived from rocks like either sample 14310 or 14053, but the third type is distinctive and similar to 14073.

Hence, it seems likely that most of the fragmental rocks at the Apollo 14 site will be composed of rocks with ages similar to these few dated samples. It might be noted that all lithic fragments at both the Apollo 11 and 12 sites, with the exception of rock 12013 had a limited age span suggesting local or closely related origin of the rocks.

Orthopyroxene grains in the soil, orthopyroxene basalt fragments with distinctive petrologic, chemical, and mineralogic features, and glass (fragments) with similar chemical composition have now been reported from the Apollo 11 samples [6,15], from the Apollo 12 samples [14,16,17,23], and the Apollo 14 samples ([1], this paper). Sources for this material, therefore, must be widely available on the lunar surface. It has been suggested that such material is the 'magic', 'cryptic' or 'KREEP' component invoked to explain the chemical and isotopic differences observed between the Apollo 11 and 12 soils and the dominant rock fragments which they contain [17].

Sample 14073 is an orthopyroxene basalt, and judging by its mineral content, is rich in K, REE, U and Th. Thus, it exhibits chemical similarities to the 'magic' and 'cryptic' components and 'KREEP'. It has an age of 3.88 AE and an initial $^{87}Sr/^{86}Sr$ of 0.70034. Rocks like rock 14073 may be the source of orthopyroxene crystals, orthopyroxene fragments, K_2O-rich glass and REE which occur as components in the soil.

As described earlier, Luny Rock 1 from Apollo 11 [6] and 14001,7,1 are notably similar in both their pre-shock and their shock features. They have model ages, T_{BABI}, of 4.44 and 4.30 AE respectively [2,24]. Assuming for argument's sake that they are cogenetic, the resulting two point isochron has an age of 3.95 AE and an initial $^{87}Sr/^{86}Sr$ of 0.70068. Data for a similar orthopyroxene basalt fragment [17] also fall, well within its error bars, on this isochron.

Comparing these points it seems important to recognize that the 'magic' or 'cryptic' component, which was invoked to account for the chemical and isotopic differences of the lunar soils from their dominant rock fragments, need not be granitic rock like 12013, but may be a lithic type like 14073 or its shocked counterparts (?) like 14001,7,1 and Luny Rock 1.

Acknowledgements

We gratefully acknowledge G.J.Wasserburg for his care and foresight in selecting fragments from the soil and breccia samples. Continuing discussions with G.J. Wasserburg and other Lunatics have proved invaluable. E.L.Haines provided the fission track data and Mr. Joe Brown meticulously prepared the micro-thin sections.

This work was supported by NASA contract NAS-9-8074. The microprobe laboratory has been developed with the support of NSF, JPL and the Union Pacific Foundation.

References

[1] Lunar Sample Preliminary Examination Team, Preliminary examination of lunar samples, in: NASA Manned Spacecraft Center, Apollo 14 Preliminary Science Report SP-272 (1971) 109.

[2] D.A.Papanastassiou and G.J.Wasserburg, Rb-Sr ages of igneous rocks from the Apollo 14 mission and the age of the Fra Mauro Formation, Earth Planet. Sci. Letters 12 (1971) 36–48.

[3] G.Turner, J.C.Huneke, F.A.Podosek and G.J.Wasserburg, ^{40}Ar-^{39}Ar ages and cosmic ray exposure ages of Apollo 14 samples, Earth Planet. Sci. Letters 12 (1971) 19–35.

[4] A.E.Bence and A.L.Albee, Empirical correction factors for the electron microanalysis of silicates and oxides, J. Geol. 76 (1968) 382.

[5] A.L.Albee and L.Ray, Correction factors for electron probe micro-analysis of silicates, oxides, carbonates, phosphates and sulfates, Analytical Chem. 42 (1970) 1408.

[6] A.L.Albee and A.A.Chodos, Microprobe investigations on Apollo 11 samples, Geochim. Cosmochim. Acta, Suppl. I, vol. 1 (1970) 135.

[7] L.H.Fuchs, Fluorapatite and other accessory minerals in Apollo 11 rocks, Geochim. Cosmochim. Acta, Suppl. I, vol. 1 (1970) 475.

[8] NASA Manned Spacecraft Center, Apollo 14 Preliminary Science Report, SP-272 (1971).

[9] G.J.Wasserburg, private communication.

[10] N.L.Carter, I.S.Leung, H.G.Ave'Lallemant and L.Fernandez, Growth and deformational structures in silicates from Mare Tranquillitatis, Geochim. Cosmochim. Acta, Suppl. I, vol. 1 (1970) 267.

[11] S.E.Haggerty and H.O.A.Meyer, Apollo 12: opaque oxides, Earth Planet. Sci. Letters 9 (1970) 379.

[12] E.Roedder and P.W.Weiblen, Lunar petrology of silicate melt inclusions, Apollo 11 rocks, Geochim. Cosmochim. Acta, Suppl. I, vol. 1 (1970) 801.

[13] N.M.Short, The nature of the moon's surface: evidence from shock metamorphism in Apollo 11 and 12 samples, Icarus 13 (1970) 383.

[14] L.H.Fuchs, Orthopyroxene-plagioclase fragments in the lunar soil from Apollo 12, Science 169 (1970) 866.

[15] J.A.Wood, U.B.Marvin, B.N.Powell and J.S.Dickey Jr., written communication.

[16] J.A.Wood, U.B.Marvin, J.B.Reid Jr., G.J.Taylor, J.F. Brown, B.N.Powell and J.S.Dickey Jr., written communication.

[17] N.J.Hubbard, C.Meyer Jr., P.W.Gast and H.Weismann, The composition and derivation of Apollo 12 soils, Earth Planet. Sci. Letters 10 (1971) 341.

[18] Lunatic Asylum, Mineralogic and isotopic investigations on lunar rock 12013, Earth Planet. Sci. Letters 9 (1970) 137.

[19] E.L.Haines, A.L.Albee, A.A.Chodos and G.J.Wasserburg, Uranium-bearing minerals of lunar rock 12013, Earth Planet. Sci. Letters, to be published.

[20] N.J.Page, L.C.Calk and M.H.Carr, Problems of small particle analysis with the electron microprobe, U.S. Geol. Survey Prof. Paper 600-C (1968) C31.

[21] E.L.Haines, private communication.

[22] C.Fick, T.C.Highes, J.F.Lovering, A.F.Reid, N.G.Ware and D.A.Wark, Electron probe, fission track and activation analysis of lunar samples, Second Lunar Science Conference, Houston, Texas, January (1971).

[23] K.Keil, M.Prinz and T.E.Bunch, Mineralogical and petrological aspects of Apollo 12 rocks, Second Lunar Science Conference, January (1971).

[24] A.L.Albee, D.S.Burnett, A.A.Chodos, O.J.Eugster, J.C. Huneke, D.A.Papanastassiou, F.A.Podosek, G.Price Russ III, G.Sanz, F.Tera and G.J.Wasserburg, Ages, irradiation history, and chemical composition of lunar rocks from the Sea of Tranquility, Science 167 (1970) 463.

MINERALOGY, PETROLOGY, AND CHEMISTRY OF LUNA 16 SAMPLE B-1

A. L. Albee, A. A. Chodos, A. J. Gancarz, E. L. Haines, D. A. Papanastassiou, L. Ray, F. Tera, G. J. Wasserburg, and T. Wen, Lunatic Asylum, Division of Geological and Planetary Sciences, California Institute of Technology, Pasadena, California 91109. Contribution No. 2095

Luna 16 sample B-1 was the largest fragment (62 mg) obtained in the sample exchange with the USSR. Petrologic, mineralogic, and chemical investigations have been made on this fragment in conjunction with isotopic investigations. A Rb-Sr internal isochron and Ar^{39}/Ar^{40} release patterns indicate an age of about 3.45 aeons for this fragment. The exterior surface of the equant fragment was coated with an irregular, thin, vitreous-appearing glaze and contained numerous zap pits. The rock is a fine-grained ophitic basalt composed predominantly of clinopyroxene (50%), plagioclase (40%), and ilmenite (7%) with minor amounts of chromian ulvöspinel, olivine cores in pyroxene, troilite, mesostasis, apatite, and whitlockite. The texture suggests that olivine and pyroxene crystallized first, followed by plagioclase laths.

Plagioclase ranges from $Or_{0.4}Ab_{7.6}An_{9.2}$ to $Or_2Ab_{22}An_{76}$ and contains Fe, Mg, K and Ba concentrations similar to those found in other lunar samples (Fig. 1). Two distinct compositional trends occur in pyroxene (Figs. 2,3): 1) Ca-rich grains become less calcic with little change in Mg/Fe (e.g., Wo_{35} En_{41} Fs_{24} grades into Wo_{16} En_{49} Fs_{35}) and 2) Ca-poor grains become more Fe-rich (e.g. Wo_{16} En_{49} Fs_{35} grades into $Wo_{20}En_5Fs_{75}$). No evidence exists for the simultaneous crystallization of more than one pyroxene. The lines on Fig. 3 are the altitudes of the triangles, which indicate the percentage of components other than Wo, En and Fs. The more calcic pyroxenes are highest in Ti, Al and Cr; and the principal coupled substitution is $R^{2+}Ti^{4+}$ (Al_2O_6).

The bulk composition of sample B-1, as determined by defocused electron beam analyses, is: SiO_2, 45.5 weight %; Al_2O_3, 13.5; TiO_2, 4.04; MgO, 5.95; FeO, 17.8; MnO, 0.26; CaO, 12.0; BaO, 0.06; Na_2O, 0.63; K_2O, 0.21; P_2O_5, 0.15; total 100.48. Isotope dilution analyses give: Li, 10.7 ppm; K, 1396 ppm; Rb, 1.58 ppm; Cs, 53.6 ppb; Ca, 8.25%; Sr, 437 ppm; Ba, 218 ppm. A uranium content of 0.30 ± 0.03 ppm was determined by fission-track counting on a 1.2 mm^2 thin section. Compared to Apollo 11 basalts the K content is intermediate to that of the low-K and high-K groups; its K/Rb is high, and it contains more Si and Al and less Ti. Compared to Apollo 12 basalts sample B-1 contains similar concentrations of Ti and Si, more Al and K, and less Ca. Compared to Apollo 14310 it contains less K, Si, and Al and more Ti and Fe. The K/U value and the Sr content is much higher than in Apollo 11 and 12 basalts.

Isotope dilution analyses of soil sample A-2 give: Li, 8.5 ppm; K, 844 ppm; Rb, 1.79 ppm; Ca, 65.1 ppb; Ca, 8.25%; Sr, 271 ppm; Ba 168 ppm.

MINERALOGY, PETROLOGY, AND CHEMISTRY OF LUNA 16 SAMPLE B-1

A. L. Albee

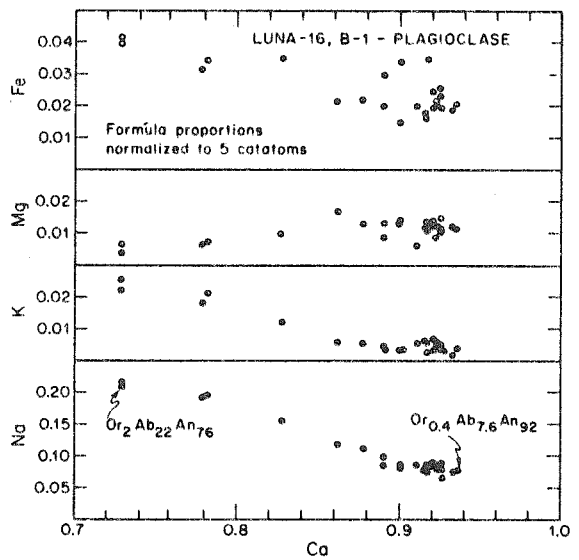

Figure 1

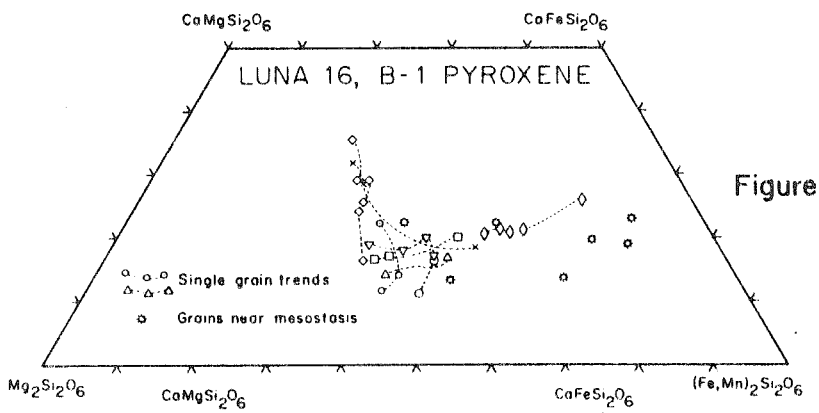

Figure 2

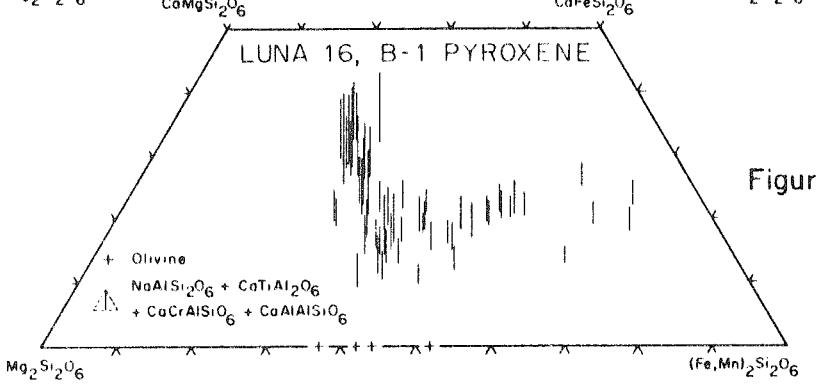

Figure 3

EARTH AND PLANETARY SCIENCE LETTERS 13 (1972) 353–367. NORTH-HOLLAND PUBLISHING COMPANY

MINERALOGY, PETROLOGY, AND CHEMISTRY OF A LUNA 16 BASALTIC FRAGMENT, SAMPLE B-1 *

A. L. ALBEE, A. A. CHODOS, A. J. GANCARZ, E. L. HAINES, D. A. PAPANASTASSIOU, L. RAY, F. TERA, G. J. WASSERBURG and T. WEN

The Lunatic Asylum, Division of Geological and Planetary Sciences, California Institute of Technology, Pasadena, California 91109, USA

Received 16 November 1971
Revised version received 29 November 1971

Luna 16 sample B-1 was the largest fragment (62 mg) obtained in the sample exchange with the USSR. Petrologic, mineralogic, and chemical investigations have been made on this fragment in conjunction with Rb–Sr and $^{40}Ar/^{39}Ar$ investigations by our colleagues. Sample B-1 is a fine-grained ophitic basalt but is distinguished from the Apollo samples by containing a single pyroxene, predominantly pigeonitic, an ilmenite content (7%) intermediate to that of the Apollo 11 and 12 samples, and subequal amounts of pyroxene (50%) and plagioclase (40%). Chemically it is distinguished by a high Sr content (437 ppm) and a high K/U value (4700). The K-content (1396 ppm) is higher than that of Luna 16 soil sample A-2.

1. Introduction

Luna 16 sample B-1 was the largest fragment obtained in the sample exchange with the USSR. Rb–Sr and $^{40}Ar/^{39}Ar$ studies, which indicate an age of about 3.45 aeons for this fragment, are described in companion papers [1, 2]. This paper describes our petrologic and chemical investigations.

Sample B-1 was a 62 mg fragment from the 15–28 cm depth zone of the Luna 16 core tube (zone B in Russian, but zone C in English translation [3]). The Russian sample number is Luna 16-10B-09; the NASA sample number is Luna 16, B-1.

The equant fragment, about 2.5 mm in diameter, weighed 61.5 mg when received in our clean lab. After binocular study, surface dust was removed by washing with acetone in an ultrasonic cleaner. The surface cleaned well with very little loss, and the fragment remained coherent.

The extent to which the fragment was significantly heated or shocked and the amount of surficial glass is extremely important in interpreting ages measured on such a small fragment. The fragment was covered with an irregular, thin, vitreous-appearing "glaze", and numerous zap pits were present on all surfaces. The "glaze" varied in color and apparent thickness but was nowhere thick enough to obscure the basaltic texture of the fragment. Feldspar grains on the exterior surface appeared milky-white just as they do in the vicinity of zap pits. However, despite the abundance of shock features, the fragment was internally tough and coherent.

Numerous small vugs were exposed on the exterior, and one side of the fragment (~2 mm) appeared to have been a vug wall. These vugs contained ilmenite plates up to 50 μm, brown pyroxene laths up to 75 μm, and plagioclase crystals.

The fragment was broken into flakes using stainless-steel surgical tools. Flakes were examined under the binocular microscope for surface glaze as flaking continued and interior portions reserved for the $^{40}Ar/^{39}Ar$ studies. The portions used for the "total" rock Rb–Sr and other chemical studies may have included a small portion of the exterior surface although every effort was made to exclude this material. Microthin sections were prepared from five thin flakes. A

* Contribution No. 2095.

section (FQM-150) with an area of 1.2 mm^2 was chosen to give a cross section from the glazed exterior into the interior of the fragment. Another section (FQM-151) with an area of about 0.5 mm^2 was a flake parallel to the surface, which was a vug wall. Three other thin sections with areas of about 0.3 mm^2 (FQM-152), 0.2 mm^2 (FQM-153), and 0.1 mm^2 (FQM-154) were simply small flakes parallel to the exterior surface.

2. Analytical techniques

The electron probe analyses were made with a M.A.C. 5-SA3 electron microprobe interfaced with a PDP-8/L computer. Standard operating conditions were 15 kV with beam current integration and pulse height selection. Peak and background counting for up to 13 elements and on-line data processing was done at each spot analyzed. Programmed peak searches were run at each spot for Si and Al in feldspar and for Si and Mg in pyroxene and olivine. The samples were analyzed relative to a standard set of simple silicates, oxides, and phosphates using the inter-element correction factors of Albee and Ray [4]. Known samples were analyzed periodically and indicate a relative standard deviation varying from 6 to 2% for oxide concentrations varying from 1 to 8 wt% and less than 2% for higher concentrations.

The alkali and alkaline earth analyses were determined on a 3.1 mg "total" rock sample by isotope dilution. The analytical procedures have been described in detail by Tera et al. [5].

3. Mineralogy and petrology

Luna 16 sample B-1 is a fine-grained ophitic basalt composed predominantly of clinopyroxene (50%), plagioclase (40%), and ilmenite (7%) with minor amounts of chromian–ulvöspinel, olivine, troilite, mesostasis, and other minor phases. With a total thin section area of about 2 mm^2, the modal abundances can only be estimated. However, the rock is so fine-grained that the modal abundance and texture are similar in each of the tiny thin sections and it is probable that the modal estimate is reasonably representative of the total rock. Similarly, it is probable that the 3.1 mg "total" rock sample is reasonably representative of the total rock.

The approximate chemical and normative composition of sample B-1 is given in table 1. The catatom percent of the normative minerals (which is approximately volume percent) indicates mineral proportions close to those obtained by point counting. The Al and Ti content of the actual pyroxene would somewhat increase the amount of pyroxene and of free SiO_2 and would decrease the amount of anorthite. It should be noted that both analyses are very close to the boundary between normative free SiO_2 and olivine, and analytical error alone could result in either normative SiO_2 or normative olivine (i.e., negative values for normative SiO_2).

As shown in figs. 1 and 2, sample B-1 is ophitic-textured with slender laths of plagioclase (~0.1 mm long) enclosed in pyroxene grains ranging in length to 0.3 mm. Locally, clusters of plagioclase laths are enclosed by pyroxene but are interstitial to the larger pyroxene grains. Ilmenite occurs in laths (~0.1 mm long), predominantly interstitial to the pyroxene grains. The texture suggests that olivine and pyroxene began to crystallize first followed by ilmenite and plagioclase. Mesostasis occurs in tiny patches interstitial to plagioclase laths, and no large patches are present in the thin sections.

The thin section (FQM-151) which was cut parallel to the vuggy surface is not notably different from the others in texture but may be slightly coarser-grained. However, chromian–ulvöspinel and Fe-rich pyroxene are more abundant in this thin section.

A portion of the exterior, vitreous-appearing glaze can be seen in fig. 1, which shows the thin section (FQM-150) selected as a representative cross-section of sample B-1. In the transmitted light photomicrographs the glaze can be seen as the opaque-appearing border, which forms a small projecting tail on one edge of the fragment. The glaze is much like the matrix of some breccias, apparently opaque at low magnification but deep brown in color and isotropic at high magnification. It has a maximum thickness of about 50 μm but is irregular in thickness. Although it fills surface irregularities, it does not extend into the fragment. The average of two similar analyses on the projecting tail is: Na_2O, 0.4 wt%; MgO, 8.2; Al_2O_3, 13.2; SiO_2, 43.2; K_2O, 0.1; CaO, 10.9; TiO_2, 3.3; Cr_2O_3, 0.2; FeO, 16.9; total 96.4. This composition is quite similar, except for MgO, to that of the rock fragment itself (table 1).

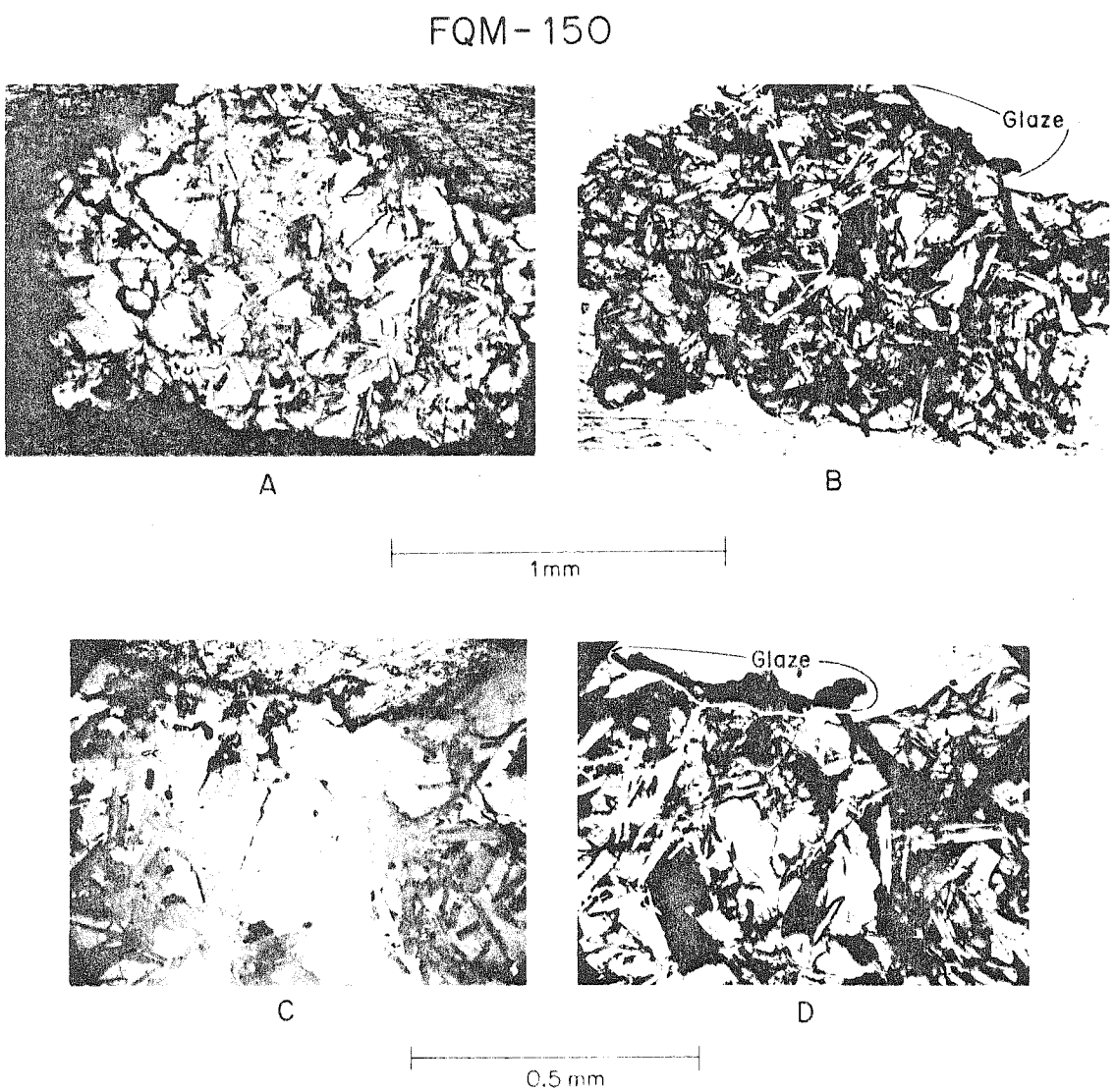

Fig. 1. Photomicrographs in reflected and transmitted light in a 1.2 mm² micro-thin section of Luna 16, B-1 (FQM-150). This thin section shows a cross section from the glazed exterior into the interior. The exterior glaze can be seen in photographs B and D as the opaque-appearing border which forms a small projecting tail on one side of the fragment; it does not extend into the interior.

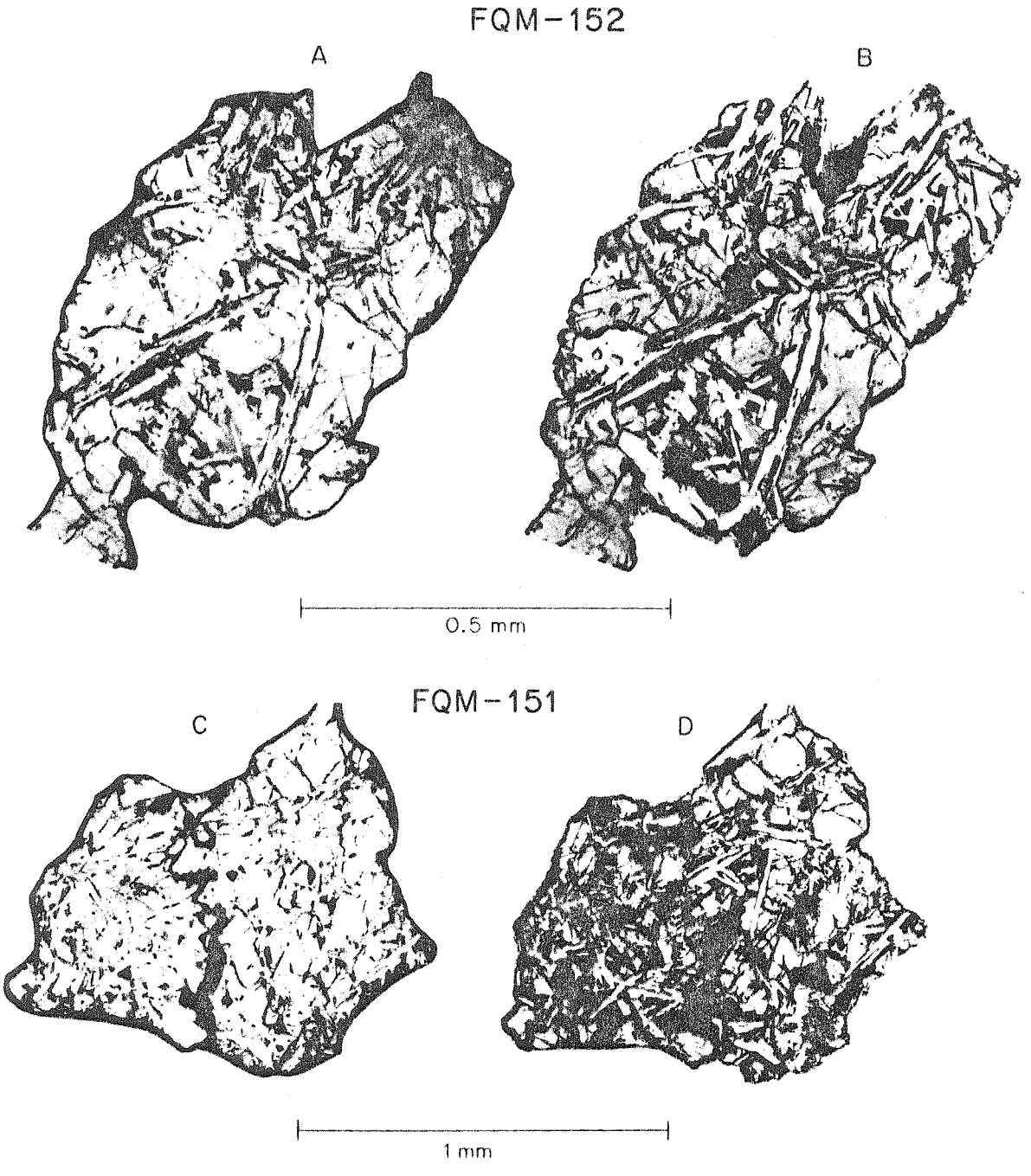

Fig. 2. Photomicrographs in reflected and transmitted light of the 0.3 mm² thin section, FQM-152 (A and B), and the 0.5 mm² thin section, FQM-151 (C and D) of Luna 16, B-1. Photos C and D show the thin section parallel to the exterior surface, which was a vug wall.

Table 1
Chemical composition of Luna 16 crystalline rocks. The analysis for sample B-1 is the average of 27 electron probe analyses on 50 μm spots at grid points within a 1.7 mm² area.

	Sample B-1	Vinogradov [3]
	[weight percent]	
SiO_2	45.50	43.8
Al_2O_3	13.95	13.65
TiO_2	4.04	4.9
MgO	5.95	7.05
FeO	17.77	19.35
MnO	0.26	0.20
CaO	11.96	10.4
BaO	0.06	0.02
Na_2O	0.63	0.38
K_2O	0.21	0.15
P_2O_5	0.15	0.12
Cl	<0.001	n.a.
Cr_2O_3	n.a.	0.28
ZrO_2	n.a.	0.04
S	n.a.	0.17
	100.48	100.5
	normative minerals (catatom percent)	
SiO_2	+0.03	−0.28
$KAlSi_3O_8$	1.30	0.95
$BaAl_2Si_2O_8$	0.10	0.05
$NaAlSi_3O_8$	5.85 } 42.0%	3.60 } 40.3%
$CaAl_2Si_2O_8$	36.1	36.7
$CaSiO_3$	9.96	6.58
$MgSiO_3$	17.2 } 50.5%	20.3 } 50.6%
$FeSiO_3$	22.9	23.4
$MnSiO_3$	0.44	0.32
$FeTiO_3$	5.88	7.14
$Ca_5(PO_4)_3F$	0.32	0.27
FeS	–	0.62
$FeCr_2O_4$	–	0.33
ZrO_2	–	0.02

As can be seen in the reflected light photomicrographs, there are numerous fractures in these microthin sections which have been accentuated by the polishing. Although many of these fractures may have formed during our breaking of the sample, there are a large number extending into the fragment immediately under the glazed surface (fig. 1). However, there appears to be no other unequivocal evidence of shock effects in the interior of the fragment. Undulatory extinction in the plagioclase appears to be related to compositional zoning, and intergrowth and irregular extinction in the pyroxene appears to be related to the mosaic structure. No clear-cut offsets of plagioclase twin lamellae were observed.

The plagioclase grains are polysynthetically twinned parallel to the laths. Zoning is present; one grain ranges from An_{83} to An_{76} and another from An_{92} to An_{88}. Most analyzed points have compositions between An_{90} and An_{92} (fig. 3), but the observed compositional extremes are $Or_{0.4}Ab_{7.6}An_{92}$ and $Or_2Ab_{22}An_{76}$ (table 2, analyses 7 and 8). The concentrations of Fe, Mg, K, and Ba are similar to those found in plagioclase from the Apollo samples. K, Fe, and Ba increase with Ab content, but Mg apparently decreases (fig. 4).

The clinopyroxene has an extensive range in composition (fig. 5; table 2, analyses 1–5), similar to that found in the Apollo samples. No orthopyroxene was observed optically, and no pyroxenes were found to have the chemical compositions typical of orthopyroxenes. The pyroxenes are pinkish-brown in thin-section and exhibit an irregular mosaic structure like that seen in the Apollo samples [6, 7]. Individual grains display compositional trends similar to the general trends suggested by all the analyzed points (fig. 5a). External grain morphology is poorly developed, hence the correlation of compositional trends with the growth direction must be inferred. In general, two distinct composition trends occur: 1) Ca-rich grains become less calcic with little change in Fe/Mg (e.g., $Wo_{35}En_{41}Fs_{24}$ grades into $Wo_{16}En_{49}Fs_{35}$) and 2) Ca-poor grains become more Fe-rich (e.g., $Wo_{16}En_{49}Fs_{35}$ grades into $Wo_{20}En_5Fs_{75}$). The most Fe-rich pyroxenes (fig. 5) occur in a 70 μm cluster of grains, possibly parts of a single crystal, associated with patches of K-rich mesostasis in the thin section (FQM-151) cut parallel to the surface which was a vug wall. Although portions of these grains have the composition of pyroxferroite, they are brown and do not have the characteristic yellow color of pyroxferroite. The Ca-rich pyroxenes contain much more Ti, Cr, and Al than do the Ca-poor and more Fe-rich pyroxenes as is indicated by the variation in length of the line symbol for the individual points on fig. 5b. Representative analyses are given in table 2, analyses 1–5. Extreme ranges of composition in individual grains are included for several grains.

The compositional trends shown in fig. 5 differ in several respects from those found in the Apollo samples. Pyroxene in the Apollo 11 samples is predomi-

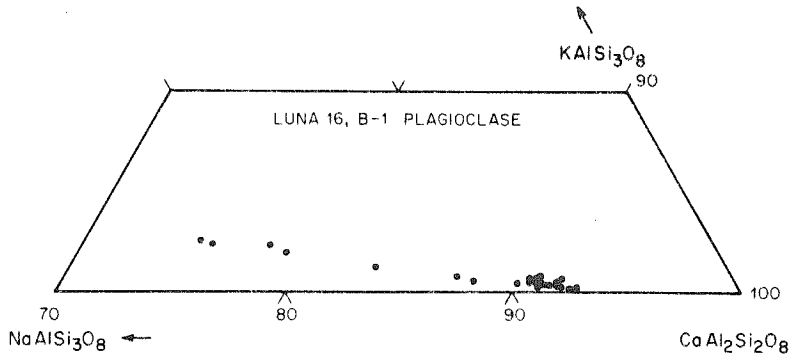

Fig. 3. Composition of plagioclase, Luna 16, B-1.

Table 2
Representative electron probe analyses of pyroxene, olivine, and plagioclase

				pyroxene					olivine	plagioclase	
wt%	1a *	1b	2a	2b	3	4a	4b	5	6	7	8
SiO_2	49.24	50.47	49.56	48.06	50.01	48.56	49.36	46.28	35.42	51.13	45.18
Al_2O_3	3.03	2.14	2.70	1.25	1.66	1.18	1.17	0.98	<0.01	30.63	33.87
Cr_2O_3	0.59	0.45	0.58	0.19	0.34	0.21	0.10	0.10	0.12	n.a.	n.a.
TiO_2	2.48	1.80	2.16	1.71	1.26	1.15	1.01	1.16	0.21	n.a.	n.a.
MgO	13.22	16.57	13.95	10.60	16.56	9.83	4.16	3.13	26.80	0.05	0.16
FeO	13.27	20.42	15.99	28.21	23.60	28.65	32.09	38.67	37.55	1.08	0.54
MnO	0.28	0.36	0.34	0.52	0.42	0.50	0.49	0.55	0.41	n.a.	n.a.
CaO	18.01	8.42	14.88	8.90	5.80	9.74	11.40	8.75	0.39	14.85	18.80
BaO	n.a.	n.a.	n.a.	n.a.	n.a.	n.a.	n.a.	n.a.	n.a.	0.05	0.04
Na_2O	0.09	0.05	0.09	0.07	n.a.	0.06	0.04	0.01	0.03	2.38	0.86
K_2O	0.01	0.02	0.02	<0.01	n.a.	0.03	0.03	<0.01	0.01	0.38	0.06
Total	100.22	100.70	100.27	99.51	99.65	99.91	99.85	99.63	100.94	100.55	99.51
atom prop.											
Si	1.86	1.91	1.88	1.91	1.92	1.93	2.03	1.94	0.99	2.34	2.10
Al	0.14	0.09	0.12	0.06	0.07	0.05	0.06	0.05	–	1.65	1.85
Cr	0.02	0.01	0.02	0.006	0.01	0.007	0.003	0.003	0.003	–	–
Ti	0.07	0.05	0.06	0.05	0.04	0.03	0.03	0.04	0.004	–	–
Mg	0.74	0.93	0.79	0.63	0.95	0.58	0.25	0.20	1.11	0.004	0.01
Fe	0.42	0.65	0.51	0.94	0.76	0.95	1.10	1.36	0.87	0.04	0.02
Mn	0.009	0.01	0.01	0.02	0.01	0.02	0.02	0.002	0.01	<0.001	–
Ca	0.73	0.34	0.60	0.38	0.24	0.42	0.50	0.40	0.01	0.73	0.93
Ba	–	–	–	–	–	–	–	–		<0.001	<0.001
Na	0.006	0.003	0.006	0.005	–	0.004	0.003	0.001	0.001	0.21	0.08
K	<0.001	<0.001	<0.001	–	–	0.002	0.001	–	–	0.02	0.004
	4.00	3.99	4.00	4.00	4.00	3.99	4.00	4.00	3.00	4.99	4.99

* Numbers indicate individual grains and letters indicate points within a single grain.

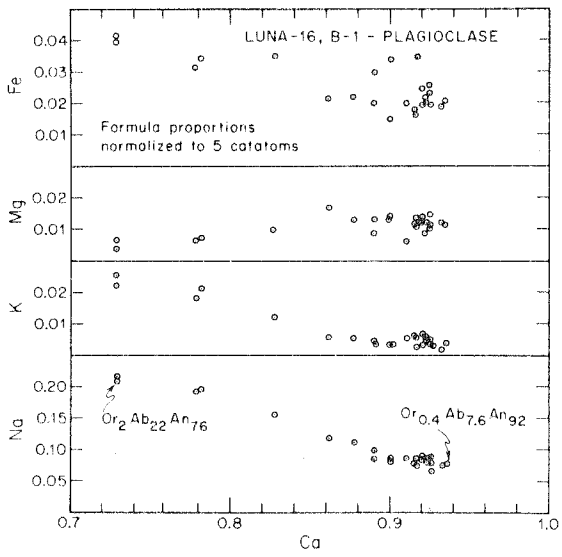

Fig. 4. Minor element content of plagioclase, Luna 16, B-1.

nantly augite which displays extensive Fe-enrichment in single grains extending to a pyroxferroite composition of about $Wo_{13}En_2Fs_{85}$. The Apollo 12 samples contain both pigeonite and augite in complicated intergrowths, but extreme Fe-enrichment trends are less common than in Apollo 11 pyroxenes. The Apollo 14 samples contain orthopyroxene, pigeonite, and augite in complicated intergrowths. In general, there is very limited Fe-enrichment in the Apollo 14 pyroxenes, but in 14053 Fe-enrichment extends toward ferrohedenbergite and fayalite occurs in the mesostasis.

In Luna 16, B-1 the initial pyroxene is more Fe-rich than is typical of the Apollo samples. The early pyroxenes display continuous variation in Ca with little variation in Fe/Mg (i.e., from augite to pigeonite), suggestive of a ternary end-point at an unusually low Ca composition. However, there is no evidence of more than one pyroxene crystallizing simultaneously from the melt as in the Apollo 12 and 14 samples. The Fe-enrichment trend initiates from a pigeonitic composition rather than from an augitic composition as in most Apollo 11 and 12 samples and extends toward a pyroxferroite composition. However, the extreme Fe-enrichment trend was found only in a single 70 μm grain adjacent to the large surface vug and not in the rims of other large grains.

Coupled substitutions and, by inference, valence states can be discussed using fig. 6 which is a plot of formula proportions normalized to 4 catatoms for all analyzed points. To a first approximation the data show that $Si + Al \cong 2$ and $Al \cong 2Ti$, indicating extensive substitution of the end member $R^{2+}TiAl_2O_6$, which was also extensive in the Apollo 11 pyroxenes, and almost no substitution of the end member $R^{2+}Al\,AlSiO_6$, which was extensive in the Apollo 12 pyroxenes. However, Si + Al is slightly less than two, and consequently there is insufficient Al to balance both the Ti as $R^{2+}TiAl_2O_6$ and the Cr as $R^{2+}CrAlSiO_6$. This relationship remains true even when the additional end member $NaCrSi_2O_6$ is utilized. The deficiency may result from minor systematic analytical errors. However, it could indicate that some Cr and/or Ti is in a reduced valence state or that some Cr and/or Ti, most likely Cr^{3+}, substitutes for Si in the four-fold coordinated position.

Olivine occurs rarely as cores within larger pyroxene grains. Analyses of two such cores range from Fa_{37} to Fa_{52} (table 2, analysis 6) with considerable compositional range in individual cores. Minor elements exhibit little variation: TiO_2 ranges from 0.10–0.21 wt%, CaO from 0.35 to 0.47, Cr_2O_3 from 0.08 to 0.21, and MnO from 0.32 to 0.44.

Most of the ilmenite occurs in laths, ~0.1 mm in length, distributed throughout the rock, but a portion occurs in very small grains interstitial to the pyroxene and plagioclase grains. The average and range for 19 analyses of ilmenite are given in table 3 along with a representative analysis of a single grain. The 19 analyses include both the larger laths and the smaller interstitial grains.

Chromian ulvöspinel occurs in equidimensional grains which show no exsolution lamellae. Seven analyses indicate compositions between $Usp_{85}Cr_{15}$ and $Usp_{65}Cr_{35}$. The minor elements show a systematic variation between the two extremes, analyses of which are given in table 3. Troilite occurs only as very small, spherical grains (< 5 μm) and contains rare, tiny blebs (< 1 μm) of Fe-metal, which are too small to analyze, and whose presence makes it difficult to obtain reliable analyses of troilite. No Ni was detected in microprobe beam scans of these metal blebs. The restriction of Fe metal to the troilite grains and its low Ni content is similar to the Apollo 11 rocks.

The mesostasis occurs in small patches disseminated throughout the rock and commonly in the interstices

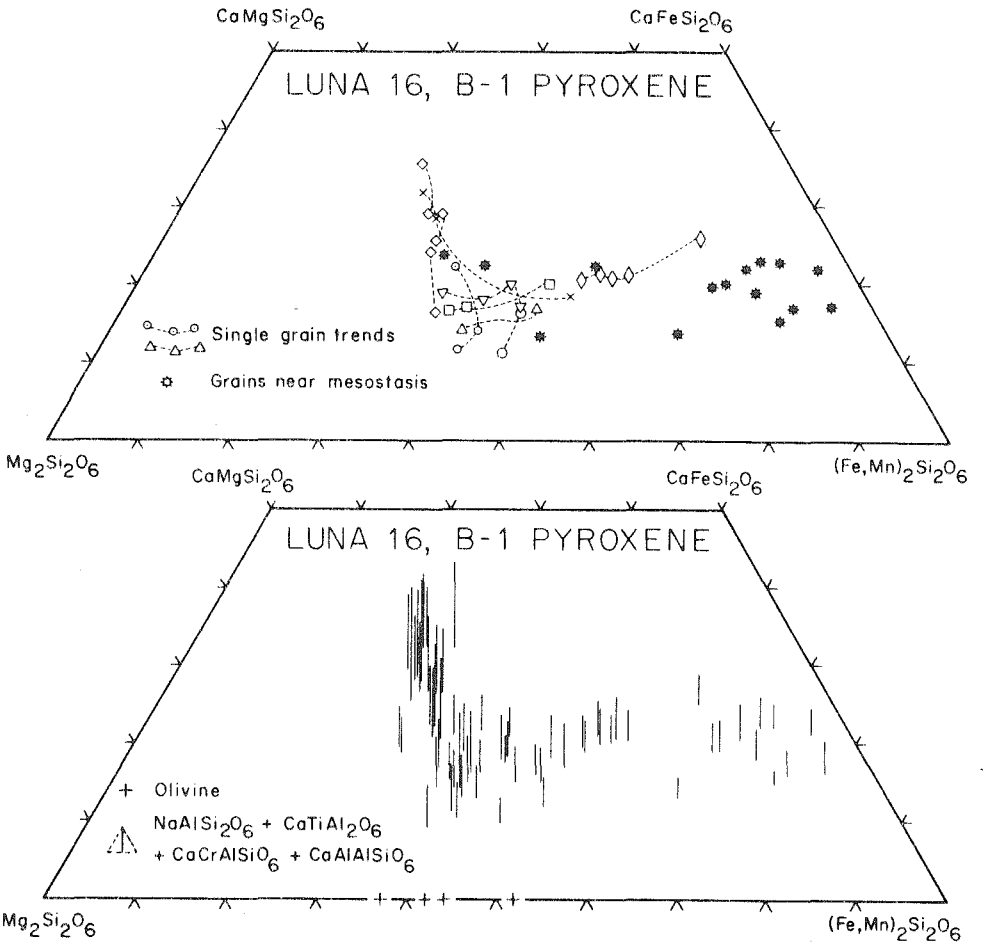

Fig. 5. Composition of pyroxene and olivine, Luna 16, B-1. Compositional trends within single grains are shown in the upper diagram (5a). The lower figure (5b) shows the composition of all analyzed points; the length of the line is the altitude of the triangle representing the percentage of components $NaAlSi_2O_6$, $CaTiAl_2O_6$, $CaCrAlSiO_6$, and $CaAlAlSiO_6$.

between plagioclase laths. Obtaining accurate analyses is difficult because the areas are very small. The average of analyses on 4 different patches of K- and Si-rich glass (?) is given in table 4. It was not possible to verify that any of the patches are actually isotropic because they do not extend entirely through the thin section. However, the 4 analyses are very similar and are similar to mesostasis glass from many Apollo samples. Four other analyses of K-rich areas indicate a high Fe content (8.4, 9.1, 18.3, and 33.1 wt%) as well as high K- and Ba-contents (table 4). Optical examination indicates that the measured Fe content is not due to adjacent pyroxene, ilmenite, or troilite; these areas are brown in color, partially anisotropic, and exhibit a globular pattern in reflected light. These analyses may represent a homogeneous glass, partially devitrified, but it is possible that they represent a mixture of K-rich globules in a Fe-rich residual phase, possibly fayalitic olivine.

Most phosphorous-rich areas were either too small for successful analysis or their analysis suggested that they are mixtures of phosphate minerals. Two analyses

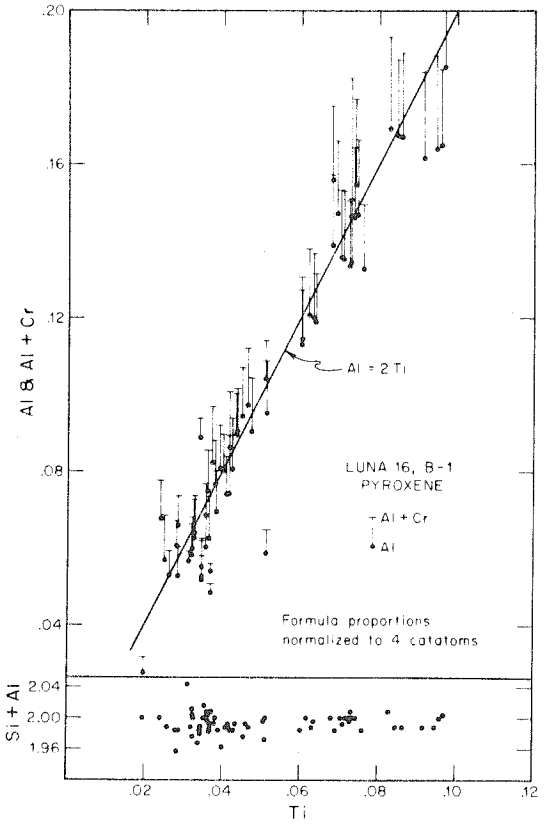

Fig. 6. Stoichiometric relationships in pyroxenes, Luna 16, B-1.

of phosphate grains about 300 μm apart are tabulated in table 5. One grain appears to be a fluorapatite with a high content of rare earth elements; its composition is similar to two other analyzed grains. The other grain appears to be a whitlockite, but the F content suggests that as much as 5% apatite may be present. The whitlockite also has a high content of rare earth elements. The analyses of these phosphate phases are generally similar to those found in the Apollo samples.

The distribution of U in the micro-thin sections was studied by fission track methods. The U is quite uniformly distributed in the largest thin section (FQM-150), and microprobe investigation indicates that the areas of high-track density are rich in P and/or Zr and are interstitial to the major minerals. Using F as a criterion to distinguish between whitlockite and apatite, qualitative microprobe analyses indicate that both phosphate minerals contain U. Zr is present as zircon, but none of the U-rich, Fe–Zr–Ti phases, such as those in the Apollo samples [8–10], are present. The zircon is generally associated with phosphate minerals. A small grain of baddeleyite (?) was also found.

In summary, although all the lunar basalts consist predominantly of pyroxene, plagioclase, and ilmenite, some distinctive differences can be recognized. The Apollo 11 basalts include fine-grained basalts and microgabbro, both of which are characterized by dominant augite and a high ilmenite content. The Apollo 12 basalts exhibit a wide variety of textures and grain size, commonly contain both pigeonite and augite, and contain much less ilmenite than Apollo 11

Table 3
Representative electron probe analyses of Fe–Ti–Cr oxides.

wt%	Ilmenite av. (19)	Range	Chromian-ulvospinel high-Cr	Chromian-ulvospinel low-Cr
SiO_2	0.13	0.16	(0.11–0.35)	0.15	0.15
Al_2O_3	0.18	0.10	(0.05–0.24)	4.06	1.90
Cr_2O_3	0.43	0.40	(0.17–0.62)	18.08	6.68
V_2O_3	0.09	0.06	(<0.01–0.12)	0.53	0.18
TiO_2	53.37	51.87	(50.76–53.37)	24.14	30.16
MgO	0.60	0.44	(0.04–0.95)	1.72	0.17
FeO	45.23	45.56	(44.35–46.66)	50.07	60.04
MnO	0.37	0.40	(0.32–0.46)	0.47	0.31
CaO	0.11	0.13	(0.06–0.29)	0.19	0.05
	100.51	99.12		99.41	99.64
Atom prop.					
Si	0.003	0.004		0.01	0.006
Al	0.01	<0.001		0.17	0.08
Cr	0.009	0.004		0.52	0.20
V	<0.001	<0.001		0.02	0.005
Ti	1.00	1.00		0.66	0.84
Mg	0.02	0.02		0.09	0.009
Fe	0.95	0.97		1.52	1.85
Mn	0.008	0.009		0.01	0.01
Ca	0.003	0.004		0.01	0.002
Total	2.00	2.01		3.01	3.00

Table 4
Representative electron probe analyses of K-rich mesostasis.

wt%	av. (4)	high-Fe
SiO_2	80.07	52.37
Al_2O_3	10.48	14.21
Cr_2O_3	0.01	n.a.
TiO_2	0.59	0.60
MgO	0.05	0.02
FeO	2.72	18.32
MnO	0.03	0.21
CaO	1.60	2.86
BaO	0.68	4.89
Na_2O	0.34	0.53
K_2O	4.14	6.00
Total	100.71	100.01

Table 5
Representative electron probe analyses of phosphate minerals.

	apatite wt%	apatite atom prop. *	whitlockite wt%	whitlockite atom prop. †
F	3.78	F 1.06	0.08	F 0.02
Cl	0.06	Cl 0.01	<0.01	Cl –
SiO_2	3.20	Si 0.28	6.89	Si 0.39
P_2O_5	36.46	P 2.75	38.04	P 1.81
Na_2O	0.07	Na 0.01	0.15	Na 0.02
MgO	0.02	Mg<.01	0.07	Mg<.01
CaO	46.90	Ca 4.47	36.23	Ca 2.19
FeO	2.62	Fe 0.19	8.54	Fe 0.40
Al_2O_3	0.96	Al 0.10	0.47	Al 0.03
Y_2O_3	1.44	Y 0.07	2.06	Y 0.05
La_2O_3	0.53	La 0.02	0.45	La 0.01
Ce_2O_3	1.88	Ce 0.06	2.39	Ce 0.05
Nd_2O_3	1.19	Nd 0.04	1.86	Nd 0.04
Total	99.11		97.23	

* Cations normalized to 8; † cations normalized to 5.

basalts. Apollo 14 sample 14310 and similar small fragments are low in ilmenite like the Apollo 12 samples, but contain dominant plagioclase, more mesostasis, and two or three pyroxenes, including orthopyroxene. Luna 16 sample B-1 contains a single pyroxene, predominantly pigeonitic in composition, subequal amounts of pyroxene and plagioclase, and an ilmenite content intermediate to that of the Apollo 11 and 12 samples. Although not dissimilar in texture and gross mineralogy to other fine-grained lunar basalts, it is not "most-like" the rocks of any one of the Apollo missions.

4. Chemistry

An analysis for major elements in Luna 16 sample B-1 is given in table 1. This analysis is the average of 27 microprobe analyses of 50 μm spots located at grid points distributed across a surface area of about 1.7 mm^2. The CaO, K_2O, and BaO values are in reasonable agreement with values determined by isotope dilution on the 3.1 mg "total" rock sample. This agreement suggests that the defocused beam analysis of these micro-thin sections gives a reasonable estimate of the chemical composition of sample B-1. The chemical analysis of Luna 16 basalt reported by

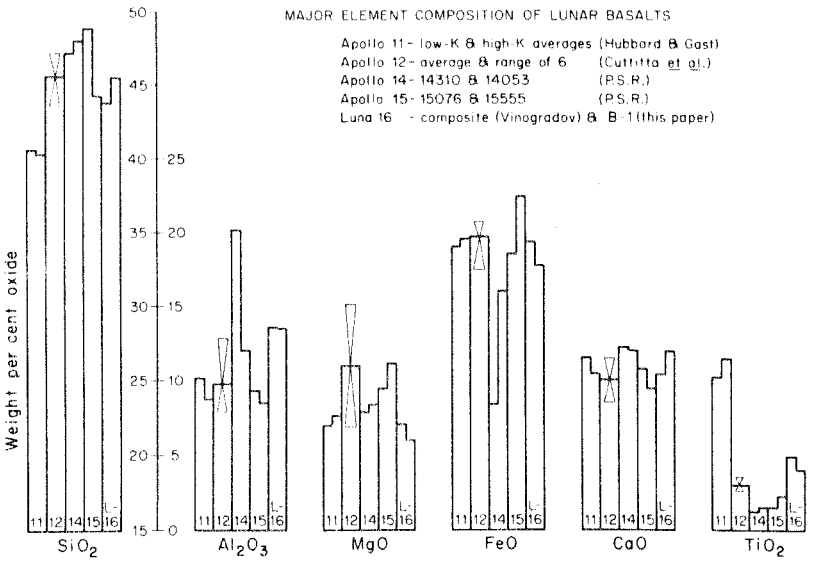

Fig. 7. Major element composition of lunar basalts. Apollo 11 is represented by an average for low-K and for high-K basalts [12]. Apollo 12 is represented by an average of 6 samples [13] with the maximum and minimum indicated by the hourglass. Apollo 14 is represented by samples 14310 and 14053 [14], which are the two large samples from that locality. Apollo 15 is represented by 15076, which is from the Elbow station, and 15555, which is from the Rille station [15]. Luna 16 is represented by a composite of basaltic fragments [3] and by sample B-1 [this paper].

Vinogradov [3] is also tabulated in table 1. We believe that this analysis represents a composite made up of a number of different fragments from the core. A comparison of our analysis and the proportions of normative minerals with that reported by Vinogradov [3] (table 1) shows them to be very similar. Hence, we conclude that sample B-1 is "typical" of basaltic fragments from the Luna 16 site.

Fig. 7 summarizes the major element composition of large crystalline rocks obtained from each of the lunar missions (or localities). Luna 16 sample B-1 does not closely correspond to any of them, nor is it grossly different in its major element chemistry. The SiO_2 content of sample B-1 is higher than that of Apollo 11 samples but similar to those from other localities. Its FeO content is somewhat low but is higher than both 14310 and 14053. The CaO content is slightly high but comparable to 14310, and its TiO_2 content is higher than all localities except Apollo 11.

This general bulk composition reflects a relatively high plagioclase to pyroxene ratio, although lower than 14310, and a higher ilmenite content than for all localities except Apollo 11. The low MgO content is reflected in the slightly lower Mg/Fe of the pyroxene.

Analyses for alkali, alkaline earths, and U are given in table 6 for a number of representative lunar samples. Included are new analyses for Luna 16 sample B-1, Luna 16 soil sample A-2, and Apollo 12 samples 12040,15 and 12070,5. Li, K, Rb, Cs, Ca, Sr, and Ba were determined by isotope dilution using the procedures described by Tera et al. [5]. The U content of Luna 16, A-2 was determined by procedures described by Tera and Wasserburg [11]. A U-content of 0.30 ± 0.03 μg/g was measured on the 1.2 mm^2 micro-thin section (FQM-150) by fission-track methods.

The K, Rb, Ba, and U content of sample B-1 is greater than that found in low-K Apollo 11 rocks, and the Apollo 12 rocks, but less than in the high-K Apollo 11 rocks and 14310. However, the Sr content is higher than for rocks from all other localities including 14310. This high Sr content is not simply due to a high plagioclase content as is demonstrated by the anomalously-high Sr found in the plagioclase

Table 6
Alkali, alkaline earths, and U in representative lunar samples.

Sample	Ref.	Li ppm	Na %	K ppm	Rb ppm	Cs ppb	Ca %	Sr ppm	Ba ppm	U ppm	K/Rb	K/Ba	K/Ca	K/Sr	K/U
10017,32	[5]	18.1	0.348	2388	5.57	159	7.35	156.5	280	0.854 [16]	429	8.53	0.0325	15.3	2796
Av. high-K rocks	[17]	nd *	nd	2400	nd	nd	nd	nd	nd	0.8	–	–	–	–	3000
10050,24	[5]	11.0	0.273	664	0.750	29	8.17	171.3	92	0.156 [16]	885	7.2	0.0081	3.88	4260
Av. low-K rocks	[17]	nd	nd	500	nd	nd	nd	nd	nd	0.25	–	–	–	–	2000
12040,15 "total"	[this paper]	6.91	0.161	364	0.762	33.5	5.83	102.4	47.7	0.24 [18]	478	7.63	0.0062	3.55	1500
plagioclase	[this paper]	nd	1.15	463	0.253	nd	13.1	355	46.5	nd	–	–	–	–	–
Av. Apollo 12	[17]	nd	nd	520	nd	nd	nd	nd	nd	0.25	–	–	–	–	2100
14310	[14]	19	nd	4900	15	nd	nd	250	630	3.7	330	7.78	–	19.6	1300
14053	[14]	11	nd	880	2	nd	nd	180	190	0.64	400	4.63	–	4.9	1400
Luna 16, B-1 "total"	[this paper]	10.7	nd	1396	1.58	53.6	8.25	436.6	218.2	0.30	884	6.40	0.0169	3.20	4700
plagioclase	[this paper]	nd	nd	nd	1.42	nd	nd	1084	nd	nd					
Soils															
10084,12	[5]	12.5	0.314	1110	2.68	101	8.52	162.8	169	0.544 [16]	414	6.57	0.0130	6.82	2040
12070,5	[this paper]	18.3	0.324	1986	6.36	273	7.34	142.4	377	nd	312	5.27	0.0271	13.9	–
12070,0	[17]	nd	nd	2030	nd	nd	nd	nd	nd	1.65	–	–	–	–	1230
14163	[19]	nd	0.54	4100	16	680	7.2	185	748	3.4	260	5.48	0.057	22.2	1200
14163	[20]	31.2	nd	4530	15.35	nd	nd	186	818	nd	295	5.77	–	24.3	–
Luna 16, A-2	[this paper]	8.5	nd	844	1.79	65.1	8.25	271.4	168.4	0.338	472	5.01	0.0102	3.11	2500

* Not determined.

(table 6). As observed by other workers, both Eu and Sr are concentrated by about a factor of three in plagioclase relative to the whole rock in typical Apollo 11 rocks, and the Sr/Eu value is about 130 in plagioclase [21]. Whole rock Sr/Eu values for Apollo 11 and 12 rocks range from about 70 to 120 [12]. From these relationships and the high Sr content we infer that B-1 will show an anomalously high Eu content of about 8 ppm in the plagioclase and about 4–6 ppm in the total rock of sample B-1. Such high values could result in a positive Eu anomaly if the trivalent rare earths do not show a similar enrichment. Since the soil is also comparatively high in Sr (table 6), [1], this could also account for the small magnitude of the negative Eu anomaly in the soil (see other papers, this issue).

The K/Rb value is high but similar to that in the low-K Apollo 11 rocks. The K/Ca value is notably higher than in the low-K Apollo 11 and Apollo 12 rocks but less than in the high-K Apollo 11 rocks. The K/U value is much higher than for any other samples for which both K and U were determined on the same sample split and is closer to terrestrial values (see also O'Kelly et al. [17]). The high value for sample 10050,24 is based on Tera's [5] K-value and Tatsumoto's [16] U-value. It is much higher than the average value, or of any of the values, obtained on the low-K Apollo 11 rocks by gamma-ray spectrometry, and it should be verified by that technique.

In summary the high K/U value and high Sr-content of Luna 16 sample B-1 distinguishes it from the Apollo samples.

Luna 16 soil sample A-2 is a < 125 μm split of the Russian sample Luna 16-17A from the A-layer of the core. Compared to the Apollo soil samples it is low in K, Rb, Cs, Ba, and U but high in Sr. The K/Rb, K/Ba, and K/U do not differ sharply from the other soils, but the K/Sr is significantly lower. In general the soils from the various lunar localities have a higher K content than the low-K rocks at each site; e.g., Apollo 11 soils are higher in K than the low-K rocks but less than the high-K rocks; Apollo 12 soils have a higher K content than all rocks except 12013; and Apollo 14 soils have a K content greater than 14053 but less than 14310. The K content and the K/Rb, K/Ba, and K/U values are much less in the soil sample than in the basaltic fragment. Assuming that this size fraction has a K content similar to that of the entire soil sample (see Vinogradov [3]), there may exist basalt fragments at this site lower in K than sample B-1. It is of course possible that low-K, non-basaltic rocks balance the composition, but the Ca contents indicate that such other rocks cannot have a plagioclase content substantially higher than sample B-1. On the basis of this data, the Luna 16 soil will be found to contain little or no "magic", "cryptic" or "KREEP" component (see also Reid et al. [22]). This same conclusion can be drawn from a detailed comparison of Vinogradov's [3] analyses of basalt fragments and of the various soil zones, including zone A.

5. Conclusions

Crystalline rock samples have now been collected from five lunar sites located in different selenographic settings. Comparison of the individual rocks within localities and among localities should indicate any relationships between parent melts of the individual rocks and constraints on the generation and solidification of these melts.

The lunar basalts have certain chemical and petrologic characteristics in common with each other distinguishing them from any terrestrial basalt. Probably the most distinctive bulk chemical difference common to all the lunar samples which have been examined is the low Na content. The Fe, Ti, and U contents are generally higher than in terrestrial basalts. The K content is lower than in terrestrial alkali-olivine (continental) basalts and, except for the high-K Apollo 11 rocks and 14310, is lower than in the tholeiitic oceanic ridge basalts. Other distinctive features which are well documented for the Apollo 11 and 12 sites include: the higher content of refractory elements and trivalent rare earth elements; the lower content of volatile, chalcophile, siderophile, and alkali elements; and a marked depletion of Eu relative to the other rare earth elements.

The lunar basaltic rocks consist predominantly of pyroxene, plagioclase, and ilmenite, all three of which coprecipitated throughout most of the crystallization history of the rock. Most rocks exhibit abundant evidence of rapid crystallization and extreme internal differentiation, indicated by strong zoning in pyroxene and plagioclase and the presence of mesostasis. The compositional range in the pyroxenes of most

rocks and even in single pyroxene grains is similar to that found in extensive layered gabbros on earth and the fractionation culminates in an interstitial, residual mesostasis equivalent to the "red rock" differentiates of layered gabbros. The zoning in plagioclase is restricted to the calcic region, reflecting the low Na content characteristic of lunar rocks. This extreme in situ differentiation over a similar range, the general absence of phenocrysts and xenocrysts, the absence of cumulate textures, and the presence of aphanitic and vitrophyric textures suggests that these rocks crystallized from a completely molten magma whose bulk composition was close to that of the individual rock specimens. Any effects of fractional crystallization are restricted to those produced by these phases initially appearing on the liquidus for these bulk compositions.

Despite these similarities differences exist between the individual rocks and between the rocks from the various localities. Textural evidence indicates that the order of initial crystallization of ilmenite, pyroxene, and plagioclase, as well as olivine and spinel, differs from rock to rock. Experimental studies suggest that the slight, but distinct, differences in the proportion of the major elements, as discussed above, are probably sufficient to account for this variation in order of appearance of the phases.

The varied crystallization histories and compositional zoning trends characteristic of the pyroxenes from the various localities are petrologically distinctive. Some localities had only one pyroxene phase crystallizing from the melt, whereas others had two, or even three, pyroxenes coprecipitating, and some pyroxenes contain cores of olivine or of another pyroxene phase. These relations and the detailed compositional trends indicate distinct differences in the position of the pyroxene cotectic and in the topology of the intersection of the melt field with the subsolidus phase regions of the pyroxene quadrilateral. These different evolutionary histories of pyroxenes have been variously attributed to a number of variables. However, since the basaltic rocks at each locality seem to have crystallized from melts with characteristic bulk compositions and seem to have characteristic compositional trends in their pyroxenes, it seems likely that the different trends are predominantly due to apparently minor differences in the bulk composition of the systems.

Although compositional differences between the localities do not appear to be related to fractionation (either gain or loss) of early crystallizing phases, many differences among the rocks at a given locality may be related to fractional crystallization (see, for example [23–26]). Major variation in minor elements may result from migration of the late residual liquid. This process would explain variations in Ba, U, K, REE, P, and other such elements, but these could also be explained by varying degrees of crustal contamination of the melts [27].

Even without the demonstrated age differences, petrologic and chemical evidence prohibits the derivation of the rocks from the various localities from one another by fractional crystallization. Since their compositions seem to represent melt compositions, it must be possible to generate lunar melts of distinctly different compositions. They may form by fractional melting of inhomogeneous source materials or by fractional melting under different conditions, but they do not form by different degrees of fractional melting from a single source under identical conditions.

Acknowledgments

We are grateful to the Academy of Sciences of the USSR for making it possible for us to work on these samples. We greatly appreciate the confidence which The Lunar Sample Analysis Planning Team and the curator of the lunar samples have shown by entrusting us with the handling of such a extrenely valuable sample. We are indebted to Jack Huneke for valid criticism of the manuscript and to Paul Gast for a useful discussion of the Sr/Eu relationships. Joe Brown meticulously prepared the micro-thin sections.

The work was supported by NASA contracts NAS 9-8074 and NA 7-100. The microprobe laboratory has been developed with the support of NSF, JPL, and the Union Pacific Foundation.

References

[1] D.A. Papanastassiou and G.J. Wasserburg, The Rb-Sr age of a basaltic pebble from the Luna 16 site, Earth Planet. Sci. Letters 13 (1972) 000.

[2] J.C. Huneke, F.A. Podosek and G.J. Wasserburg, Gas retention and cosmic-ray exposure ages of a basalt frag-

ment from Mare Fecunditatis, Earth Planet. Sci. Letters 13 (1972) 375.

[3] A.P. Vinogradov, Preliminary data on lunar ground brought to Earth by automatic probe "Luna 16", Geochim. Cosmochim. Acta, Suppl. 2, vol. 1 (1971) 1.

[4] A.L. Albee and L. Ray, Correction factors for electron probe micro-analysis of silicates, carbonates, phosphates, and sulfates, Analytical Chem. 42 (1970) 1408.

[5] F. Tera, O. Eugster, D.S. Burnett and G.J. Wasserburg, Comparative study of Li, Na, K, Rb, Cs, Ca, Sr and Ba abundances in achondrites and in Apollo 11 lunar samples, Geochim. Cosmochim. Acta, Suppl. 1, vol. 2 (1970) 1637.

[6] A.L. Albee and A.A. Chodos, Microprobe investigations on Apollo 11 samples, Geochim. Cosmochim. Acta, Suppl. 1, vol. 1 (1970) 135.

[7] N.L. Carter, I.S. Leung, H.G. Avé Lallement and L. Fernandez, Growth and deformational structures in silicates from Mare Tranquillitatis, Geochim. Cosmochim. Acta, Suppl. 1, vol. 1 (1970) 267.

[8] J.F. Lovering, D.A. Wark, A.F. Reid, N.G. Ware, K. Keil, M. Prinz, T.E. Bunch, A. El Goresy, P. Ramdohr, G.M. Brown, A. Peckett, R. Phillips, E.N. Cameron, J.A.V. Douglas and A.G. Plant, Tranquillityite: A new silicate mineral from Apollo 11 and Apollo 12 basaltic rocks, Geochim. Cosmochim. Acta, Suppl. 2, vol. 1 (1971) 39.

[9] J.F. Lovering and D.A. Wark, Uranium-enriched phases in Apollo 11 and Apollo 12 basaltic rocks, Geochim. Cosmochim. Acta, Suppl. 2, vol. 1 (1971) 151.

[10] E.L. Haines, A.L. Albee, A.A. Chodos and G.J. Wasserburg, Uranium-bearing minerals of lunar rock 12013, Earth Planet. Sci. Letters 12 (1971) 145.

[11] F. Tera and G.J. Wasserburg, U, Th and Pb analyses on soil samples returned from the Luna 16 mission, Earth Planet. Sci. Letters 13 (1972) 457.

[12] N.J. Hubbard and P.W. Gast, Chemical composition and origin of nonmare lunar basalts, Geochim. Cosmochim. Acta, Suppl. 2, vol. 2 (1971) 999.

[13] F. Cuttitta, H.J. Rose, Jr., C.S. Annell, M.K. Carron, R.P. Christian, E.J. Dwornik, L.P. Greenland, A.W. Helz and D.T. Ligan, Jr., Elemental composition of some Apollo 12 lunar rocks and soils, Geochim. Cosmochim. Acta, Suppl. 2, vol. 2 (1971) 1217.

[14] Lunar Sample Preliminary Examination Team, Preliminary examination of the lunar samples, in: NASA Manned Spacecraft Center, Apollo 14 Preliminary Science Report SP-272 (1971) 109.

[15] Lunar Sample Preliminary Examination Team, A preliminary description of the Apollo 15 lunar samples in: NASA Manned Spacecraft Center, Apollo 15 Preliminary Science Report, in press.

[16] M. Tatsumoto, Age of the moon: an isotopic study of U-Th-Pb systematics of Apollo 11 lunar sample II, Geochim. Cosmochim. Acta, Suppl. 1, vol. 2 (1970) 1595.

[17] G.D. O'Kelley, J.S. Eldridge, E. Schonfeld and P.R. Bell, Abundances of the primordial radionuclides K, Th, and U in Apollo 12 lunar samples by nondestructive gamma-ray spectrometry: Implications for the origin of lunar soils, Geochim. Cosmochim. Acta, Suppl. 2, vol. 2 (1971) 1159.

[18] D. Burnett, M. Monnin, M. Seitz, R. Walker and D. Yuhas, Lunar astrology-U-Th distribution and fission track dating of lunar samples, Geochim. Cosmochim. Acta, Suppl. 2, vol. 2 (1971) 1503.

[19] A.O. Brunfelt, K.S. Heier, E. Steinnes and B. Sundvoll, Determination of 36 elements in Apollo 14 bulk fines 14163 by activation analysis, Earth Planet. Sci. Letters 11 (1971) 351.

[20] C.C. Schnetzler and D.F. Nava, Chemical composition of Apollo 14 soils 14163 and 14259, Earth Planet. Sci. Letters 11 (1971) 345.

[21] J.A. Philpotts and C.C. Schnetzler, Apollo 11 lunar samples: K, Rb, Sr, Ba and rare-earth concentrations in some rocks and separated phases, Geochim. Cosmochim. Acta, Suppl. 1, vol. 2 (1970) 1471.

[22] J.B. Reid, Jr., G.J. Taylor, U.B. Marvin and J.A. Wood, Luna 16: Relative proportions and petrologic significance of particles in the soil from Mare Fecunditatis, Earth Planet. Sci. Letters 13 (1972) 286.

[23] P.W. Gast, N.J. Hubbard and H. Weismann, Chemical composition and petrogenesis of basalts from Tranquillity Base, Geochim. Cosmochim. Acta, Suppl. 1, vol. 2 (1970) 1143.

[24] O.B. James and E.D. Jackson, Petrology of the Apollo 11 ilmenite basalts, J. Geophys. Res. 75 (1970) 5793.

[25] C.C. Schnetzler and J.A. Philpotts, Alkali, alkaline earths, and rare-earth element concentrations in some Apollo 12 soils, rocks, and separated phases, Geochim. Cosmochim. Acta, Suppl. 2, vol. 2 (1971) 1101.

[26] Apollo Soil Survey, Apollo 14: Nature and origin of rock types in soil from the Fra Mauro Formation, Earth Planet. Sci. Letters 12 (1971) 49.

[27] G.J. Wasserburg and D.A. Papanastassiou, Age of an Apollo 15 mare basalt; lunar crust and mantle evolution, Earth Planet. Sci. Letters 13 (1971) 97.

THE URANIUM DISTRIBUTION IN LUNAR SOILS AND ROCKS 12013 and 14310 (1) E. L. Haines, A. J. Gancarz, A. L. Albee, and G. J. Wasserburg, Jet Propulsion Laboratory and Division of Geological and Planetary Sciences, California Institute of Technology, Pasadena, Calif. 91109.

The U distribution in lunar samples 12013,14; 12013,15 and 14310,6 and in soils 10084,8; 12070,5; 14259,97 and 15221,46 was studied by fission track (2) and electron microprobe mapping techniques. The major U-bearing phases are whitlockite, apatite, zircon, baddeleyite, thorite and Zr-Ti rich phases. Zr-Ti rich phases have been reported by many authors (3,4) but the extremely high U, Th and Pb concentrations are rare. A Zr-Ti rich phase in rock 12013 contains major Ca, Fe, Nb, Y, REE and up to 4.2 wt% PbO, 4.7 wt% ThO_2 and 3.6 wt% UO_2 (3). Thorite was identified in soil sample 14259,97.

Grains containing more than 10^9 U atoms were recorded and identified with the electron microprobe. They contain from 1.8 to 29.9 atomic percent of the total sample U. Tables 1 and 2 list the minimum atomic percentages of the total sample U contained in the major U-bearing phases. The percentages ascribed to "unidentified hosts" collectively refers to major phases with very low U concentration and/or very small grains of the U-bearing phases containing less than 10^9 U atoms and/or U adsorbed on the grain surfaces.

Lunar rock 12013 is distinguished among the rocks returned by the Apollo mission by its lithic heterogeniety and by its high abundance of Si, K, Rb, Y, Zr, Nb, Ba, REE, Th and U. It consists of a heterogeneous mixture of a "dark" clastic lithology and a "light" K-feldspar-rich lithology. In the dark lithology much of the U resides in phosphate and zircon and is relatively uniformly distributed (Table 1). The light lithology contains rare grains of a Zr-Ti rich phase. Although rich in U, Th, and Pb, these grains apparently do not dominate the U, Th, Pb systematics as was suggested earlier (3). Zircon and phosphates are also present in the light lithology, and while their U and Th concentrations are much lower than those of the Zr-Ti-rich phase, their larger modal abundances make their U contribution to the total rock U budget as significant as the Zr-Ti-rich phase (Table 1).

Concentrations of U, Th and Pb are sufficiently high in the Zr-Ti rich phase of rock 12013 to permit calculation of ages from electron microprobe analyses of these three elements. These ages average 4.0 ± 0.1 AE (3). Reasonable agreement with the Rb-Sr and Ar^{39}/Ar^{40} ages suggests that these phases represent closed systems with respect to U, Th, and Pb.

Rock 14310 was investigated because it is the most U-rich crystalline rock known. The identified U-bearing phases include baddeleyite, phosphate, zircon and Zr-Ti rich phases (Table 1) but 95 atomic percent of the U resides in grains with less than 10^8 atoms of U per grain. If this U is present in these U-rich phases, their grain size must be ≤ 1 μm.

Haines et al. (3) suggested that the Zr-Ti-rich phase may significantly affect the U, Th, and Pb systematics of the lunar soils. Table 2 gives U distribution data in soils from all the lunar missions. The data suggest that

a Zr-Ti rich phase is an important U-bearing phase, and contains more of the soils' U than either zircon or phosphate. However, in no case do these coarser grained (10^9 U atoms/grain)U-rock phases dominate the soils U,Th,and Pb budget. However, in sample 14259,97 the one grain of thorite does dominate the U content of the sample, thus a few grains of thorite in a soil sample would seriously alter the total U content of the soil and the U, Th, Pb systematics.

References: (1) This research was supported by the Director's Discretionary Fund, Jet Propulsion Laboratory and by the National Aeronautics and Space Administration, contracts NAS 7-100 and NAS 9-8074.

(2) E. Haines, "Precise Coordinate Control in Fission Track Uranium Mapping" Nucl. Instr. Methods (in press).

(3) E. Haines, A. Albee, A. Chodos, G. Wasserburg, Earth Plan. Sci. Lett. 12, 145 (1971).

(4) D. Burnett, M. Monnin, M. Seitz, R. Walker, D. Yuhas, Second Lunar Sci. Conf., Geochim. Cosmochim. Acta, Suppl. 2, 2, 1503 (1971); J. Lovering, D. W[illegible] A. Reid, N. Ware, K. Keil, M. Prinz, T. Bunch, A. El Goresy, P. Ramdohr, G. Brown, A. Peckett, R. Phillips, E. Cameron, J. Douglas, A. Plant, Ibid., 1, 39 (1971); J. Lovering, D. Wark, Ibid., 1, 151 (1971); C. Rice, S. Bowie, Ibid., 1, 159 (1971); A. Gancarz, A. Albee, A. Chodos, Earth Plan. Sci. Lett. 12, 1 (1971); F. Busche, M. Prinz, K. Keil, G. Kurat,"Lunar Zirkelite: A uranium-bearing phase", (submitted for publication).

Table 1. Uranium Distribution in Rocks 12013 and 14310 (atomic %)

	sample		
	14310,6	12013,14	12013,15
Unidentified hosts	95.6	89.0	95.1
Phosphate minerals	2.2(12)*	9.5(8)	1.9(10)
Zr-Ti rich phases	0.9(13)	0.9(7)	2.0(22)
Zircon	0.5(7)	0.6(7)	1.0(12)
Baddeleyite	0.7(6)	<0.1(0)	<0.1(0)

* (1) number of grains identified

Table 2. Uranium Distribution in Lunar Soils (atomic %)

	sample			
	10084,8	12070,5	14259,97	15221,46
Unidentified hosts	98.2	89.1	70.0	93.5
Phosphate minerals	0.2(1)*	2.4(5)	1.5(13)	2.2(6)
Zr-Ti rich phases	1.5(1)	7.3(7)	5.3(23)	2.5(5)
Zircon	0.1(1)	0.7(2)	1.2(7)	1.8(3)
Thorite	<0.1(0)	<0.1(0)	21.6(1)	<0.1(0)
Baddeleyite	<0.1(0)	0.5(1)	0.4(3)	<0.1(0)

PETROLOGY OF APOLLO 15 SAMPLE 15486. A. L. Albee, A. A. Chodos and A. J. Gancarz, California Institute of Technology, Pasadena, Calif. 91109.*

Sample 15486 is one of three samples—15485, 15486 and 15499—collected from a large (>1m) vesicular block at station 4 on the south rim of Dune Crater. $^{40}Ar/^{39}Ar$ studies by Huneke et al. [1] show that 15499 has an age of 3.40 AE and a Rb-Sr model age has been reported [2]. Silver and Jakes [3] describe 15486 as a blocky, angular porphyritic basalt fragment (47 gm), 5.6 x 3 x 2.5 cm, with a grey coating on fracture surfaces and some zap pits on the exterior surfaces. They describe pyroxene prisms up to 10mm in length and about 5% vugs.

The sample was studied in polished thin section 15486,20(area $\approx$ 75mm^2). It is a porphyritic, clinopyroxene vitrophyre composed of elongate pyroxene prisms (53%) in a matrix of opaque devitrified glass (44%) with 3% globulose vugs and about 0.1% each of spinel and Fe-metal. Olivine phenocrysts are reported in other samples from this block [4-5], but are not present in this sample.

The matrix appears to be a devitrified glass composed of extremely fine-grained segregations of crystallites. It is predominantly opaque, but a "fingerprint-like" pattern is visible under reflected light at high magnification. The striations in the "fingerprint" pattern are made up of alternating subparallel segregations about 1μm wide, consisting of crystallites of either pyroxene or plagioclase and opaque minerals. At their edges light is partially transmitted and the opacity appears to be due to a myriad of wormlike rods, about 0.2μm in diameter, of opaque minerals, predominantly troilite.

Despite the devitrification-segregation the matrix is quite homogeneous at the 20μm level. Five analyses of 20μm diameter spots are nearly identical (analysis 9). The matrix contains about 53% normative feldspar, 35% pyroxene, 7% SiO_2, and 4% opaque minerals. This may be compared to the norm for a chemical analysis of 15499 [4] which contains about 28% feldspar, 68% pyroxene and 0.4% SiO_2. A devitrified glass inclusion within a pyroxene prism (analysis 10) has an intermediate composition.

Pyroxene occurs as elongate skeletal prisms, which commonly enclose matrix (see photomicrographs of 15485 [4] and 15499[5]). Many of the larger grains contain low-Ca clinopyroxene cores enclosed by high-Ca clinopyroxene (figs. 2 and 3). As illustrated, $CaAlAlSiO_6$, $NaAlSi_2O_6$, and $CaTiAl_2O_6$ increase outward and $CaCrAlSiO_6$ decreases outward. This minor element variation is similar to that described for 15499 by Bence and Papike [5], who note that Al/Si increases in lunar pyroxene continuously until the onset of plagioclase crystallization, which never began in this rock. Some areas of the slide contain many small pyroxene grains with rather uniform augitic composition similar to that of the rims of larger pyroxene phenocrysts.

Spinels and Fe-metal are present in minor amounts (<0.5%), but ilmenite and troilite are absent as phenocrysts and are present only in the devitrified matrix. Cr-spinel occurs in euhedral grains, 20-100μm, both in pyroxene and in the matrix. These grains become more Al-rich and more Fe-rich from the core outward and many of them are rimmed by Fe-rich ulvöspinel (fig. 1). These rims

Table 1: Selected electron microprobe analyses from sample 15486,20

	Pyroxene				Spinel				"Glass"			
wt.%	1	2	3	4	5	6	7	8		9		10
SiO_2	52.08	50.45	48.14	44.61	0.26	0.72	1.12	0.35	SiO_2	48.84	±0.62	43.98
Al_2O_3	2.32	4.09	6.33	9.23	11.25	7.93	12.42	11.27	Al_2O_3	16.83	±0.95	14.99
Cr_2O_3	1.14	1.20	0.76	0.06	53.40	9.44	30.82	51.15	Cr_2O_3	0.01	±0.01	0.04
TiO_2	0.50	1.22	1.67	2.23	2.35	24.72	11.11	5.93	TiO_2	2.30	±0.23	3.05
MgO	23.12	13.96	11.89	7.41	7.76	0.61	1.32	7.19	MgO	0.77	±0.10	2.83
FeO	17.14	14.10	16.01	26.53	24.32	54.16	42.47	26.07	FeO	20.34	±1.80	22.98
MnO	0.28	0.30	0.27	0.35	0.72	0.35	0.49	0.72	MnO	0.21	±0.02	0.30
CaO	3.43	15.39	16.45	10.89	n.a.	n.a.	n.a.	n.a.	CaO	9.98	±0.43	10.99
Na_2O	0.02	0.05	0.07	0.08	n.a.	n.a.	n.a.	n.a.	BaO	0.02	±0.03	0.02
									Na_2O	0.88	±0.09	0.44
Total	100.03	100.76	101.59	101.39	100.06	97.93	99.75	102.63	K_2O	0.15	±0.01	0.09
									P_2O_5	0.18	±0.03	0.14
									SO_3	0.15	±0.11	0.05
									NiO	<0.01		<0.01
Formula proportions									ZrO_2	<0.01		<0.01
									Total	100.66	±0.85	99.90
Si	1.91	1.89	1.81	1.74	0.01	0.03	0.04	0.01				
Al	0.10	0.18	0.28	0.42	0.44	0.34	0.51	0.43		"Glass Norms"		
Cr	0.03	0.04	0.02	<0.01	1.41	0.27	0.85	1.32	an	44.11		41.49
Ti	0.01	0.03	0.05	0.07	0.06	0.68	0.29	0.15	ab	8.40		4.24
Mg	1.27	0.78	0.67	0.43	0.39	0.03	0.07	0.35	or	0.94		0.57
Fe	0.53	0.44	0.50	0.87	0.68	1.64	1.23	0.71	cel	0.04		0.04
Mn	0.01	0.01	0.01	0.01	0.02	0.01	0.01	0.02	en	2.26		8.22
Ca	0.14	0.62	0.66	0.46	n.a.	n.a.	n.a.	n.a.	fs	30.20		33.37
Na	0.01	<0.01	0.01	0.01	n.a.	n.a.	n.a.	n.a.	wo	2.90		6.43
									fo	0.0		0.13
Total	4.01	3.99	4.01	4.01	3.01	3.00	3.00	2.99	fa	0.0		0.53
									Q	7.12		0.0
									C	0.0		0.0
									il	3.41		4.54
									cm	0.01		0.05
									FeS	0.22		0.08
									ap	0.40		0.31
									Z	0.0		0.0
									NiO	0.0		0.0

n.a. ≡ not analyzed for

Petrology of Apollo 15 Sample 15486

A. L. Albee

tend to be broader on grains in the matrix than on grains enclosed in pyroxene. Fe-metal occurs as equidimensional spherical blebs or aggregates of equidimensional blebs. It is both associated with spinel and independent of spinel in the matrix. An average of 8 analyses gives the following composition: $Fe_{92.16}$ wt%, $Ni_{6.28}$, and $Co_{1.42}$. A computer printout of all electron microprobe analyses from sample 15486,20 is available upon request.

REFERENCES

[1] J.C. Huneke, F.A. Podosek, and G.J. Wasserburg, personal communication.
[2] D.A. Papanastassiou and G.J. Wasserburg, Rb-Sr ages and initial strontium in basalts from Apollo 15 (in press).
[3] Lunar Sample Information Catalog: Apollo 15, NASA pub. MSC 03209 (1971).
[4] Lunar Sample Preliminary Examination Team, Preliminary examination of lunar samples in: Apollo 15: Preliminary Science Report NASA SP-289 (1972).
[5] A.E. Bence and J.J. Papike, Pyroxenes as recorders of lunar basalt petrogenesis: I. Chemical data for liquidus trends (in press).

*Contribution number 2211

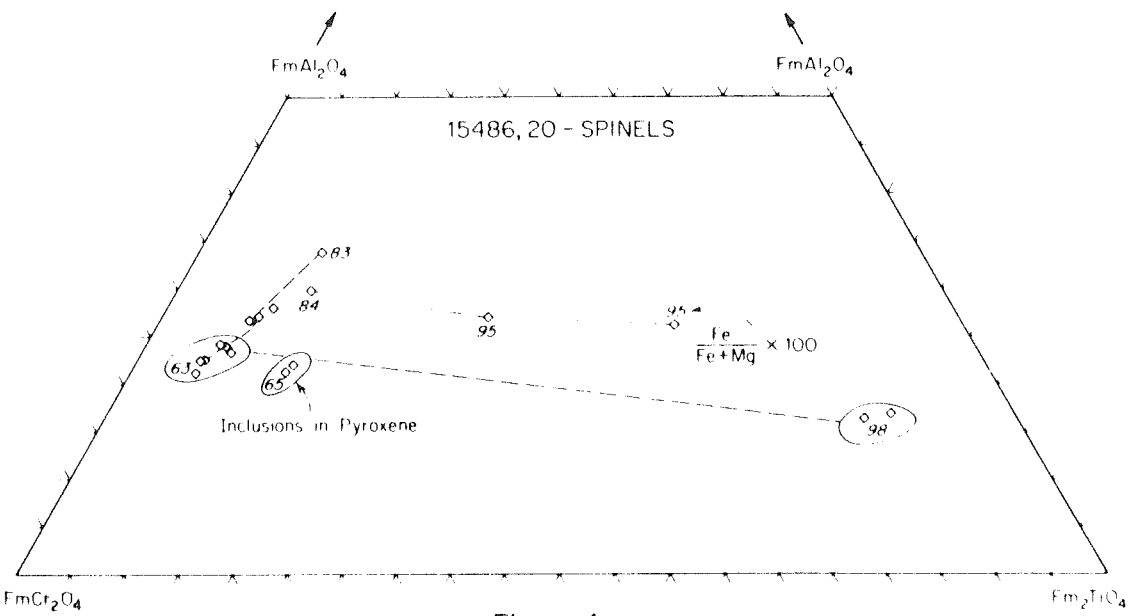

Figure 1

Petrology of Apollo 15 Sample 15486

A. L. Albee

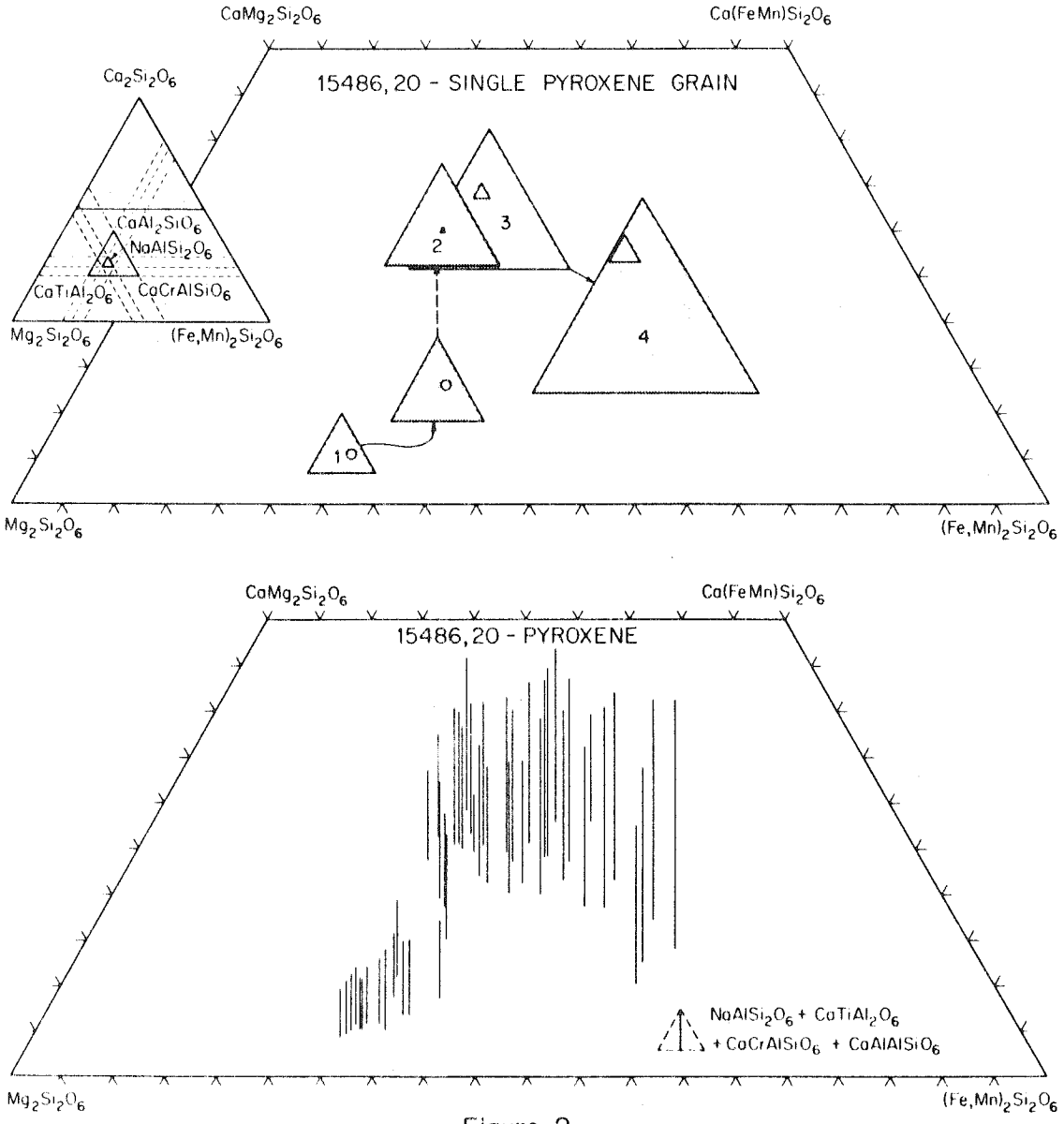

Figure 2

Petrology of Apollo 15 Sample 15486

A. L. Albee

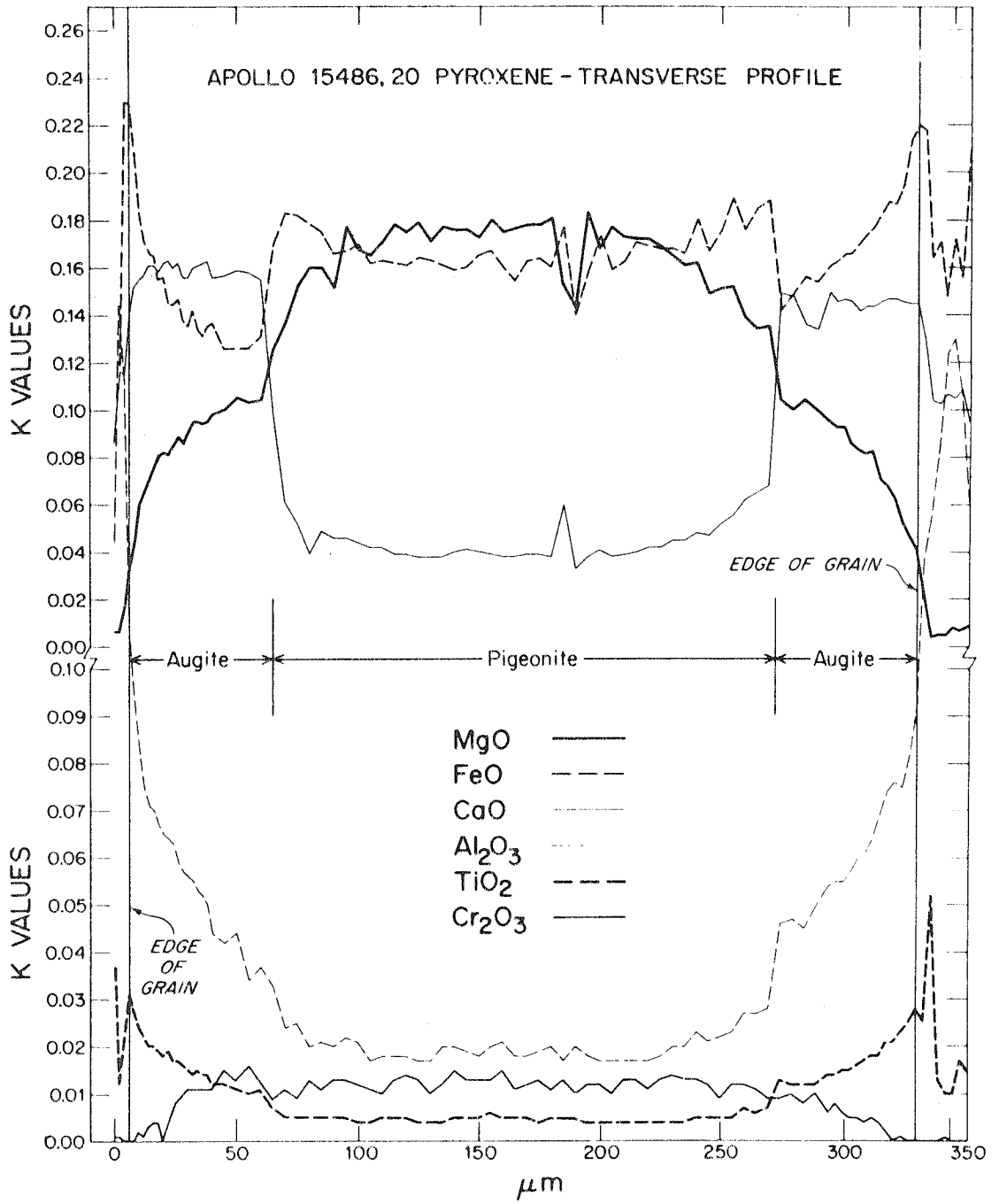

Figure 3

Petrology of Apollo 15 Sample 15486

A. L. Albee

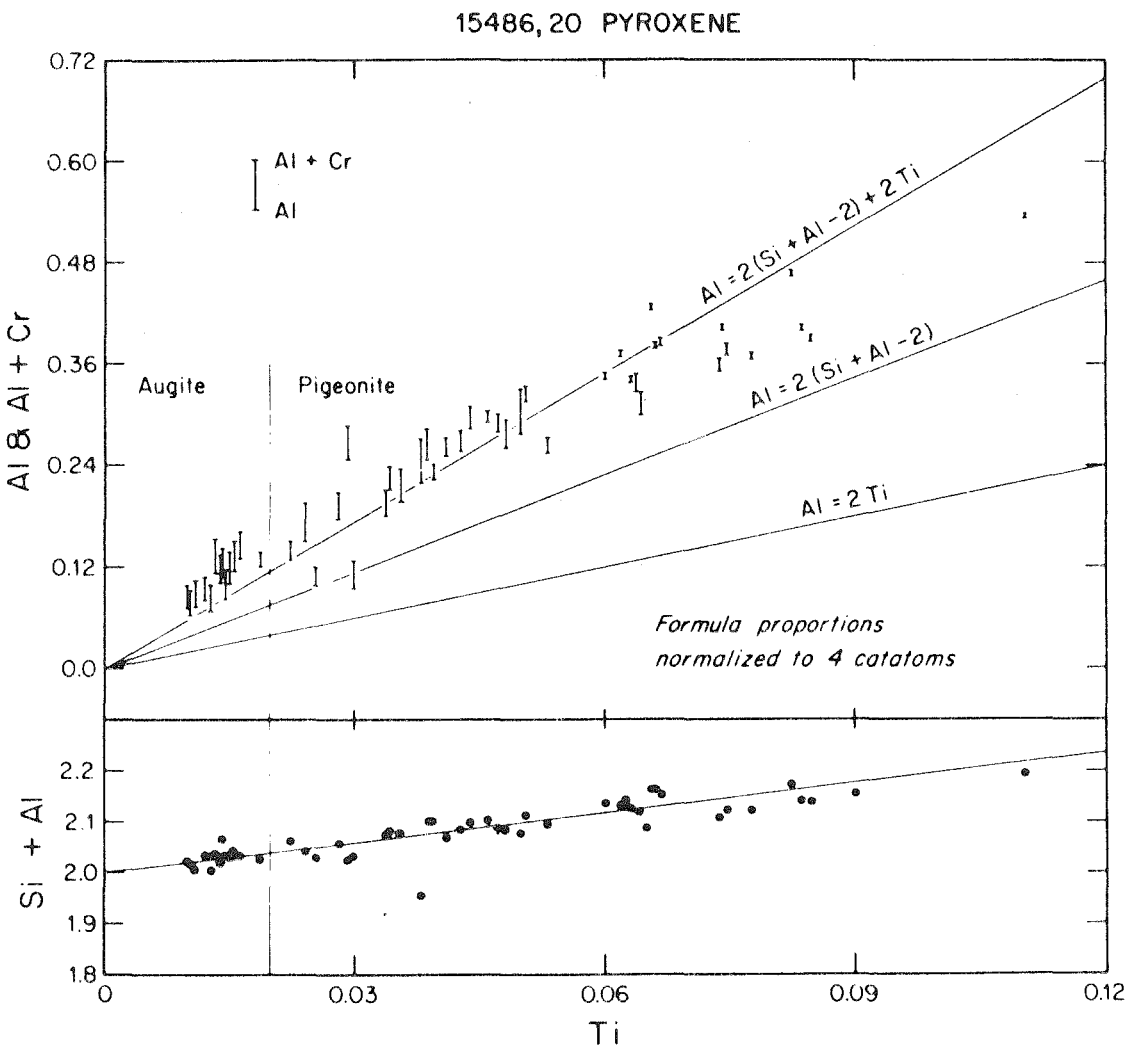

Figure 4

EARTH AND PLANETARY SCIENCE LETTERS 16 (1972) 307–330. NORTH-HOLLAND PUBLISHING COMPANY

COMPARATIVE PETROLOGY OF APOLLO 16 SAMPLE 68415 AND APOLLO 14 SAMPLES 14276 AND 14310

A.J. GANCARZ, A.L. ALBEE and A.A. CHODOS
*California Institute of Technology, Division of Geological and Planetary Sciences *, Pasadena, Calif. 91109, USA*

Received 25 September 1972

Petrographic and electron microprobe studies of Apollo 16 igneous rock 68415 and Apollo 14 rocks 14276 and 14310 show that all three samples differ from the mare basalts and are characterized by plagioclase as the first liquidus phase and by the abundance of plagioclase which is in part cumulate in origin. Major and minor element abundances and isotopic data prohibit the derivation of rocks like any of these samples from one another by magmatic fractionation during their crystallization. They could have originated by partial melting of an old, more Al-rich source material without isotopic equilibration with the residuum, by complete melting of three independent sources, or by contamination with old radiogenic material. The existence of such feldspathic basalts indicates that the generation of Al-rich magmas may have been an important and widespread lunar process.

1. Introduction

Lunar sample 68415, a feldspathic basalt, is one of the few large Apollo 16 samples "that can be unambiguously categorized as holocrystalline igneous rock" [1]. The extremely high plagioclase content and texture is similar to that of the Fra Mauro basalts, but very different from that of most of the mare basalts returned by the Apollo 11, 12, and 15 and Luna 16 missions. Anorthosite and anorthositic gabbro form a significant percentage of the coarser fragments in the lunar soil and large samples were returned by the Apollo 15 and 16 missions, indicating that highly feldspathic rocks represent a common lunar lithologic type. However, the feldspathic soil fragments and anorthosites typically exhibit a complex history of deformation and recrystallization [2, 5], which tends to obscure the primary petrogenetic processes producing such rocks. This paper will examine two questions: (1) whether the feldspathic basalts represented by 68415 and the Fra Mauro basalts are closely related to the anorthosites and anorthositic gabbros and hence provide significant information about the primary petrogenetic processes producing such rocks; and (2) whether the feldspathic basalts are representatives of another common lunar lithologic type, but unrelated to the anorthosites and anorthositic gabbros.

The fine-grained ophitic texture of 68415 is similar to that of the Apollo 14 feldspathic rocks (14310, 14073, and 14276) from Fra Mauro. Comprehensive descriptions have been published of the first two of these samples [6–9]. A comprehensive description of 14276 and some additional data on 14310 are given here for the purpose of making a detailed petrologic comparison with 68415.

The three Apollo 14 feldspathic rocks have been dated at 3.87–3.88 by by the Rb–Sr internal isochron method and by the ^{40}Ar–^{39}Ar stepwise heating method [10–12]. Apollo 16 sample 68415 has been dated by the Rb–Sr internal isochron method as 3.84 ± 0.01 by [13]. Although these ages are the same within analytical error, the initial $^{87}Sr/^{86}Sr$ values are distinctly different, 0.70036–0.70019, for the Apollo 14 rocks and 0.69920 for the Apollo 16 sample.

2. Apollo 16 sample 68415

2.1. *Sample description*

Apollo 16 samples 68415 and 68416, originally 20–30 cm apart, were chipped from an angular half-meter block perched on the outside rim of a 5-meter

* Contribution No. 2225.

Table 1a
Phase abundances, "average" phase compositions and bulk chemical composition of 68415.

	plagioclase	pigeonite	augite	olivine	ilmenite	mesostasis	Fe-metal	Bulk chemical composition	
								calculated	LSPET [15]
vol %	$82.2_3 \pm 2.1_3$	$7.5_4 \pm 0.6_4$	$4.4_6 \pm 0.5_0$	$3.1_9 \pm 0.4_2$	$0.1_7 \pm 0.1_0$	$2.1_5 \pm 0.3_4$	$0.2_2 \pm 0.1_1$		
wt %	79.1_2	8.9_6	5.2_6	3.8_3	0.2_8	1.9_9	0.5_6		
SiO_2	43.72	53.50	50.63	37.18	0.44	79.54	n.a.	45.06	45.40
Al_2O_3	36.36	1.28	1.77	0.08	0.21	11.42	n.a.	29.21	28.63
Cr_2O_3	n.a.	0.71	0.75	0.15	0.48	0.06	n.a.	0.11	0.10
TiO_2	n.a.	0.48	1.66	0.09	49.86	0.06	n.a.	0.27	0.32
MgO	0.06	23.29	14.83	36.04	0.89	0.03	n.a.	4.30	4.38
FeO	0.17	14.72	13.78	26.27	44.70	1.06	89.60 *	3.98 **	4.25
MnO	n.a.	0.28	0.28	0.27	0.47	< 0.01	n.a.	0.05	0.06
CaO	19.43	5.86	16.08	0.20	n.a.	0.70	n.a.	16.77	16.39
BaO	< 0.01	n.a.	n.a.	n.a.	n.a.	0.31	n.a.	0.01	n.r.
Na_2O	0.29	0.05	0.13	<0.01	n.a.	0.06	n.a.	0.24	0.41
K_2O	0.02	n.a.	n.a.	n.a.	n.a.	1.32	n.a.	0.04	0.06
P_2O_5	n.a.	n.a.	n.a.	n.a.	n.a.	0.19	n.a.	< 0.01	0.07
SO_3	n.a.	n.a.	n.a.	n.a.	n.a.	0.01	n.a.	< 0.01	0.10
Ni	n.a.	n.a.	n.a.	n.a.	n.a.	< 0.01	9.18	0.05	n.r.
ZrO_2	n.a.	n.a.	n.a.	n.a.	0.18	0.44	n.a.	< 0.01	n.r.
Total	100.05	100.17	99.91	100.28	97.58	95.81	98.78	100.09	100.17

n.a. not analyzed; n.r. not reported; * Fe; ** total iron as FeO.

Table 1b
Phase abundances, "average" phase compositions and bulk chemical composition of 14276.

	plagioclase	ortho-pyroxene	pigeonite	augite	mesostasis	ilmenite	Fe-metal	phosphate **	Bulk chemical composition	
									calculated	Rose et al. [23]
vol %	$64.6_5 \pm 1.8_2$	$15.7_0 \pm 0.9_0$	$9.3_4 \pm 0.6_9$	$4.0_5 \pm 0.4_6$	$3.5_4 \pm 0.4_2$	$1.2_8 \pm 0.2_6$	$0.3_6 \pm 0.1_3$	$0.6_7 \pm 0.1_8$		
wt %	59.9_2	17.9_8	10.7_0	4.6_0	3.1_5	2.0_3	0.9_1	0.7_2		
SiO_2	46.25	53.52	50.67	51.73	73.58	0.24	n.a.	0.56	47.4_6	47.60
Al_2O_3	34.18	1.60	1.39	2.56	12.85	0.35	n.a.	0.06	21.4_5	21.34
Cr_2O_3	n.a.	0.56	0.48	0.81	< 0.01	0.28	n.a.	n.a.	0.1_9	0.26
TiO_2	n.a.	0.59	0.82	1.07	0.52	49.58	n.a.	n.a.	1.2_7	1.20
MgO	0.19	25.35	18.66	17.67	0.04	1.44	n.a.	1.15	7.5_2	7.10
FeO	0.21	16.41	20.81	12.49	1.21	47.62	n.a.	1.74	7.9_6 ***	7.94
MnO	n.a.	0.27	0.29	0.22	< 0.01	0.42	91.71 *	n.a.	0.1_0	0.12
CaO	17.55	2.43	6.32	14.35	0.99	0.16	n.a.	47.96	12.6_7	13.18

Table 1b (cont'd.)

	plagioclase	ortho-pyroxene	pigeonite	augite	mesostasis	ilmenite	Fe-metal	phosphate **	Bulk chemical composition	
									calculated	Rose et al. [23]
vol %	$64.6_5 \pm 1.8_2$	$15.7_0 \pm 0.9_0$	$9.3_4 \pm 0.6_9$	$4.0_5 \pm 0.4_6$	$3.5_4 \pm 0.4_2$	$1.2_8 \pm 0.2_6$	$0.3_6 \pm 0.1_3$	$0.6_7 \pm 0.1_8$		
wt %	59.9_2	17.9_8	10.7_0	4.6_0	3.1_5	2.0_3	0.9_1	0.7_2		
Na_2O	1.37	0.02	0.06	0.09	0.92	< 0.01	n.a.	0.32	0.8_7	0.72
K_2O	0.19	< 0.01	< 0.01	< 0.01	7.41	0.01	n.a.	n.a.	0.3_5	0.48
BaO	0.05	n.a.	n.a.	n.a.	0.07	n.a.	n.a.	n.a.	0.0_3	0.08
P_2O_5	n.a.	n.a.	n.a.	n.a.	n.a.	n.a.	n.a.	41.16	0.3_0	0.40
Ni	n.a.	n.a.	n.a.	n.a.	n.a.	n.a.	7.45	n.a.	0.0_7	0.01
F	n.a.	n.a.	n.a.	n.a.	n.a.	n.a.	n.a.	1.67	0.0_1	n.r.
Total	99.99	100.75	99.50	100.99	97.97	100.10	99.16	94.62	100.24	100.34

* Fe; ** average of apatite and whitlockite; *** total iron as FeO; n.a. not analyzed; n.r. not reported.

Table 1c
Phase abundances, "average" phase compositions and bulk chemical composition of 14310.

	plagioclase	ortho-pyroxene	pigeonite	augite	mesostasis	ilmenite	phosphate *	Fe-metal	Bulk chemical composition	
									calculated	Rose et al. [23]
vol %	$59.0_0 \pm 2.0_6$	$16.3_1 \pm 1.0_8$	$10.5_3 \pm 0.8_7$	$6.1_3 \pm 0.6_6$	$4.4_7 \pm 0.5_7$	$1.8_8 \pm 0.3_6$	$0.3_6 \pm 0.1_6$	$0.1_4 \pm 0.1_0$		
wt %	54.6_4	18.6_6	12.0_5	6.9_5	3.9_7	2.9_8	0.3_9	0.3_5		
SiO_2	46.36	53.89	51.42	50.66	61.32	0.39	1.28	n.a.	47.55	47.81
Al_2O_3	33.97	1.08	1.48	2.25	19.82	0.10	n.a.	n.a.	19.89	21.54
Cr_2O_3	n.a.	0.40	0.42	0.56	n.a.	0.38	n.a.	n.a.	0.18	0.25
TiO_2	n.a.	0.42	0.95	1.67	n.a.	52.66	n.a.	n.a.	1.88	1.11
MgO	0.29	26.30	18.40	14.68	0.01	0.83	1.03	n.a.	8.33	7.48
FeO	0.07	15.41	20.34	15.62	0.23	44.62	2.29	85.39 **	8.18 ***	7.62
MnO	n.a.	0.27	0.33	0.36	n.a.	0.32	0.04	n.a.	0.12	0.10
CaO	17.05	2.60	6.35	15.05	0.77	0.12	46.75	n.a.	11.83	12.92
Na_2O	1.43	0.01	0.04	0.11	1.00	< 0.01	0.05	n.a.	0.84	0.68
K_2O	0.21	< 0.01	0.01	< 0.01	12.63	0.03	n.a.	n.a.	0.62	0.48
BaO	0.18	n.a.	n.a.	n.a.	3.99	n.a.	n.a.	n.a.	0.26	0.09
P_2O_5	n.a.	n.a.	n.a.	n.a.	n.a.	n.a.	40.50	n.a.	0.16	0.43
Ni	n.a.	n.a.	n.a.	n.a.	n.a.	n.a.	n.a.	12.68	0.04	0.01
F	n.a.	n.a.	n.a.	n.a.	n.a.	n.a.	1.68	n.a.	0.01	n.r.
Total	99.56	100.38	99.70	100.96	99.77	99.45	93.62	98.07	99.89	100.51

* average apatite and whitlockite; ** Fe; *** total iron as FeO; n.a. not analyzed; n.r. not reported.

crater at Station 8 [14]. Station 8 is located on a light-colored ray of ejecta from South Ray Crater and much of the surface in its vicinity is covered with angular fragments and blocks. Sample 68415 consisted of two fragments, one about 6 × 8 × 10 cm weighing 203 g, and one about 3.5 × 5 × 10 cm weighing 168 g. They are notably inhomogeneous, having a "patchy distribution of light- and dark-colored parts" on a 10–20 mm scale with unevenly distributed clusters and trains of miarolitic cavities which contain projecting, white plagioclase crystals [1]. A 15 × 20 mm patch of coarser-grained material includes up to 10% void. Large irregular "plagioclase lumps" are sparsely distributed throughout the rock and there are "strips" of fine-grained material bordered by plagioclase laths in parallel-preferred orientation. Sample 68416, although it is coarser-grained and contains more and larger plagioclase phenocrysts (see photomicrograph in [15]), is like 68415 [1].

2.2. *Petrography and bulk composition*

This petrographic study utilized polished thin section 68415,8, which has an area of 61 mm^2. In addition, some microprobe analyses were made on grain mounts of mineral separates from 68415,10 which were utilized in the Rb–Sr isotopic studies on this rock [13].

The electron microprobe was used to simultaneously obtain modal estimates and estimates of the average composition of each phase so that the bulk chemical composition could be calculated for the thin section. Averaged defocussed beam analyses were not used because certain elements, in particular Al, are strongly biased in basaltic rocks with average grain size close to or greater than beam size. Using a MAC-5-SA3 electron microprobe under computer control, analyses of 1μm spots for Fe, Ca, and Si were made at 1818 equally-spaced grid points on section 68415,8. The program identifies the phase analyzed at each point, determines the volume percent of each phase, and calculates the average Fe, Ca, and Si content of each phase. The volume percents, calculated errors, and calculated weight percents of the phases are given in table 1a. The modal abundances are nearly identical to those obtained by optical point counts by us on 68415,8 and by Bass on 68415,8 and 68415,9 [1]. An actual microprobe analysis, with Fe, Ca, and Si contents closely corresponding to the average Fe, Ca, and Si contents, was selected from all of the complete quantitative analyses * to represent the average composition of each phase; these analyses are included in table 1a. The calculated bulk composition is compared in table 1a with that obtained by X-ray fluorescence analysis of a 280 mg aliquot from the same chip of this sample [15]. The good agreement suggests that this section reasonably samples the composition of this particular portion of sample 68415 even though it is texturally inhomogeneous and no single chip can be totally representative of the rock.

This thin section is of a subophitic, intersertal plagioclase-rich basalt composed predominantly of plagioclase (82%), augite (4%), pigeonite (8%), olivine (3%) and mesostasis (2%) with less than 1% of ilmenite, chromite, ulvöspinel, troilite, Fe-metal, cristobalite and glass. The texture is like that of most lunar basalts. However, in detail the texture is distinct from most of the Apollo 11, 12, and 15 basalt samples, but is similar to that of the Fra Mauro basalts, represented by 14310, 14276, and 14073 (compare plate Ia with photomicrographs in [6]). This similarity is basically due to the high abundance of randomly-oriented plagioclase laths between which the other phases occur interstitially in an ophitic to intersertal texture.

These rocks have a similar mineralogic composition to those lunar rocks which have been called anorthosite or anorthositic gabbro. However, the anorthosite and anorthositic gabbro samples typically exhibit textures indicative of deformation and recrystallization [2–5], whereas samples like 68415 and the Fra Mauro basalts exhibit well-developed primary igneous textures. Therefore, we will refer to samples like 68415 and the Fra Mauro basalts as plagioclase-rich or feldspathic basalts to emphasize the differences in texture and petrogenetic history.

Thin section 68415,8 contains several types of relict features which predate the main crystallization period during which the dominant ophitic texture formed. These relict features are like those described in rock 14310 by Brown and Peckett [7] and in rock 14276 [this paper]. As shown in plate I, plagioclase phenocrysts occur in a groundmass of interlocking plagioclase laths. Residual areas within the groundmass contain even smaller plagioclase microlaths. These

* A complete tabulation of microprobe analyses can be obtained upon request from the authors.

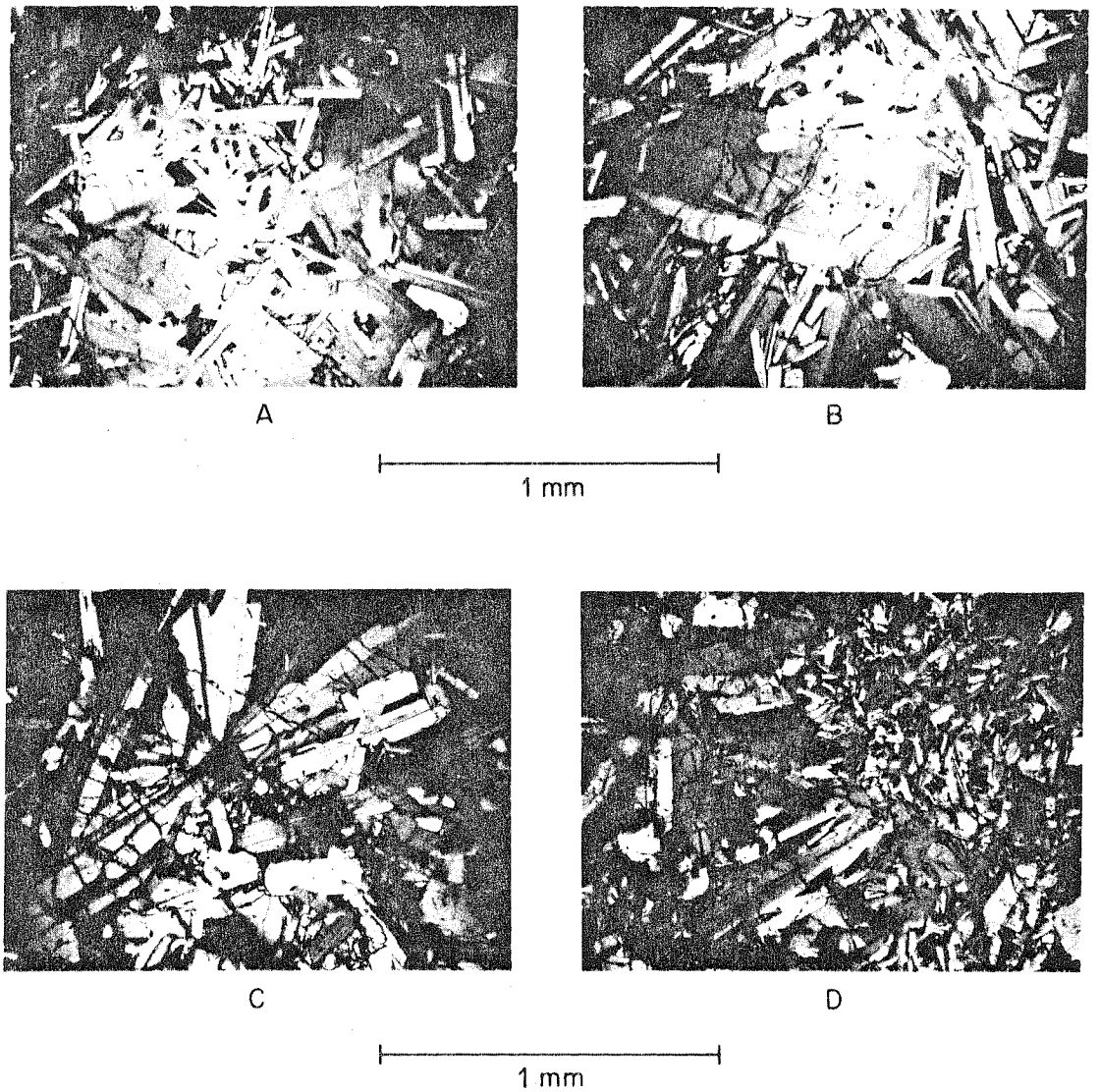

Fig. 1. Photomicrographs of thin section 68415,8; A. Typical ophitic-intersertal texture. B. Phenocryst plagioclase surrounded by groundmass laths. Like many of the plagioclase phenocrysts, this particular phenocryst contains inclusions of troilite. C. Radial aggregate of plagioclase phenocrysts which may be cumulate in origin. D. Fine-grained patch of plagioclase and pyroxene crystals which appears to be a cognate inclusion.

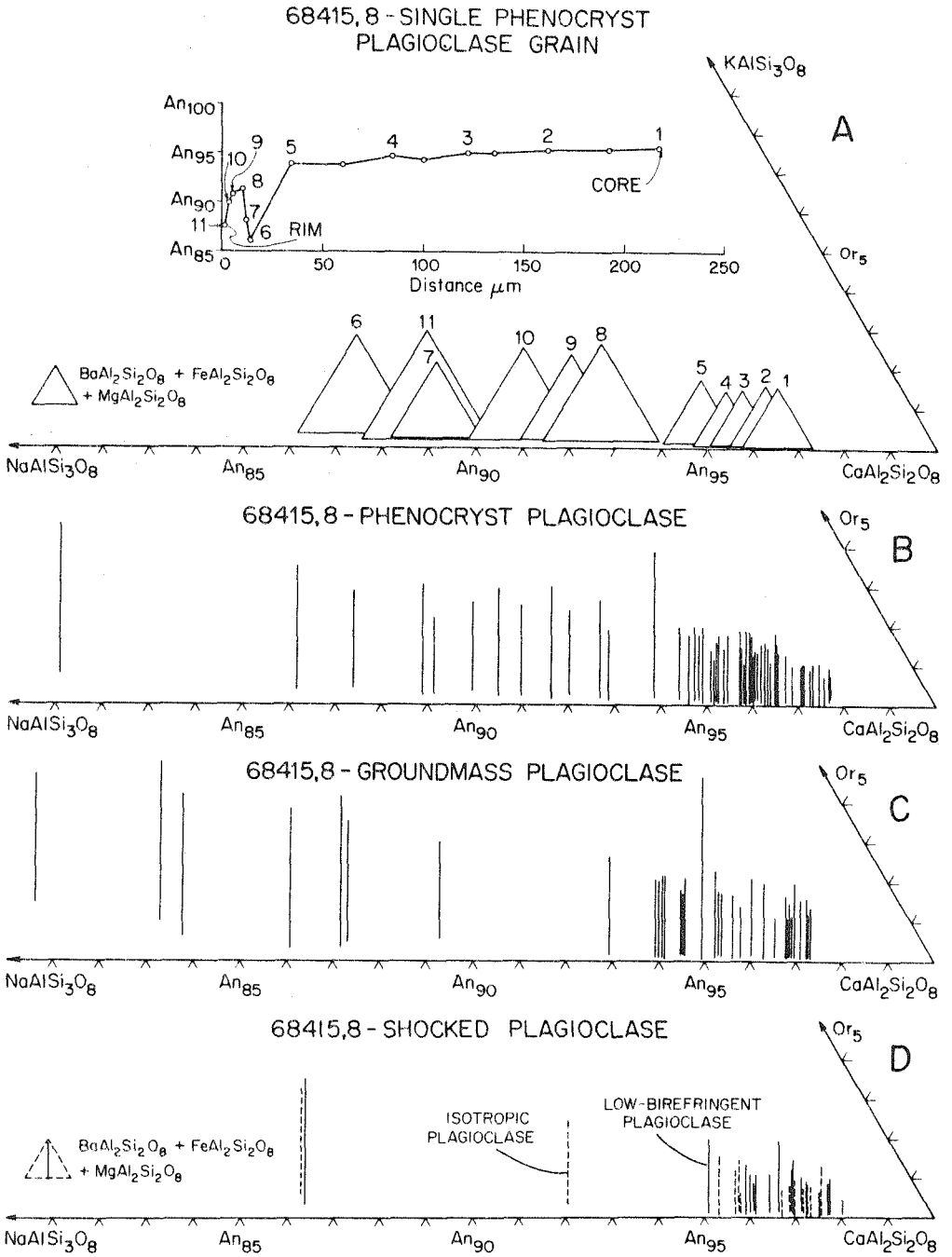

Fig. 2. Plagioclase analyses from sample 68415,8. Fig. 2a illustrates the compositional variation from core to rim and the compositional reversal in a single plagioclase phenocryst from the radial aggregate shown in fig. 1C. The numerals on the profile correspond to the numbered triangles plotted below. Fig. 2D shows the range of composition of shocked plagioclase, which can be contrasted to the composition of the plagioclase phenocrysts (fig. 2B) and of the groundmass plagioclase (fig. 2C).

Table 2
Representative analyses[a/] of feldspar, pyroxene, and olivine
from samples 68415 and 14276

	68415,8 phenocryst grains			68415,8 groundmass grain	68415,8 isotropic plagioclase	14276,13 phenocryst grains			14276,13 mesostasis	14276,13 potassium-feldspar
	(3)[b]	(6)[b]	(8)[b]			(2)[c]	(5)[c]	(14)[c]		
SiO_2	44.40	46.53	44.68	43.72	43.92	44.46	47.20	48.99	53.65	61.44
Al_2O_3	35.35	33.84	35.02	36.36	36.54	35.76	34.37	31.37	28.99	19.45
Na_2O	0.39	1.26	0.68	0.29	0.27	0.75	1.38	2.31	3.73	1.73
K_2O	0.02	0.07	0.04	0.02	<0.01	0.06	0.11	0.40	0.70	12.02
CaO	19.42	17.63	18.77	19.43	19.19	18.84	17.69	15.64	12.42	0.61
BaO	<0.01	0.02	0.05	0.01	0.03	0.06	0.03	<0.01	0.11	4.35
FeO	0.12	0.24	0.36	0.17	0.10	0.12	0.18	0.34	0.47	0.02
MgO	0.14	0.23	0.16	0.06	0.06	0.23	0.33	0.19	0.08	0.02
Total	99.84	99.82	99.76	100.05	100.11	100.28	101.29	99.24	100.25	99.84
Formula proportions										
Si	2.06	2.15	2.07	2.02	2.03	2.04	2.14	2.26	2.44	2.91
Al	1.93	1.84	1.91	1.98	1.99	1.94	1.84	1.71	1.56	1.09
Na	0.04	0.11	0.06	0.03	0.02	0.07	0.12	0.21	0.33	0.16
K	0.01	<0.01	<0.01	<0.01	<0.01	<0.01	0.01	0.02	0.04	0.73
Ca	0.96	0.87	0.93	0.96	0.95	0.93	0.86	0.77	0.61	0.03
Ba	<0.01	<0.01	<0.01	<0.01	<0.01	<0.01	<0.01	<0.01	<0.01	0.08
Fe	<0.01	0.01	0.01	<0.01	<0.01	<0.01	0.01	0.01	0.02	<0.01
Mg	0.01	0.02	0.01	0.01	<0.01	0.02	0.03	0.01	0.01	<0.01

	68415,8 pyroxene				68415,8 olivine		14276,13 pyroxene			
							(1)[d]	(2)[d]	(3)[d]	(4)[d]
SiO_2	53.53	51.00	48.32	52.77	37.18	37.71	54.73	51.47	52.04	47.68
Al_2O_3	0.98	1.35	0.57	2.24	0.08	0.09	2.29	2.62	1.40	1.02
Cr_2O_3	0.68	0.56	0.12	0.80	0.15	0.15	0.58	0.85	0.41	0.04
TiO_2	0.41	1.21	0.71	0.97	0.09	0.03	0.40	1.15	0.78	0.67
MgO	24.12	15.31	9.21	22.15	36.04	35.37	29.65	18.86	19.29	7.59
FeO	14.85	15.73	33.63	15.32	26.27	26.92	11.44	11.40	20.26	32.97
MnO	0.30	0.29	0.55	0.36	0.27	0.28	0.16	0.22	0.34	0.39
CaO	5.16	14.24	4.71	5.82	0.20	0.19	1.66	16.22	6.81	9.25
Na_2O	0.04	0.10	0.02	0.05	n.a.	n.a.	0.03	0.12	0.06	0.09
Total	100.07	99.79	97.84	100.48	100.28	100.74	100.94	100.91	101.89	99.70
Formula proportions										
Si	1.95	1.93	1.99	1.93	0.98	1.00	1.92	1.90	1.93	1.93
Al	0.04	0.06	0.03	0.10	<0.01	<0.01	0.09	0.11	0.06	0.05
Cr	0.02	0.02	<0.01	0.02	<0.01	<0.01	0.02	0.02	0.01	<0.01
Ti	0.01	0.03	0.02	0.03	<0.01	<0.01	0.01	0.03	0.02	0.02
Mg	1.31	0.86	0.57	1.21	1.42	1.39	1.55	0.93	1.06	0.46
Fe	0.45	0.50	1.16	0.47	0.58	0.59	0.34	0.35	0.63	1.12
Mn	0.01	0.01	0.02	0.01	<0.01	0.01	<0.01	0.01	0.01	0.01
Ca	0.20	0.58	0.21	0.23	<0.01	0.01	0.06	0.64	0.27	0.40
Na	<0.01	0.01	<0.01	<0.01	n.a.	n.a.	<0.01	0.01	<0.01	0.01

a/ A complete tabulation of microprobe analyses can be obtained upon request from A.Albee.
b/ Number corresponds to numbers of Fig. 2A.
c/ Number corresponds to numbers of Fig. 7A.
d/ Number corresponds to numbers of Fig. 8B.

distinctions between phenocrysts, groundmass plagioclase, and microlaths, are clear in much of the thin section and are illustrated in figs. 1A–C, but there is no sharp distinction in size or other properties. The phenocrysts tend to be larger (to ~ 1.5 mm), more equant, and more complexly-twinned than the groundmass laths and, as was observed in sample 14310 [16], may include laths of the groundmass projecting into their outermost edges (fig. 1B). Most of the plagioclase occurs as groundmass laths (0.9 X 0.2 mm to 0.09 X 0.02 mm) producing the ophitic texture with an interstitial residuum including plagioclase microlaths, pyroxene, and mesostasis. There appears to be no real distinction between the groundmass laths and the residuum microlaths, but the texture suggests that much of the plagioclase that co-precipitated with pyroxene formed the smaller grains. It should also be noted that the companion sample (68416) from the same block contains much larger phenocrysts of plagioclase (see figs. 10A and 11A in [15]).

The radial cluster of large plagioclase laths shown in fig. 1C is probably an aggregate of early phenocrysts. The thin section also contains possible cognate inclusions somewhat similar to the finer-grained patches in 14310. As shown in fig. 1D, the inclusion is ophitic-intergranular and finer-grained than the groundmass of the rock. It occupies a 0.3 X 0.4 mm area at one edge of the thin section and is bordered by plagioclase laths, oriented in a radial aggregate normal to the inclusion, which in turn are bordered by relatively finer-grained groundmass.

The crystallization history of sample 68415, as reflected in these textures, is sketched in fig. 3. Comparison with similar diagrams [17] for Apollo 11, 12, 14, and 15 samples emphasizes that the mare basalts, unlike this rock and the Apollo 14 plagioclase-rich basalts, do not contain plagioclase as cumulate grains nor as the initial phase to crystallize. We estimate that as little as 5% and as much as 25% of the plagioclase in this rock may represent crystal accumulation.

2.3. *Plagioclase feldspar*

Plagioclase is the dominant mineral in this rock and occurs in several habits. Larger semi-equant phenocrysts, which may be cumulate grains, are enclosed in an ophitic groundmass of laths with a wide range of size. Many of the larger grains have complex twinning whereas the groundmass laths typically have only polysynthetic twinning.

The composition of plagioclase in these different habits is illustrated on fig. 2 and typical analyses are given in table 2. Many of the larger grains exhibit

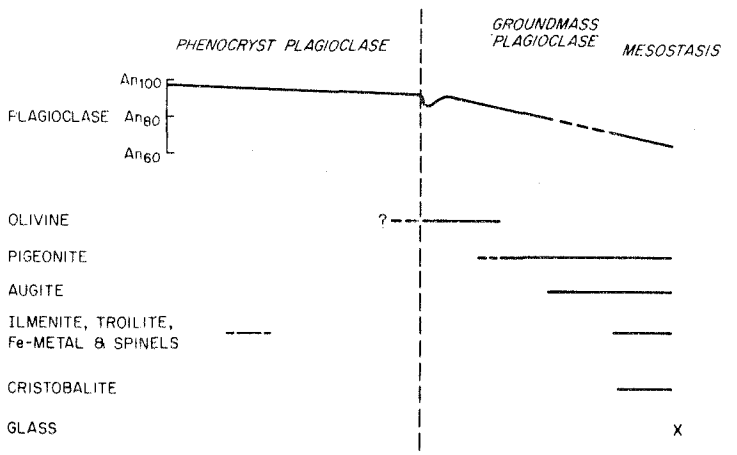

Fig. 3. Summary of crystallization history of 68415 as inferred from petrographic relationships and phase composition data. The vertical dashed line indicates the event responsible for the compositional reversal at the edges of the plagioclase phenocrysts and the initiation of groundmass plagioclase crystallization.

Plate 1a. Photomicrograph of section 68415,8 (crossed polarizers) illustrating typical intersertal texture. Field of view 2.1 × 3.2 mm.

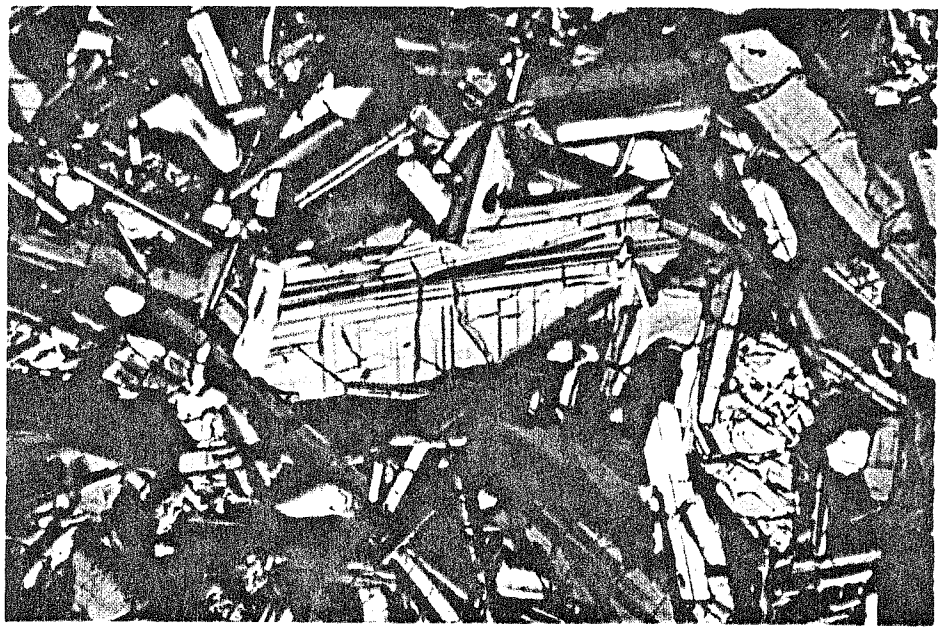

Plate 1b. Photomicrograph of section 68415,8 (crossed polarizers) showing a plagioclase phenocryst surrounded by smaller groundmass plagioclase laths. Field of view 1.1 × 1.6 mm.

zoning with an optical discontinuity near the rim generally reflecting a reversal in composition. Fig. 2a shows the compositional variation in a single plagioclase grain from the radial cluster shown in fig. 1C. It shows a variation from An_{97} near the core to An_{86} near the rim and a marked reversal in the zoning pattern near the rim. The laths in the groundmass show little optical zoning and are typically quite homogeneous in composition, ranging from An_{97} to An_{92} (fig. 2C). The less-anorthitic compositions shown in fig. 2C are from plagioclase microlaths in or bordering areas of mesostasis.

The overlap in composition of the phenocrysts and the groundmass grains is not readily explainable. The cores of the phenocrysts are about as An-rich as the most An-rich groundmass grains and their rims are less An-rich than the typical groundmass grains. Moreover, there is a compositional reversal and/or discontinuity near the borders of many of the larger grains. Under normal magmatic conditions or in rapid cooling and rapid nucleation of plagioclase in a closed system, the groundmass plagioclase would have a composition close to that of the rim of the phenocrysts. Brown and Peckett [7] have studied similar textures with a similar compositional reversal from sample 14310 and concluded that the only mechanism likely to produce such a drastic effect would be the loss of Na and K from the system by volatilization from the surface of a lava lake at this stage. In addition to the experimental data [16, 18], the systematics of the Rb–Sr isotopic data seem to make such an explanation untenable. (Extensive loss of volatiles would result in much higher model ages than are observed.) A decrease in total pressure could account for it, but would probably require much too great a pressure drop. An explanation which simultaneously accounts for the overlap in composition between the phenocryst and groundmass grains, and for the compositional reversal near the rims of the phenocrysts, is the intrusion of a magma into a partially-crystallized magma resulting in the admixture of plagioclase phenocrysts into a higher temperature melt with rapid crystallization of the groundmass laths and concomitant mantling of the rims on some plagioclase phenocrysts. Such a process might occur with overturning in a lava lake or with eruption upward through partially-crystalline layers which would be at a lower temperature.

As in other lunar plagioclase, the substitution of minor elements increases with decreasing An-content [19]. On fig. 2, the feldspars are plotted in terms of Or, Ab, and An with the vertical line representing the altitude of the triangle indicating the amount of $BaAl_2Si_2O_8 + MgAl_2Si_2O_8 + FeAl_2Si_2O_8$. It is useful to treat Mg and Fe as feldspar end-members, because their concentrations are so high in the lunar plagioclase. No significant differences in these minor elements differentiate between phenocryst and groundmass grains of plagioclase.

2.4. *Pyroxene and olivine*

Clinopyroxene occurs as small (~ 0.2 mm) anhedral to irregular grains interstitial to the plagioclase frame-

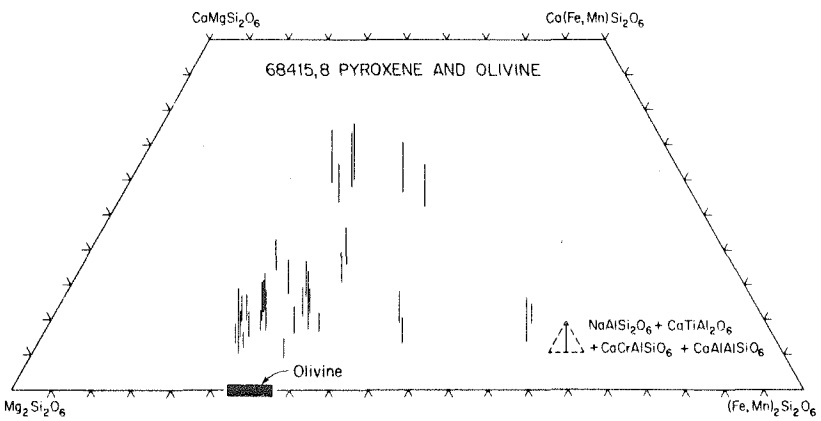

Fig. 4. Pyroxene and olivine analyses from 68415,8. The four most Fe-rich analyses are of grains in the mesostasis.

work. No good examples of systematic zoning were found. The analyzed points, which were selected rather randomly, suggest that Ca-rich compositions are about half as abundant as Ca-poor compositions and this is substantiated by the microprobe point count. Although many pyroxene grains contain cores of olivine, no orthopyroxene cores were observed, unlike in the Fra Mauro feldspathic basalts. Moreover, the presence of orthopyroxene is not suggested by any of the microprobe analyses.

Typical analyses are given in table 2, average compositions of the low-Ca and high-Ca pyroxenes are given in table 1a, and the analytical data are summarized on fig. 4. Most of the pyroxenes are Mg-rich and do not display extensive zoning to Fe-rich compositions as in many lunar rocks. The six most Fe-rich compositions were found by a deliberate search for small pyroxene grains within mesostasis areas.

The Ti, Al, Cr, and Na contents are lower in the low-Ca pyroxene than in the high-Ca pyroxene. In both, these minor elements have concentrations similar to those found in other lunar pyroxenes with similar major element concentration. As in the Apollo 11 rocks, the coupled-substitution $CaAlAlSiO_6$ is low and the major substitutions are (Ca, Fe, Mg) $TiAl_2O_6$, (Ca, Fe, Mg) $CrAlSiO_6$, and $NaCrSi_2O_6$.

Olivine occurs throughout the thin section as small anhedral to irregular grains interstitial to plagioclase laths. Typically, it occurs as cores in pyroxene or rimmed by pyroxene, but it also occurs mantled by plagioclase without a pyroxene rim. The textures suggest that the crystallization of olivine preceded that of pyroxene and that it reacted with the melt to form pyroxene rims except where mantled by plagioclase (fig. 3).

Ten analyses of olivine lie within the range shown on fig. 4 and there is little variation in its composition within individual grains or between grains. The Fe/Mg ratio is similar to that of the most magnesian pyroxene (fig. 4). The average composition is given in table 1a and typical analyses are given in table 2. Minor element contents exhibit some differences (MnO, 0.23–0.33 wt %; Cr_2O_3, 0.07–0.17 wt %; TiO_2, 0.05–0.09 wt %; CaO, 0.02–0.29 wt%), but show no apparent correlation with Fe/Mg.

2.5. *Mesostasis and opaque minerals*

The mesostasis areas in this rock contain silicate glass, cristobalite, phosphate minerals, and opaque minerals, as well as more Fe-rich pyroxene and more Ab-rich plagioclase which continued to crystallize during the final stages of solidification. This mesostasis is dominated by opaque minerals including ilmenite, Fe-metal, troilite, ulvöspinel, and chromite. The opaque minerals are not abundant in the rock and their crystallization was confined to the latest stages of crystallization. This feature differs from most other lunar igneous rocks in which ilmenite is an early liquidus phase and crystallized throughout the entire crystallization sequence.

Ilmenite typically occurs as thin plates, rarely translucent, oriented parallel to plagioclase laths or pyroxene grains, which surround the mesostasis, or are included in the outermost rims of the surrounding grains during late stage growth. The ZrO_2 content of ilmenite analyses ranges from 0.05 to 0.18 wt %; a typical analysis is given in table 1a. Ulvöspinel and chromite are rare and each occurs in close association with ilmenite, the ulvöspinel partially rimmed by ilmenite and the chromite in a complex intergrowth with ilmenite. The composition of the chromite is $[Fe_{1.06}Mg_{0.16}Mn_{0.02}Cr_{1.15}Al_{0.27}Ti_{0.32}Si_{0.02}]O_{\sim 4}$; that of ulvöspinel is $[Fe_{1.90}Mg_{0.03}Mn_{0.01}Cr_{0.08}Al_{0.12}Ti_{0.84}Si_{0.01}]O_{\sim 4}$ (ZrO_2 = 0.04 wt %).

Troilite and Fe-metal typically occur as blebs in the residual glass. Less commonly they are included within the bordering plagioclase and pyroxene. The spherical or globular shape of these phases suggests separation due to liquid immiscibility. The Fe-metal has a high-Ni and low-Co content (see fig. 5) and by the criteria of Goldstein and Yakowitz [20] would be of meteoritic origin.

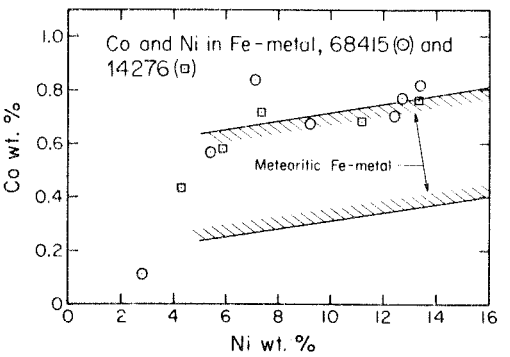

Fig. 5. Co and Ni in Fe-metal in 68415, 8, 10 and 14276, 13. The field of meteoritic Fe-metal is taken from Goldstein and Yakowitz [20].

The silicate glass is light-colored and occurs in tiny patches which include opaque phases. The glass analyses indicate a considerable range in composition similar to that found in 14310 [6]. Relative to glasses found in other lunar basalts, these glasses are high-Si and low-K (SiO_2, 64–85 wt %; K_2O, 0.2–5.0 wt %; FeO, 0.5–3.9 wt %). No evidence was found of an immiscible Fe-rich silicate liquid. Grains, which had been optically identified as cristobalite, yielded analyses ranging from 94.8 to 97.9 wt % SiO_2 but the analyzed points could have included some glass.

Mineral separates of cristobalite and/or glass (i.e., $\rho < 2.5$ g/cm^3) which were made for the Rb–Sr isotopic investigations, yielded one grain with high K and Ba (K_2O, 4.7 wt %, BaO, 4.0 wt %) and a few relatively Na-rich plagioclase grains ($An_{65}Ab_{30}Or_2$ $other_3$).

Cryptocrystalline aggregates of phosphate minerals occur in the mesostasis, commonly associated with the globules of troilite and Fe-metal. Qualitative analyses of 40 such aggregates indicated that about 60% are whitlockite and about 40% are apatite. No grains large enough for quantitative analysis were found. Several tiny ($\ll 1$ μm) grains of unidentified Zr-rich phases were found with the microprobe.

Individual areas of mesostasis have quite different percentages of the various constituent minerals. Although this could be simply a happenstance of the orientation of the thin section, it suggests that the final liquid had different compositions in different interstices within the rock.

2.6. *Shock features*

An abundance of shock features and zap pits have been described in the sample from which thin section 68415,8 was cut [1]. In addition, this thin section contains an exceptionally good cross-section of the transition from highly-shocked to unshocked crystalline rock. A projecting point on one edge of the thin section, presumably an exterior surface of the rock, has been highly shocked. A photomicrograph and line drawing of this feature is shown in fig. 6A. Although the ophitic texture is retained, the plagioclase is isotropic for up to 0.8 mm into the rock where it has a sharp interface with highly-shattered, low-birefringent plagioclase (see fig. 6A). Normal rock with only minor shattering is about 2.2 mm from the edge of the isotropic plagioclase. Pyroxene and olivine have lowered birefringence due to intense shattering (fig. 6B), but are not isotropic. Larger grains of Fe-metal, troilite, and ilmenite do not show obvious evidence of deformation or compositional change.

As shown in fig. 6A, a circular 0.1-mm hole occurs in the isotropized plagioclase. It is not obvious whether this represents a relict vug or a gas cavity formed as a consequence of the shock. However, on another edge of the thin section there is a similar circular hole, ~ 0.5 mm in diameter, bounded by about 0.1 mm of low-birefringent plagioclase (see fig. 6C). Because this hole is bounded by low-birefringent plagioclase, it seems possible that it represents shock-intensification about a cavity [21], although this could be a section of a zap pit.

Microprobe analyses of isotropized and of low-birefringent plagioclase from these two features are illustrated in fig. 2D. Most of the analyses range from An_{98} to An_{94}, and are not dissimilar to plagioclase in the undeformed rock. The three low-An analyses are from the edge of the hole shown in fig. 6C and the lower An content could support the suggestion that the hole is a relict vug. One small part of the isotropized area was inferred to be a relict mesostasis area on the basis of the distribution of opaque minerals; its composition was found to be similar to the residual glass with 86 wt % SiO_2.

The shocked area of rock is bordered by a smooth exterior surface which is coated with minute ($\ll 1$ μm) opaque particles. Most appear to be Fe-metal or troilite. This surface forms a gray layer in fig. 6A that looks like a glass coating because it is at a small angle to the thin section. Brown wisps of glass within the isotropized rock (fig. 6A) also owe their color to abundant, small ($\ll 1$ μm) Fe-metal balls, which were characterized by a microprobe analysis indicating 13.6 wt % FeO, 0.4 wt % NiO, and less than 0.3 wt % of TiO_2, Cr_2O_3, and SO_3. Since there is no evidence of flowage, these wisps may represent penetration of a surficial glass coating into grain boundaries of the rock prior to or during the shock event.

3. Apollo 14 sample 14276

Sample 14276 was collected near the landing site as part of the "comprehensive sample" and weighed 12.75 g. It is described in the Apollo 14 Sample Infor-

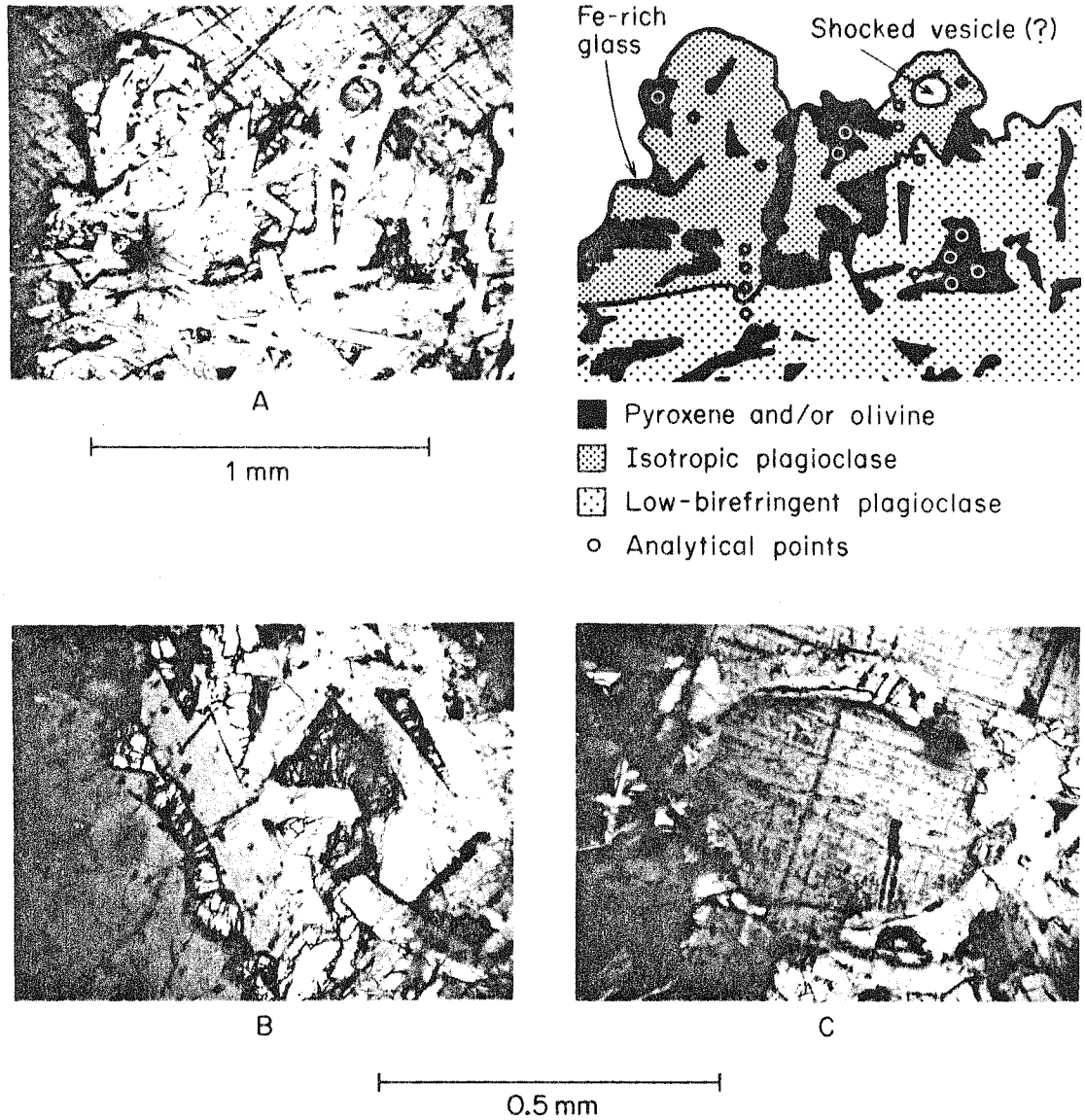

Fig. 6. Photomicrographs illustrating shock features in sample 68415,8. A. Photograph of the boundary between shock isotropized plagioclase and low-birefringent plagioclase. B. Enlargement of the boundary between shock isotropized plagioclase and low-birefringent plagioclase shown in fig. 6A. Despite the highly fractured and shocked nature of the pyroxene and olivine, the ophitic intersertal texture is preserved. C. A shocked vug (?) on an exterior surface of 68415,8.

mation Catalog [22] as a blocky, subrounded, crystalline rock fragment, 3.0 × 2.2 × 2.0 cm, without surface glass or shock features. A few glass-lined pits were present on the surface, averaging about 1 mm in diameter. Irregular to sub-spherical vugs, which range in size from 0.2 to 1 mm and which make up about

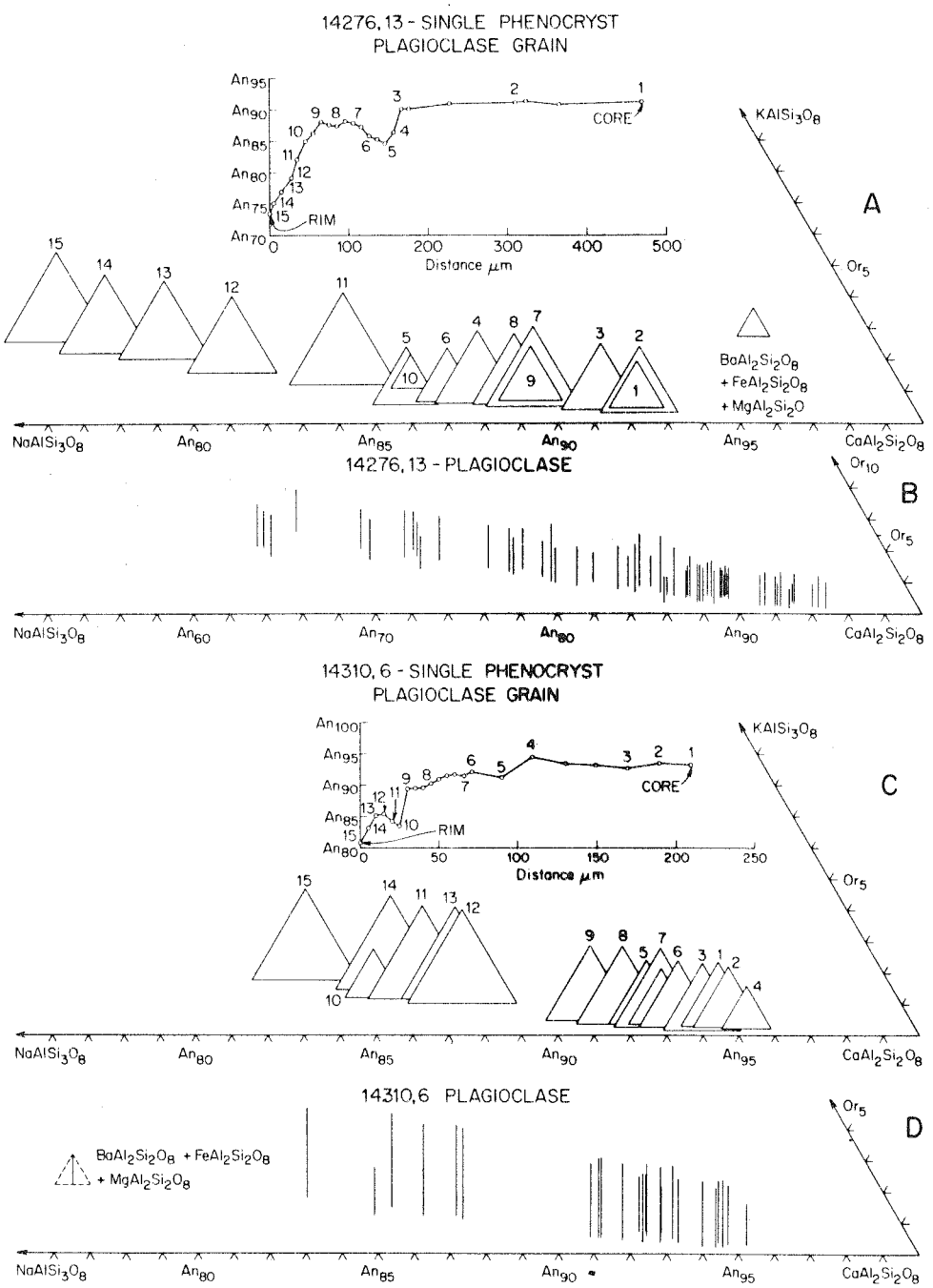

Fig. 7. Plagioclase analyses from samples 14310,6 and 14276,13. Figs. 7A and 7C show the compositional variation from the core to rim and the compositional reversal in single plagioclase phenocrysts from samples 14276,13 and 14310,6 respectively. The numerals on the profiles correspond to the numbered triangles plotted directly below the profile. Figs. 7B and 7D are composite diagrams of all the plagioclase analyses from samples 14276,13 and 14310,6, respectively.

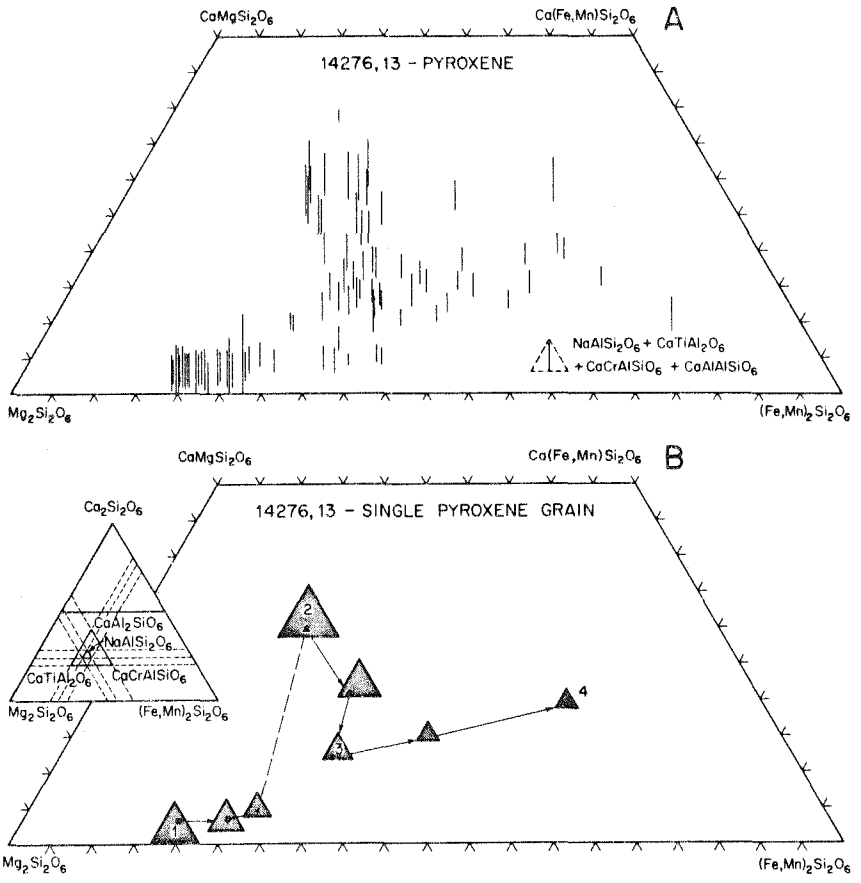

Fig. 8. Pyroxene analyses from sample 14276,13. Fig. 8A is a composite of all the pyroxenes from the sample. On fig. 8B, selected analyses from a core to rim traverse are plotted in terms of the seven principal end-members. The numerals correspond to the numbered analyses in table 2.

10% of the rock, are uniformly distributed. These vugs contain projecting crystals of plagioclase, ilmenite, and pyroxene.

The sample was studied in polished thin section 14276,13, which has an area of about 68 mm^2. The section is of a subophitic, intergranular to interstitial, basalt composed predominantly of plagioclase (65%) and pyroxene (33%) with 2% opaque minerals, predominantly ilmenite, and 4% mesostasis containing glass and other minor phases. The texture is like that of 68415 and 14310 and distinct from the Apollo 11 and 12 samples and 14053 (see photos in Gancarz et al. [6]). Euhedral plagioclase laths (~ 0.5 mm long) form an interlocking framework, the interstices of which contain anhedral pyroxene grains (~ 0.3 mm) and mesostasis. Locally the plagioclase laths are in radial aggregates or in finer-grained patches which could represent cognate inclusions. No prominent shock features were observed in the thin section.

For comparison with 68415 and 14310, table 1b gives the mode, "average" mineral compositions and calculated bulk composition determined by the microprobe. The similarity of the calculated composition with that determined by chemical analysis of a bulk sample [23] suggests that the mode and "average" mineral compositions are accurate.

The plagioclase occurs in several distinctive habits nearly identical to those described for sample 68415.

Like the phenocrysts in rock 68415, the phenocrysts in 14276,13 exhibit an optical discontinuity near the rim and a reversal in composition, and, as is shown on fig. 7a, the cores of the phenocrysts are relatively homogeneous in composition. However, unlike those in sample 68415, the rims of the phenocrysts in 14276,13 are larger and are zoned to more Ab-rich compositions (i.e., An_{74} vs. An_{87}). Selected plagioclase analyses are given in table 2.

External morphology and symmetrical zoning are not well developed in the pyroxene because it grew interstitial to the plagioclase. However, individual pyroxene grains typically have a low-birefringent orthopyroxene core surrounded by higher-birefringent clinopyroxene which displays a weak mosaic structure. A similar variation in composition is indicated in fig. 8, both by all the analyses and by selected points from a traverse from core to rim in a single pyroxene grain. Typical analyses are presented in table 2. The orthopyroxene core becomes more iron-rich outward to the optical discontinuity; jumps to a high-Ca clinopyroxene (augite) which grades with oscillations to a low-Ca clinopyroxene (pigeonite) and then grades near the edge to a Fe-rich composition. Many of the most Fe-rich compositions on fig. 8A occur as tiny, high birefringent grains in the mesostasis, although some mesostasis grains have Mg > Fe. Both orthopyroxene and high-Ca clinopyroxene tend to have higher $CaCrAlSiO_6$ and $CaAl_2SiO_6$ contents than the low-Ca clinopyroxene. The zoning pattern is nearly identical to that in 14310 (see also Bence and Papike [17]).

The mesostasis is a complex of fine-grained material including glass, K-Ba feldspar, Fe-rich pyroxene, apatite, whitlockite, tranquillityite, and opaque phases. The SiO_2 content of the glass ranges from 69 to 78 wt % (14 analyses), falling in the high-Si range of glass from other Apollo 14 samples [6]. The low-Si, high-K and Ba glass found in other Apollo samples apparently occurs as K-Ba feldspar in this rock. An analysis of a K-Ba feldspar grain about 0.2 mm across ($2V = 31 \pm 4^\circ$) is given in table 2.

Opaque phases include ilmenite, troilite, ulvöspinel, and Fe-metal. Ulvöspinel is rare $(Fe_{1.88}Mg_{0.07}Mn_{0.01})(Ti_{0.86}Cr_{0.05}Al_{0.13})O_{\sim 4}$ and is rimmed by ilmenite (see table 1b). The average ZrO_2 content in six ilmenite grains is 0.30 wt %, ranging from 0.16 to 0.67 wt %. One zircon grain was observed enclosed in ilmenite. Fe-metal occurs as grains both associated with and independent of troilite. The Ni ranges from 4.3 to 13.3 wt % and the Co from 0.45 to 0.76 wt % (see fig. 5). There is no apparent compositional distinction between Fe-metal included in FeS and that in independent grains.

Both apatite and whitlockite occur in the mesostasis, typically as needles (0.05–0.07 mm). Electron beam scans indicate that distinct grains of apatite may be included within whitlockite. Their compositions (table 3) are similar to those reported for other Apollo 14 samples. Analyses were made for Ce_2O_3, La_2O_3, and Nd_2O_3 and the total RE_2O_3 were estimated by normalization to the values for total rock 14310. These estimates range from 1.1 to 6.0 wt % for apatite (3 analyses) and 5.3 to 11.7 wt % (6 analyses) for whitlockite.

Table 3
Apatite, whitlockite and tranquillityite analyses from sample 14276, 13.

	Apatite	Whitlockite
F	3.33	< 0.01
Cl	0.21	< 0.01
P_2O_5	40.78	41.54
SiO_2	0.43	0.68
CaO	53.85	42.07
FeO	0.45	3.03
MgO	0.05	2.24
Na_2O	0.09	0.54
Al_2O_3	0.04	0.07
Y_2O_3	0.35	2.29
La_2O_3	0.05	0.95
Ce_2O_3	0.51	2.60
Nd_2O_3	0.23	1.22
ΣRE_2O_3	0.31	2.75
Total	100.68	99.98
$O \equiv F + Cl$	1.45	
	99.23	
	Formula proportions	
F	0.90	< 0.01
Cl	0.03	< 0.01
P	2.94	1.91
Si	0.04	0.04
Ca	4.92	2.45
Fe	0.03	0.14
Mg	0.01	0.18
Na	0.01	0.06
Al	< 0.01	< 0.01
Y	0.02	0.06
ΣRE	0.02	0.16

Table 3 (cont'd.)

	Tranquillityite			
Nb_2O_5	< 0.01	(0.00) *	< 0.01	(0.00) *
P_2O_5	0.03	(0.01)	0.26	(0.04)
SiO_2	15.43	(3.13)	14.55	(2.93)
TiO_2	21.19	(3.23)	23.90	(3.62)
ZrO_2	13.21	(1.31)	11.27	(1.11)
HfO_2	0.72	(0.05)	0.55	(0.03)
UO_2	0.08	(0.00)	0.21	(0.01)
ThO_2	0.03	(0.00)	0.08	(0.00)
Y_2O_3	0.27	(0.03)	0.60	(0.06)
La_2O_3	< 0.01	(0.00)	< 0.01	(0.00)
Ce_2O_3	0.30	(0.02)	0.30	(0.02)
Nd_2O_3	< 0.01	(0.00)	< 0.01	(0.00)
Pr_2O_3	0.06	(0.00)	< 0.01	(0.00)
Gd_2O_3	0.12	(0.02)	0.10	(0.01)
Dy_2O_3	< 0.01	(0.00)	< 0.01	(0.00)
Cr_2O_3	0.01	(0.00)	0.07	(0.01)
Al_2O_3	0.88	(0.21)	1.24	(0.29)
FeO	43.20	(7.33)	42.28	(7.12)
MgO	1.08	(0.33)	1.17	(0.35)
MnO	0.34	(0.06)	0.27	(0.05)
CaO	1.31	(0.28)	1.47	(0.32)
PbO	0.04	(0.00)	0.03	(0.00)
K_2O	< 0.01	(0.00)	0.02	(0.01)
Na_2O	< 0.01	(0.00)	0.02	(0.01)
Total	98.30		98.31	

* Numbers in parentheses are formula proportions with the cations normalized to 16.

Tranquillityite occurs as small (1–5 μm), red translucent plates in the mesostasis and is relatively abundant as in the other Fra Mauro basalts. The two analyses given in table 3 are basically different from those reported for tranquillityite in the Apollo 11 and 12 basalts [24]; the TiO_2 and SiO_2 contents are higher and the ZrO_2 content is significantly lower (~ 30%). Similar differences in Apollo 14 tranquillityite have been reported by El Goresy and Ramdohr [25].

These differences appear to be real and not the result of contamination by other phases adjacent to the analyzed grains. Optical examination of the analyzed tranquillityite grains indicates that they are surrounded by glass and that ilmenite and other opaque phases are absent. Therefore, the higher TiO_2 content is not due to contamination from ilmenite. The analyses were performed with the electron microprobe in the computer-controlled automated mode. Since the microprobe is preprogrammed for a total analysis (i.e., counting on the peak and respective background positions for all 25 elements), the sample is never moved. Therefore, the problem of precisely relocating the exact sample position is alleviated. The points were initially located by maximizing the Zr signal.

In addition to the elements which typically occur in tranquillityite, the total analyses included S, P, K, and Na as internal checks for possible contamination. The very low SO_3 values (table 3) indicate no contamination by troilite and the low P_2O_5 values indicate that contamination by either apatite or whitlockite is relatively minor. Since both of the analyzed grains are surrounded by glass which contains K_2O and Na_2O, it is possible that the SiO_2 value for analysis # 2 is 3% to 7% in excess of the true value because of contamination. However, this is still not sufficient to account for the compositional differences between these and the Apollo 11 and 12 tranquillityites.

Fission-track studies on 14276, 13 indicate the absence of the extremely U- and Th-rich phases found in other Fra Mauro basalts [6].

4. Apollo 14 sample 14310

Sample 14310 has been described by a number of workers [6–9, 26]. For comparison with 68415 and 14276, table 1c gives the mode, "average" mineral compositions, and calculated bulk composition determined by the microprobe.

The similarity of the calculated composition with that determined by chemical analysis of a bulk sample [23] suggests that the mode and "average" mineral compositions are accurate although quite different modal estimates, especially of the relative proportions of the pyroxenes, have been published.

Brown and Peckett [7] have described a reversal in plagioclase composition between larger phenocrysts and groundmass laths in this rock. The texture and the compositional discontinuities in the plagioclase are present in thin section 14310,6 (figs. 7C and D), but are not as evident as in thin section 68415,8.

Additional analyses of pyroxene are shown on fig. 9. The microprobe point counts indicate two quite distinct groups of low-Ca pyroxene compositions. As noted by Bence and Papike [17], the pyroxene trends are nearly identical in 14276 and 14310, and the dominant pyroxene is orthopyroxene although we previously [6] described the group lowest in Ca as clinopyroxene.

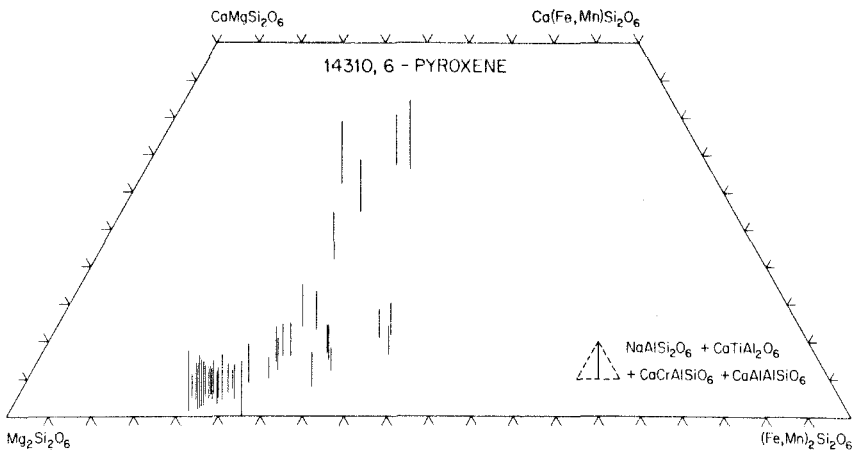

Fig. 9. Pyroxene analyses from sample 14310,6.

5. Discussion

5.1. *Characteristics of feldspathic basalts*

Petrographically, samples 68415 and the Fra Mauro basalts, represented by samples 14310, 14276, and 14073 are remarkably similar to one another in many respects and very different from the mare basalts, represented by the Apollo 11 and 12 and Luna 16 samples: (1) they have similar, ophitic intersertal textures; (2) they are characterized by a high plagioclase content; (3) textural relationships and compositional data demonstrate that there are two generations of plagioclase, the earlier of which was cumulate in origin; (4) the pyroxenes, unlike those in most of the mare basalts, show rather limited Fe-enrichment; (5) ilmenite enters relatively late as a liquidus phase. The presence of early orthopyroxene in the Fra Mauro basalts versus olivine in sample 68415 does not basically distinguish these basalts [27].

Chemically, both sample 68415 and the Fra Mauro basalts have a high Al_2O_3 content and low FeO and TiO_2 content compared to the mare basalts. However, they differ markedly in their minor element content. Compared to the mare basalts, the Fra Mauro basalts have much higher K, trivalent REE, P, Ba, U, and Th concentrations, whereas sample 68415 has lower or similar concentrations of these elements [28, 15]. In terms of the chemical classification adopted by Reid et al. [29], sample 68415 would be classified as a gabbroic anorthosite or "Highland basalt".

In the following discussion, we will group all of the plagioclase-rich basalts with primary, ophitic intersertal texture as feldspathic basalt. The reasons for this petrogenetic grouping, despite the chemical differences, is to emphasize the petrogenetic importance of such high plagioclase contents. If these rocks crystallized from parent magmas generated by partial melting, then such magmas were all derived from even more aluminous source material. Alternatively, such plagioclase-rich basalts would have to represent accumulation of early-formed feldspar from a parental basaltic liquid.

The nature and origin of feldspathic basalts is of fundamental importance to questions relating to the formation of the highlands regions and lunar magmatic differentiation processes. Numerous investigators have suggested that plagioclase separation played an important role in the genesis of lunar rocks. This suggestion was based on the presence of anorthositic fragments in the lunar soil samples, the high albedo of the highlands, the Surveyor VII analyses, and the chemistry of the mare basalts, particularly the large negative europium anomaly. Since the europium anomaly is observed not only in all the mare basalts, but also in the Fra Mauro feldspathic basalts and in the soil samples, it has been further suggested by numerous investigators that the plagioclase separation occurred at an early stage in lunar history. Furthermore, the Rb–Sr and U–Th–Pb systematics, summarized by Papanastassiou and Wasserburg [30, 13] and Tera and

Wasserburg [31], provide clear evidence that major differentiation and chemical fractionation occurred earlier than 4.3 by in lunar history and resulted in the formation of two rock reservoirs with very distinctive concentrations of K, Rb, U, and Th.

The feldspathic basalts discussed here range in age from 3.84 to 3.88 by [10, 12, 13]. They are older than most of the dated mare basalts, but seem young relative to the inferred major differentiation early in lunar history. Questions posed by "young" highly feldspathic basalts are as follows: (1) how, if at all, are they related to one another; (2) did they crystallize from a melt formed by impact melting of regolith; (3) how are they related to the anorthositic fragments found in the soils and to anorthosite samples such as 15415; (4) are these feldspathic basalts a major constituent of the highlands?

5.2. *Relationships among the feldspathic basalts*

We have emphasized the petrographic and chemical similarities of sample 68415 and of the Fra Mauro samples (14310, 14276, and 14073). These similarities suggest that the eruptive processes and the major element compositions of the magmas from which they were produced were similar or might even suggest that these samples were derived from the same magma. However, there are distinctive trace element and isotopic characteristics which indicate that sample 68415 and the Fra Mauro samples not only originated independently of each other, but also that Fra Mauro samples 14310 and 14073 originated independently of sample 14276. Hence, we will discuss each of these samples as representatives of different magma bodies, collectively representing an important lunar magma type.

Fig. 10 is a K versus Al_2O_3 plot showing the compositions of 68415, 14310, and 15415. Sample 14276 is nearly identical to 14310 and its composition is not plotted. This plot is useful because the chemical behavior of many elements, such as K, Rb, U, trivalent REE, and Ba, which tend to be highly concentrated into the mesostasis, can be illustrated by the differences in K concentration and can be correlated with the mesostasis content. Similarly, the behavior of elements such as Sr, Eu, and Al, which are highly concentrated into plagioclase, can be illustrated by the Al_2O_3 concentration and can be correlated with the plagioclase content. A point lying on a line passing

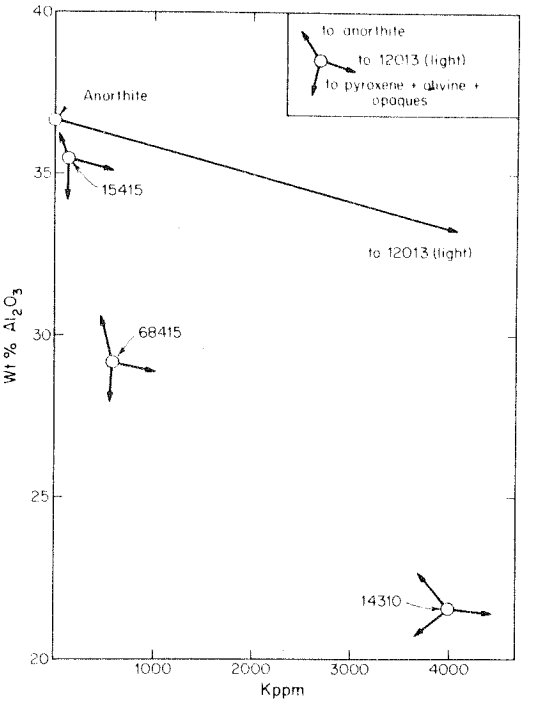

Fig. 10. A K versus Al_2O_3 plot showing the compositions of 15415, 68415, and 14310 [15, 23]. The arrows show the trajectories for the addition of either 12013 (light), pure anorthite, or low-K and low Al_2O_3-bearing phases such as pyroxene, olivine, and opaques. Along such a trajectory there is no change in the proportions of the other two components.

through any other two points on such a diagram can be represented as a linear combination of the other two samples. For example, a sample of intermediate composition could be produced by an additive relation between the two samples with extremal compositions, *or* a sample with an extremal composition could be produced through a subtractive relation between the other two samples. These two relations represent physically quite different processes, but they cannot be distinguished from the diagram alone.

The arrows of the point of fig. 10 indicate the trajectories formed by addition of each of the following end-members: anorthite, mesostasis represented by 12013 (light), and the origin, representing low-K and low-Al_2O_3 phases, such as pyroxene, olivine, and opaque minerals.

Along such a trajectory representing the addition

or subtraction of a single end-member there can be no change in the proportions of the other two end-members. Since a straight line can be passed through 15415, 68415, and anorthite, rocks represented by these two samples could be related by addition or subtraction of plagioclase without a change in the proportions of the other components. However, since no straight line can be passed through 14310, 68415, and any one of the end-members, these two rock compositions cannot be related solely by addition or subtraction of any one of the end-members. They can be related only by a change in the proportions of all three end-members. This statement remains true even if each of the "average" mesostasis compositions given in table 1, which differ by a factor of 8 in K content, is substituted for 12013 (light).

The chemical data restrict any genetic relationships between rocks with 68415- and 14310-like compositions by simple magmatic fractionation which results from the addition or subtraction of a single phase. A relationship by some more complicated process of magmatic fractionation cannot be ruled out by chemical data alone.

The Rb–Sr isotopic data provide much more rigorous restraints on the processes involved. Rb–Sr isotopic measurements show that samples 68415, 14310, and 14276 have within experimental error the same internal isochron age (3.84 to 3.88 by) and the same model age (4.35–4.39 by), but radically different initial values of $^{87}Sr/^{86}Sr$ (0.69920 ± 3, 0.70036 ± 8, and 0.70019 ± 2) [10, 12, 13]. These data impose stringent boundary conditions on any petrogenetic model which might be proposed to explain the origin of the rocks represented by each of these samples.

Based on the element and mineral compositions, it would be possible to postulate that the composition of 68415 could have been derived from that of 14276 or 14310 (or 14073 or 14001, 7, 3) by a complex magmatic fractionation, for example, addition of plagioclase with some concomitant change in the composition of the mesostasis. However, the hypothesis that these three rocks were derived from the same magma by magmatic differentiation during crystallization of the melt is *strictly* prohibited by the Rb–Sr isotopic systematics. The initial $^{87}Sr/^{86}Sr$ is the value of $^{87}Sr/^{86}Sr$ in the rock and all its phases at the time of the most recent homogenization and closure of the rock and mineral systems. This value is obtained from the intercept of the internal isochron line on the Rb–Sr evolution diagram. The distinctly different initial $^{87}Sr/^{86}Sr$ indicate that, even considering the maximum analytical errors, none of these three rocks can be related to one another by the addition or subtraction of either the plagioclase or of the mesostasis actually present in these rocks at the time of crystallization. Since all phases in the crystallizing magma had isotopic compositions identical to that of the total system (melt + crystals), there is no way in which the addition or removal of cognate phenocrysts from any of the magmas can change the Sr isotopic composition of one magma to that of one of the other magmas.

Simple magmatic differentiation at the time of crystallization from the melt is thus excluded as a process relating the rocks represented by these samples. Although the rocks show textural evidence of plagioclase accumulation, such accumulation cannot explain the Rb–Sr data.

All three rocks have the same model age relative to BABI within analytical error (~ 4.35 by) indicating that all three rocks, if they evolved as closed systems, would have had the same $^{87}Sr/^{86}Sr$ value 4.35 by ago, and that this value would have been that of basaltic achondrites [32]. Hence, these rocks can only be related to one another by addition or subtraction of material which, if analyzed today, would fall on the isochron formed by the total rock values (i.e., would have the same total rock isochron age and the same model age) [33, 32].

Wilshire and Jackson [34] suggest that "local temperatures were high enough (about 1000° C) to reset partially or completely certain radiogenic systems used to date the Apollo 14 rocks". These possibilities are excluded by the Rb–Sr systematics for the two petrographically distinct groups of samples [6]. One group of Fra Mauro basalt samples (14310, 14276, 14073, and 14001, 7, 3, a small clast from the soil) has the identical age within analytical error (3.88 by) based on a precise internal isochron. The other group of mare basalt samples (14053 and 14321,199, a clast from a "coherent to moderately coherent" breccia [34]) also has the identical internal isochron age within analytical error (3.95 by). For igneous

rocks, internal isochron ages are generally considered to represent the time since the rock crystallized from the melt. In the absence of textural evidence the internal isochron could represent a *complete* metamorphic re-equilibration, but a *partial* re-equilibration of a rock will result in phases whose composition does not fit the internal isochron age (i.e., it falls off the internal isochron line on the Rb–Sr evolution diagram [33]). The Rb–Sr data for the Apollo 14 samples exclude the possibility of a *partial* thermal metamorphic re-equilibration and, in conjunction with the zoning exhibited by the minerals, excludes the possibility of a *complete* thermal metamorphic re-equilibration. The agreement between the ^{40}Ar–^{39}Ar [11] and the Rb–Sr ages should also be noted since Ar loss might be expected at lower temperatures than Sr redistribution.

It has been suggested that certain characteristics of sample 14310 are compatible with near-surface crystallization of a large sheet of magma produced by impact melting of regolith containing a significant meteoritic component [35]. These characteristics include the compositional similarity of 14310 to the Apollo 14 soils and fragmental rocks, the presence of fragments and of schreibersite in the rock, and the composition of the Fe-metal in the rock [35–38, 26]. No conclusive evidence seems to exclude the possibility that all of these feldspathic basalts formed from melts which originated by impact melting of regolith of the proper composition. However, the precise internal isochrons indicate that *complete* melting and rehomogenization occurred and that the early phenocrysts in these rocks cannot represent clasts from the soil. It is possible that the rehomogenization only occurred on a scale of several centimeters. Cliff et al. [3] report a higher model age and suggest the possibility of heterogeneity in this rock. Feldspathic basalt clasts are reported in the coherent breccias of the Fra Mauro formation [34]. If these clasts are like the feldspathic basalts described here and contain a complex textural history, it seems impossible to attribute both the origin of the pool of impact melt and the Fra Mauro breccias to the Imbrian event. It appears quite possible that 14310 (and other feldspathic basalts) originated from impact-generated melts. However, alternative origins are discussed in this paper, in as much as assumption of an impact origin implies that these rocks do not provide information on important lunar processes which is basically different from that provided by the analyses of bulk regolith samples and by studies of glass fragments and balls contained in the regolith [40, 29].

The Rb–Sr isotopic data do allow two reasonable petrogenetic hypotheses consistent with the elemental and mineralogic data. The three magmas represented by samples 68415, 14276, and 14310 could have evolved with different plagioclase contents in the same or a similar magmatic reservoir. Upon eruption or ascent to a shallow environment, rocks such as 14276 and 14310 were then contaminated by different amounts of material with high $^{87}Sr/^{86}Sr$ and Rb/Sr ratios, equivalent to a model age of about 4.35 by today, and rich in trace elements such as Ba, U, K, REE, P, and Th [10, 12]. Although it seems possible that 68415 may have a positive europium anomaly owing to its high plagioclase content and low abundance of REE-bearing minerals, the admixture of a small amount of material with a high REE concentration and a large negative europium anomaly could produce the negative europium anomaly observed in samples 14276 and 14310.

Conceptually, we encounter difficulties in accepting such contamination and homogeneous assimilation of very small amounts of a very special material as a general and widespread process. It is generally recognized that the extent of assimilation of felsic inclusions by mafic melts is limited and that felsic inclusions in mafic melts are likely to be preserved, surrounded by fine-grained quenched rock, unless the cooling rate is very slow and the crystal settling rate rapid [41]. Hence, it seems likely that a general and widespread contamination process would have resulted in petrographic evidence of its existence.

The Rb–Sr isotopic restraints would also be satisfied if magmas represented by these three rocks were related to one another by subtraction of plagioclase, which has a Rb–Sr composition lying on the total rock isochron for the three rocks. This process could occur by the following sequence of events: (1) source material, more aluminous than the feldspathic basalts, formed during an early lunar differentiation at about 4.35 by or earlier; (2) partial melting occurred at about 3.85 by and these melts separated *without* isotopic equilibration with the plagioclase-rich residuum. These residual plagioclase crystals formed during the earlier differentiation and would necessarily have a

very low Rb/Sr and a $^{87}Sr/^{86}Sr$ close to BABI. Different degrees of such partial melting and separation without isotopic equilibration could result in the formation of melts with different Rb/Sr and $^{87}Sr/^{86}Sr$ ratios from the same reservoir. A somewhat different alternative would be the *total* melting of a higher Rb/Sr (i.e., a composition like 14310) source volume formed during the early differentiation and the assimilation of varied amounts of plagioclase from the surrounding more plagioclase-rich rocks, which also formed during the early differentiation. This could also result in the formation and derivation of melts with different Rb/Sr and $^{87}Sr/^{86}Sr$ ratios from the same reservoir. A less likely alternative would be that each rock was derived by the *total* melting of different source rocks with distinct compositions owing directly to the early differentiation. All three of these processes can explain the observed Rb–Sr, element abundance, and petrologic data without recourse to contamination by highly radiogenic material during eruption or ascent to a shallow environment.

5.3. *Relationship of feldspathic basalts to anorthositic rocks*

Once the existence of younger feldspathic rocks like 68415 is established, it becomes necessary to ask whether they are basically different or whether they are actually derived from anorthositic rocks, or vice versa. In general, the anorthositic fragments from the soil samples, including those from Apollo 16, and the "Genesis Rock" (15415) have undergone a complex history of deformation and recrystallization [2–5, 15]. Although some of the fragments display relict ophitic textures, most appear to have been originally coarse-grained rocks with more equant grains, and many consist almost entirely of plagioclase.

No precise age can be assigned to 15415 from the Rb–Sr data, but the U–Th–Pb isotopic data indicates an age between 3.8 and 4.1 by [42] and the $^{40}Ar–^{39}Ar$ data indicate an age between 3.9 and 4.3 by [43, 44]. These age observations permit an age older than that of the three feldspathic basalts described in this paper. The low $^{87}Sr/^{86}Sr$ of 15415 prohibits it from having been exposed for a significant time to a high Rb/Sr environment, even one as high as the Apollo 11 low-K rocks, which is about a tenth that of 68415 and about a hundredth that of 14310 [10, 12, 13]. Therefore, if 68415 was derived by partial melting of basement material with a composition similar to 15415, it must represent only a fraction of a percent of partial melting and the derivation of the Fra Mauro type basalts, such as 14310 and 14276, in such a manner, appears even more implausible.

The anorthositic fragments in the soils include a considerable compositional variety and it appears that anorthositic gabbros are more common than anorthosites [29]. The major element and major mineral abundances of the feldspathic basalts are quite similar to those of the anorthositic gabbro fragments, but the Fra Mauro basalts are distinguished by the high K, REE, P, Ba, U, and Th abundances. It seems possible that 68415 is a relatively undeformed fragment derived from the same magmatic reservoir that produced some of the highly-shocked anorthositic fragments and that some of the anorthositic fragments are 3.85 by old. However, any mechanism for the origin of the feldspathic basalts by partial melting requires the existence of a more aluminous source material formed earlier in lunar history. Such material very likely forms some portion of the anorthositic fragments in the soils.

5.4. *Chemical composition and nature of the highlands*

The high albedo of the highlands combined with the Surveyor VII data, the europium anomaly, and the discovery of anorthositic fragments in the Apollo 11 soil led to the early suggestion that the highlands consisted of early-formed anorthositic crust [2, 45, 46]. Norms for analyses of Surveyor VII [47], Luna 20 [47], Apollo 14 [48], and Apollo 16 [15] soils indicate that these highland soils are too poor in plagioclase to represent a true anorthosite with greater than 90% plagioclase. In addition, the Al-rich glasses from the soil samples, which show a very restricted range of composition, have been interpreted as representing a common rock composition in the highlands [40, 29]. These glass samples are also too poor in normative plagioclase to represent a true anorthosite.

Although it is possible that the highlands consist of a plagioclase-rich basalt or anorthositic gabbro rather than of anorthosite [29], it may well be too simplistic an idea to imagine that the highlands are composed of a homogeneous rock of any sort. On the contrary, the highlands may consist of a complex mixture of darker and lighter rocks, albeit all rather feldspathic, covered by a regolith well mixed by a long

history of impact, so as to produce the characteristic light albedo and an average composition like the Al-rich glasses from the soils.

The existence of rock fragments and glass of the Fra Mauro or KREEP-type in all the soils and their affinities with the anorthositic fragments has suggested that they were derived from the highlands [40–49]. It seems entirely possible that relict portions of an earlier K-rich crust may still be present in the highlands. The orbiter gamma ray data indicate that the highlands have an average U content of about 0.5 ppm [50, 51]. This would suggest an average K content of about 800 ppm, assuming K/U typical of lunar rocks. This value is similar to that of 68415. Since the spatial resolution of the orbiter data is quite low, rather large area of higher-K rocks may be present. Such old K-rich areas would have been subjected to repeated bombardment and may be covered with a high albedo regolith. Consequently, the bulk of such an early crust may actually now reside in the lunar soil. However, such highly radioactive masses are more likely to be remelted than the typical highland rock, assimilating varied proportions of more typical plagioclase-rich material and possibly resulting in the formation of the higher-K magmas represented by 14276 and 14310.

6. Conclusions

Feldspathic basalts apparently are a common and widespread lithologic type, and may be a major rock type in the lunar highlands. Feldspathic basalts from the Apollo 14 and 16 missions cannot be derived from one another by magmatic fractionation during their crystallization. We conclude that feldspathic basalt magmas could have been derived from pre-existent highly feldspathic source regions by partial melting *without* isotopic equilibration between the melt and the residual crystals.

These source regions must have had a range of compositions corresponding to that exhibited by the highly-deformed anorthositic and anorthositic gabbro fragments found in the lunar soils. We suggest that only a small part of the anorthositic fragments in the soils are derived by deformation and recrystallization of younger feldspathic basalts and that most such fragments are derived from the source regions of the feldspathic basalts and were originally formed during a major differentiation event early in lunar history.

Acknowledgements

We have greatly benefited from a series of heated discussions with G.J. Wasserburg and D. Papanastassiou, and from detailed comments upon the manuscript by R. Dymek, C. Gray, J.C. Huneke, D. Papanastassiou, and G.J. Wasserburg. E. Haines provided fission-track data on sample 14276. This work was supported by NASA contract NAS-9-8074. The microprobe laboratory has been developed with the support of NSF, JPL, and the Union Pacific Foundation.

References

[1] Lunar Receiving Laboratory, Lunar sample information catalog, Apollo 16, MSC 03210 (1972) 372 pp.
[2] J.A. Wood, J.S. Dickey Jr., U.B. Marvin and B.N. Powell, Lunar anorthosites and a geophysical model of the moon, Proc. Apollo 11 Lunar Sci. Conf., Geochim. Cosmochim. Acta Suppl. 1, 1 (1970) 965.
[3] U.B. Marvin, J.A. Wood, G.J. Taylor, J.B. Reid Jr., B.N. Powell, J.S. Dickey Jr. and J.F. Bower, Relative proportions and probable sources of rock fragments in the Apollo 12 soil samples, Proc. Second Lunar Sci. Conf., Geochim. Cosmochim. Acta Suppl. 2, 1 (1971) 679.
[4] O.B. James, Lunar anorthosite 15415: Texture, mineralogy, and metamorphic history, Science 175 (1972) 432.
[5] H.G. Wilshire, G.G. Schaber, L.T. Silver, W.C. Phinney and E.D. Jackson, Geologic setting and petrology of Apollo 15 anorthosite (15415), Geol. Soc. Am. Bull. 83 (1972) 1083.
[6] A.J. Gancarz, A.L. Albee and A.A. Chodos, Petrologic and mineralogic investigation of some crystalline rocks returned by the Apollo 14 mission, Earth Planet. Sci. Letters 12 (1971) 1.
[7] G.M. Brown and A. Peckett, Selective volatilization on the lunar surface: Evidence from Apollo 14 feldspar-phyric basalts, Nature 234 (1971) 262.
[8] W.G. Melson, B. Mason, J. Nelen and S. Jacobson, Apollo 14 basaltic rocks, Revised Abstr. Third Lunar Sci. Conf., ed. C. Watkins (1972) 535.
[9] W.I. Ridley, R.J. Williams, R. Brett, H. Takeda and R.W. Brown, Petrology of lunar basalt 14310, Revised Abstr. Third Lunar Sci. Conf., ed. C. Watkins (1972) 648.
[10] D.A. Papanastassiou and G.J. Wasserburg, Rb–Sr ages of igneous rocks from the Apollo 14 mission and the age of the Fra Mauro formation, Earth Planet. Sci. Letters 12 (1971) 36.

[11] G. Turner, J.C. Huneke, F.A. Podosek and G.J. Wasserburg, $^{40}Ar-^{39}Ar$ ages and cosmic ray exposure ages of Apollo 14 samples, Earth Planet. Sci. Letters 12 (1971) 19.

[12] G.J. Wasserburg and D.A. Papanastassiou, Age of an Apollo 15 mare basalt; lunar crust and mantle evolution, Earth Planet. Sci. Letters 13 (1971) 97.

[13] D.A. Papanastassiou and G.J. Wasserburg, The Rb–Sr age of a crystalline rock from Apollo 16, Earth Planet. Sci. Letters (in press).

[14] Apollo Lunar Geology Investigation Team, U.S.G.S., Documentation and environment of the Apollo 16 samples: A preliminary report, U.S.G.S. Interagency Rep.: Astrogeology 51 (1972) 252 pp.

[15] Apollo 16 Preliminary Examination Team, The Apollo 16 lunar samples: A petrographic and chemical description of samples from the lunar highlands, Science (in press).

[16] D.H. Green, N.G. Ware and W.O. Hibberson, Experimental evidence against the role of selective volatilization on the lunar surface, Nature 238 (1972) 450.

[17] A.E. Bence and J.J. Papike, Pyroxenes as recorders of lunar basalt petrogenesis: I. Chemical data for liquidus trends (in press).

[18] I. Kushiro, Petrology of lunar high-alumina basalt, Revised Abstr. Third Lunar Sci. Conf., ed. C. Watkins (1972) 466.

[19] J.V. Smith, Minor elements in Apollo 11 and Apollo 12 olivine and plagioclase, Proc. Second Lunar Sci. Conf., Geochim. Cosmochim. Acta Suppl. 2, 1 (1971) 143.

[20] J.I. Goldstein and H. Yakowitz, Metallic inclusions and metal particles in the Apollo 12 lunar soil, Proc. Second Lunar Sci. Conf., Geochim. Cosmochim. Acta Suppl. 2, 1 (1971) 177.

[21] T.J. Ahrens and J.D. O'Keefe, Shock melting and vaporization of lunar rocks and minerals, The Moon 4 (1972) 214.

[22] Apollo 14 lunar sample information catalog, NASA Tech. Memo., NASA TM X-48062 (1971).

[23] H.J. Rose Jr., F. Cuttitta, C.S. Annell, M.K. Carron, R.P. Christian, E.J. Dwornik, L.P. Greenland and D.T. Ligon Jr., Compositional data for twenty-one Fra Mauro lunar materials, Proc. Third Lunar Sci. Conf., Geochim. Cosmochim. Acta Suppl. 3 (1972) (in press).

[24] J.F. Lovering, D.A. Wark, A.F. Reid, N.G. Ware, M. Keil, M. Prinz, T.E. Bunch, A.E. Goresy, P. Ramdohr, G.M. Brown, A. Peckett, R. Phillips, E.N. Cameron, J.A.V. Douglas and A.G. Plant, Tranquillityite: A new silicate mineral from Apollo 11 and Apollo 12 basaltic rocks, Proc. Second Lunar Sci. Conf., Geochim. Cosmochim. Acta Suppl. 2, 1 (1971) 39.

[25] A. El Goresy and P. Ramdohr, Fra Mauro crystalline rocks: Petrology, geochemistry and subsolidus reduction of the opaque minerals, Revised Abstr. Third Lunar Sci. Conf., ed. C. Watkins (1972) 224.

[26] L. Hollister, W. Trzcienski Jr., R. Dymek, C. Kulick, P. Weigand and R. Hargraves, Igneous fragment 14310, 21 and the origin of the mare basalts, Revised Abstr. Third Lunar Sci. Conf., ed. C. Watkins (1972) 386.

[27] D. Walker, J. Longhi and J.F. Hays, Experimental petrology and origin of Fra Mauro rocks and soil, Revised Abstr. Third Lunar Sci. Conf., ed. C. Watkins (1972) 770.

[28] A.L. Albee, A.A. Chodos, A.J. Gancarz, E.L. Haines, D.A. Papanastassiou, L. Ray, F. Tera, G.J. Wasserburg and T. Wen, Mineralogy, petrology and chemistry of a Luna 16 basaltic fragment, Sample B-1, Earth Planet. Sci. Letters 13 (1972) 353.

[29] A.M. Reid, W.I. Ridley, R.S. Harmon and R. Brett, Highly aluminous glasses in lunar soils and the nature of the lunar highlands, Geochim. Cosmochim. Acta 36 (1972) 903.

[30] D.A. Papanastassiou and G.J. Wasserburg, Lunar chronology and evolution from Rb–Sr studies of Apollo 11 and 12 samples, Earth Planet. Sci. Letters 11 (1971) 37.

[31] F. Tera and G.J. Wasserburg, U–Th–Pb systematics in three Apollo 14 basalts and the problem of initial Pb in lunar rocks, Earth Planet. Sci. Letters 14 (1972) 281.

[32] D.A. Papanastassiou and G.J. Wasserburg, Initial strontium isotopic abundances and the resolution of small time differences in the formation of planetary objects, Earth Planet. Sci. Letters 5 (1969) 361.

[33] M.A. Lanphere, G.J.F. Wasserburg, A.L. Albee and G.R. Tilton, Redistribution of strontium and rubidium isotopes during metamorphism, World Beater Complex, Panamint Range, California, in: Isotopic and Cosmic Chemistry, eds. H. Craig, S.L. Miller and G.J. Wasserburg (North-Holland, Amsterdam, 1964) 553 pp.

[34] H.G. Wilshire and E.D. Jackson, Petrology and stratigraphy of the Fra Mauro Formation at the Apollo 14 site, U.S. Geol. Surv., Prof. Paper 785 (1972) 26 pp.

[35] M.R. Dence, A.G. Plant and R.J. Traill, Impact-generated shock and thermal metamorphism in Fra Mauro lunar samples, Revised Abstr. Third Lunar Sci. Conf., ed. C. Watkins (1972) 174.

[36] A.E. Ringwood, D.H. Green and N.G. Ware, Experimental petrology and petrogenesis of Apollo 14 basalts, Revised Abstr. Third Lunar Sci. Conf., ed. C. Watkins (1972) 654.

[37] Lunar Sample Preliminary Examination Team, Preliminary examination of lunar samples from Apollo 14, Science 173 (1971) 681.

[38] H.J. Axon and J.I. Goldstein, Temperature–time relationships from lunar two-phase metallic particles (14310, 14163, 14003) (in press).

[39] R.A. Cliff, C. Lee–Hu and G.W. Wetherill, K, Rb and Sr measurements in Apollo 14 and 15 material, Revised Abstr. Third Lunar Sci. Conf., ed. C. Watkins (1972) 146.

[40] A.L. Albee and A.A. Chodos, Microprobe investigations on Apollo 11 samples, Proc. Apollo 11 Lunar Sci. Conf., Geochim. Cosmochim. Acta Suppl. 1, 1 (1970) 135.

[41] N.L. Bowen, The Evolution of the Igneous Rocks (Dover, New York, 1928) 332 pp.

[42] F. Tera, L.A. Ray and G.J. Wasserburg, Distribution of Pb–U–Th in lunar anorthosite 15415 and inferences about its age (abstract) (in press).

[43] L. Husain, O.A. Schaefer and J.F. Sutter, Age of a lunar anorthosite, Science 175 (1972) 428.
[44] G. Turner, $^{40}Ar-^{39}Ar$ age and cosmic ray irradiation history of the Apollo 15 anorthosite, 15415, Earth Planet. Sci. Letters 14 (1972) 169.
[45] J.V. Smith, A.T. Anderson, R.C. Newton, E.J. Olsen and P.J. Wyllie, A petrologic model for the moon used on petrogenesis experimental petrology, and physical properties, J. Geol. 78 (1970) 381.
[46] A.T. Anderson Jr., A.V. Crewe, J.R. Goldsmith, P.B. Moore, C.C. Newton, E.J. Olsen, J.V. Smith and P.J. Wyllie, Petrologic history of moon suggested by petrography, mineralogy, crystallography of Apollo 11 rock, Science 167 (1970) 587.
[47] A.L. Turkevich, The chemical composition of the lunar surface (to be published in "Accounts of Chemical Research").
[48] C.C. Schnetzler and D.F. Nava, Chemical composition of Apollo 14 soils 14163 and 14259, Earth Planet. Sci. Letters 11 (1971) 345.
[49] N.J. Hubbard and P.W. Gast, Chemical composition and origin of nonmare lunar basalts, Proc. Second Lunar Sci. Conf., Geochim. Cosmochim. Acta Suppl. 2, 2 (1971) 999.
[50] A.E. Metzger, J.I. Trombka, L.E. Peterson, R.C. Reedy and J.R. Arnold, A first look at the lunar orbital gamma ray data, Revised Abstr. Third Lunar Sci. Conf., ed. C. Watkins (1972) 540.
[51] A.E. Metzger, oral communication, September 1972.

EARTH AND PLANETARY SCIENCE LETTERS 17 (1973) 433–445. NORTH-HOLLAND PUBLISHING COMPANY

6

CONSTRAINED LEAST-SQUARES ANALYSIS OF PETROLOGIC PROBLEMS WITH AN APPLICATION TO LUNAR SAMPLE 12040

M.J. REID, A.J. GANCARZ AND A.L. ALBEE

Division of Geological and Planetary Sciences, California Institute of Technology, Pasadena, Calif. 91109, USA *

Received 22 August 1972

Revised version received 25 October 1972

Many petrologic problems, which may be expressed as a set of linear equations, have been solved by least-squares analysis. In many cases insufficient attention has been paid to the physical conditions of the model resulting in incorrect application of the method. This paper presents a systematic treatment of the application of least-squares analysis to petrologic problems including the direct utilization of physical constraints and weighting factors in the problem,and the assessment of uncertainties in the solution. As an example, least-squares analysis is used to examine, in detail, the mass balance equations for lunar rock 12040 and to determine the consistency of the available analytical data.

1. Introduction

A wide variety of geologic problems have been investigated with a form of least-squares analysis described by Bryan, Finger and Chayes [1] and Wright and Doherty [2]. Specifically, this method has been used by Goles et al. [3], Lindstrom et al. [4] and Schonfeld [5] to develop lunar soil mixing models; and by Wright and Fiske [6] and Wright [7] to develop magmatic differentiation models.

The authors of this paper first attempted to duplicate and then expand upon lunar soil analyses of the type done by Goles et al. [3]. It became apparent that Goles et al. [3] incorrectly weighted the problem, neglected certain physically important constraints, did not describe procedures for excluding non-physical solutions, and did not discuss the uncertainties in the solution. Further, these problems are not limited to this work, but some of these or other problems are present in all of the papers previously cited.

Because of these problems, the conclusions reached by these authors is difficult to evaluate, especially for those papers in which no description of the uncertainties in the values of the parameters estimated by the least-squares solution is given. In only a few cases was sufficient raw data presented to allow reanalysis of the problem. For example, Goles et al. [3] reported 0.3 – 1.5 wt% of carbonaceous chondrite component in three of five lunar soil mixing models. However, we reanalyzed one of the two cases in which no carbonaceous chondrite component was reported and found an estimated 1σ range of from 1.1 to −1.5 wt%. This is consistent with the carbonaceous chondrite abundance in other models. Further, Goles et al. [3] appear to have normalized the estimated component abundance to sum to 100 wt% rather than imposing a constraint in the least-squares analysis. Consequently, the estimated abundances are not least-squares estimates and direct comparison of different models is difficult.

Any changes introduced by the treatment suggested by this paper probably would not be large for homogeneous data and well-defined systems. In fact, the conclusions reached by the authors previously cited [1–7] would probably be strengthened by application of the techniques discussed in this paper. However, the differences between treatments can be quite dramatic in more complex systems. When we

* Contribution No. 2185.

attempted generalized analyses of lunar samples, including many mixing phases and a wide variety of data (e.g., isotopic as well as chemical data), it became evident that good solutions could only be obtained by a careful examination of the *physical* meaning of the mixing model. Such an examination revealed the necessity to deal carefully with the subjects of weighting least-squares problems, constraining the solutions, and analyzing the uncertainties on the values of the estimated parameters. Therefore, this paper presents a systematic method of least-squares analysis, readily applicable to geologic problems, which deals with such problems.

1.1. *The problem*

Many geologic problems involve a set of mass balance equations of the form:

$$s_i = c_{i1}x_1 + c_{i2}x_2 + \ . \ . \ . \ + c_{im}x_m \qquad (1)$$

where c_{ij} represents the amount of the ith component in the jth phase, s_i represents the amount of the ith component in the sample being modeled, and x_j represents the amount of the jth phase required to model the sample. The values of all x_j's are then calculated to minimize the sum of the squares of the differences of the modeled and real sample component abundances (i.e., to minimize the sum of the squares of the residuals). The units chosen for the c_{ij}'s, the s_i's and the x_j's are arbitrary, but must be defined in a manner consistent with the mass balance equations. For example, the c_{ij}'s and the s_i's may represent weights and the x_j's parts or fractions; or the c_{ij}'s may represent proportions (e.g., weight percent or atomic percent) and the s_i's and x_j's weights.

Perry [8] and Carmichael [10] solved a set of mass balance equations in considering problems of metamorphic petrology. They restricted the number of mass balance equations, n, to equal the number of phases, m, thus obtaining exact solutions for the x_j's. Bryan et al. [1] noted that if n is greater than m (i.e., more mass balance equations than phases), the set of equations can be solved for the best least-squares estimate of the x_j's.

Most of these authors used only the mass balance equations to solve for the x_j's, but additional information usually is available, all of which should be used to obtain the best solutions. Typically such information includes the errors of the chemical analyses (which should be used to weight the importance of each equation), and closure requirements for the entire system (which should constrain the estimates of the x_j's).

2. Theory

The least-squares approach presented in this paper is as follows: denote the measured amount of the ith component in the sample to be modeled by s_i and the ith component in the jth phase by c_{ij}. In this problem the values of all s_i's are considered experimentally determined with absolute errors, e_i's. The values of all c_{ij}'s are defined with zero error. Then a set of mass balance equations (one equation for each s_i) is defined as follows:

$$\begin{aligned}
s_1 &= c_{11}x_1 + c_{12}x_2 + \ . \ . \ . \ + c_{1m}x_m + e_1 \\
s_2 &= c_{21}x_1 + c_{22}x_2 + \ . \ . \ . \ + c_{2m}x_m + e_2 \\
&\ . \quad . \quad . \quad . \quad . \\
&\ . \quad . \quad . \quad . \quad . \\
&\ . \quad . \quad . \quad . \quad . \\
s_n &= c_{n1}x_1 + c_{n2}x_2 + \ . \ . \ . \ + c_{nm}x_m + e_n
\end{aligned} \qquad (2)$$

where x_j is the amount of the jth phase. Thus, the sample ($\mathbf{S}$) and the jth phase ($\mathbf{C}_j$) are represented by the column vectors

$$\mathbf{S} = \begin{pmatrix} s_1 \\ s_2 \\ \cdot \\ \cdot \\ \cdot \\ s_n \end{pmatrix} \quad \text{and} \quad \mathbf{C}_j = \begin{pmatrix} c_{1j} \\ c_{2j} \\ \cdot \\ \cdot \\ \cdot \\ c_{nj} \end{pmatrix} \quad \text{for } j = 1, 2, \ldots, m$$

where n is the number of components and m is the number of phases. For a least-squares solution to exist, n must be greater than m. If n is less than m, an infinite number of solutions exist; and if n is equal to m, an exact solution exists. For all cases the $\mathbf{C}_j$'s must be linearly independent.

The equations can be represented in the following matrix form:

$$\mathbf{S} = \mathbf{CX} + \mathbf{E} \qquad (3)$$

where $\mathbf{C}$ is the n by m matrix of c_{ij}'s, $\mathbf{X}$ is the column vector of x_j's, and $\mathbf{E}$ is the column vector of absolute errors e_i's. The least-squares solution for $\mathbf{X}$ is designated as $\hat{\mathbf{X}}$ [12]

where

$$\hat{\mathbf{X}} = \mathbf{B}^{-1}\mathbf{C}^{\dagger}\mathbf{M}_s^{-1}\mathbf{S}, \tag{4}$$

and

$$\mathbf{B}^{-1} = (\mathbf{C}^{\dagger}\mathbf{M}_s^{-1}\mathbf{C})^{-1}, \tag{5}$$

and

$$\mathbf{M}_s = \begin{pmatrix} \sigma_1^2 & \sigma_{12}^2 & \cdots & \sigma_{1n}^2 \\ \sigma_{21}^2 & \sigma_2^2 & \cdots & \sigma_{2n}^2 \\ \cdot & \cdot & & \cdot \\ \cdot & \cdot & & \cdot \\ \cdot & \cdot & & \cdot \\ \sigma_{n1}^2 & \sigma_{n2}^2 & \cdots & \sigma_n^2 \end{pmatrix}$$

$\mathbf{B}^{-1}$ is the inverse of $\mathbf{B}$ and $\mathbf{C}^{\dagger}$ is the transpose of $\mathbf{C}$. σ_{ij}^2 is the covariance of the measurement of the ith and jth components of the sample, σ_i^2 is the variance of the measurements of the ith component of the sample, and $\mathbf{M}_s$ is the variance-covariance matrix of $\mathbf{S}$, which weights the mass balance equations. If, for example,

$$\mathbf{M}_s = \mathbf{I} = \begin{pmatrix} 1 & 0 & \cdots & 0 \\ 0 & 1 & \cdots & \cdot \\ \cdot & \cdot & \cdots & \cdot \\ \cdot & \cdot & \cdots & 1 \\ 0 & \cdot & \cdots & 0 \; 1 \end{pmatrix} \quad \text{then } \mathbf{B} = \mathbf{C}^{\dagger}\mathbf{C}$$

and all eqs. (2) carry equal weight. Eqs. (3) and (4) are basically those presented by Bryan et al. [1] modified by weighting factors which can be different from unity.

A least-squares solution of (3) may be subject to a set of inexact linear constraints. Such constraints do not alter the analytic form of the least-squares solution and are discussed in detail in sect. 2.2. A least-squares solution to eq. (3) also may be subject to a set of k exact linear constraints. Such a set of constraints is as follows:

$$\begin{aligned} z_1 &= q_{11}x_1 + q_{12}x_2 + \cdots + q_{1m}x_m \\ z_2 &= q_{21}x_1 + q_{22}x_2 + \cdots + q_{2m}x_m \\ &\cdots \\ z_k &= q_{k1}x_1 + q_{k2}x_2 + \cdots + q_{km}x_m \end{aligned} \tag{6}$$

This can be represented in matrix form as

$$\mathbf{QX} = \mathbf{Z} \tag{7}$$

where $\mathbf{Q}$ is the k by m matrix of q_{ij}'s, $\mathbf{X}$ is again the column vector of x_j's and $\mathbf{Z}$ is the column vector of z_i's. The constrained least-squares estimate of $\mathbf{X}$, designated as $\hat{\hat{\mathbf{X}}}$ [12], is

$$\hat{\hat{\mathbf{X}}} = \hat{\mathbf{X}} + [(\mathbf{Z}^{\dagger} - \hat{\mathbf{X}}^{\dagger}\mathbf{Q}^{\dagger})(\mathbf{QB}^{-1}\mathbf{Q}^{\dagger})^{-1}\mathbf{QB}^{-1}]^{\dagger} \tag{8}$$

For this solution to exist, the number of independent constraint equations must be less than the number of variables to be estimated. Exact constraints and their physical significance are also discussed in detail in sect 2.2.

2.1. *Weighting factors*

A rigorous solution of the least-squares problem requires a priori knowledge of the variance-covariance matrix of $\mathbf{S}(\mathbf{M}_s)$, but generally this is not available. However, in most types of geochemical analyses either the absolute errors are known, or the magnitude of the absolute errors can be estimated relative to one another. Therefore, σ_i^2 can be expressed as

$$\sigma_i^2 = \sigma^2 e_i^{*2}$$

where σ^2 is a (possibly unknown) constant and the e_i^*'s are the relative values of the absolute errors normalized to any one e_i. Secondly, if the measurements of s_i and s_j are nearly independent, then σ_{ij} is approximately equal to zero. For most modern instrumental analytical techniques (e.g., electron microprobe analysis and neutron activation analysis) inter-element correction factors are known and are used in reducing the analytical data. Consequently, we assume that the values of all σ_{ij}'s are small and can be neglected. Under these conditions the variance-covariance matrix of $\mathbf{S}$ can be expressed as

$$\mathbf{M}_s = \sigma^2 \begin{pmatrix} e_1^{*2} & 0 & \cdots & 0 \\ 0 & e_2^{*2} & \cdots & \cdot \\ \cdot & \cdot & \cdots & \cdot \\ \cdot & \cdot & & \cdot \\ \cdot & \cdot & & 0 \\ 0 & \cdots & 0 & e_n^{*2} \end{pmatrix}$$

Then eq. (5) can be rewritten as

$$\mathbf{B}^{-1} = \sigma^2(\mathbf{C}^{*\dagger}\mathbf{C}^*)^{-1} \quad \text{where } \mathbf{C}^* = \begin{pmatrix} c_{11}/e_1^* & c_{12}/e_1^* & \cdots & c_{1m}/e_1^* \\ c_{21}/e_2^* & c_{22}/e_2^* & \cdots & c_{2m}/e_2^* \\ \cdot & \cdot & & \cdot \\ \cdot & \cdot & & \cdot \\ \cdot & \cdot & & \cdot \\ c_{n1}/e_n^* & c_{n2}/e_n^* & \cdots & c_{nm}/e_n^* \end{pmatrix}$$

and the term $\mathbf{C}^{\dagger}\mathbf{M}_s^{-1}\mathbf{S}$ in eq. (4) can be rewritten as

$$\mathbf{C}^{\dagger}\mathbf{M}_s^{-1}\mathbf{S} = \frac{1}{\sigma^2}\mathbf{C}^{*\dagger}\mathbf{S} \text{ where } \mathbf{S}^* = \begin{pmatrix} s_1/e_1^* \\ s_2/e_2^* \\ \cdot \\ \cdot \\ \cdot \\ s_n/e_n^* \end{pmatrix}$$

Substituting these terms in eq. (4), the solution $\hat{\mathbf{X}}$ becomes

$$\hat{\mathbf{X}} = (\mathbf{C}^{*\dagger}\mathbf{C}^*)^{-1}\mathbf{C}^{*\dagger}\mathbf{S}^* \tag{9}$$

Therefore, the entire problem can be treated as unweighted (i.e., $\mathbf{M}_s = \mathbf{I}$) by multiplying the ith mass balance equation by a weighting factor $1/e_i^*$ and redefining the mass balance equations as:

$$\mathbf{S}^* = \mathbf{C}^*\mathbf{X} + \Sigma \tag{10}$$

where Σ is the column vector whose elements are all identically σ^2.

The use of weighting factors is of fundamental importance in all least-squares problems, especially in the cases where the errors, e_i, vary over several orders of magnitude. If no weighting factors are used, one must recognize that equal absolute errors are assumed. For example, if a component whose abundance is 1 μg/g and another component whose abundance is 1000 μg/g have been measured with percent errors of 10 and 1%, the absolute error of the first component is 0.1 μg/g and the absolute error of the second component is 10 μg/g. If no weighting procedure is used, then the solution would be dominated by the mass balance equation for the more abundant component. In fact, the first equation should be weighted by 1/0.1 (e_1 = 0.1) and the second equation should be weighted by 1/10 (e_2 = 10). In this case e_2 is 100 times larger than e_1 and e_2^* may be set equal to 100 and e_1^* set equal to 1. The mathematical effect of the weighting factors in most geochemical problems is to assign an importance to each mass balance equation commensurate with the inverse of its absolute error. The individual mass balance equations are equally important when the percent errors on all the values of the s_i's are equal.

One final point on the subject of weighting deserves attention. In many real problems the c_{ij}'s are determined experimentally rather than defined. Thus, an experimental error, $e_{c_{ij}}$, can be associated with each c_{ij}. It seems physically reasonable that these errors should affect the weighting of the mass balance equations. This can be accomplished by redefining the error, e_i, as the error in each mass balance equation – that is the error expected in the value of

$$s_i - (c_{i1}x_1 + c_{i2}x_2 + \cdots + c_{im}x_m)$$

rather than the error in the measurement of s_i. Formally, this error is given by

$$\sqrt{e_i^2 + \sum_{j=1}^{m} (e_{c_{ij}}x_j)^2} \tag{11}$$

Exact determination of this error requires the values of the x_j's. In most cases reasonable approximations for the values of the x_j's will suffice. However, after solving for the $\hat{x}_j$'s using some initial approximation for the x_j's to evaluate the errors (eq. (11)), the $\hat{x}_j$'s can be used to reevaluate eq. (11) and obtain a better estimate of the errors. Thus, any degree of precision is attainable by iterative methods. As in the original case, knowledge of the absolute experimental errors relative to any one absolute error is all that is required to weight the mass balance equations.

2.2. *Linear constraints*

In this section methods for incorporating two types of linear constraints into the least-squares solution are developed. In contrast to the weighting factors which *must* be considered in solving the mass balance equations, the use of linear constraints is necessitated only by the definition of the problem. Consequently, it is important to carefully consider the physical significance of each constraint before it is applied to the problem.

The first type of linear constraint is an inexact constraint. These constraints contain additional independent data related to the problem such as independent modal estimates, density measurements on the phases and on the total sample, or additional information such as the requirement for the conservation of mass. Since the inexact constraints do contain additional independent information, they should be used to obtain the best least-squares estimate of the x_j's.

The form of the inexact linear constraint is as follows:

$$d_i = p_{i1}x_1 + p_{i2}x_2 + \ . \ . \ . \ + p_{im}x_m + e_{d_i} \quad (12)$$

where d_i is experimentally determined, the p_{ij}'s are either experimentally determined or defined, the x_j's are the amount of the jth phase needed to model the sample, and e_{d_i} is the absolute error of d_i.

The constraint equations are added to the set of mass balance equations and treated just as additional mass balance equations. Consequently, a term is included in the sum of the squares of the residuals which are to be minimized. Therefore, redefine eq. (3) as follows:

$$\mathbf{S}' = \mathbf{C}'\mathbf{X} + \mathbf{E}'$$

where

$$\mathbf{S}' = \begin{pmatrix} s_1 \\ s_2 \\ \cdot \\ \cdot \\ \cdot \\ s_n \\ d_1 \\ d_2 \\ \cdot \\ \cdot \\ \cdot \\ d_r \end{pmatrix} \quad \mathbf{C}' = \begin{pmatrix} c_{11} & c_{12} & \cdots & c_{1m} \\ c_{21} & c_{22} & \cdots & c_{2m} \\ \cdot & \cdot & & \cdot \\ \cdot & \cdot & & \cdot \\ \cdot & \cdot & & \cdot \\ c_{n1} & c_{n2} & \cdots & c_{nm} \\ p_{11} & p_{12} & \cdots & p_{1m} \\ p_{21} & p_{22} & \cdots & p_{2m} \\ \cdot & \cdot & & \cdot \\ \cdot & \cdot & & \cdot \\ \cdot & \cdot & & \cdot \\ p_{r1} & p_{r2} & \cdots & p_{rm} \end{pmatrix} \quad \mathbf{E}' = \begin{pmatrix} e_1 \\ e_2 \\ \cdot \\ \cdot \\ \cdot \\ e_n \\ e_{d_1} \\ e_{d_2} \\ \cdot \\ \cdot \\ \cdot \\ e_{d_r} \end{pmatrix}$$

where r is the number of inexact constraint equations. The solution, $\hat{\mathbf{X}}$, is obtained as described before only using $\mathbf{S}'$, $\mathbf{C}'$ and $\mathbf{E}'$ in place of $\mathbf{S}$, $\mathbf{C}$ and $\mathbf{E}$.

A specific constraint important in many real problems requires that the total mass of the components be conserved within experimental error, and is as follows:

$$\bar{s} = \bar{c}_1x_1 + \bar{c}_2x_2 + \ . \ . \ . \ + \bar{c}_mx_m + \bar{e} \quad (13)$$

where $\bar{c}_j = \sum_{i=1}^{n} c_{ij}$, $s = \sum_{i=1}^{n} s_i$ and $\bar{e} = \sqrt{\sum_{i=1}^{n} e_i^2}$

The $\bar{c}_j$ is the sum of the analyzed components of the jth phase, $\bar{s}$ is the sum of the analyzed components of the sample, and $\bar{e}$ is the absolute error of $\bar{s}$. To include errors in the c_{ij}'s, $\bar{e}$ may be redefined as follows:

$$\bar{e} \equiv \sqrt{\sum_{i=1}^{n}\sum_{j=1}^{m} ((e_{c_{ij}}x_j)^2\, x_j^2) + \bar{e}^2}$$

Exact determination of such an error has been discussed previously.

The second type of linear constraint is an exact constraint, as in eq. (6), for which the values of the q_{ij}'s and the z_i's are constants specified by the nature of the problem. These linear equations impose stringent limitations on the least-squares solution. First, the equations are exact, and they are required to be obeyed absolutely by the values of the $\hat{x}_j$'s. Second, the imposition of exact constraints always causes an increase in the sum of the squares of the weighted residuals. Consequently, they must be applied with caution.

Many geologic problems naturally define exact constraints. For example, real systems being modeled are often hypothesized to be completely closed. Such an hypothesis assumes neither mass loss nor gain, not only for the analyzed components, but also for the unanalyzed components. This hypothesis implies that

$$a_{\text{model sample}} = \hat{x}_1a_1 + \hat{x}_2a_2 + \ . \ . \ . \ + \hat{x}_ma_m \quad (14)$$

where a_j is the amount of all components, both analyzed and unanalyzed, in phase j and $a_{\text{model sample}}$ is the amount of the model sample defined by the least-squares estimate of the x_j's. Secondly, modeled samples are physically significant only if the amounts of the real and modeled sample are equivalent, but this condition has been ignored [1–7].

This implies the following:

$$a_{\text{model sample}} = a_{\text{real sample}} \quad (15)$$

where $a_{\text{real sample}}$ is the amount of all components, both analyzed and unanalyzed, in the real sample. Therefore, eqs. (14) and (15) imply

$$a_{\text{real sample}} = \hat{x}_1a_1 + \hat{x}_2a_2 + \ . \ . \ . \ + \hat{x}_ma_m \quad (16)$$

Commonly, the units of the components composing the a_j's and $a_{\text{real sample}}$ are defined as weight percent (i.e., g/100 g). Therefore, the amount of all the analyzed and unanalyzed components is 100 weight percent (i.e., 100 g/100 g) and eq. (16) becomes

$$1 = \hat{x}_1 + \hat{x}_2 \ . \ . \ . \ + \hat{x}_m \quad (17)$$

This specific form of the exact linear constraint eq. (16) is applicable to many geologic problems.

Without the use of the constraint (17) the $\hat{x}_j$'s do not necessarily sum to unity. If the best, *unconstrained* least-squares estimate of the x_j's sums to a value dif-

ferent from unity, then the amount of modeled sample is different from the amount of real sample. The values of the $\hat{x}_j$'s must not be normalized to unity, as Goles et al. [3] appear to have done, because normalization changes the amounts of the components in the modeled sample and the sum of the squares of their residuals is no longer the minimum – that is, normalized $\hat{x}_j$'s are not the least-squares estimates.

Since there is a strong functional dependence between the sum of the squares of the residuals and the sum of the $\hat{x}_j$'s, the residuals of different models whose $\hat{x}_j$'s sum to different values cannot be readily compared. Therefore, the use of the constrained over the unconstrained least-squares estimates not only yields values of the $\hat{x}_j$'s which have more physical significance, but also yields values which are readily comparable with the values of other models. This is significant as the comparison may be used to test the quality of various models.

Putting the constraint eq. (17) into the matrix form (7) defines $\mathbf{Z} = 1$ and $\mathbf{Q} \equiv (1,1, \ldots ,1)$. Thus eq. (8) becomes

$$\hat{\hat{\mathbf{X}}} = \hat{\mathbf{X}} + \frac{(1 - \sum_{j=1}^{m} \hat{x}_j)}{\sum_{i=1}^{m}\sum_{j=1}^{m} b_{ij}^{-1}} \begin{pmatrix} \sum_{i=1}^{m} b_{i1}^{-1} \\ \sum_{i=1}^{m} b_{i2}^{-1} \\ \vdots \\ \sum_{i=1}^{m} b_{im}^{-1} \end{pmatrix} \tag{18}$$

where b_{ij}^{-1} is the ijth element of B^{-1}. It is interesting to note that the second term on the righthand side of eq. (18) can be thought of as a 'correction term' to the unconstrained estimate of $\mathbf{X}$, because its magnitude decreases towards zero the closer the unconstrained estimates come to satisfying the constraint. Furthermore, the constraint is incorporated as a 'correction term' which uses the weighting matrix, $\mathbf{M}_s$, and the matrix, $\mathbf{C}$, and is not just a normalization of the $\hat{x}_j$'s. Finally, eq. (13) is satisfied automatically by eq. (17) in the case that amounts of the components for the various phases sum either to unity or to equivalent values.

2.3. *Errors of $\hat{x}_j$'s*

Since there are assigned errors e_i's, in the set of mass balance equations, there are uncertainties in the least-squares estimates of the values of the x_j's. While it is necessary to know these uncertainties in order to assess the significance of the solution, only Wright and Doherty [2] have attempted to determine them. These uncertainties are available from the variance-covariance matrix of $\mathbf{X}$,$\mathbf{M}_x$. An estimate of $\mathbf{M}_x$ is as follows:

$$\mathbf{M}_x \equiv \mathbf{B}^{-1} = \sigma^2(\mathbf{C}^{*\dagger}\mathbf{C})^{-1} \tag{19}$$

where an unbiased estimate of σ^2 is the sum of the squares of the residuals of the weighted equations divided by the quantity, $n+r+k-m$, where $n+r$ is the number of mass balance equations plus inexact constraint equations, k is the number of exact constraint equations, and m is the number of x_j's.

The diagonal elements of $\mathbf{M}_x$, m_{jj}'s, are the variances of the $\hat{x}_j$'s, and the off-diagonal elements, m_{ij}'s, are the covariances of the $\hat{x}_i$'s and the $\hat{x}_j$'s. The variances of the $\hat{x}_j$'s become less significant as the correlation coefficients approach unity. The correlation coefficient, ρ_{ij}, is as follows:

$$\rho_{ij} = \frac{m_{ij}}{\sqrt{m_{ii}m_{jj}}}$$

A more complete discussion of correlation coefficients and statistical tests is given by Hamilton [12].

2.4. *Normalization of the c_{ij}'s*

A common procedure in defining the phases, $\mathbf{C}_j$'s, is to normalize to unity the sum of the components of each phase, apparently in the hope that this will result in the normalization of the solution, but there is no reason for doing this. This is particularly common in models involving chemical analyses which total close to 100 weight percent, Moreover, normalization of components does not normalize the solution (x_j's), nor does it yield more physically significant results. Such a procedure is equivalent to a separate change of units for each phase and seriously complicates the problem. If the values of the c_{ij}'s are normalized, then the values of the constants, q_{ij}'s and z_i's, in the exact constraint eq. (6) and d_i's and p_{ij}'s in

the inexact constraint eq. (12) must be accordingly changed to derive the correct least-squares estimate of the x_j's. Furthermore, the values of the errors, e_i's, also must be changed and there is no a priori knowledge of how to do this.

2.5. *Additional constraints*

In many problems additional constraints need to be imposed upon the solution ($\hat{x}_j$'s). For example, non-negative values for any of the $\hat{x}_j$'s may be the only physically acceptable values. We know of no direct method for imposing such a 'non-negativity' constraint. Wright and Doherty [2] and Trombka [13] discuss systematic methods for obtaining least-squares solutions constraining the signs of the $\hat{x}_j$'s. Wright and Doherty [2] indicate that the best solution that excludes negative values of the $\hat{x}_j$'s can only be found by examining least-squares solutions using all combinations of phases. They suggested the use of separable programming to test for and exclude phases whose $\hat{x}_j$ values are likely to be negative before doing the least-squares solution. Trombka [13] has demonstrated that the 'non-negativity' constraint is satisfied by solving for the $\hat{x}_j$'s using any two phases, and continuing to solve for the $\hat{x}_j$'s by adding one phase at a time and deleting any phase whose $\hat{x}_j$ value is negative. Furthermore, he showed that the order of addition of phases is irrelevant and hence it is not necessary to test all the various combinations of phases. However, Trombka [14] also indicates that this procedure is rigorous only if all phases are orthogonal, but may be applied subject to the condition that correlation coefficients are small (e.g., $\rho_{ij} \leqslant 0.25$). Since this condition is seldom satisfied by any set of geologically important phases, this method has limited applicability to petrologic problems.

In problems where only positive values for the $\hat{x}_j$'s are physically realistic, $\hat{x}_j$'s with negative values, but with uncertainties which permit positive values, are still physically meaningful. Componets with such negative $\hat{x}_j$'s should not be dropped from the analysis as appears to have been done by others [2,3]. However, large negative or other non-physically meaningful values for the $\hat{x}_j$'s implies that an error(s) has been made in the definition of the problem. Among the possible errors are: (1) an incorrect or incomplete set of phases; (2) incorrect or incomplete phase compositions; (3) inaccurate assignment of errors; and (4) the presence of a phase whose composition can be closely approximated by a linear combination of one or more of the other phases (i.e., correlation coefficients $\cong 1$). Therefore, application of 'non-negativity' constraints without examination of the unconstrained estimates may be dangerous.

3. Discussion

The procedures described in this paper are well illustrated by an application to lunar sample 12040. This sample was selected because of the extensive chemical data available for both the total rock and individual phases. The data chosen for the **C** matrix and the **S** vector are given in table 1. Most of the data are from published sources [15–27], supplemented by some arbitrary zero values as indicated in the table, and by some unpublished data as indicated below. Detailed rare-earth element analyses are only available for mineral separates of augite, pigeonite and plagioclase [20]. Hence, only Ce and Y were used to represent the rare earth elements, because microprobe analyses for other rare earth elements in both apatite and whitlockite were not available.

Initially the compositions of the phases which show extensive chemical variation were chosen by estimating median points on published diagrams or by averaging analyses. The solution using these values was physically unrealistic (i.e., values greater than 100 wt% for some phase abundances and large negative values of phase abundances for other, highly correlated, phases). It became apparent that the solution of such a complex set of mass balance equations can only yield reasonable results if the compositions of the phases are known quite accurately.

The electron microbe was utilized to simultaneously obtain modal estimates and more realistic estimates of the average concentration of the major components in the variable phases. Using a MAC-5-SA3 electron microprobe under computer control [28], analyses of 1 μm spots for Fe, Ca and Si were made at 1194 equally-spaced grid points on thin section 12040,47 ($\approx$ area 70 mm^2). The program identifies the phase analyzed at each point, determines the volume percent of each phase, and calculates the Fe, Ca and Si content of each phase. Actual analyses closely corresponding to

Table 1
Analytical data for lunar sample 12040

Element		Total rock	absolute error	percent error	plagioclase 16.1 ± 1.1	pigeonite* 35.4 ± 1.7	pigeonite†	augite* 18.8 = 1.3	augite†	olivine* 23.4 ± 1.4
Li	ppm	6.91	± 0.07	1	9.07	7.71	7.71	5.60	5.60	(0)
F	ppm	30	± 4.5	15	(0)	(0)	(0)	(0)	(0)	(0)
Na_2O	wt%	0.217	± 0.003	1.5	1.55	0.01	0.01	0.02	0.01	(0)
MgO	wt%	16.3	± 0.82	5	0.16	21.47	18.86	16.05	15.63	28.85
Al_2O_3	wt%	7.3	± 0.37	5	34.16	1.09	0.97	1.93	1.89	0.03
SiO_2	wt%	43.9	± 2.2	5	47.06	53.16	53.11	51.89	52.04	36.47
P_2O_5	wt%	0.065	± 0.033	50	(0)	(0)	(0)	(0)	(0)	(0)
S	wt%	0.05	± 0.025	50	(0)	(0)	(0)	(0)	(0)	(0)
K	ppm	364	± 7.28	2	463	109	109	109	109	(0)
CaO	wt%	8.16	± 0.41	5	18.33	6.16	6.62	13.76	14.62	0.34
TiO_2	wt%	2.5	± 0.25	10	0.08	0.75	0.79	1.41	1.21	0.07
Cr_2O_3	wt%	0.61	± 0.061	10	(0)	0.44	0.38	0.49	0.44	0.09
MnO	wt%	0.26	± 0.026	10	0.01	0.34	0.33	0.32	0.28	0.33
FeO	wt%	21.0	± 1.05	5	0.52	18.27	21.23	15.36	14.68	34.74
Co	ppm	56	± 5.6	10	(0)	(0)	(0)	(0)	(0)	(0)
Ni	ppm	45	± 4.5	10	(0)	(0)	(0)	(0)	(0)	(0)
Rb	ppm	0.762	± 0.015	2	0.253	0.31	0.31	0.31	0.31	(0)
Sr	ppm	102.4	± 1.54	1.5	355	13.2	13.2	13.2	13.2	(0)
Y	ppm	26.5	± 0.53	2	(0)	(0)	(0)	(0)	(0)	(0)
Zr	ppm	82	± 8.2	10	(0)	(0)	(0)	(0)	(0)	(0)
Cs	ppb	33.5	± 1.01	3	(0)	(0)	(0)	(0)	(0)	(0)
Ba	ppm	47.7	± 0.72	1.5	46.5	16.3	16.3	16.3	16.3	(0)
Ce	ppm	15.3	± 0.31	2	2.95	3.67	3.67	4.65	4.65	(0)
Hf	ppm	2.39	± 0.12	5	(0)	(0)	(0)	(0)	(0)	(0)

Table 1 (continued).

Element		olivine†	ilmenite	Fe-metal	troilite	apatite	whitlockite	baddeleyite	Ti-spinel	Cr-spinel	mesostasis
			2.4 ± 0.6	n.d.	n.d.	0.1 ± 0.1		n.d.	1.6 ± 0.5	2.2 ± 0.6	n.d.
Li	ppm	(0)	(0)	(0)	(0)	(0)	(0)	(0)	(0)	(0)	23.0
F	ppm	(0)	(0)	(0)	(0)	27000	(0)	(0)	(0)	(0)	(0)
Na_2O	wt%	(0)	(0)	(0)	(0)	(0)	(0)	(0)	(0)	(0)	0.67
MgO	wt%	31.21	3.12	(0)	(0)	0.15	3.32	(0)	2.54	4.59	0.10
Al_2O_3	wt%	0.04	0.0	(0)	(0)	0.0	0.0	(0)	4.47	12.20	11.40
SiO_2	wt%	37.06	0.10	(0)	(0)	0.21	0.46	(0)	0.0	0.0	76.60
P_2O_5	wt%	(0)	(0)	(0)	(0)	42.17	44.27	(0)	(0)	(0)	0.10
S	wt%	(0)	(0)	(0)	36.48	0.0	(0)	(0)	(0)	(0)	(0)
K	ppm	(0)	(0)	(0)	(0)	0.0	0.0	(0)	(0)	(0)	40,400
CaO	wt%	0.32	0.02	(0)	(0)	54.18	42.26	(0)	0.01	0.06	1.27
TiO_2	wt%	0.06	53.86	(0)	(0)	(0)	(0)	(0)	24.07	7.39	0.06
Cr_2O_3	wt%	0.08	0.55	(0)	(0)	(0)	(0)	(0)	16.23	40.40	0.07
MnO	wt%	0.32	0.36	(0)	(0)	(0)	(0)	(0)	0.52	0.72	0.01
FeO	wt%	31.78	43.35	116.43	81.62	0.60	2.30	(0)	52.90	35.20	1.10
Co	ppm	(0)	(0)	20000	(0)	(0)	(0)	(0)	(0)	(0)	(0)
Ni	ppm	(0)	(0)	75000	(0)	(0)	(0)	(0)	(0)	(0)	(0)
Rb	ppm	(0)	0.745	(0)	(0)	(0)	(0)	(0)	(0)	(0)	132.0
Sr	ppm	(0)	12.32	(0)	(0)	(0)	(0)	(0)	(0)	(0)	1052.5
Y	ppm	(0)	(0)	(0)	(0)	2760	17000	(0)	(0)	(0)	(0)
Zr	ppm	(0)	700	(0)	(0)	(0)	(0)	724000	(0)	(0)	70
Cs	ppb	(0)	(0)	(0)	(0)	(0)	(0)	(0)	(0)	(0)	6100
Ba	ppm	(0)	(0)	(0)	(0)	(0)	(0)	(0)	(0)	(0)	4500
Ce	ppm	(0)	(0)	(0)	(0)	1200	12000	(0)	(0)	(0)	(0)
Hf	ppm	(0)	(0)	(0)	(0)	(0)	(0)	15200	(0)	(0)	(0)

( ) assumed value.

* values determined from electron microbe point count.

† values determined by estimating median points on published diagrams or averaging analyses.

n.d. ≡ not determined.

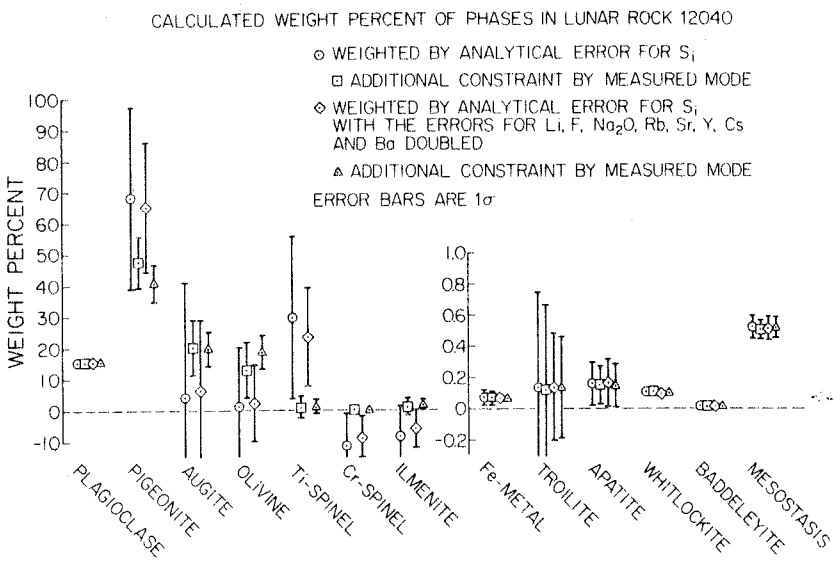

Fig. 1. Calculated weight percent of phases in lunar rock 12040.

the average content determined by the microprobe were selected to represent the phase. The weight percents and calculated errors obtained from the microprobe point count are given in table 1. Both the original choice and the composition of the variable phases obtained by this method are also presented in table 1. Although the only major differences are in the FeO and MgO contents of the pigeonite and olivine, these changes yielded a physically realistic solution.

The 24 mass balance equations using the components listed in table 1 were solved simultaneously for the weight percent of the various phases using the procedures described in this paper. Both the inexact constraint, requiring the total mass of the analyzed components to be conserved within an estimated analytical error of 5%, and the exact constraint, requiring the mass fractions of the various phases to total to unity, were imposed upon the solution. The definition of the model demands these two constraints, but no others. Consequently, four solutions using different sets of inexact constraints and weighting factors were obtained and are illustrated in fig. 1. These solutions represent all the permutations allowed by two sets of weighting factors and two sets of inexact constraints. Solutions 1 and 2 used the analytical errors given in table 1 to weight the equations. The weighting factors for solutions 3 and 4 were obtained by using twice the 'total rock' analytical errors for those components where mineral separation procedures were important (Li, F, Na_2O, K, Rb, Sr, Y, Cs and Ba). Doubling these errors is an attempt to account for additional sampling uncertainty in the mineral separates. Thus, the new errors are intended to represent the total errors for the respective mass balance equations rather than only the errors of the 'total rock' analyses. However, the analytical form for such an error (11) was not used because precise estimates of the purity of the mineral separates, and therefore the errors, were not available.

In solutions 2 and 4, additional independent information was added to the simultaneous solution in the form of measured modes, converted to the weight percent of the phases, and their errors. These data were added to the **C** matrix and **S** vector as additional independent equations (12) and provide inexact constraints to the simultaneous solution of the equations. For example, the inexact constraint eq. (12) for pigeonite takes the following form

$$x_{\text{pigeonite (measured)}} = 0(x_{\text{plagioclase}}) + (x_{\text{pigeonite}}) + 0(x_{\text{augite}}) + \ldots + 0(x_{\text{mesostasis}}) + e_{\text{pigeonite measurement}}$$

Consequently, in this example all the p_{ij}'s of eq. (12), except for pigeonite, are zero.

Solutions 1 and 2 (or solutions 3 and 4) are markedly different in their estimates of the weight percent of the various phases required to model the sample. However, nearly all the estimates of solution 2 (or 4) lie within the error bars on the estimates from solution 1 (or 3). Consequently solutions 1 and 2 are consistent with each other (as are solutions 3 and 4).

The large uncertainties in the weight percent estimates of the phases in solutions 1 and 3 reflect the high correlations among many of the phases. For example, the correlation coefficients between augite and pigeonite, and both the spinels and ilmenite, are greater than 0.9. Such high correlation coefficients indicate that small changes in the values of the components listed in table 1 are likely to produce large changes in the least-squares estimate of the x_j's. However, the addition of inexact constraint equations containing modal data (solutions 2 and 4) decreases the correlation among the phases by introducing information about each phase abundance independent of all other phase abundances, and decreases the uncertainties of the estimates of the mass fractions of the phases.

By comparing solutions 1 with 3 (or 2 with 4) the effects of weighting are illustrated. The uniform decrease in the uncertainties associated with the estimates of the mass fractions indicates that weighting by the total error on each mass balance equation yields more physically reasonable solutions than only weighting by the analytical error in the s_i's.

The effect upon the residuals of these inexact constraints is illustrated by comparing solutions 1 and 2 (or 3 and 4). Table 2 presents the weighted residuals for the components in the four solutions. Also presented in table 2 are the weighted residuals for those phases for which inexact constraint equations were included, the sum of the squares of the weighted residuals, and σ^2. The weighted residuals are just the absolute residual divided by the assigned errors and hence are unitless. For example, a weighted residual of 2 means that the residual is twice the absolute error. One should note that the addition of constraints to a least-squares problem automatically results in an increase in the sum of the squares of the weighted residuals. However, a quantity better describing the quality of the fit is σ^2. This quantity can be used to compare results for least-squares solutions where different inexact constraints have been imposed upon the solution. However, the comparison of solutions is not valid for mass balance equations which are weighted by different sets of e_i^*'s. Therefore, the σ^2's for solutions 1 and 2 cannot be compared with the σ^2's for solutions 3 and 4.

Table 2
Weighted residuals for four least-squares solutions of lunar sample 12040.

	1	2	3	4
Li	− 0.9	8.4	− 0.1	7.8
F	− 2.6	− 2.3	− 1.6	− 1.0
Na_2O	− 10.8	− 11.8	− 6.1	− 6.9
MgO	0.8	− 1.3	0.6	− 1.5
Al_2O_3	3.2	2.6	2.9	2.3
SiO_2	− 1.1	− 2.0	− 1.3	− 1.3
P_2O_5	− 1.4	− 1.4	− 1.4	− 1.2
S	< 0.1	0.2	< 0.1	< 0.1
K	0.6	1.9	0.4	1.0
CaO	1.2	− 1.3	0.6	− 0.5
TiO_2	0.3	3.4	< 0.1	2.0
Cr_2O_3	− 0.1	− 0.5	− 0.1	− 0.8
MnO	− 1.4	− 0.9	− 1.2	− 0.9
FeO	− 1.0	3.0	< 0.1	1.9
Co	7.5	7.5	7.5	7.5
Ni	− 1.6	− 1.6	− 1.6	− 1.6
Rb	− 8.3	− 11.1	− 4.5	− 5.6
Sr	21.8	21.3	10.6	10.4
Y	8.5	8.7	6.1	6.0
Zr	2.2	− 3.4	0.7	− 3.8
Cs	1.8	2.6	1.1	0.9
Ba	7.6	9.2	3.9	4.9
Ce	− 7.0	− 7.1	− 2.5	− 2.4
Hf	− 1.5	2.4	− 0.5	2.6
$x_{\text{plagioclase}}$	−	0.5	−	0.3
$x_{\text{pigeonite}}$	−	− 7.1	−	− 3.2
x_{augite}	−	− 1.1	−	− 0.8
x_{olivine}	−	7.4	−	3.3
x_{ilmenite}	−	2.0	−	0.8
$x_{\text{apatite + whitlockite}}$	−	− 1.5	−	− 1.4
$x_{\text{Ti-spinel}}$	−	0.9	−	0.8
$x_{\text{Cr-spinel}}$	−	3.4	−	3.0
Σ mass analyzed	− 0.2	− 0.2	− 0.2	− 0.2
Σ (weighted residuals)^2	935	−1252	306	451
σ^2	72	60	24	21

The values in table 2 illustrate the change in the residuals upon adding modal data. While the change from solution 1 to 2 is large, the change in the residuals from solutions 3 to 4 is relatively small. This small change in conjunction with the large decrease in the uncertainties of the estimates of the mass fractions suggests that solution 4 is the best of the four

solutions. Although solution 4 appears the best of the four solutions, the large absolute values of the weighted residuals in table 2 indicate inconsistencies in the analytical data and suggest that certain component abundances in various phases are incorrect. These inconsistencies may be the result of impure mineral separates used to represent a phase, systematic differences between the various analytical procedures or between the mineral separates used, or actual inhomogeneities in the total rock samples.

When a solution is highly overdetermined it is possible to solve simultaneously for the amounts of the various phases and for the amounts of various components in a limited number of phases. This requires the use of non-linear least-squares (see Hamilton [12] for a discussion). This method is not detailed here because an application to lunar sample 12040 indicated that it would require exceptionally consistent data to have any meaning. If such a solution is attempted, additional equations reflecting stoichiometric restrictions should be included as constraints. When the solution is highly overdetermined it would also be possible to calculate the average composition of a phase, such as pyroxene, by defining fictitious end-member phases meeting the stoichiometric requirements, and recombining them after the least-squares solution.

In conclusion we suggest that a detailed mass balance analysis for *all* components in all phases of a rock is exceptionally difficult. It is nearly an impossible task when various components are analyzed by different techniques on different mineral separates taken to represent a phase. However, the least-squares solution is a systematic method for determining the presence of inconsistencies, and the nature of these inconsistencies.

Acknowledgments

We are grateful to D. Muhleman for a long series of discussions on various aspects of this paper and to D. Muhleman, S. DeLong, and R. Dean for their comments on a preliminary draft of the paper. G.J. Wasserburg initiated the work on sample 12040 and pointed out that we do not really understand a rock unless we can explain the complete phase distribution of every element. The work was supported by NAS contract NAS-9-8074 and NSF grant GA-12867. The microprobe laboratory has been developed with the support of the Jet Propulsion Laboratory, National Science Foundation, and the Union Pacific Foundation. One of us (A.J.G.) holds a National Science Foundation Graduate Fellowship.

References

[1] W.B. Bryan, L.W. Finger and F. Chayes, Estimating proportions in petrographic mixing equations by least-squares approximation, Science 163 (1969) 926.

[2] T.L. Wright and P.C. Doherty, A linear programming and least squares computer method for solving petrologic mixing problems, Geol. Soc. Am. Bull. 81 (1970) 1995.

[3] G.G. Goles, A.R. Duncan, D.J. Lindstrom, M.R. Martin, R.L. Beyer, M. Osawa, K. Randle, L.T. Meek, T.L. Steinborn and S.M. McKay, Analysis of Apollo 12 specimens: compositional variations, differentiation processes, and lunar soil mixing models, Geochim. Cosmochim. Acta Suppl. 2 (1971) 1063.

[4] M.M. Lindstrom, A.R. Duncan, J.S. Fruchter, S.M. McKay, J.W. Stoeser, G.G. Goles and D.J. Lindstrom, Compositional characteristics of some Apollo 14 clastic materials (in press).

[5] E. Schonfeld, Component abundance and ages in soils and breccia, in: Revised abstracts of papers presented at the Third Lunar Sci. Conf., C. Watkins, ed. (1972) 685.

[6] T.L. Wright and R.S. Fiske, Origin of differentiated and hybrid lavas of Kilauea Volcano, Hawaii, J. Petrol. 12 (1971) 1.

[7] T.L. Wright, Chemistry of Kilauea and Mauna Loa lava in space and time, U.S. Geol. Surv. Prof. Paper 735 (1971).

[8] K. Perry Jr., Methods of petrologic calculation and the relationship between mineral and bulk chemical composition, Contrib. Geol. 6 (1967) 5.

[9] H.J. Greenwood, Matrix methods and the phase rule in petrology, Proc. XXIII Int. Geol. Congr. 6 (1968) 267.

[10] D.M. Carmichael, Intersecting isograds in the Whetstone Lake Area, Ontario, J.Petrol. 11 (1970) 147.

[11] K. Perry Jr., An application of linear algebra to petrologic problems: Part 1, Mineral classification, Geochim. Cosmochim. Acta 31 (1967) 1043.

[12] W.C. Hamilton, Statistics in physical science: estimation, hypothesis testing, and least squares (Ronald Press, New York, 1964) 230 pp.

[13] J.I. Trombka and R.L. Schmadebeck, A numerical least-square method for resolving complex pulse height spectra, National Aeronautics and Space Admin. pub. SP-3044 (1968) 170 pp.

[14] J.I. Trombka, oral communication, July 1972.

[15] G. Arrhenius, J.E. Everson, R.W. Fitzgerald and H. Fujita, Zirconium fractionation in Apollo 11 and Apollo 12 rocks, Geochim. Cosmochim. Acta, Suppl. II (1971) 169.

[16] L.S. Walter, B.M. French, K.F.J. Heinrich, P.D. Lowman Jr., A.S. Doan and I. Adler, Mineralogical studies of Apollo 12 samples, Geochim. Cosmochim. Acta, Suppl. II (1971) 343.

[17] R.C. Newton, A.T. Anderson and J.V. Smith, Accumulation of olivine in rock 12040 and other basaltic fragments in light of analysis and syntheses, Geochim. Cosmochim. Acta, Suppl. II (1971) 575.

[18] G.M. Brown, C.H. Emeleus, J.G. Holland, A. Peckett and R. Phillips, Picrite basalts, ferrobasalts, feldspathic norites, and rhyolites in a strongly fractionated lunar crust, Geochim. Cosmochim. Acta, Suppl. II (1971) 583.

[19] E. Anders, R. Ganapathy, R.R. Keays, J.C. Laul and J.W. Morgan, Volatile and siderophile elements in lunar rocks: Comparison with terrestrial and meteoritic basalts, Geochim. Cosmochim. Acta, Suppl. II (1971) 1021.

[20] C.C. Schnetzler and J.A. Philpotts, Alkali, alkaline earths, and rare-earth element concentrations in some Apollo 12 soils, rocks, and separated phases, Geochim. Cosmochim. Acta, Suppl. II (1971) 1101.

[21] J.H. Scoon, Chemical analyses of lunar samples 12040 and 12064, Geochim. Cosmochim. Acta, Suppl. II (1971) 1259.

[22] W. Compston, H. Berry, M.J. Vernon, B.W. Chappell and M.J. Kaye, Rubidium-strontium chronology and chemistry of lunar material from the Ocean of Storms, Geochim. Cosmochim. Acta, Suppl. II (1971) 1471.

[23] S.E. Haggerty and H.O.A. Meyer, Apollo 12: opaque oxides, Earth Planet. Sci Letters 9 (1970) 379.

[24] D.A. Papanastassiou and G.J. Wasserburg, Lunar chronology and evaluation from Rb-Sr studies of Apollo 11 and 12 samples, Earth Planet. Sci. Letters 11 (1971) 37.

[25] G.W. Reed, S. Jovanovic and L. H. Fuchs, Fluorine and other trace elements in lunar plagioclase concentrates, Earth. Planet. Sci. Letters 11 (1971) 354.

[26] A.L. Albee, A.A. Chodos, A.J. Gancarz, E.L. Haines, D.A. Papanastassiou, L. Ray, F. Tera, G.J. Wasserburg and T. Wen, Mineralogy, petrology and chemistry of a Luna 16 basaltic fragment, sample B-1, Earth Planet. Sci. Letters 13 (1972) 353.

[27] I. Kushiro and H. Haramura, Major element variation and possible source materials of Apollo 12 crystalline rocks, Science 171 (1971) 1235.

[28] A.A. Chodos and A.L. Albee, Quantitative microprobe analysis and data reduction using an on-line mini computer, Proc. Sixth Nat. Conf. on Electron Probe Analysis (1971) 15A.

SANIDINITE FACIES METAMORPHISM OF APOLLO 16 SAMPLE 65015.

A.L. Albee, A.J. Gancarz, and A.A. Chodos; Division of Geological and Planetary Sciences, Calif. Inst. Tech., Pasadena, Calif., 91109

Sample 65015 was collected at station 5, ~ 4.5 km northeast of South Ray Crater. The 1802gm block has the highest reported K (4000ppm), U (3ppm), and Th (10ppm) content of the Apollo 16 samples [1]. It is a prime example of a BaUKREEPTh-rich polymict rock formed prior to 3.93 b.y. [2], which has undergone partial, but extensive recrystallization and reequilibration by sanidinite facies metamorphism at 3.93 b.y. following the Imbrium Event.

The sample was studied in two polished thin sections (~81mm² and ~26mm²). About 5% of the rock consists of rock and mineral clasts, predominantly angular plagioclase (0.1-0.5mm), set in a finer-grained metaclastic matrix. These larger clasts also include a 0.4mm "ball" of Fe-metal, an equant 0.6mm grain of olivine, and about 28 lithic fragments (0.1-1.0mm), including polygonal anorthosite (14), intersertal basalt (7), gabbroic anorthosite (3), and devitrified plagioclase glass (4). This variety of clasts indicates a polymict origin.

The matrix consists of plagioclase, high-Ca pyroxene, olivine, Fe-metal, and troilite grains, poikilitically enclosed in a polygonal mosaic of larger (0.3-0.7mm) low-Ca pyroxene grains. The irregular boundaries between these pyroxene grains typically contain more abundant plagioclase grains, especially the larger, more-angular clasts, poikilitic ilmenite grains, and irregular troilite and Fe-metal grains. The low-Ca pyroxene grains are peppered with blocky plagioclase grains (≤ 0.1 mm) and with olivine and high-Ca pyroxene inclusions, both of which are markedly embayed.

The table gives the mode (1603 points), "average" mineral compositions, and calculated bulk chemical composition as determined by the electron microprobe [3]. The "average" plagioclase composition is An_{93}, but observed compositions range from An_{88} to An_{97}. There are no major compositional differences between the larger clasts and the smaller grains. Many clasts have a core of uniform composition, bordered by a discontinuity, which is marked by a string of tiny olivine granules, and overgrown by a lower An-content rim. High-Ca pyroxene and olivine occur as partially-resorbed clasts with only a limited range in composition. The "average" olivine composition is $Ca_{.01}Fe_{.48}Mg_{1.49}Si_{1.01}O_{\sim 4}$ and the "average" high-Ca pyroxene is $Ca_{.84}Fe_{.29}Mn_{.01}Mg_{.97}Cr_{.02}Al_{.12}Ti_{.05}Si_{1.90}O_{\sim 6}$. The olivine has a higher Fe/Mg than the high-Ca pyroxene, suggesting derivation from independent igneous rock sources. Low-Ca pyroxene ("average" $Ca_{.11}Fe_{.57}Mn_{.01}Mg_{1.28}Cr_{.01}Al_{.04}Ti_{.02}Si_{1.95}O_{\sim 6}$) shows a greater range of composition than high-Ca pyroxene and olivine.

K-rich areas are irregularly dispersed in very fine patches, but are commonly associated with ilmenite. The areas are too small for accurate analysis but the "average" analysis contains normative troilite, corundum, and quartz. No isotropic areas were found and the K-rich areas appear to be devitrified glass. Whitlockite is very abundant and occurs as slender needles up to 40μm in length. No apatite was found. Fourteen grains were analyzed for Y_2O_3 (2.33± 0.29 wt%), Ce_2O_3 (2.34±0.32 wt%), La_2O_3 (0.86±0.24 wt%), and Nd_2O_3 (1.39±0.25 wt%). Other REE were calculated assuming a chondritic abundance pattern. The rock has a high REE content (see table) and the absence of apatite indicates a low Cl and F content.

SANIDINITE FACIES METAMORPHISM

ALBEE, A. L.

Ilmenite occurs as irregular poikilitic grains and as smaller laths. The larger grains have a uniform composition (38analyses) with an extremely high MgO content (5.06±0.35wt%) and low ZrO_2 content (0.05±0.06 wt%), and contain exsolution lamellae of rutile and Cr-spinel on different crystallographic planes, and tiny baddeleyite grains. The high MgO content suggests homogenization of ilmenite grains containing armalcolite cores [4] which was followed by exsolution of Cr-spinel, rutile, and baddeleyite. The globules of Fe-metal are uniform in composition and contain: Ni=5.44±0.85wt%, Co=0.21±0.07wt%, and P=0.14±0.04wt%; 20 analyses. The composition falls slightly outside the meteoritic range.

A most important characteristic of rock 65015 is that it has undergone partial, but extensive sub-solidus recrystallization and reequilibration. This is suggested by the texture, including the polygonal mosaic of poikilitic, low-Ca pyroxene, and is corroborated by Rb-Sr isotopic studies [2]. An internal isochron indicates that most phases equilibrated at 3.93±0.02 b.y., but that the large plagioclase clasts did not equilibrate at that time [2]. Lower-An rims on plagioclase clasts, embayed relic clasts, and subhedral form of the finer-grained plagioclase enclosed in the low-Ca pyroxene matrix--all indicate a reaction relationship between clasts and surrounding matrix. The texture suggests that this is a metaclastic rock and that the low-Ca pyroxene did not crystallize from a melt.

Sub-solidus recrystallization at a relatively low temperature is also suggested by the abundance in ilmenite of rutile, Cr-spinel, and baddeleyite, and by the low ZrO_2 content of ilmenite. In addition, both apatite and whitlockite occur in nearly all lunar igneous rocks, commonly associated with mesostasis. In this rock whitlockite occurs as large crystals not restricted to high-K areas and no apatite was found. This may be the result of Cl and F loss during metamorphic recrystallization with conversion of apatite to whitlockite. Such Cl loss could well be accompanied by loss of volatile $PbCl_2$ [5], especially since lunar apatite and whitlockite are typically high in U and Th and hence radiogenic Pb.

The rock as a whole is high in K, U, Th [1], and Ba, REE, and P (see table) and has a composition similar to "KREEP" fragments [6]. The abundance of such rocks in Apollo 16 soils was estimated by broad-beam analysis for K of 24 2-4mm fragments from stations 4, 8, 10 and 11. About 1/3 of these have a K-content equal to or greater than 65015.

We infer that the most probable protolith of sample 65015 was a glassy agglutinate of mineral and lithic fragments comented by "KREEP" glass which was extensively recrystallized with incipient melting of the interstitial K-rich material during sanidinite facies metamorphism at 3.93 b.y. Such "KREEP"-glass agglutinates are figured by Meyer et al. [6,p.399]. Alternatively, 65015 might be derived by metamorphism of "annealed brecciated KREEP", such as the fragments figured by Meyer et al. [6,p.403]. However, the peculiar nature of the low-Ca pyroxene might be more readily attributed to metamorphism of a glass containing clasts. The variety of lithic clasts indicates that 65015 was not simply derived by brecciation of an igneous rock. Hence, the 4.42 b.y. Rb-Sr isochron, defined by the total rock and plagioclase clast composition [2] cannot be interpreted as the primary age of the protolith.

SANIDINITE FACIES METAMORPHISM

ALBEE, A. L.

We are grateful to S. Epstein and H. Taylor for lending us thin section 65015,83, and to R. Dymek for assistance in the data reduction. This work was supported by NASA Contract NAS-9-8074. C.I.T. Contribution # 2297.

REFERENCES

[1] P.E.T., Science 179(1973)23; [2] D. A. Papanastassiou and G. J. Wasserburg, Earth Planet. Sci. Letters 17(1972)52 and F. Tera et al., this volume; [3] A. J. Gancarz et al., Earth Planet. Sci. Letters. 16 (1972)307; [4] S. E. Haggerty, Earth Planet. Sci. Letters 13(1972)328; [5] F. Tera and G. J. Wasserburg, Earth Planet. Sci. Letters 17(1972)36; [6] C. Meyer, Jr. et al., Proc. 2nd Lunar Sci. Conf. 1(1971)393.

Phase abundances, "average" phase compositions and calculated bulk-chemical composition of 65015

	plagioclase	low-Ca pyroxene	high-Ca pyroxene	mesostasis	ilmenite	olivine	whitlockite*	Fe-metal**	troilite**	bulk composition
vol %	$57.1_3 \pm 1.8_9$	$28.9_4 \pm 1.3_4$	$6.4_9 \pm 0.63$	$3.6_2 \pm 0.4_8$	$1.2_5 \pm 0.2_8$	$1.1_9 \pm 0.2_7$	$0.7_5 \pm 0.2_2$	$0.4_4 \pm 0.1_7$	$0.1_9 \pm 0.1_1$	
wt %	51.2_2	32.5_5	7.1_5	3.4_2	1.9_2	1.5_1	0.7_8	1.1_5	0.3_0	
P_2O_5	n.a.	n.a.	n.a.	0.06	n.a.	n.a.	40.28±1.39	0.17	0.01	0.3_2
SiO_2	43.76	51.80	51.31	60.43	0.26	38.85	2.29±1.28	0.07	0.06	45.6_2
TiO_2	n.a.	0.78	1.68	0.16	53.58	0.17	n.a.	0.01	n.a.	1.4_1
ZrO_2	n.a.	n.a.	n.a.	<0.01	0.05	n.a.	n.a.	n.a.	n.a.	<0.01
Al_2O_3	36.93	1.27	2.64	21.95	0.13	0.14	1.26±1.21	n.a.	n.a.	20.2_8
Cr_2O_3	n.a.	0.47	0.77	<0.01	0.54	0.07	n.a.	n.a.	0.06	0.2_2
MgO	0.11	24.41	17.61	0.05	5.00	38.28	3.28±0.34	0.02	n.a.	9.9_6
CaO	18.80	2.43	16.18	2.75	n.a.	0.26	39.94±1.12	0.01	0.01	11.9_9
FeO	0.13	18.42	9.30	3.35	39.57	22.25	0.89±0.36	94.98	63.43	9.5_9
MnO	n.a.	0.36	0.20	<0.01	0.32	0.15	n.a.	0.04	n.a.	0.1_4
NiO	n.a.	n.a.	n.a.	0.21	n.a.	0.01	n.a.	4.55	0.04	0.0_7
BaO	0.09	n.a.	n.a.	2.47	n.a.	n.a.	n.a.	n.a.	n.a.	0.1_3
Na_2O	0.60	0.02	0.08	0.73	n.a.	n.a.	0.47±0.13	n.a.	n.a.	0.3_5
K_2O	0.06	n.a.	n.a.	7.73	n.a.	n.a.	n.a.	n.a.	n.a.	0.3_0
S	n.a.	n.a.	n.a.	0.83	n.a.	n.a.	n.a.	n.a.	36.39	0.1_4
Co	n.a.	n.a.	n.a.	n.a.	n.a.	n.a.	n.a.	0.19	n.a.	<0.01
$\Sigma RE_2O_3 + Y_2O_3$	n.a.	n.a.	n.a.	n.a.	n.a.	n.a.	10.71	n.a.	n.a.	0.0_8
Total	100.48	99.96	99.77	100.72	99.45	100.18	99.18	100.04	100.00	100.60

Geochimica et Cosmochimica Acta, 1973, Vol. 37, pp. 887 to 904. Pergamon Press. Printed in Northern Ireland

The age and petrography of two Luna 20 fragments and inferences for widespread lunar metamorphism

F. A. PODOSEK, J. C. HUNEKE, A. J. GANCARZ and G. J. WASSERBURG
The Lunatic Asylum of the Charles Arms Laboratory, Division of Geological and Planetary Sciences,* California Institute of Technology, Pasadena, California 91109

(*Received* 30 *January* 1973; *accepted in revised form* 8 *February* 1973)

Abstract—Ages were determined by the ^{40}Ar–^{39}Ar method on two metaclastic rocks returned from the lunar highlands north of Mare Fecunditatis by the Luna 20 probe. Both samples gave very well-defined argon retention ages of 3·90 ± 0·04 AE which are indistinguishable from each other within a resolution of 0·02 AE. Both fragments, 22006 and 22007, are highly recrystallized polymict breccias; there is no evidence for loss of radiogenic ^{40}Ar, and the age almost surely dates the time of recrystallization. The cosmic ray exposure ages of these fragments are similar and high: 900 million years for 22006, 1300 million years for 22007. 22007 also contains substantial trapped argon with a high $^{40}Ar/^{36}Ar$ ratio.

The Luna 20 results greatly extend the area of the Moon's surface exhibiting a well-defined record of metamorphism at 3·9 AE. So far, lunar history in the interval 4·6–3·9 AE is not preserved in the ages of surface rocks. This obliteration suggests lunar-wide metamorphic conditions occurring or terminating at this time as a result of major impacts.

INTRODUCTION

THE UNMANNED probe Luna 20 returned samples from the lunar highlands region north of Mare Fecunditatis. In this paper we report petrographic descriptions and the results of argon analyses of neutron-irradiated specimens of two of the largest lithic fragments transferred to the United States in the lunar sample exchange program with the USSR. The principal scientific result of the argon experiment is the determination of a gas retention age by the ^{40}Ar–^{39}Ar method. The analyses also provide information on cosmic-ray exposure history, trapped argon and elemental abundances (K, Ca and Cl).

The samples studied in this work are designated 22006 and 22007. Prior to our work these specimens were included in a non-destructive instrumental neutron activation analysis (INAA) experiment by LAUL and SCHMITT (1973). Extensive INAA chemical data for these fragments are reported elsewhere in this issue (LAUL and SCHMITT, 1973).

SAMPLES

Fragments 22006 and 22007, as received in this laboratory, weighed 12·2 and 6·0 mg, respectively. As received, they were both coated with dust. After preliminary examination and photographic documentation, the dust was removed by individually washing them in methyl alcohol in an ultrasonic cleaner. A micro-thin section was made from two chips of 22006 which broke off during the washing. The specimens were then transferred to LAUL and SCHMITT (1973) for INAA analysis.

When the samples were returned after the INAA experiment, both were stained with a fine layer of rust, not present before the irradiation. This botryoidal orange-brown material was on the exterior surfaces, and appeared to be particularly

* Contribution number 2315.

clustered around opaque phases. An additional chip was then removed from 22006 and a chip taken from 22007 for thin sections. No apparent differences were observed between the thin sections prepared before and after the INAA, suggesting that the rust was only on the surface and, therefore, did not compromise the subsequent argon analyses, since argon associated with this surface would be expected to be released at very low temperatures.

The material remaining after removal of the thin section chips was then irradiated with fast neutrons for the ^{40}Ar–^{39}Ar analysis.

In addition to 22006 and 22007, we also received a 5·0 mg sample designated 22004. Chemical analyses for 22004 are reported by Laul and Schmitt (1973). This specimen appeared to be a soil breccia, and contained clasts of plagioclase and lithic fragments. It partially disaggregated during preliminary washing and completely disaggregated after the INAA. No further experiments were performed.

Mineralogy and Petrology

Rock 22006 was a tough, dense, fine-grained rock, approximately 2 × 2 × 2 mm. Under the binocular microscope it appeared very light-colored and opalescent or milky. Blebs of Fe-metal were also present on the surface. The thin sections of 22006, labeled FQM-201 and FQM-212 (total area ~1·4 mm^2), were studied optically and with the electron microprobe. Despite the small size of the thin sections, the binocular microscope observations and the small grain-size in the rock suggest that the thin sections are reasonably representative of the material analyzed for argon. 22006 is a fine-grained, metaclastic rock composed primarily of plagioclase (~65 per cent) and pyroxene (~30 per cent) with minor amounts of olivine, ilmenite, chromian ulvöspinel, troilite and Fe-metal. No glass or areas of mesostasis were observed. The rock contains a few clasts of plagioclase and polygonal anorthosite which are surrounded by an abundant granular groundmass (see Fig. 1a) composed of small (~25–50 μm) grains of plagioclase, pyroxene, olivine and large (to 0·25 mm) aggregates of anastomosing crystals.

The groundmass includes high- and low-Ca pyroxene, both of which are quite homogeneous and have nearly the same Fe/Mg. The low-Ca pyroxene is much more abundant than the high-Ca pyroxene. The high-Ca group contains higher concentrations of Al, Cr, Na and Ti than the low-Ca group (see Table 1, No. 1 and No. 2). This groundmass pyroxene occurs as grains independent of one another and of olivine. Like the pyroxene, the groundmass olivine exhibits little compositional variation. The composition ranges from Fo_{66} to Fo_{64} and the olivine has a slightly higher Fe/Mg than the groundmass pyroxene (see Table 1, No. 3).

Individual grains of groundmass plagioclase are generally uniform in composition. The total range in composition is from An_{95} to An_{85}. A typical analysis is given in Table 1 (No. 4). Like other lunar plagioclase, the concentrations of Ba, Fe and Mg increase with decreasing An content.

The large plagioclase clasts occur as single subhedral grains to 250 μm in diameter or as clusters of a few crystals. Many of these clasts exhibit undulatory extinction and ragged twinning suggestive of mild shock. In addition, they exhibit weak compositional zoning. The greatest variation observed within a single grain is from An_{94} in the core to An_{84} at the rim (typical analysis, Table 1, No. 5). Similarly,

22006

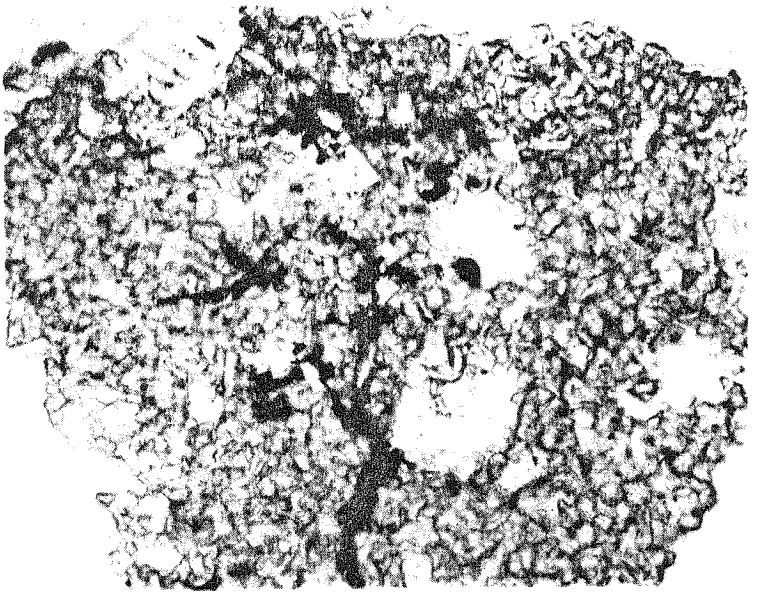

22007

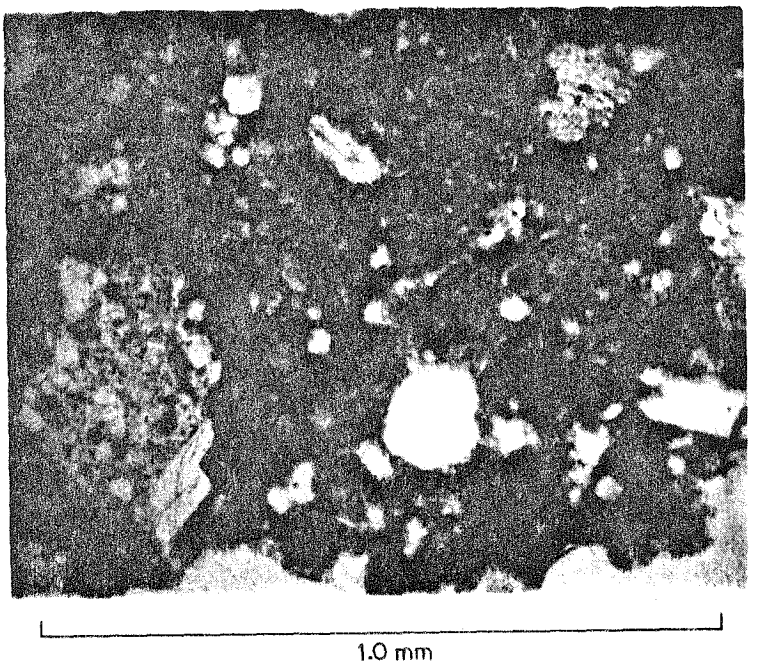

Fig. 1a. Photomicrograph of Luna 20 sample 22006 illustrating the granular groundmass, plagioclase clasts containing pyroxene inclusions, and the anastomosing ilmenite grains.

Fig. 1b. Photomicrograph of Luna 20 sample 22007 illustrating the very fine-grained matrix, and clasts of plagioclase and lithic clasts.

Table 1. Representative electron microprobe analyses of 22006 and 22007

	22006					22007		
	Pyroxene		Olivine	Plagioclase Ground-mass	Clast	Matrix	Plagio-clase	Olivine
wt.%	No. 1	No. 2	No. 3	No. 4	No. 5	No. 6	No. 7	No. 8
SiO_2	50·63	53·08	36·22	44·31	44·83	46·67	43·69	39·41
Al_2O_3	2·65	1·58	0·19	35·78	35·91	26·52	36·35	0·23
Cr_2O_3	0·81	0·31	0·19	n.a.	n.a.	0·11	n.a.	0·22
TiO_2	1·94	0·93	0·09	n.a.	n.a.	0·66	n.a.	0·16
MgO	15·56	21·65	32·89	0·09	0·11	5·24	0·14	43·25
FeO	9·88	17·44	30·49	0·24	0·37	4·93	0·23	17·14
MnO	0·20	0·34	0·30	n.a.	n.a.	<0·01	n.a.	<0·01
CaO	18·08	4·94	0·25	18·88	18·62	15·70	19·62	0·27
BaO	n.a.	n.a.	n.a.	0·08	<0·01	0·11	0·16	n.a.
Na_2O	0·10	0·07	0·01	0·55	0·60	0·52	0·39	n.a.
K_2O	n.a.	n.a.	n.a.	0·17	0·18	0·22	0·07	n.a.
NiO	n.a.	n.a.	n.a.	n.a.	n.a.	<0·01	n.a.	<0·01
P_2O_5	n.a.	n.a.	n.a.	n.a.	n.a.	0·06	n.a.	n.a.
SO_3	n.a.	n.a.	n.a.	n.a.	n.a.	0·03	n.a.	n.a.
Total	99·85	100·34	100·63	100·10	100·62	100·77	100·65	100·68
catatom prop.								
Si	1·89	1·96	0·97	2·04	2·05	—	2·01	0·99
Al	0·12	0·07	0·01	1·95	1·94	—	1·97	0·01
Cr	0·02	0·01	<0·01	—	—	—	—	<0·01
Ti	0·05	0·03	<0·01	—	—	—	—	<0·01
Mg	0·87	1·19	1·32	0·01	0·01	—	0·01	1·62
Fe	0·31	0·54	0·68	0·01	0·01	—	0·01	0·36
Mn	0·01	0·01	0·01	—	—	—	—	—
Ca	0·72	0·20	0·01	0·93	0·92	—	0·97	0·01
Ba	—	—	—	0·001	<0·001	—	0·003	—
Na	0·01	<0·01	<0·01	0·05	0·05	—	0·03	—
K	—	—	—	0·01	0·01	—	<0·01	—
Ni	—	—	—	—	—	—	—	<0·01
P	—	—	—	—	—	—	—	—
S	—	—	—	—	—	—	—	—
Total	4·00	4·01	3·00	5·00	4·99	—	5·00	2·99

n.a. = not analyzed.

polygonal anorthosite occurs as subhedral fragments to 200 μm in diameter. The individual plagioclase grains range in size from 10 μm to 100 μm. These polygonal anorthosite fragments are like those described by Wood *et al.* (1970); these particular fragments contain more than 99 per cent plagioclase. Low-Ca pyroxene occurs as small anhedral grains (<10 μm) within the plagioclase clasts and within the plagioclase grains in the anorthosite fragments. Their composition is the same as the low-Ca pyroxene in the groundmass. These plagioclase clasts and polygonal anorthosite fragments may have been derived from the same source. The presence of the

pyroxene-rich groundmass which is distinctly different in composition from the plagioclase-rich lithic fragments, indicates that this rock was originally a breccia whose components were derived from at least two different lithic types.

Individual pyroxene and olivine grains in most lunar rocks are chemically zoned, with a significant variation in Fe/Mg, indicative of their rapid crystallization. However, in this sample the pyroxene and olivine grains are uniform in composition. This homogeneity of pyroxene and olivine and the granoblastic texture suggest that the rock has been metamorphosed to a degree sufficient to equilibrate the Fe and Mg within pyroxene and olivine. In addition, the two pyroxenes are probably in equilibrium with each other. The metamorphism, however, was insufficient to homogenize the large subhedral plagioclase clasts. The considerably larger BaO content in the groundmass plagioclase in comparison to the plagioclase clasts also indicates incomplete homogenization. Similar recrystallized polymict breccias have been described by Warner (1972) and Albee *et al.* (1973).

Rock 22006 is a 'recrystallized anorthositic norite' according to the classification of the Luna 20 soil fragments of Taylor *et al.* (1973), and is transitional between 'high-alumina basalt' and 'anorthositic norite' according to the classification of Prinz *et al.* (1973). These classification schemes, which are based on bulk chemical composition (Prinz *et al.*, 1973) and on the abundance of different minerals (Taylor *et al.*, 1973), include a variety of textural types. Included within the classification of lithic fragments by Taylor *et al.* (1973) are the highly metamorphosed breccias which are the more common type of lithic fragment. Thus, the comparison of the mineralogic, petrographic and bulk chemical characteristics of this rock with the study of other fragments in the Luna 20 soil suggest that it is indeed a common rock type at the Luna 20 site.

22007 was a fine-grained, mesocratic rock approximately $2 \times 2 \times 2$ mm with abundant vesicles or vugs present at the surfaces. One side of the specimen was coated with a thin, sugary layer of plagioclase-rich material, quite distinct from the bulk of the sample. The sample was studied in thin section FQM-211 with an area of approximately 1·6 mm^2. It is a metaclastic rock, but texturally very distinct from 22006. The sample consists of subangular plagioclase clasts (to $\sim$200 μm), set in a very fine-grained matrix (see Fig. 1b). The fine-grained, semi-opaque matrix is composed of small euhedral laths of plagioclase surrounded by submicron-size particles of ferromagnesian silicates, Fe-metal, troilite and ilmenite (?). No glass appears to be present in the matrix and the opacity is due to the numerous small grains of opaque minerals.

The matrix is somewhat inhomogeneous on a scale of 50 μm. Five quantitative electron microprobe analyses (beam diameter $\sim$50 μm) of the matrix are all olivine normative. The amount of normative pyroxene is nearly constant (22 to 25 catatom per cent), but the amounts of normative olivine and plagioclase range from 1 to 21 catatom per cent and 52 to 75 catatom per cent, respectively. An analysis of the groundmass of intermediate composition is presented in Table 2, No. 6.

The subangular plagioclase clasts exhibit little zoning. They range in composition from An_{92} to An_{95}.

Three lithic fragments are present in the thin section of 22007 (see Fig. 1b). One is a polygonal anorthosite. Its plagioclase is extremely uniform in composition, An_{93}

to An_{95}. The other two fragments are fine-grained troctolites, similar to those described by TAYLOR *et al.* (1973). In these fragments the plagioclase ranges in composition from An_{90} to An_{93} and the olivine ranges from Fo_{72} to Fo_{82} (see Table 1, Nos. 7 and 8).

The euhedral form of the small groundmass plagioclase crystals indicates that they are products of recrystallization and not fragments originally in the progenitor. Although this rock is texturally very different from 22006 and the other fragments described from the Luna 20 site, its bulk chemistry (LAUL and SCHMITT, 1973) and mineralogy are similar to the other fragments.

ARGON ANALYSES

The experimental and computational procedures and techniques used in this work differ only in minor detail from those described elsewhere (TURNER *et al.*, 1971; PODOSEK and HUNEKE, 1973a).

The irradiation in which 22006 and 22007 were included is designated LAV3, a 9-day irradiation performed in November 1972, in the shuttle-tube facility of the General Electric Test Reactor (GETR), Pleasanton, California. Nominal neutron fluences for this irradiation estimated by GETR personnel were $9{\cdot}0 \times 10^{19}$ neutrons/cm^2 below 0·17 eV and $1{\cdot}2 \times 10^{19}$ neutrons/cm^2 above 0·18 MeV. Spatial variations in neutron fluence were monitored by counting ^{58}Co activity induced by ^{58}Ni(n, p) in Ni wires packaged between samples. All relative fluences for this irradiation are referred to an arbitrary normalization at the center of the irradiation capsule.

Following convention, we will use an asterisk (*) to designate kaliogenic argon: ^{39}Ar* produced by ^{39}K(n, p) and ^{40}Ar* produced by natural decay of ^{40}K. This notation indicates that corrections have been applied to remove any other contributions, and also that a correction for neutron fluence variation has been applied to ^{39}Ar.

Production of ^{39}Ar* in LAV3 was monitored by determination of ^{40}Ar*/^{39}Ar* in aliquots of a hornblende (hb3gr) standard (TURNER *et al.*, 1971) of known ^{40}Ar*/K. Measurements of the two hornblende aliquots in LAV3 yielded ^{40}Ar*/^{39}Ar* values of $7{\cdot}04 \pm 0{\cdot}02$ and $7{\cdot}21 \pm 0{\cdot}04$; the 2·4 per cent difference in these values is within their $\pm 1{\cdot}6$ per cent variability in ^{40}Ar*/K (TURNER *et al.*, 1971). Production of ^{39}Ar* for unit fluence in LAV3 will be based on ^{40}Ar*/^{39}Ar* = 7·10, with an uncertainty of 2 per cent; rather than average the two monitor values, we have weighted more heavily the one located in a region of lesser fluence gradient. For ^{40}Ar*/K = $5{\cdot}69 \times 10^{-3}$ cm^3 STP/g (TURNER *et al.*, 1971), this gives $C_{39}(K) = {}^{39}Ar^*/K = 8{\cdot}02 \times 10^{-4}$ cm^3 STP/g.

Production of ^{37}Ar by ^{40}Ca(n, α) and ^{38}Ar by ^{37}Cl$(n, \gamma\beta)$ are computed by comparison of ^{40}Ar*/^{39}Ar* in LAV3 with the same quantity in other irradiations (in the same GETR position) which included appropriate Ca (TURNER *et al.*, 1971) and Cl (PODOSEK, 1973) calibrations. Determination of absolute K and Ca abundances is uncertain by 10 per cent (due to uncertainty in mass spectrometer sensitivity); absolute Cl abundances are subject to a 25 per cent uncertainty in the calibration (PODOSEK, 1973).

The INAA experiment on the Luna 20 samples (LAUL and SCHMITT, 1973) involved

a neutron irradiation. To monitor possible interference with the ^{40}Ar–^{39}Ar experiment, the INAA irradiation included an aliquot of the hb3gr monitor. In the mass spectrometric measurement of this aliquot (not irradiated in LAV3) $^{39}Ar^*$ was essentially undetectable with an upper limit of $^{39}Ar^*/^{40}Ar^* < 0{\cdot}0001$, less than 10^{-3} of the LAV3 level. This is in agreement with the stated fluence level of Laul and Schmitt (1973), which is $\sim 0{\cdot}5 \times 10^{-3}$ times the LAV3 fluence level. Accordingly, the INAA irradiation is ignored in subsequent calculations.

Because of the small sample size of the Luna 20 specimens we have applied a background correction to ^{39}Ar. Procedural blanks indicate the presence of mass 39 in the spectrometer essentially at our detection limit of 3×10^{-12} cm^3 STP Ar, and unrelated to signal strength of other isotopes. We have accordingly subtracted $(3 \pm 3) \times 10^{-12}$ cm^3 STP (independent of sample amount) from measured ^{39}Ar. These corrections are typically about half the statistical error in measured ^{39}Ar and, in view of uncertainties in other corrections and calculations, represent only a minor contribution to overall uncertainty in quantities of interest here. Spectrometer background Cl and HCl have been reduced below the detection limit, and correction to masses 36, 37 and 38 are unnecessary.

Results

The results of thermal-release argon analyses of the Luna 20 samples are presented in Table 2. A preliminary report of these data was given by Huneke *et al.* (1973).

Table 2. Argon† analyses of neutron-irradiated (LAV3) Luna 20 samples

Extraction temperature[e] (°C)	^{40}Ar[a] cm^3 STP/g $\times 10^{-8}$	$^{36}Ar/^{40}Ar$	^{37}Ar[b]$/^{40}Ar$	$^{38}Ar/^{40}Ar$	^{39}Ar[bc]$/^{40}Ar$	Apparent age[d] (AE)
		22006				
	(sample weight 7·5 mg; relative neutron fluence 1·002 ± 0·003)					
455	88	0·003	0·089	0·0232	0·0024	
		±0·002	0·003	0·0009	0·0014	
515	34	0·013	0·330	0·046	0·0098	3·8
		±0·003	0·010	0·004	0·0020	0·7
600	101	0·0172	0·354	0·0226	0·0141	3·81
		±0·0010	0·003	0·0006	0·0007	0·16
695	516	0·01637	0·3484	0·0139	0·01447	3·96
		±0·00013	0·0011	0·0002	0·00016	0·03
770	736	0·0185	0·4369	0·01481	0·01504	3·91
		±0·0003	0·0004	0·00006	0·00012	0·02
825	781	0·0172	0·4762	0·01563	0·01518	3·906
		±0·0003	0·0005	0·00011	0·00009	0·020
885	820	0·01748	0·5022	0·01614	0·01497	3·933
		±0·00020	0·0005	0·00008	0·00011	0·020
975	798	0·01609	0·5590	0·01766	0·01539	3·900
		±0·00017	0·0006	0·00006	0·00017	0·025
1135	1366	0·01572	0·6171	0·02041	0·01568	3·891
		±0·00012	0·0005	0·00009	0·00005	0·013
1265	387	0·0168	0·8004	0·0248	0·01553	3·86
		±0·0003	0·0014	0·0003	0·00020	0·05

Table 2 (*continued*)

Extraction temperature[e] (°C)	^{40}Ar[a] cm³ STP/g × 10^{-8}	$\frac{^{36}Ar}{^{40}Ar}$	$\frac{^{37}Ar}{^{40}Ar}$[b]	$\frac{^{38}Ar}{^{40}Ar}$	$\frac{^{39}Ar}{^{40}Ar}$[bc]	Apparent age[d] (AE)
1360	597	0·01532	0·7778	0·0235	0·01521	3·92
		±0·00019	0·0005	0·0002	0·00011	0·04
1590	214	0·0149	0·706	0·0221	0·0129	3·9
		±0·0004	0·002	0·0005	0·0003	0·2
Total	6437	0·01637	0·5521	0·01861	0·01494	
		±0·00008	0·0020	0·00007	0·00005	
		22007				
	(sample weight 4·4 mg; relative neutron fluence 1·004 ± 0·003)					
455	167	0·008	0·028	0·0191	0·0015	
		±0·002	0·003	0·0010	0·0007	
515	78	0·0331	0·117	0·0312	0·0084	4·2
		±0·0012	0·006	0·0006	0·0014	0·5
600	225	0·0506	0·122	0·0203	0·0077	4·72
		±0·0009	0·002	0·0005	0·0007	0·20
695	1022	0·08473	0·1203	0·02129	0·00696	4·91
		±0·00020	0·0007	0·00015	0·00014	0·06
795	1333	0·10917	0·2382	0·02936	0·01098	4·04
		±0·00019	0·0005	0·00011	0·00014	0·06
885	867	0·0896	0·3102	0·0287	0·01242	3·92
		±0·0005	0·0007	0·0004	0·00015	0·05
975	672	0·0629	0·3902	0·0264	0·01349	3·89
		±0·0004	0·0005	0·0003	0·00019	0·05
1135	1680	0·04342	0·4376	0·02487	0·01441	3·91
		±0·00011	0·0003	0·00012	0·00008	0·02
1460	5176	0·01249	0·4367	0·01912	0·01554	3·911
		±0·00004	0·0002	0·00010	0·00004	0·010
1590	111	0·0111	0·153	0·011	0·0063	3·3
		±0·0011	< 0·010	0·003	0·0012	2·0
Total	11331	0·0447	0·355	0·02257	0·01320	
		±0·0009	0·002	0·00012	0·00008	

† Except as noted below, tabulated data are raw, corrected only for mass discrimination, but not for any contributions produced by neutron irradiation or for procedural blanks. Blank levels of ^{40}Ar (with ^{36}Ar and ^{38}Ar in assumed atmospheric ratio) in cm³ STP × 10^{-8} are: 0·11 up to 975°C, 0·13 at 1135°C, 0·15 at 1265°C, 0·18 at 1360°C, 0·20 at 1460°C and 0·35 at 1590°C. Tabulated errors in isotopic ratio are one standard deviation.

(a) Absolute gas amounts uncertain by 10%; relative gas amounts uncertain by 5%.

(b) Corrected for radioactive decay.

(c) Corrected for (3 ± 3) × 10^{-12} cm³ STP background at mass 39.

(d) Tabulated errors are based on statistical uncertainty in $^{39}Ar^*/^{40}Ar^*$; comparison of ages of different samples involves additional uncertainty due to uncertainty in relative neutron fluence (~0·01 AE); a further systematic uncertainty in absolute age of 0·04 AE is attributable to uncertainty in monitor calibration. Constants used in age calculations are $\lambda_\beta = 4{\cdot}72 \times 10^{-10}$ yr^{-1}, $\lambda_e = 0{\cdot}585 \times 10^{-10}$ yr^{-1} and $^{40}K/K = 1{\cdot}19 \times 10^{-4}$.

(e) Temperatures above 900°C are measured by optical pyrometer assuming a spectral emissivity (for silicates) of 0·5. Lower temperatures are extrapolated on the basis of oven power input.

Tabulated data differ from measured isotopic ratios only by the incorporation of corrections for mass discrimination in the spectrometry, radioactive decay of ^{37}Ar and ^{39}Ar before analysis, and mass 39 background. Other corrections which must be made prior to calculation of any quantities of interest are those for neutron irradiation interferences, flux normalization and procedural blanks; the data in Table 2 do *not* include these corrections. All these corrections are straightforward and are made in accordance with previous practice (Turner *et al.*, 1971; Podosek and Huneke, 1973a). The data in Table 2, together with parameters and procedures detailed below and in these references, are sufficient to reproduce all calculations used in this paper.

As usual, the largest corrections are for non-kaliogenic ^{39}Ar from $^{40}Ca(n, \alpha)$ (typically a few per cent) and for procedural blanks (typically a few per cent or less of ^{40}Ar, but larger in small fractions at the lowest and highest temperatures). The calcium correction to ^{39}Ar is well-established and does not contribute significant error. We assign a ± 50 per cent uncertainty to the blank correction; this is the principal error introduced by the corrections and typically is comparable to the statistical error involved in measurement of the $^{39}Ar/^{40}Ar$ ratio.

Subsequent discussion is based on data which have been corrected for irradiation interferences, fluence variation and blanks. Further corrections necessary before age computations are those for spallogenic and trapped ^{40}Ar; these are discussed in detail below.

K and Ca Abundances

$^{39}Ar^*$ and ^{37}Ar are attributable solely to neutron reactions with K and Ca, respectively, and are used to determine average K and Ca abundances in the sites degassed in each release fraction. The K/Ca ratios for individual sites often constitute a useful diagnostic tool in interpreting the age release pattern, and are plotted in Fig. 3. Total K and Ca abundances are given in Table 3, and are in reasonable agreement with the more precise determinations of Laul and Schmitt (1973).

In 22006, essentially all of the K and Ca in the total sample resides in the plagioclase, as seen by combining plagioclase composition (Table 1) and plagioclase abundance (65 per cent). This is also consistent with the apparent absence of K-rich mesostasis areas. In 22007, K and Ca cannot be contained in the plagioclase alone; a substantial portion, particularly of K, must be in the 'matrix' (see Table 1). Since no glass was observed in the thin section, the K in the 'matrix' is probably in K-rich feldspar grains too small to be resolved in the electron microprobe analyses.

Trapped and Spallogenic Argon–Chlorine–Cosmic Rays

Partitioning. After corrections for procedural blanks and production by neutron irradiation of Ca and K, there remain three sources of ^{36}Ar and ^{38}Ar: trapped gas, for which we assume $(^{38}Ar/^{36}Ar)_t = 0{\cdot}187$; spallogenic gas, for which we assume $(^{38}Ar/^{36}Ar)_s = 1{\cdot}54$, and monoisotopic ^{38}Ar produced in the neutron irradiation by $^{37}Cl(n, \gamma)$ (production of ^{36}Ar is negligible because of the long half-life of ^{36}Cl). All three are of intrinsic interest, and in the present case their resolution is important in applying a correction to ^{40}Ar. In general, a mixture of three components cannot be uniquely and rigorously resolved in a two isotope system, so that any resolution is necessarily indirect and involves other considerations.

The patterns of ^{36}Ar and ^{38}Ar variation for both the Luna 20 samples are similar and can be decomposed with confidence. Temporarily ignoring ^{38}Ar produced from Cl, lever-rule partitioning of ^{36}Ar and ^{38}Ar between trapped and spallation leads to a reasonable sequence in which ^{36}Ar and ^{38}Ar are mostly spallogenic at the highest temperatures, grading monotonically to increasing proportions of trapped gas at lower temperatures. This sequence is to be expected if spallogenic gas is uniformly distributed and trapped gas is concentrated near the surface. The ratio of spallogenic $^{38}Ar_s$ to Ca-derived ^{37}Ar inferred by this partitioning is also constant down to 795°C in both cases ($^{38}Ar_s/^{37}Ar = 0{\cdot}030$ in 22006, and $^{38}Ar_s/^{37}Ar = 0{\cdot}043$ in 22007), consistent with production of ^{38}Ar principally by cosmic-ray induced spallation reactions on Ca, without appreciable diffusive loss. At 695°C and below, in both 22006 and 22007, the apparent proportion of spallation and the apparent $^{38}Ar_s/^{37}Ar$ ratio rise, which we take as an indication of the presence of Cl-derived ^{38}Ar. With the assumption that $^{38}Ar_s/^{37}Ar$ in these low temperature fractions is the same as at high temperatures, the non-spallogenic gas may be partitioned between trapped Ar and Cl-derived ^{38}Ar.

Chlorine. The identification of Cl-derived ^{38}Ar described above leads to the Cl abundances in Table 3. These are somewhat lower than but comparable to Cl values for a Luna 20 anorthosite (12 ppm) and soil (14 ppm) (VINOGRADOV, 1972).

We wish to caution that an accurate determination of Cl-abundances is not an integral part of the present experiment design. In addition to possible errors in spectral decomposition, there are systematic uncertainties concerning which we have no control information. Our abundances will be too low if significant Cl-derived ^{38}Ar is released during our preliminary sample-bake (90°C); such low-temperature release has been observed for other halogens (Br and I) by ALEXANDER *et al.* (1972). Alternatively, we have no estimate of possible superficial Cl contamination during sample handling. While the tabulated abundances probably reflect reasonably well the Cl contributions in our data there is thus no guarantee that they reflect true lunar abundances.

Cosmic-ray exposure. The observed constancy (within a few per cent) of $^{38}Ar_s/^{37}Ar$ in five or more high temperature fractions allows computation of a cosmic-ray exposure age (TURNER *et al.*, 1971). For a surface production rate of $^{38}Ar/Ca = 1{\cdot}4 \times 10^{-8}$ cm^3 STP/g-10^6 yr (TURNER *et al.*, 1971), with minor corrections for production of ^{38}Ar from Fe (LAUL and SCHMITT, 1973; HUNEKE *et al.*, 1972a), we obtain exposure ages of 900 million years for 22006 and 1300 million years for 22007 (Table 3).

The cosmic ray exposure ages of both fragments are longer than typical of lunar soils or soil fragments in general (cf. KIRSTEN *et al.*, 1972), and Luna 20 soil in particular (HEYMANN *et al.*, 1973). One other feldspathic Luna 20 fragment measured has essentially the same exposure age as 22006 (HEYMANN *et al.*, 1973).

We make a small correction for spallogenic ^{40}Ar on the basis of $(^{40}Ar/^{38}Ar)_s = 0{\cdot}15 \pm 0{\cdot}15$ (HUNEKE *et al.*, 1972b).

Trapped argon. Total trapped ^{36}Ar in 22006 is small but not insignificant: $3{\cdot}3 \times 10^{-7}$ cm^3 STP/g. ^{36}Ar in 22007 is a decade higher: $3{\cdot}9 \times 10^{-6}$ cm^3 STP/g. These levels require detailed consideration of the possible contribution of trapped ^{40}Ar.

The relationship between trapped ^{36}Ar, $^{39}Ar^*$ and ^{40}Ar (trapped plus $^{40}Ar^*$) in

22007 is displayed in Fig. 2, a standard three-isotope correlation diagram. If the gas represented by these data is a mixture of a well-defined kaliogenic component (a unique $^{39}Ar^*/^{40}Ar^*$, corresponding to a well-defined gas retention age without diffusive loss of $^{40}Ar^*$) and a well-defined trapped component (a unique $^{36}Ar/^{40}Ar$ ratio), the data array will be linear. As seen in Fig. 2, only the four high-temperature

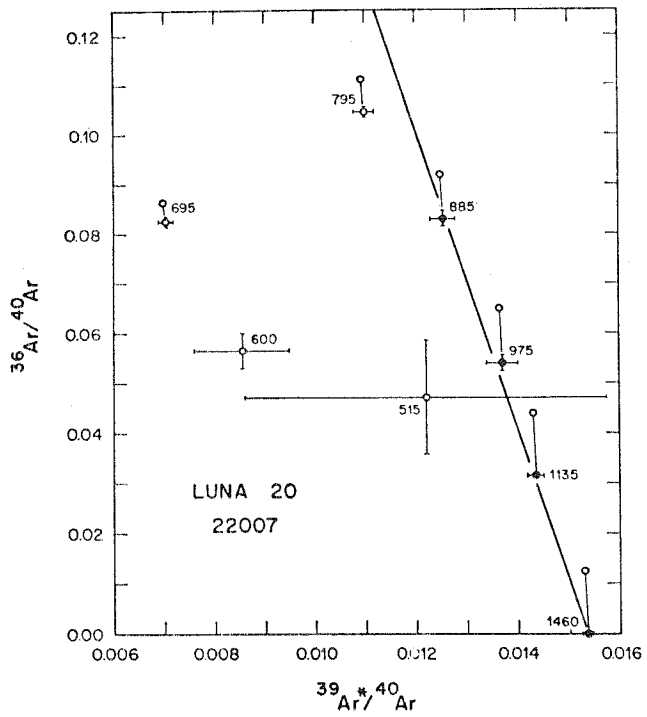

Fig. 2. Three isotope correlation for 22007. Data have been corrected for all contributions other than trapped Ar (both ^{36}Ar and ^{40}Ar) and kaliogenic Ar ($^{40}Ar^*$ and $^{39}Ar^*$). Labels indicate release temperature (°C). The magnitude of spallation corrections to both ^{36}Ar and ^{40}Ar is illustrated by tie-lines between uncorrected data (without error bars) and corrected data (with error bars). The four (corrected) high-temperature points (solid) are consistent with mixing of a single trapped component and a single kaliogenic component whose compositions are determined by the intercepts of the least-squares correlation line with the axes. Lower-temperature data indicate the presence of another trapped component richer in ^{40}Ar and, at the lowest temperatures (515°C and probably 600°C), partial diffusive loss of $^{40}Ar^*$.

points (895°–1460°C, accounting for 83 per cent of total $^{39}Ar^*$) are consistent with this interpretation. The corresponding trapped composition is $^{40}Ar/^{36}Ar = 2{\cdot}15$, the intercept of a least-squares correlation line (York, 1966) with the y-axis. At lower temperatures the data trend away from this correlation in the direction of increasing ^{40}Ar, opposite to the direction corresponding to diffusive loss of ^{40}Ar. Only at 600°C and below, where the data trend back toward higher $^{39}Ar^*/^{40}Ar$ ratios, is there evidence for diffusive loss of $^{40}Ar^*$. More detailed arguments leading to the same

conclusions in a similar but more extreme case have been presented by PODOSEK and HUNEKE (1973b).

The contribution of the low temperature Ar changes the composition of total trapped Ar in 22007 to $(^{40}Ar/^{36}Ar)_t = 4{\cdot}3$, higher than typical lunar soil values (YANIV and HEYMANN, 1972), and in particular higher than other Luna 20 samples (HEYMANN *et al.*, 1973). Following a model in which positive correlation of $(^{40}Ar/^{36}Ar)_t$ with site age reflects a greater availability of ^{40}Ar in the lunar atmosphere in more ancient times (YANIV and HEYMANN, 1972), this result suggests that the immediate-surface exposure of 22007 has been skewed toward the early part of its age to avoid integration of the secular decrease of $^{40}Ar/^{36}Ar$ available for trapping.

On the basis of the observed high-temperature correlation we have made a correction for trapped ^{40}Ar in 22007 by $(^{40}Ar/^{36}Ar)_t = 2{\cdot}15 \pm 0{\cdot}22$. This will be an *undercorrection*, resulting in high apparent ages, in those release fractions (795°C and below) in which we infer the presence of the trapped Ar richer in ^{40}Ar.

While non-negligible, the amount of trapped Ar in 22006 is too small to permit independent evaluation of a trapped $^{40}Ar/^{36}Ar$ ratio in the same fashion as for 22007. In accordance with the value used for 22007, we have applied a correction for trapped ^{40}Ar in 22006 in the ratio of $2{\cdot}15 \pm 0{\cdot}22$ to trapped ^{36}Ar.

The similarity of the two unusually high exposure ages suggests a common origin, such as excavation from depth in a single cratering event. The different calculated ages must then reflect different average shielding histories, i.e. a shallower average depth for 22007 than for 22006. This inequality is also suggested by the larger amount of trapped ^{36}Ar found in 22007, indicative of a longer direct surface exposure.

The origin of trapped noble gases in lunar samples is usually presumed to be direct surface implantation of solar wind and ion-pumped lunar atmosphere subsequent to the event defined by the gas retention age. An alternative possibility for 22006 and 22007 is suggested by comparison of ^{36}Ar abundances with petrographic characteristics. 22007 has more ^{36}Ar than does 22006, and is also more vesicular, finer-grained and less metamorphosed. These correlations are consistent with origin of presently observed trapped Ar either as a relict of surface-implanted gas in a pre-metamorphic breccia or implantation associated with the metamorphic event itself. The latter possibility of implantation from an ambient gas phase, e.g. in a base-surge type event, has been suggested for trapped gas in Apollo 15 green glass spherules by LAKATOS *et al.* (1973). A common mechanism, of whatever nature, for the origin or redistribution of trapped Ar in both 22007 and the green glass balls is in any case suggested by their close similarity in release patterns and the similar 1:2 relationship between high-temperature $^{40}Ar/^{36}Ar$ to total trapped $^{40}Ar/^{36}Ar$ (PODOSEK and HUNEKE, 1973b).

AGE EVALUATION

Following all corrections to both ^{40}Ar and ^{39}Ar, including those for spallogenic and trapped ^{40}Ar described in the previous section, apparent ages are computed from $^{40}Ar^*/^{39}Ar^*$ in each release fraction. These ages are included in Table 2 and displayed in Fig. 3. Each age is uncertain by 0·04 AE, the uncertainty inherent in the LAV3 irradiation calibration. Comparison of the ages of different release fractions of a single sample involves only the statistical errors (as tabulated and displayed in

Fig. 3), however, and is independent of the monitor. Comparison of relative ages of two samples in the same irradiation is also independent of the monitor calibration but must include an error due to uncertainty in relative neutron fluence (0·01 AE for comparison of 22006 and 22007).

Apparent ages in the ^{40}Ar–^{39}Ar method are only formal calculations based on the ratio of $^{40}Ar^*$ to $^{39}Ar^*$, i.e. the ratio of radiogenic $^{40}Ar^*$ to ^{40}K. Only when the

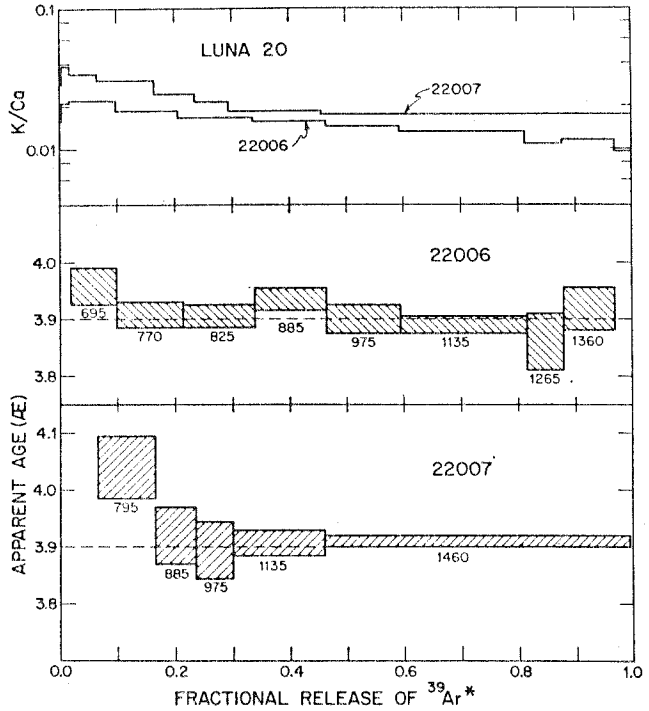

Fig. 3. K/Ca ratios and apparent ages of thermal release fractions of Luna 20 samples 22006 and 22007 (irradiated in LAV3), plotted as functions of cumulative release of $^{39}Ar^*$. The length of each entry is the fraction of total $^{39}Ar^*$ included in each fraction, labeled by release temperature (°C); the height of each box in the age plot spans the statistical error in the apparent age. The age scales for the two fragments are separate: a common reference line is shown at 3·90 AE for each sample.

apparent ages are equal in several thermal-release fractions, i.e. only when we observe the same ratio of $^{40}Ar^*$ to ^{40}K in several sites of different retentivity, may we associate the age with a specific event in the history of the sample. When displayed as in Fig. 3, a sequence of equal apparent ages defines a 'plateau', the existence of which is the usual criterion for identification of a 'well-defined' gas retention age.

As seen in Fig. 3, the four high-temperature points of 22007 define a plateau, and the gas retention age is accordingly well-defined. This plateau is of course a consequence of the particular correction made for trapped ^{40}Ar on the basis of the correlation discussed in the previous section. This is not a trivial result; the chronological significance lies in the fact that in these four high-temperature fractions, which

represent 83 per cent of the total potassium in the sample, we *can* identify a component of well-defined $^{40}Ar^*/^{39}Ar^*$. The actual age assignment rests on these four points, and it is immaterial whether we calculate the age by the $^{39}Ar^*/^{40}Ar^*$ intercept on the x-axis of Fig. 2 or the plateau average (Table 2, Fig. 3). The age is 3·91 ± 0·01 AE.

At lower temperatures (795°C and below) the release fractions of 22007 have higher apparent ages. As noted in the previous section, this represents an undercorrection for trapped ^{40}Ar and is not chronologically significant.

Apparent ages of the release fractions of 22006, also shown in Fig. 3, define a plateau extending over the entire release of $^{39}Ar^*$.

The correction for trapped ^{40}Ar is insignificant in the high temperature fractions (>800°C). The uncorrected ages of the 675°C and 770°C fractions are perceptibly higher, and a correction of the approximate magnitude actually applied is clearly indicated. The high apparent age of the 675°C fraction for 22006 presumably reflects an undercorrection for trapped ^{40}Ar similar to that inferred for 22007. The plateau age is 3·90 ± 0·01 AE.

The difference between the plateau ages of 22006 and 22007 (Table 3) is not significant, being well within the range of compounded statistical errors and fluence uncertainties. Within a resolution of about 0·02 AE these two samples have indistinguishable ages. The absolute age is 3·90 ± 0·04 AE, the error originating primarily in the irradiation monitor calibration.

While there is no difficulty in making these age evaluations, we must also recognize that previous investigations of ^{40}Ar–^{39}Ar systematics, particularly concerning relationships between whole rock and constituent mineral phases, have indicated that whole-rock ^{40}Ar–^{39}Ar analyses of lunar samples sometimes yield ambiguous or misleading results. In many cases whole rock patterns exhibit a characteristic decrease in apparent age at high temperatures, an inversion of the normal diffusive loss pattern (Turner *et al.*, 1971, 1972). While not well-understood, this phenomenon is accompanied by very low K/Ca ratios, and has been clearly associated with pyroxenes (Turner *et al.*, 1972). A second distinctive pattern, disparity of whole rock and plagioclase ages, occurs in some rocks in which whole-rock K is dominated by high-K mesostasis glass and the whole rock pattern shows a high degree of low-temperature

Table 3. Summary of argon results

Sample	[K]† (%)	[Ca]† (%)	[Cl]‡ (ppm)	Cosmic ray† exposure age (million years)	Gas-retention age§ (AE)
22006	0·12	8·2	4	900	3·90 ± 0·001
22007	0·18	9·3	6	1300	3·91 ± 0·001

† Uncertain by 10%.

‡ Uncertain by 25%. Additional possible systematic errors are discussed in text.

§ Quoted errors are statistical; comparison of different samples must allow ~0·01 AE systematic error due to uncertainty in neutron fluence levels. Absolute age and comparison with ages of samples in other irradiations must allow an uncertainty of 0·04 AE inherent in irradiation monitor calibration.

diffusive loss (Podosek *et al.*, 1972; Turner *et al.*, 1972). This pattern is always accompanied by K/Ca ratios which decrease strongly from very high initial values. In both cases, plagioclase separates exhibit substantially better-defined patterns which, when comparison is possible, agree with Rb–Sr internal isochron ages even when the whole-rock ages do not.

No evidence for either effect appears in the Luna 20 data. K/Ca ratios for both 22006 and 22007 (Fig. 3) show quite modest variation for whole-rock samples, and, as discussed earlier, exhibit principally the value appropriate for the constituent plagioclase. Both the extremely high K/Ca ratios (at low temperatures) characteristic of mesostasis and the extremely low K/Ca ratios (at high temperatures) characteristic of pyroxenes are absent from the Luna 20 data. The age-release patterns also show no evidence for the high-temperature decrease in apparent age, and any gas loss is apparently minor and confined to the first few per cent of total $^{39}Ar^*$.

Within the experimental limitations imposed by the small sample sizes, the systematic relationships between $^{40}Ar^*$ and ^{40}K are as well-defined as any which have been observed by the ^{40}Ar–^{39}Ar method. We feel correspondingly secure in the interpretation that the resultant gas retention age dates a clearly identifiable event in the history of the samples. In conjunction with the petrographic observation of thorough metamorphic recrystallization of these samples it also seems reasonably secure that this age is the time of the recrystallization.

It is possible, particularly if trapped ^{36}Ar survived or was acquired in the metamorphism, that some or even all of the ^{40}Ar which we have identified as trapped results from a local redistribution of existing radiogenic ^{40}Ar during the metamorphic event, in the sense of complete disassociation from parent ^{40}K and isotopic homogenization with ^{36}Ar to form the observed trapped component. If this has happened, it does not affect our age computation and the identification of the 3·90 age as the time of metamorphism, since calculated ages are based on $^{40}Ar^*$, by definition the component which correlates with potassium ($^{39}Ar^*$) and which has been corrected for any ^{40}Ar which correlates with ^{36}Ar.

A redistribution of ^{40}Ar without significant loss is evidently operative in some shocked Apollo 14 breccias (Turner *et al.*, 1971; Huneke *et al.*, 1972c). In these cases age release patterns show decreases in apparent age with temperature with no indication of plateaux at any level. Interpretation of such patterns remains obscure, but Turner *et al.* (1971) have noted that in these cases the integrated ratio of ^{40}Ar to $^{39}Ar^*$ agrees with Rb–Sr ages of clasts within the breccias and with K–Ar ages of other Apollo 14 samples. Extension of such lines of reasoning to pre-metamorphic history of the Luna 20 samples is unjustified, however, since we have no way of distinguishing any redistributed radiogenic ^{40}Ar from ^{40}Ar acquired from external sources.

Discussion

Both 22006 and 22007 are clastic rocks which have experienced metamorphic recrystallization. Well-defined ^{40}Ar–^{39}Ar ages for both samples indicate that the metamorphism occurred simultaneously (within 20 million years) 3·90 ± 0·04 AE ago. These samples are similar to other lithic fragments in the Luna 20 core, and it

appears that the 3·9 AE age can be associated with the Luna 20 site with as much validity as the equivalent associations made for other sites.

This result significantly extends the already large area and variety of samples characterized by a 3·9 AE age, as found by a number of methods and authors. These include two ring-structure sites associated with major impact basins: Luna 20, located between the Crisium, Fecunditatis and Tranquillitatis basins (age determined in this paper), and Apollo 15 Apennine Front samples from the edge of the Imbrium basin (representative ages given by STETTLER *et al.*, 1972, and HUSAIN, 1972). Also included are a highlands region not identified with a major basin (Apollo 16; cf. TERA *et al.*, 1973), the ejecta blanket from the Imbrium basin (Apollo 14; cf. TURNER *et al.*, 1971, 1972), and one maverick rock found at a mare site (Apollo 12 sample 12013; cf. LUNATIC ASYLUM, 1970; TURNER, 1971). The persistence of the 3·9 AE age, and the apparent absence of any significantly older rocks, suggests that a wide area of at least the Earth-facing side of the Moon was either blanketed with materials produced in an event about this time or that processes at that time virtually obliterated any more ancient, near-surface rocks. The general observation that the known ages of lunar rocks are confined to a relatively narrow interval between 3·2 and 4·0 AE has not escaped previous notice (cf. PAPANASTASSIOU and WASSERBURG, 1971).

Interpretation of an age of a lunar rock depends critically on the nature of the rock considered. For lunar igneous rocks, it is not *a priori* evident whether the parent magma was produced by large impact or internal heat sources. For metamorphic rocks, the problem is more complex. Metamorphism as a result of large impacts is widely accepted at present, although the detailed mechanisms for producing mature metamorphic textures and large scale melts are not well understood. A wide scale of metamorphic textures may be produced in a large impact, and some of the more mature metamorphic textures observed in 22006 suggest burial at considerable depth in a hot ejecta blanket. The depth of such burial is uncertain because of our lack of knowledge of the appropriate kinetics, but a conservative estimate would be at least a few hundred meters, requiring a rather large cratering event.

Alternatively, rocks can be metamorphosed at depth by internal lunar heat sources. The lunar temperature gradient indicates that depth of 10–20 km or more would be required. If present concepts of lunar tectonics are basically correct, impacts are the only means of exposing rock buried at depth. The large impacts required to excavate to depths of 10–20 km or more would very likely cause melting and metamorphism themselves. Even if they did not, but the rocks were still hot when excavated, their subsequent cooling would date their excavation, i.e. the impact.

The generation of regional metamorphic rocks may also be accomplished at relatively shallow depths by the injection and extrusion of magmas into the outer crust and regolith. Shallow cratering at later times could then expose metamorphic rocks without requiring such large impacts as would likely cause remetamorphism and remelting. For local metamorphism by this mechanism, we would also expect the local regolith to contain abundant unmetamorphosed igneous rocks. The contrary observation in the Luna 20 soil (e.g. TAYLOR *et al.*, 1973) suggests that the metamorphism of 22006 and 22007 is not due to local magmatic activity.

On these grounds we conclude that the metamorphism age we find for the Luna 20 samples dates a very large impact. Two possibilities for the identity of the impact are immediately apparent. One is that the Luna 20 site is covered with Imbrium ejecta, and its chronology is the same as that of at least two other sites already identified with the Imbrium impact: Apollo 14 (Fra Mauro Formation) and Apollo 15 (Apennine mountains). If this is true, debris from the Imbrium impact must have covered very large areas of the near-side of the Moon.

The other immediate possibility is that the Luna 20 samples date a major impact other than Imbrium, presumably associated with a nearby basin such as Mare Crisium, or possibly Mare Fecunditatis or Mare Tranquillitatis. Formation of two major basins at essentially the same time would be either a remarkable coincidence or a strong suggestion that several other basins were also contemporaneous. This in turn suggests that 3·9 AE would have been not just the date of the last of the major mare basins, but a special set of circumstances for at least the Earth–Moon system.

The infalling planetary objects which excavated the basins could represent general solar system debris. Alternatively, it is plausible that one or more Earth orbiting moonlets were the source of the impacting material. In this model we propose that the lunar orbital parameters were undergoing relatively rapid change as a result of strong tidal effects, and swept up the other Earth-orbiting moonlets over a short period of time at ~4·0 AE. In the extreme limit, the collisions resulting in formation of all or most of the major basins might have been essentially a single event. This could have generated the front–back asymmetry presently observed on the Moon.

Present interpretation of chemical and isotopic systematics of the lunar surface indicates that the Moon has enjoyed an existence as an independent astronomical object since about 4·6 AE ago (cf. Papanastassiou and Wasserburg, 1971; Tera and Wasserburg, 1972; Tera *et al.*, 1973). The lack of data for the history of the Moon in the interval between ~4·6 AE and the cataclysm at ~3·9–4·0 AE leaves many fundamental questions unanswered about the nature of the Earth–Moon system in this time interval. It is possible that the Moon was captured at ~4·0 AE causing major heating of that planet, and a destruction of the previous record. However, from the evidence at hand it appears necessary to conclude that major basin forming impacts and concurrent metamorphism occurred subsequent to such capture. It is possible that this lacuna between 4·6 and 4·0 AE is the result of a rather continuous massive bombardment which terminated at ~3·9 AE, or that subsequent to the original major accretion process, there was a relatively quiescent period followed by a narrow interval at ~4·0–3·9 AE in which most of the major impact basins were formed. In either model we must conclude that the late event has essentially erased any intermediate record of lunar evolution.

We note that the 3·9 AE 'magic number' is actually a spread of at least 10^8 yr, most prominently at Apollo 14 (cf. Tera *et al.*, 1973). If this age represents a bombardment 'cataclysm', single or multiple, other effects must be postulated to account for the finite duration of igneous and metamorphic activity. If the younger igneous rocks are the product of impact melting, it is necessary for them to have been buried to a depth of at least several kilometers beneath a hot ejecta blanket and

mechanically confined in that region for an unreasonably long time prior to extrusion and later excavation. In addition to the debris produced by the impact, however, the collision could have triggered lunar volcanism which continued for a prolonged time. In this model, we should observe both metamorphic and igneous rocks of the same age and igneous rocks from internal magma sources which could be significantly younger. The point in time when impact-triggered volcanism would be terminated and the time when 'normal' mare flooding would begin is unclear.

Whichever version of a cataclysmic bombardment episode is considered, it appears necessary to consider all of the highlands sites to be covered with a veneer of relatively young impact ejecta. If so, care must be exercised in identifying the chemical or petrologic character of the 'typical highland' samples returned by Apollo 16 and Luna 20 with the rock types which comprise the highlands and the highlands basement. The highlands samples so far studied cannot yet be regarded with certainty as representatives of extensive highland basement formations occurring in the immediate regions of the areas sampled.

Acknowledgements—We are pleased to acknowledge the role of the Lunar Sample Analysis Planning Team in the design of a series of experiments which seeks to maximize the scientific information obtained from extremely limited material.

We are grateful for the friendly cooperation of J. C. LAUL and R. A. SCHMITT in coordinating cascaded experiments. The continuing interest and friendly criticism of A. L. ALBEE was greatly appreciated. We also thank T. J. GAY for flux-wire counting.

This work was supported by NASA under grant [NGL 05-002-188.]

REFERENCES

ALBEE A. L., GANCARZ A. J. and CHODOS A. A. (1973) Sanidinite facies metamorphism of Apollo 16 sample 65015. Abstracts, *Fourth Lunar Science Conference.*

ALEXANDER JR. E. C., DAVIS P. K. and REYNOLDS J. H. (1972) Rare gas analyses on neutron-irradiated Apollo 12 samples. *Proc. Third Lunar Sci. Conf., Geochim. Cosmochim. Acta Suppl.* **3,** 1787–1798. M.I.T. Press.

HEYMANN D., LAKATOS S. and WALTON J. R. (1973) Inert gases in a terra sample: measurements in six grain-size fractions and two single particles from Luna 20. *Geochim. Cosmochim. Acta* **37,** 875–885.

HUNEKE J. C., PODOSEK F. A., BURNETT D. S. and WASSERBURG G. J. (1972a) Rare gas studies of the galactic cosmic ray irradiation history of lunar rocks. *Geochim. Cosmochim. Acta* **36,** 269–301.

HUNEKE J. C., PODOSEK F. A. and WASSERBURG G. J. (1972b) Gas retention and cosmic-ray exposure ages of a basalt fragment from Mare Fecunditatis. *Earth Planet. Sci. Lett.* **13,** 375–383.

HUNEKE J. C., PODOSEK F. A., TURNER G. and WASSERBURG G. J. (1972c) ^{40}Ar–^{39}Ar systematics in lunar rocks and separated minerals of lunar rocks from Apollo 14 and 15. Revised Abstracts, *Third Lunar Sci. Conf.*, (editor C. Watkins), 413.

HUNEKE J. C., PODOSEK F. A. and WASSERBURG G. J. (1973) An argon bouillabaisse including ages from the Luna 20 site. Abstracts, *Fourth Lunar Science Conference.*

HUSAIN L. (1972) The ^{40}Ar–^{39}Ar and cosmic ray exposure ages of Apollo 15 crystalline rocks, breccias and glasses. *The Apollo 15 Lunar Samples*, (editors J. W. Chamberlain and C. Watkins), 374–377. Lunar Science Institute.

KIRSTEN T., DUEBNER J., HORN P., KANEOKA I., KIKO J., SCHAEFFER O. A. and THIO S. K. (1972) The rare gas record of Apollo 14 and 15 samples. *Proc. Third Lunar Sci. Conf., Geochim. Cosmochim. Acta Suppl.* **3,** 1865–1889. M.I.T. Press.

LAUL J. C. and SCHMITT R. A. (1973) Chemical composition of Luna 20 rocks and soil and Apollo 16 soils. *Geochim. Cosmochim. Acta* **37**, 927–942.

LAKATOS S., HEYMANN D. and YANIV A. (1973) Green spherules from Apollo 15: inferences about their origin from inert gas measurements. *The Moon.*

LUNATIC ASYLUM (1970) Mineralogic and isotopic investigations on lunar rock 12013. *Earth Planet. Sci. Lett.* **9**, 137–163.

PODOSEK F. A., HUNEKE J. C., and WASSERBURG G. J., (1972) Gas-retention and cosmic-ray exposure ages of lunar rock 15555. *Science* **175**, 423–425.

PODOSEK F. A. (1973) Thermal history of the nakhlites by the ^{40}Ar–^{39}Ar method. Submitted to *Earth Planet. Sci. Lett.*

PODOSEK F. A. and HUNEKE J. C. (1973a) Argon 40–argon 39 chronology of four calcium-rich achondrites. *Geochim. Cosmochim. Acta* **37**, 667–684.

PODOSEK F. A., and HUNEKE J. C. (1973b) Argon in Apollo 15 green glass spherules (15426): ^{40}Ar–^{39}Ar age and trapped argon. Submitted to *Earth Planet. Sci. Lett.*

PAPANASTASSIOU D. A. and WASSERBURG G. J. (1971) Lunar chronology and evolution from Rb–Sr studies of Apollo 11 and 12 samples. *Earth Planet. Sci. Lett.* **11**, 37–62.

PRINZ M., DOWTY E. and KEIL K. (1973) Mineralogy, petrology and chemistry of lithic fragments from Luna 20 fines: origin of the cumulate ANT suite and its relationship to high-alumina and mare basalts. *Geochim. Cosmochim. Acta* **37**, 979–1006.

STETTLER A., EBERHARDT P., GEISS J. and GRÖGLER N. (1972) Ar^{39}/Ar^{40} ages of Apollo 11, 12, 14 and 15 rocks. Revised Abstracts, *Third Lunar Sci. Conf.*, (editor C. Watkins), 724–726.

TAYLOR G. J., DRAKE M. J., WOOD J. A. and MARVIN U. B. (1973) The Luna 20 lithic fragments, and the composition and origin of the lunar highlands. *Geochim. Cosmochim. Acta* **37**, 1087–1106.

TERA F., PAPANASTASSIOU D. A. and WASSERBURG G. J. (1973) A lunar cataclysm at ~3·95 AE and the structure of the lunar crust. Abstracts, *Fourth Lunar Science Conf.*

TERA F. and WASSERBURG G. J. (1972) U–Th–Pb systematics in three Apollo 14 basalts and the problem of initial Pb in lunar rocks. *Earth Planet. Sci. Lett.* **14**, 281–304.

TURNER G. (1971) ^{40}Ar–^{39}Ar ages from the lunar maria. *Earth Planet. Sci. Lett.* **11**, 169–191.

TURNER G., HUNEKE J. C., PODOSEK F. A. and WASSERBURG G. J. (1971) Ar^{40}–Ar^{39} ages and cosmic-ray exposure ages of Apollo 14 samples. *Earth Planet. Sci. Lett.* **12**, 19–35.

TURNER G., HUNEKE J. C., PODOSEK F. A. and WASSERBURG G. J. (1972) Ar^{40}–Ar^{39} systematics in rocks and separated minerals from Apollo 14. *Proc. Third Lunar Sci. Conf., Geochim. Cosmochim. Acta Suppl.* **3**, 1589–1612. M.I.T. Press.

VINOGRADOV A. P. (1972) Preliminary data on lunar soil collected by the Luna 20 unmanned spacecraft. *Geokhimiya* **2**, 763–774. English translation, *Geochim. Cosmochim. Acta* **37**, 721–729 (1973).

WARNER J. L. (1972) Metamorphism of Apollo 14 breccias. *Proc. Third Lunar Sci. Conf., Geochim. Cosmochim. Acta Suppl.* **3**, 623–643. M.I.T. Press.

WOOD J. A., DICKEY JR. J. S., MARVIN U. B. and POWELL B. N. (1970) Lunar anorthosites and a geophysical model of the moon. *Proc. Apollo 11 Lunar Sci. Conf., Geochim. Cosmochim. Acta Suppl.* **1**, 965–988.

YANIV A., and HEYMANN D. (1972) Atmospheric Ar^{40} in lunar fines. *Proc. Third Lunar Sci. Conf., Geochim. Cosmochim. Acta Suppl.* **3**, 1967–1980. M.I.T. Press.

YORK D. (1966) Least-squares fitting of a straight line. *Can. J. Phys.* **44**, 1079–1086.

OPTIMIZATION OF COMPUTER-CONTROLLED QUANTITATIVE ANALYSIS OF MINERALS

A. A. Chodos, A. L. Albee, A. J. Gancarz, and J. Laird

Division of Geological and Planetary Sciences
California Institute of Technology *
Pasadena, California 91109

With the development of the computer-controlled electron microprobe, two basic approaches in programming the quantitative analysis of minerals have been used. In the first type of programming the instrument operator must input answers to a large number of questions before performing an analysis. The program is extremely flexible but requires the operator to have a thorough understanding of electron microprobe analytical techniques. In the second approach all choices, which include counting time, elements to be analyzed, and the order in which the elements are analyzed, are programmed for each mineral type. For this approach the operator does not require an extensive knowledge of analytical techniques to perform accurate quantitative analyses. This paper describes a computer program utilizing the second approach.

The program, ULTIMATE, is designed for quantitative analysis of most silicates, oxides, phosphates, carbonates, and sulfates. ULTIMATE is written in a high-level computer language, FOCAL (1969), and controls a Materials Analysis Corporation model 5-SA3 electron microprobe. The computer, a Digital Equipment Corporation 12K PDP-8/L, is interfaced to a Tennecomp Systems TP-1371 MiniDek magnetic cartridge tape deck. Control of the tape deck by FOCAL permits chaining in successive portions of the program during the actual analysis. FOCAL has been modified to include indexing of two-dimensional arrays and high speed calculation routines. These modifications increase the storage capacity for variables and constants by 67% and decrease calculation time from 50% to 80%. This increased efficiency results because the addresses of the doubly-indexed variables and constants are calculated by the computer rather than searched for by testing each entry in the list of variables and constants.

In writing ULTIMATE the main objective was to allow rapid quantitative analysis of the common minerals of geologic interest. Twenty-nine elements which are abundant in the common minerals and/or which have been shown to be significant to understanding the physical and chemical conditions of formation of the common minerals were selected to be analyzed. In addition, since all 29 elements never occur in any single phase, 22 mineral types were chosen, and the significant elements to be analyzed for each mineral type were selected from the list of elements. These combinations of elements and mineral types permit the analysis of all common rock-forming minerals and of nearly all different types of minerals in general.

*Contribution Number 2334

The basic format of the program consists of: 1) an array of constant values, 2) a subprogram to run the standards, 3) the main portion of the program to control the acquisition of data and to compute the final chemical analysis, and 4) a subroutine for each of the 22 mineral types. The array of constant values consists of a 30 x 30 matrix of correction factors for the data reduction technique of Bence and Albee (1968) as modified by Albee and Ray (1970), stage coordinate locations of the standards for all elements, approximate peak position for all elements, and the constants for the calculations specific to each mineral type. Despite the size of the array, the modified version of FOCAL permits rapid location of the constants and consequently rapid calculation.

The standards subprogram moves each standard into position for analysis, searches for the precise peak, and collects counts on the standard. The peak search routine is a simple and rapid method for determining the peak position. Counts are accumulated for one second at each of 25 equally-spaced (10^{-4} Å apart) locations in an interval centered on the approximate peak. The location with maximum counts is determined, and those locations that have greater than 95% of the maximum counts are averaged to give the final peak position.

The main part of the program controls the actual data gathering and reduction. A peak search is done for those elements whose X-radiations are subject to wavelength shifts due to different crystallographic coordinations. Counts are accumulated for peak and respective background positions simultaneously for three elements. The counting time is 90 seconds unless counting statistics give a relative standard deviation of 1% in a shorter time interval. However, since there is only one scaler-timer for all three detectors, the actual counting time is the longest time calculated for any member of the triad of elements whose abundance is greater than about 1%. The final chemical analysis is calculated using the technique of Bence and Albee (1968).

The subroutine for each mineral type determines the sequence of elements to be analyzed. The triad grouping of elements was chosen for each mineral type to maximize the counting accuracy and minimize the counting time. The subroutines also contain specific calculations for each mineral type. For example, in the "opaque" subroutine the effect of the interference of $Ti_{K\beta}$ on $V_{K\alpha}$ radiation is calculated, permitting routine quantitative analysis of V. Additional calculations include determination of the amount of H_2O or CO_2 present in the analyzed sample and correction of the other abundance values for the inter-element interferences due to H_2O or CO_2. To actually perform quantitative analyses, the appropriate subroutine is selected and the entire analysis is completed automatically.

The final chemical analysis is converted to catatom percentages and formula proportions; the normalization factors for these values are set by the mineral subroutines. The formula proportions are used to calculate additional information for each mineral type. This information includes end-member mineral formulae, normative minerals, and significant element ratios.

Although the ULTIMATE program is very specific, it is written in a conversational language and can be readily modified to include analysis of additional elements and calculation of any other desired information.

Acknowledgements

FOCAL was modified by J. Crapuchettes of Frelan Associates. This work was supported by NASA grant NGL-05-002 and NSF grant GA-12867. The microprobe laboratory has been developed with the support of the National Science Foundation, the Jet Propulsion Laboratory, and the Union Pacific Foundation.

References

Albee, A. L. and Ray, L. (1970) Correction factors for electron probe microanalysis of silicates, oxides, carbonates, phosphates, and sulfates. Anal. Chem., 42, 1408-1414.

Bence, A. E. and Albee, A. L. (1968) Empirical correction factors for the electron microanalysis of silicates and oxides. J. Geol., 76, 382-403.

FOCAL (1969): Formulating On-line Calculations in Algebraic Language, Digital Equipment Corporation, Maynard, Mass.

MICROPROBE ANALYSIS OF THE BULK COMPOSITION OF PHASE AGGREGATES

A. J. Gancarz and A. L. Albee

Division of Geological and Planetary Sciences
California Institute of Technology*
Pasadena, California 91109

Introduction

Petrologic, metallurgic, and ceramic studies often require a knowledge of the total composition and/or average phase compositions of a heterogeneous aggregate of phases. Two approaches for obtaining the total composition, the "broad-beam" method and the "point-count" method, are readily possible with a computer-controlled electron microprobe. The advantages and disadvantages of each method will be discussed using the analysis of a lunar basalt as an example.

An aggregate of phases can be described by a series of mass balance equations:

$$C_{11}X_1 + C_{12}X_2 + \cdots + C_{1n}X_n = S_1$$

$$C_{21}X_1 + C_{22}X_2 + \cdots + C_{2n}X_n = S_2$$

$$\vdots$$

$$C_{m1}X_1 + C_{m_2}X_2 + \cdots + C_{mn}X_n = S_m$$

where C_{ij} is the concentration of the i^{th} element in the j^{th} phase, X_j is the weight fraction of the j^{th} phase in the aggregate, and S_i is the concentration of the i^{th} element in the total aggregate. The "broad-beam" method attempts to directly determine the S_i's, i.e. the bulk composition, by averaging the analyses of a large number of 30 to 50μm spots. The "point-count" method measures the C_{ij}'s and X_j's, which are themselves exceedingly useful information and which also permit calculation of the S_i's. It should be noted that the basic equation for each element is correct regardless of whether the phases are compositionally variable or homogeneous. However, obtaining the C_{ij}'s is much simpler for homogeneous phases, such as occur in petrologic or metallurgic systems in approximate thermodynamic equilibrium.

*Contribution Number 2335

Point-count method

Point counting is a standard microscopy technique (Chayes, 1956). Identification of the phase present at a statistically significant number of grid points on a surface provides an estimate of the volume percent of each phase. Volume percentages are transformed to weight percentages (X_j's) by using the densities of the phases. If the phases are homogeneous a single analysis of each phase provides the C_{ij}'s, but if they are inhomogeneous a suitable average composition must be used.

The "point-count" method with the electron microprobe (Keil, 1965) applying the same principles as the standard microscopy technique, measures both C_{ij} and X_j.

The "point-count" technique was used to obtain the C_{ij}'s and X_j's for lunar basalt sample 14276. With a MAC-5-SA3 electron microprobe completely under computer control, 5 second counts for Fe, Ca, and Si were made at 1949 one micron grid points on a polished thin section. The program advanced the stage position, identified epoxy-filled cracks or holes, moved to a new traverse line when the edge of the sample was reached, identified the phase analyzed at each point, determined the volume percentage of each phase, and calculated the average Fe, Ca, and Si counts for each phase. Total running time was less than 4 hours. A large number of complete analyses of the individual mineral phases had established the general compositional range of each phase (see Gancarz et al. 1972), and these ranges were used to establish the phase identification filter. A complete microprobe analysis with Fe, Ca, and Si counts closely corresponding to the average Fe, Ca, and Si counts was selected from all of the complete quantitative analyses to represent the average composition of each phase; these average analyses are included in Table 1. The bulk composition calculated by the "point-count" method is nearly identical to that obtained by chemical analysis (Rose et al. 1972), which is also presented in Table 1. Even minor elements can be determined with considerable accuracy by the "point-count" technique when they are concentrated in measurable quantities in low abundance phases.

In this rock the compositional variation in plagioclase could be expressed in terms of two components and formed a continuous series; hence plagioclase composition was expressed as a single average. The pyroxenes -- augite, pigeonite, and orthopyroxene -- show three distinct groupings within a nearly continuous compositional variation expressable by three components. Hence, the phase identification filter in the program was written to divide the pyroxenes into 3 groups and to provide three different pyroxene averages since a single average pyroxene composition would not correspond to any actual pyroxene in the rock.

Experience has shown that Fe, Ca, and Si analyses are sufficient to identify and average the phases in the lunar basalts. A different set of filters which identify the phase at each grid point on the basis of Fe, Ca, and Si X-radiation intensity, is written for each rock based upon numerous analyses of the minerals. Rewriting the filters is relatively simple because the program is written in FOCAL, a conversational computer language.

At the expense of increased analytical time, the program can be modified to analyze several elements on each spectrometer. Alternatively, a non-dispersive system with a number of preset windows could be used. Although such modifications make it possible to apply the "point-count" method to quite heterogeneous and less well known aggregates, it is necessary to have some prior compositional information on the phases in order to set up proper identification filters.

"Broad-beam" method

A bulk analysis of lunar basalt sample 14276 was also determined by the "broad-beam"technique and is given in Table 1. The program controlled the analysis and data reduction for 13 elements; 50μm spots spaced on a grid covering the polished thin section were used, and an average for the 50 individual analyses was calculated. This average analysis required about 15 hours of probe time. The resulting bulk composition is quite different from that determined by chemical analysis and by the "point-count" method (see Table 1). Especially notable are the higher Al_2O_3 value and lower MgO and FeO values for the"broad-beam"method. These discrepancies are due to the combined results of at least 4 different biases, which could have been partially avoided by taking certain precautions.

One bias is due to the fact that the correction procedures for inter-element interactions assume a homogeneous sample. The "broad-beam" method assumes that the average grain size is so much smaller than the beam size that the area covered by the beam approximates a homogeneous sample. The grain size in this sample is too large. Hence, a large proportion of the X-rays are generated and pass through a single phase, but the corrections are based on the composition of the entire 50μm spot. As a result, Al, which is almost entirely in plagioclase ($CaAl_2Si_2O_8$), is overcorrected because of the presence of pyroxene $(Ca, Fe, Mg)_2Si_2O_6$ within the analyzed spot. With some knowledge of the C_{ij}'s and X_i's, it would be possible to calculate correction factors weighted by the phase abundance in each spot, but this calculation becomes quite complicated. Moreover it can, at best, only be an approximation because of the difficulty of calculating an average path for the emergent X-radiation in grains of varied geometry.

Two different biases were introduced by the fact that pyroxene tends to pit more than plagioclase during polishing. The program allowed the operator to focus and inspect each 50μm spot and, if it was badly pitted, to move 1/4 of a grid distance normal to the grid traverse direction. In retrospect, this procedure introduced adefinite bias toward plagioclase-rich areas. In addition, the higher degree of pitting on the pyroxene surface resulted in a change in the effective take-off angle, effective source volume, and effective depth of penetration. Both of these problems can be partially avoided by better polishing. An additional bias was due to the fact that some Al_2O_3 used in polishing was lodged in cracks and pits despite ultrasonic cleaning. This amount of Al_2O_3, although small, is also overcorrected as explained above. This problem can be avoided by using other polishing materials.

References

Chayes, F. (1956) Petrographic Modal Analysis, John Wiley & Sons, Inc. New York.

Gancarz, A. J., Albee, A. L., and Chodos, A. A. (1972) Comparative Petrology of Apollo 16 Sample 68415 and Apollo 14 Samples 14276 and 14310, Earth Planet. Sci. Letters 16, 307-330.

Keil, K. (1965) Mineralogic modal analysis with the electron microprobe X-ray analyses, Amer. Min., 50, 2089-2092,

Rose, H. J., Jr., Cuttitta, F., Annell, C. S., Carron, M. K., Christian, R. P, Dwornik, E. J., Greenland, L. D., and Ligon, D. T., Jr. (1972) Compositional data for twenty-one Fra Mauro lunar materials, Proc. Third Lunar Sci. Conf., Geochim. Cosmochim. Acta, Suppl. 3, 2, 1215-1229.

Discussion

Both the "broad-beam" and "point count" methods are useful for particular problems, providing proper precautions are taken. In most circumstances we have found the "point count" method provides more precise data in less time and provides valuable data on average phase composition and phase abundances as well as on bulk composition. In general, the use of a few "broad-beam" analyses as an estimate of the bulk composition is not a reliable procedure and can be highly misleading.

Acknowledgments

We thank A. Chodos for his assistance and help with the computer programming. This work was supported by NASA grant NGL-05-002. The microprobe laboratory has been developed with the support of the National Science Foundation, the Jet Propulsion Laboratory, and the Union Pacific Foundation.

Table 1

Phase abundances, "average" phase compositions and bulk chemical composition of 14276

									Bulk chemical composition		
	plagioclase	ortho-pyroxene	pigeonite	augite	mesostasis	ilmenite	Fe-metal	phosphate**	calculated	Rose et al.	"Broad Beam"
vol %	$64.6_5 \pm 1.8_2$	$15.7_0 \pm 0.9_0$	$9.3_4 \pm 0.6_9$	$4.0_5 \pm 0.4_6$	$3.5_4 \pm 0.4_2$	$1.2_8 \pm 0.2_6$	$0.3_6 \pm 0.1_3$	$0.6_7 \pm 0.1_8$			
wt %	59.9_2	17.9_8	10.7_0	4.6_0	3.1_5	2.0_3	0.9_1	0.7_2			
SiO_2	46.25	53.52	50.67	51.73	73.58	0.24	n.a.	0.56	47.4_1	47.60	47.89
Al_2O_3	34.18	1.60	1.39	2.56	12.85	0.35	n.a.	0.06	21.4_2	21.34	26.13
Cr_2O_3	n.a.	0.56	0.48	0.81	<0.01	0.28	n.a.	n.a.	0.1_0	0.26	0.12
TiO_2	n.a.	0.59	0.82	1.07	0.52	49.58	n.a.	n.a.	1.2_7	1.20	0.59
MgO	0.19	25.35	18.66	17.67	0.04	1.44	n.a.	1.15	7.5_2	7.10	4.98
FeO	0.21	16.41	20.81	12.49	1.21	47.62	91.71*	1.74	7.9_1***	7.94	4.89
MnO	n.a.	0.27	0.29	0.22	<0.01	0.42	n.a.	n.a.	0.1_0	0.12	0.07
CaO	17.55	2.43	6.32	14.35	0.99	0.16	n.a.	47.96	12.6_7	13.18	14.57
Na_2O	1.37	0.02	0.06	0.09	0.92	<0.01	n.a.	0.32	0.8_7	0.72	0.90
K_2O	0.19	<0.01	<0.01	<0.01	7.41	0.01	n.a.	n.a.	0.5_1	0.48	0.55
BaO	0.05	n.a.	n.a.	n.a.	0.07	n.a.	n.a.	n.a.	0.0_4	0.08	0.12
P_2O_5	n.a.	n.a.	n.a.	n.a.	n.a.	n.a.	n.a.	41.16	0.3_0	0.40	0.37
Ni	n.a.	n.a.	n.a.	n.a.	n.a.	n.a.	7.45	n.a.	0.0_7	0.01	n.a.
F	n.a.	n.a.	n.a.	n.a.	n.a.	n.a.	n.a.	1.67	0.0_3	n.r.	n.a.
Total	99.99	100.75	99.50	100.99	97.97	100.10	99.16	94.62	100.24	100.34	101.08

* Fe
** average of apatite and whitlockite
*** total iron as FeO
n.a. not analyzed
n.r. not reported

Proceedings of the Fourth Lunar Science Conference
(Supplement 4, *Geochimica et Cosmochimica Acta*)
Vol. 1, pp. 569–595

Metamorphism of Apollo 16 and 17 and Luna 20 metaclastic rocks at about 3.95 AE: Samples 61156, 64423,14-2, 65015, 67483,15-2, 76055, 22006, and 22007

A. L. ALBEE, A. J. GANCARZ, and A. A. CHODOS

Division of Geological and Planetary Sciences*
California Institute of Technology
Pasadena, California 91109

Abstract—Isotopically-dated metamorphic rocks from the Apollo 16 and 17 and Luna 20 landing sites exhibit not only similar petrographic and mineralogic characteristics, but also a limited spread of recrystallization ages at about 3.95 b.y. The rocks are typically rich in plagioclase, low-Ca pyroxene and olivine and include a variety of rock and mineral clasts. These clasts clearly indicate a polymict origin. The most probable protolith is an agglutinate of mineral and rock fragments cemented by glass, which in some samples was of KREEP composition. High-temperature metamorphism, probably accompanied by some partial melting, resulted in an intergranular reaction responsible for the development of (1) coarser matrix material, (2) reaction rims on clasts, and (3) a poikilitic texture. Such metaclastic rocks with recrystallization ages of about 3.95 b.y. appear to blanket large portions of the moon and are critical to deciphering early lunar history.

INTRODUCTION

PETROGRAPHIC AND ISOTOPIC studies of metaclastic rock samples returned by the Apollo 16 and 17 and Luna 20 missions suggest widespread lunar metamorphism at about 3.95 b.y. Petrographic, electron microprobe, and isotopic data indicate a considerable range of responses by the samples to this metamorphism. The presence of a variety of rock and mineral clasts in these samples indicates a polymict origin more complex than simple crushing of homogeneous volcanic or plutonic rock. In each sample, metamorphism produced intergranular reaction which caused the matrix to become coarser-grained, larger clasts to react with the matrix at their borders, and in several samples, large crystals (oikocrysts), predominantly low-Ca pyroxene, to grow enclosing abundant relict grains (chadacrysts) of the matrix. The extent of intergranular recrystallization and of oikocryst growth is indicative of the degree of response by the individual samples to the metamorphism.

SAMPLE DESCRIPTIONS

Analytical techniques

All of the points plotted on the various diagrams represent analyses for 8 to 16 elements made on a computer-controlled MAC-5-SA3 microprobe using techniques described by Chodos *et al.* (1973). Computer outputs of these analyses are available from A. Albee. Microprobe point counts, "average" mineral compositions, and calculated bulk-chemical compositions were obtained using techniques described by Gancarz and Albee (1973).

---

*Contribution Number: 2341.

Except where specifically noted, each of the tabulated "average" mineral compositions is a selected analysis of an individual point, which closely corresponds to the "average" determined by the point count. Ca, Fe, and Si were analyzed simultaneously using a 1 μm spot. The modal abundances of high-Ca pyroxene are probably slightly too high in rocks with an extremely fine intergrowth of plagioclase and low-Ca pyroxene, since certain proportions of these phases in the 1 μm spot may be identified by the computer program as high-Ca pyroxene. The greatest effect of this error would be a slightly low Al_2O_3 content in the calculated bulk-chemical composition.

Sample 65015

Sample 65015 was collected at Station 5, which may contain a significant amount of ejecta from South Ray Crater located about 4.5 km to the southwest. The 1802 gm (19 × 9 × 10 cm) block was partially buried and has zap pits on two surfaces. It was described in the sample catalogue as a

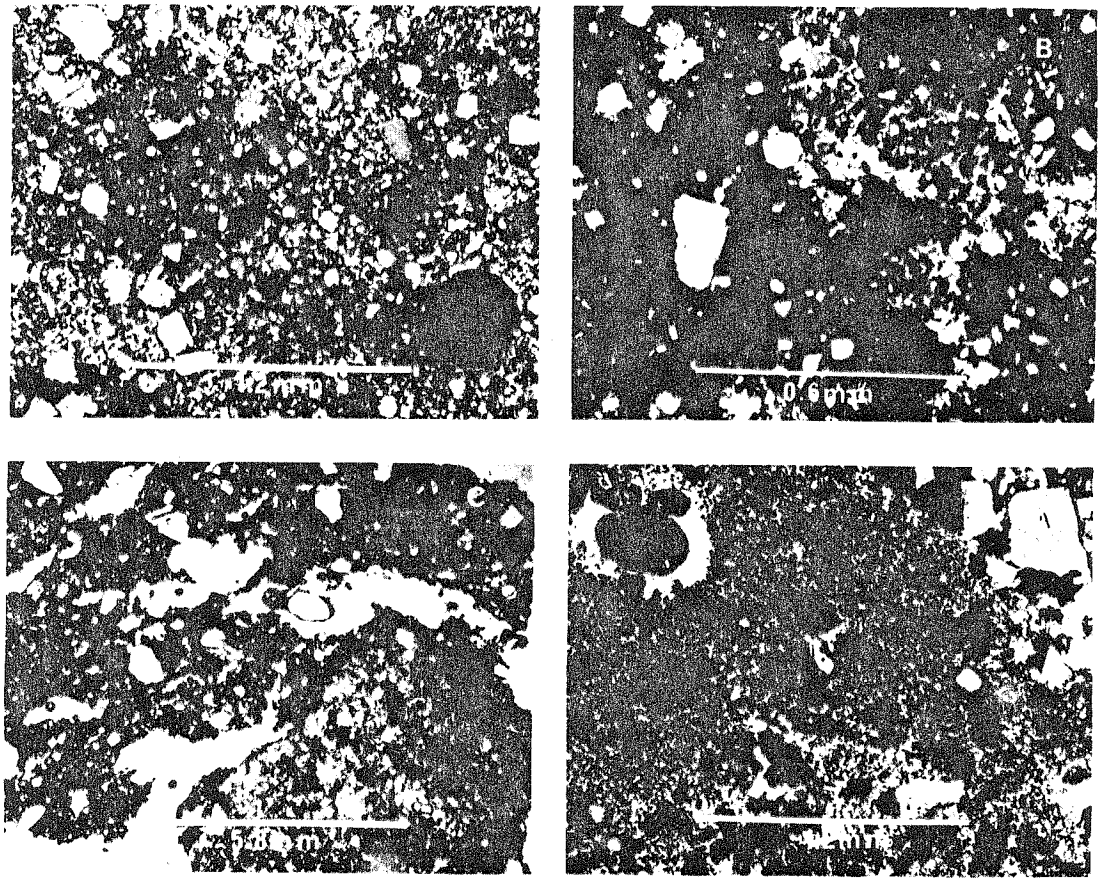

Fig. 1. (a) Photomicrograph of 65015 in crossed-polarized light illustrating metaclastic texture. The dark patch in the upper left is an oikocryst of low-Ca pyroxene at extinction position. The circular area is Fe-metal. (b) Photomicrograph of 65015 in crossed-polarized light illustrating the mosaic of coalesced oikocrysts of low-Ca pyroxene. This area is included in Fig. 1(a), just above the Fe-metal ball. (c) Photomicrograph of 76055 illustrating the contrast between the vesicular, non-poikilitic and non-vesicular, poikilitic portions. Slit-like cavities wrap around the non-vesicular pod. (d) Photomicrograph of 61156 illustrating poikilitic texture in which the oikocrysts have not coalesced and the boundary with a coarse-grained anorthositic clast.

homogeneous metaclastic rock containing only a single 1 mm vug and several subparallel features which may be crush zones. The sample has the highest K (4000 ppm), U (3 ppm) and Th (10 ppm) content of the Apollo 16 samples for which γ-ray analyses were reported (LSPET, 1973a).

The sample was studied in polished thin sections 65015,83 (area ~81 mm^2) and 65015,56, FQM-207 (area ~26 mm^2). As illustrated in Figs. 1a and 1b, about 5% of the rock consists of rock and mineral fragments, predominantly angular plagioclase clasts (100–500 μm), set in a finer-grained metaclastic matrix. The larger clasts include a 400 μm "ball" of Fe-metal, an equant 600 μm grain of olivine, and at least 28 lithic fragments (100–1000 μm), including polygonal anorthosite (14 fragments), intersertal basalt (7), gabbroic anorthosite (3), and devitrified plagioclase glass (4). O. James (written communication, November, 1972) also recognized all of these lithic types in other thin sections of the sample.

The matrix consists of < 100 μm grains of plagioclase, high-Ca pyroxene, olivine, Fe-metal and troilite, which are poikilitically enclosed by larger (300–700 μm) pyroxene oikocrysts, predominantly low-Ca, but some high-Ca pyroxene. In this sample the oikocrysts have almost completely coalesced to form a polygonal mosaic (Fig. 1b). The irregular boundaries between these pyroxene oikocrysts typically contain more abundant plagioclase grains, especially the larger, more-angular clasts, poikilitic ilmenite grains and irregular troilite and Fe-metal grains. The pyroxene oikocrysts are peppered with equant plagioclase granules and contain olivine and high-Ca pyroxene inclusions, which are markedly embayed.

Table 1 gives the mode, "average" mineral compositions, and calculated bulk-chemical composition of thin section 65015,83, as determined by the electron microprobe. Pyroxene, plagioclase, olivine, and ilmenite compositions are summarized in Fig. 2.

The "average" plagioclase composition is An_{93} and observed compositions range from An_{88} to An_{97}. Many clasts have a core of uniform composition, bordered by an optical discontinuity, which is marked by a string of tiny olivine granules, and overgrown by a lower An-content rim (Fig. 4d). There are no major compositional differences between the larger clasts and smaller granules, but there is a systematically higher Fe-content in the plagioclase granules than in the clasts (Fig. 3). Figure 3 also illustrates the generally lower An-content of the rims and the higher An-content of the cores of the clasts.

Olivine and much of the high-Ca pyroxene occur as partially-reacted clasts with only a limited range in composition. The "average" high-Ca pyroxene (Table 1) is $Ca_{0.43}Fe_{0.20}Mn_{0.01}Mg_{0.29}Cr_{0.01}Al_{0.12}Ti_{0.05}Si_{1.99}O_{6}$. No differences in composition were observed between the high-Ca pyroxene oikocrysts and the partially-reacted clasts. The average olivine composition is $Ca_{0.01}Fe_{0.48}Mg_{1.49}Si_{1.01}O_{4}$. A single large olivine clast (~650 μm) ranges from Fo_{66} (CaO, 0.23 wt.%) at the rim to Fo_{74} (CaO, 0.10 wt.%) in the center; this CaO content is lower than in typical mare basalts (Smith, 1971). Olivine has a distinctly higher Fe/Mg than the high-Ca pyroxene clasts. The large grain size and the composition of the high-Ca pyroxene and the olivine clasts suggests that they were derived from the anorthositic (gabbroic and troctolitic) rocks.

Low-Ca pyroxene ("average" $Ca_{0.11}Fe_{0.35}Mn_{0.01}Mg_{1.38}Cr_{0.01}Al_{0.04}Ti_{0.02}Si_{1.95}O_{6}$) shows a greater range of composition than high-Ca pyroxene and olivine, but only about half the total range is found in a single oikocryst. The range in composition suggests that the low-Ca pyroxene oikocrysts may include both orthopyroxene and pigeonite as found by Bence *et al.* (1973), but no X-ray investigations were made. Points were analyzed in radial traverses in several oikocrysts of both low-Ca and high-Ca pyroxene. No significant systematic variation in composition was present.

K-rich areas are irregularly dispersed throughout this rock in very fine patches, exterior to the oikocrysts. Such K-rich areas are particularly abundant in this rock and contain about 90% of the K (Table 1). The common association of K-rich material with ilmenite is reflected by a K-content of 1274 ppm in an ilmenite separate, compared to 2904 ppm for the total rock and 172 ppm for a pyroxene separate (D. A. Papanastassiou, oral communication, February, 1973). The areas are generally too small for accurate analysis but the "average" analysis contains normative FeS, Al_2O_3, and SiO_2. No isotropic areas were found and the K-rich areas appear to be devitrified glass.

Whitlockite is very abundant, occurring as slender needles up to 40 μm in length. No apatite was found. The "average" analysis (Table 1) is the average of analyses on 14 grains. Total REE were calculated, assuming a chondritic abundance pattern, from the average Y_2O_3 (2.33 ± 0.29 wt.%), La_2O_3

Table 1. 65015,83 Phase abundances, "average" phase compositions, and bulk-chemical composition.

	Plagioclase	Low-Ca pyroxene	High-Ca pyroxene	K-rich interstitial material	Ilmenite	Olivine	Whitlockite*	Fe-metal†	Troilite†	Bulk composition
vol. %	57.1 ± 1.8	28.9 ± 1.3	6.4 ± 0.63	3.6 ± 0.4	1.2 ± 0.2	1.1 ± 0.2	0.7 ± 0.2	0.4 ± 0.1	0.1 ± 0.1	(1603 points)
wt. %	51.2	32.5	7.1	3.4	1.9	1.5	0.7	1.1	0.3	
P_2O_5	n.a.	n.a.	n.a.	0.06	n.a.	n.a.	40.28 ± 1.39	0.17	0.01	0.3
SiO_2	43.76	51.80	51.31	60.43	0.26	38.85	2.29 ± 1.28	0.07	0.06	45.6
TiO_2	n.a.	0.78	1.68	0.16	53.58	0.17	n.a.	0.01	n.a.	1.4
ZrO_2	n.a.	n.a.	n.a.	< 0.01	0.05	n.a.	n.a.	n.a.	n.a.	< 0.01
Al_2O_3	36.93	1.27	2.64	21.95	0.13	0.14	1.26 ± 1.21	n.a.	n.a.	20.2
Cr_2O_3	n.a.	0.47	0.77	< 0.01	0.54	0.07	n.a.	n.a.	0.06	0.2
MgO	0.11	24.41	17.61	0.05	5.00	38.28	3.28 ± 0.34	0.02	n.a.	9.9
CaO	18.80	2.43	16.18	2.75	n.a.	0.26	39.94 ± 1.12	0.01	0.01	11.9
FeO	0.13	18.42	9.30	3.35	39.57	22.25	0.89 ± 0.36	94.98	63.43	9.5
MnO	n.a.	0.36	0.20	< 0.01	0.32	0.15	n.a.	0.04	n.a.	0.1
NiO	n.a.	n.a.	n.a.	0.21	n.a.	0.01	n.a.	4.55	0.04	0.0-
BaO	0.09	n.a.	n.a.	2.47	n.a.	n.a.	n.a.	n.a.	n.a.	0.1
Na_2O	0.60	0.02	0.08	0.73	n.a.	n.a.	0.47 ± 0.13	n.a.	n.a.	0.3
K_2O	0.06	n.a.	n.a.	7.73	n.a.	n.a.	n.a.	n.a.	n.a.	0.3
S	n.a.	n.a.	n.a.	0.83	n.a.	n.a.	n.a.	n.a.	36.39	0.1
Co	n.a.	n.a.	n.a.	n.a.	n.a.	n.a.	n.a.	0.19	n.a.	< 0.01
$\Sigma RE_2O_3 + Y_2O_3$	n.a.	n.a.	n.a.	n.a.	n.a.	n.a.	10.71	n.a.	n.a.	0.0
Total	100.48	99.96	99.77	100.72	99.45	100.18	99.18	100.04	100.00	100.60
	An 93	En 68	En 53			Fo 75				
	Ab 5	Fs 29	Fs 16			Fa 25				
	Or < 1	Wo 3	Wo 31							
	Others 2									

*Average and standard deviation of 14 analyses.
†Elemental abundances.
n.a. = Not analyzed.

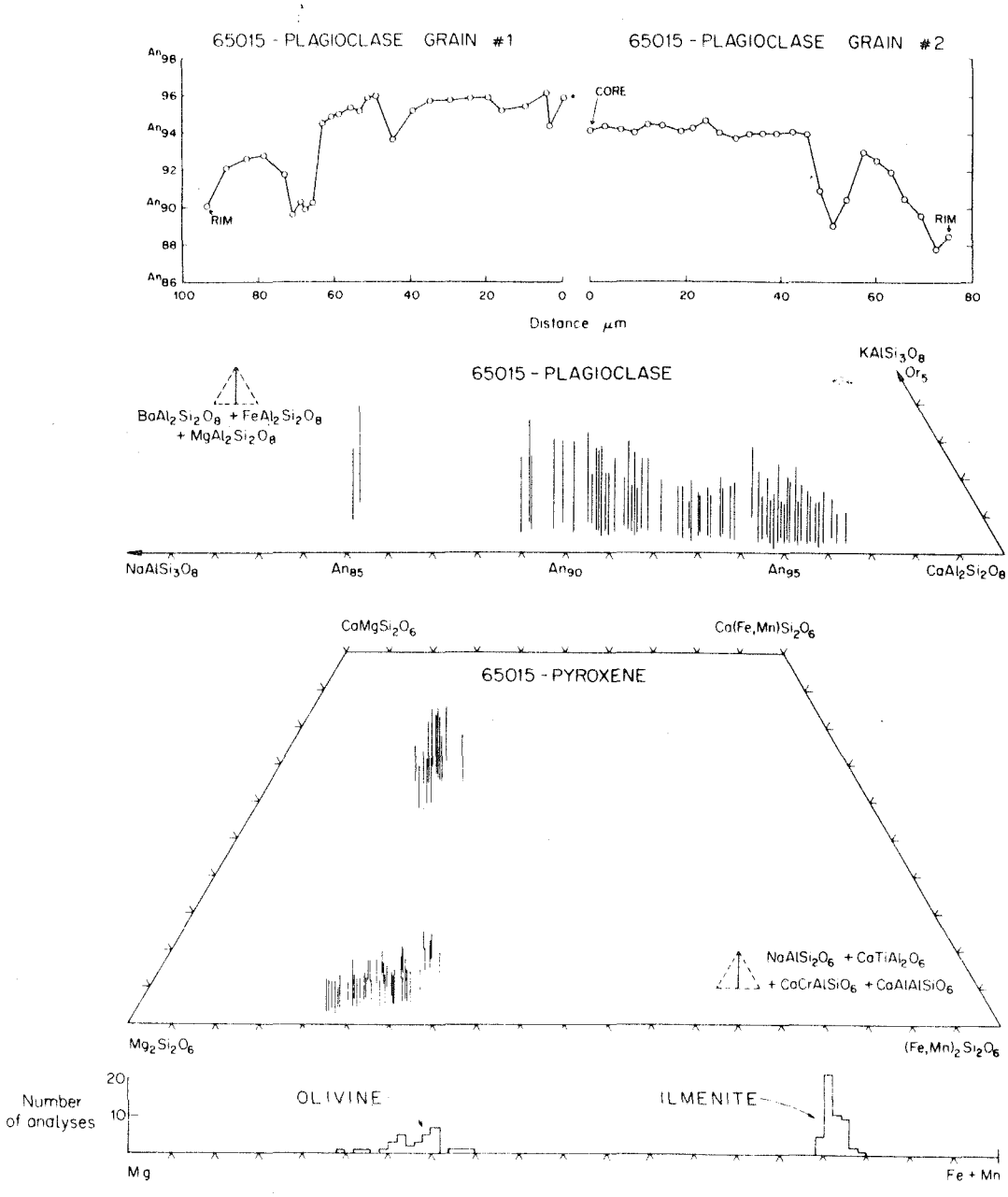

Fig. 2. Compositions of the major mineral phases in Apollo 16 sample 65015.

(0.86 ± 0.24 wt.%), Ce_2O_3 (2.34 ± 0.32 wt.%), and Nd_2O_3 (1.39 ± 0.25 wt.%). Based on these data the rock has a high REE content (Table 1) and the absence of apatite suggests a low Cl and F content.

Ilmenite occurs predominantly as irregular poikilitic grains and in part as smaller laths, which were not analyzed. The larger poikilitic grains have a uniform composition (Fig. 2) with an extremely high MgO content (5.06 ± 0.06 wt.%) and low ZrO_2 content (0.05 ± 0.06 wt.%), and contain exsolution lamellae of rutile and Cr-rich spinel (Fig. 5). The high MgO content suggests possible homogenization of ilmenite grains containing armalcolite cores (Haggerty, 1972), which was followed by exsolution of Cr-spinel, rutile, and baddeleyite. However, no armalcolite was found.

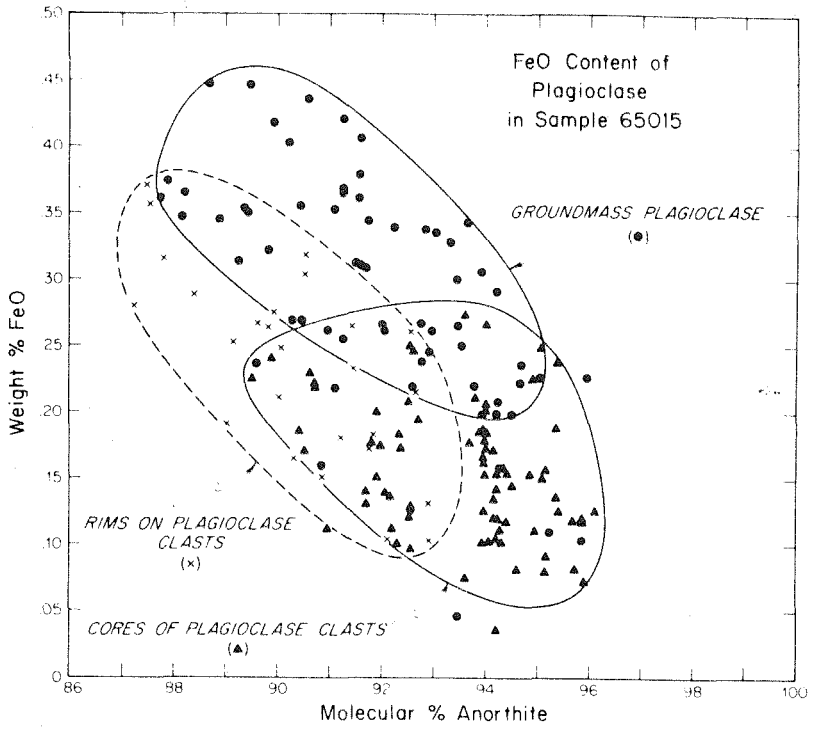

Fig. 3. FeO content of plagioclase in Apollo sample 65015.

The globules of Fe-metal, including the 400 μm "ball," are uniform in composition (Fig. 6), and contain: Ni = 5.44 ± 0.85 wt.%, Co = 0.21 ± 0.07 wt.%, and P = 0.14 ± 0.04 wt.%, 20 analyses. The composition falls slightly outside the meteoritic range (Goldstein and Yakowitz, 1971). Fe-metal also occurs associated with troilite in irregular grains interstitial to the low-Ca pyroxene oikocrysts.

Sample 61156

Sample 61156 was a 58.5 g, 4 × 2.7 × 2.5 cm, angular fragment collected from the surface of the regolith at Station 1. As indicated in the sample catalogue, the rock contained about 1 percent of irregularly-shaped and irregularly-distributed vugs and a portion of a plagioclase-rich clast on one edge.

The sample was studied in polished thin section 61156,31, which has an area of 65 mm^2. One edge of the thin section is a coarse-grained plagioclase rock, a portion of the described clast. Well-twinned plagioclase grains (200–1000 μm) with interstitial, angular plagioclase grains and minor pyroxene form a crushed texture. The contact with the matrix is irregular and matrix material penetrates between and surrounds some of the large plagioclase grains (Fig. 1d).

The matrix is a poikilitic metaclastic rock containing about 3 percent of 50–200 μm plagioclase clasts, a number of 200–400 μm Fe-metal globules, and about 5 percent holes. These holes are believed to represent vesicles rather than "plucking" during preparation because many are circular, are surrounded by matrix rich in plagioclase and poor in low-Ca pyroxene, and contain projecting crystals, predominantly low-Ca pyroxene and ilmenite with minor plagioclase and apatite (Fig. 4e). The matrix consists predominantly of plagioclase granules (20–50 μm long), and low-Ca pyroxene and olivine granules (10–20 μm). Most of the low-Ca pyroxene is oriented into oikocrysts averaging about 100 μm across, but these have not coalesced into a polygonal mosaic. Within the oikocrysts, pyroxene is the most abundant phase and plagioclase laths predominate over granules (Fig. 4f). The olivine and

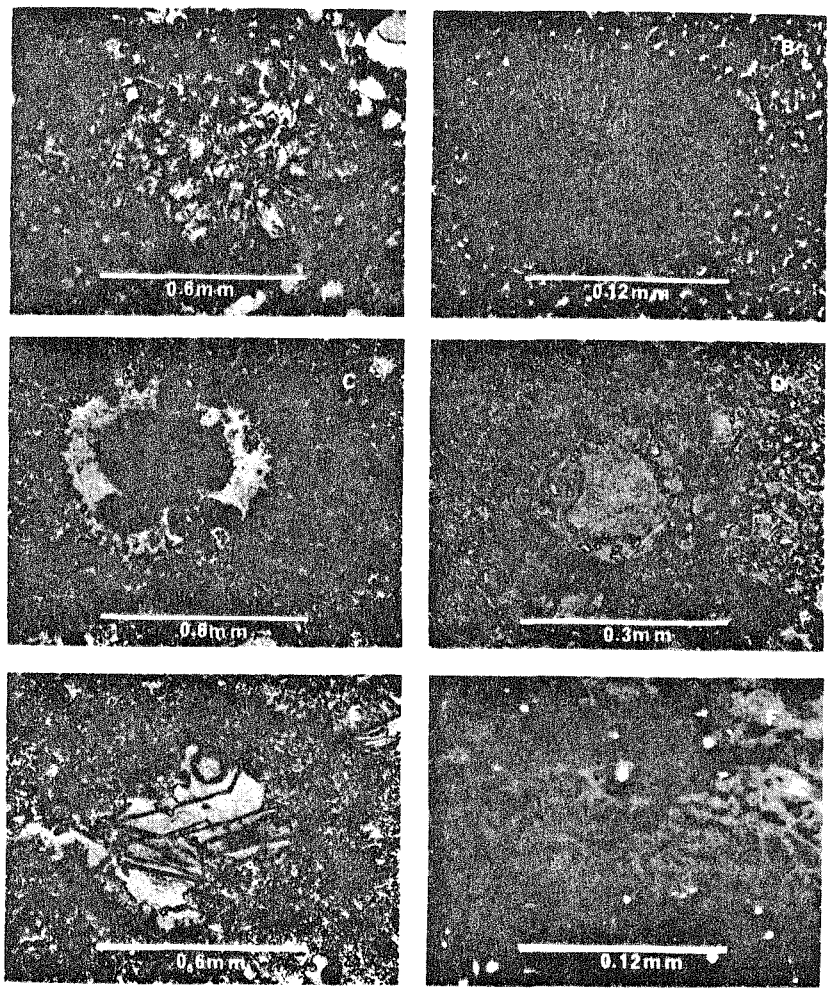

Fig. 4. (a) Photomicrograph of plagioclase-rich, intersertal basalt clast in vesicular portion of Apollo 17 sample 76055. (b) Photomicrograph of spherulitic "spherulite" clast in vesicular portion of Apollo 17 sample 76055. (c) Photomicrograph of Fe-metal "ball" surrounded by plagioclase-rich rim in Apollo 16 sample 61156. The large embayments in the "ball" contain Ca-phosphate. Also illustrated are sheaf-like aggregates of ilmenite and armalcolite. (d) Photomicrograph of a relic plagioclase clast with a string of olivine granules marking the compositional discontinuity with the rim—non-vesicular portion of Apollo 17 sample 76055. (e) Photomicrograph of low-Ca pyroxene crystals projecting into a vesicle in Apollo 16 sample 61156. (f) Photomicrograph in reflected light illustrating lath-shaped grains of plagioclase included in a low-Ca pyroxene oikocryst—Apollo 16 sample 61156.

high-Ca pyroxene generally occur exterior to the oikocrysts. Ilmenite plates typically occur in sheaf-like aggregates and show no apparent relationship to oikocryst development.

Table 2 shows the modal composition, excluding vugs and the plagioclase-rich clast along the edge of the thin section, the "average" mineral compositions, and the calculated bulk-chemical composition as determined by the electron microprobe. Compositions of the major phases are shown in Fig. 7.

The plagioclase compositions fall into two distinct groups as shown in Fig. 7. The anorthite-rich group includes analyses of feldspar from the anorthosite clast on one edge and from the cores of large

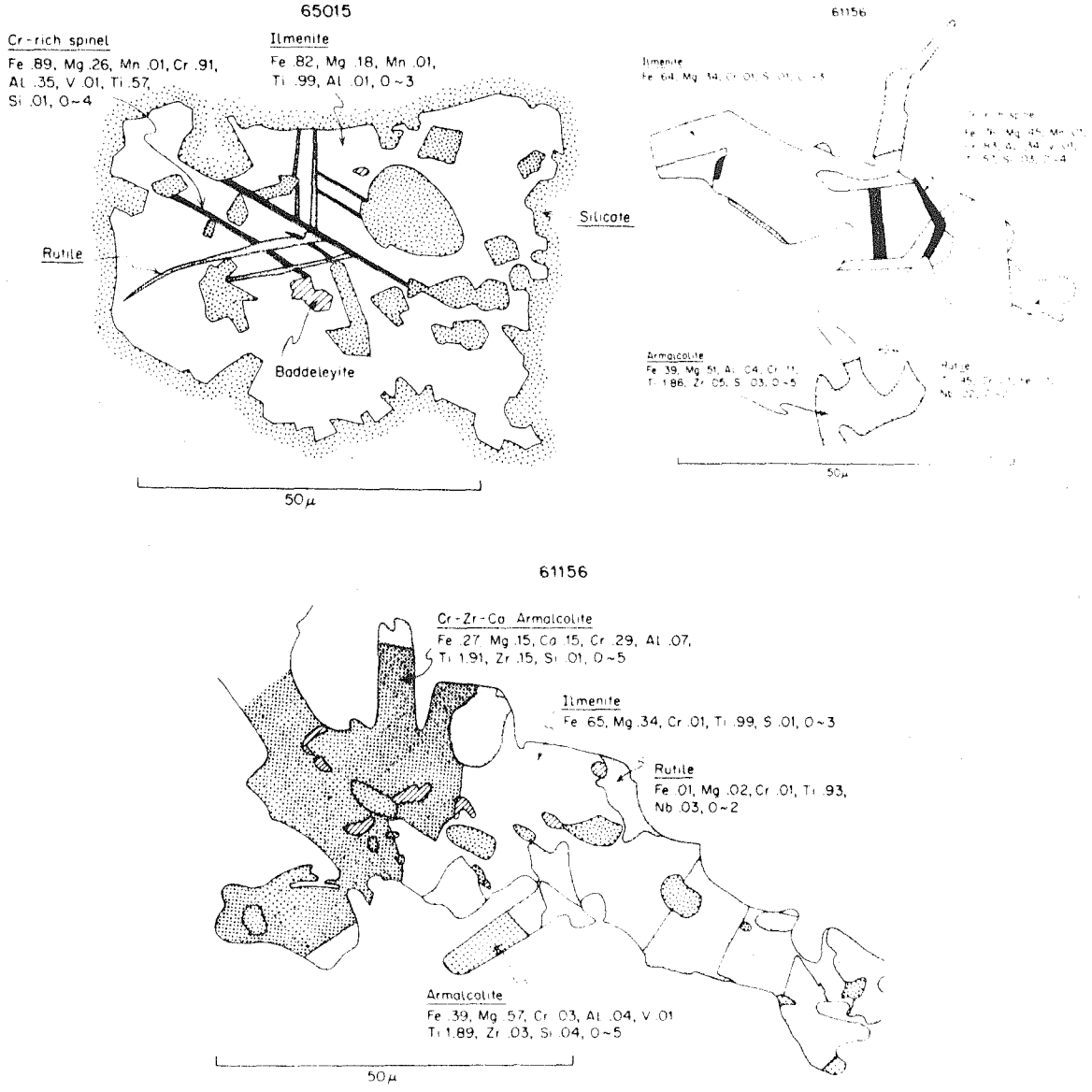

Fig. 5. Complex oxide associations in Apollo 16 samples, with formulae for representative analyses.

plagioclase clasts. The anorthite-poor group includes granules and laths from the matrix and overgrowths on large plagioclase clasts. The low-Ca pyroxene also tends to fall into two compositional groups: a lower-Ca, higher-Mg group and a higher-Ca, lower-Mg group. Many, but not all of the lower-Ca, higher-Mg group are analyses of pyroxene grains projecting into the vugs. The range in Fe/Mg is similar in all the ferromagnesian silicates.

K-rich material occurs in small patches ($< 15\ \mu$m) distributed throughout the rock, but external to the oikocrysts. Chemical composition (Table 2) and optical properties suggest that it is devitrified glass. Table 2 indicates that about 40 percent of the K in this rock is contained in the K-rich material and about 60 percent in plagioclase.

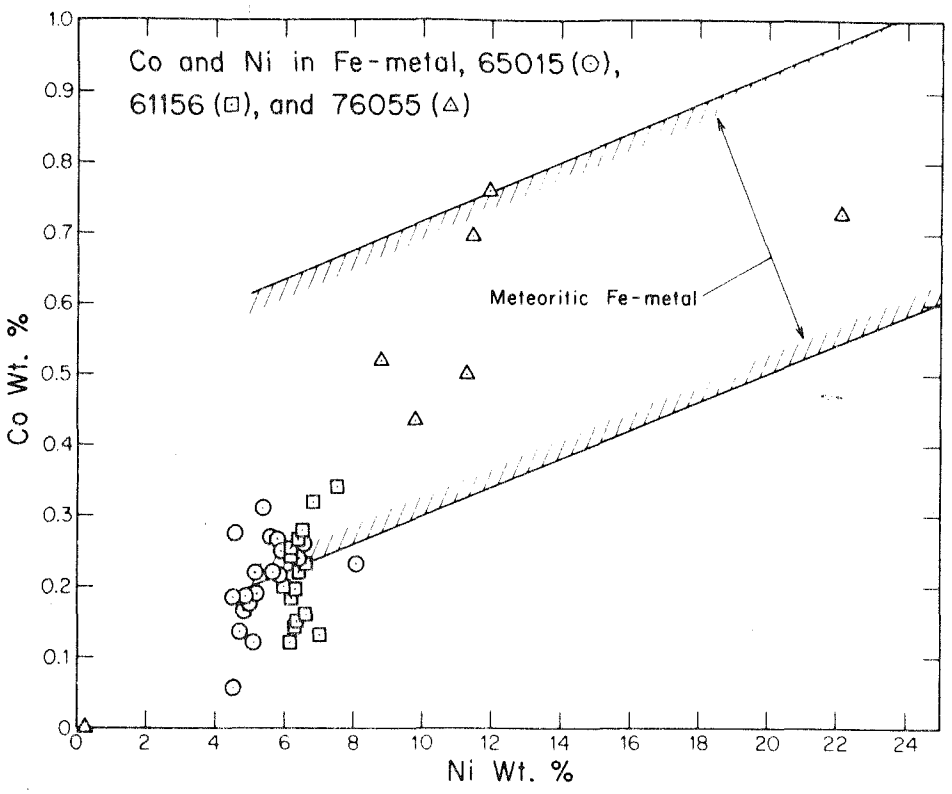

Fig. 6. Co and Ni content of Fe-metal in Apollo 16 samples 61156 and 65015 and Apollo 17 sample 76055. The field of meteoritic Fe-metal is from Goldstein and Yakowitz (1971).

The opaque minerals include armalcolite, ilmenite, Cr-rich spinel, rutile, baddeleyite, Fe-metal, troilite, and schreibersite. Armalcolite occurs as small independent grains or, more commonly, in a complex association with ilmenite, Cr-rich spinel, rutile, and baddeleyite. Two such associations are shown in Fig. 5 along with formulae for representative analyzed points. Armalcolite tends to occur on the extremities of sheafs of ilmenite blades, which contain lamellae of rutile and Cr-spinel and globules of baddeleyite. Two compositions of armalcolite occur (*see also* Haggerty, 1973); the ilmenite is high in Mg and low in Zr, and the rutile contains Nb and Zr. The association appears to represent breakdown of some preexistent phase, possibly armalcolite, or exsolution from ilmenite (Haggerty, 1973). In either case, it suggests slow cooling.

Troilite and Fe-metal occur both as independent grains and in association with one another. The Fe-metal has a rather uniform composition just within the meteoritic range of composition (Fig. 6). Schreibersite occurs as inclusions within and as small rims on Fe-metal. Typically Fe-metal globules are surrounded by a rim of plagioclase-rich rock depleted in pyroxene and commonly rimmed and embayed by Ca-phosphate grains. Goldstein *et al.* (1972) suggested that phosphates in the rock are reduced and P combines with Fe-metal at high temperature to form phosphides. The feature described here may represent the reverse process during slow cooling.

Sample 64423,14-2

This sample is a 0.031 g fragment from the 2–4 mm fraction of soil sample 64423,14, which was collected from the bottom of the trench at Station 4. It was studied in a 4 mm^2 micro-thin section (FQM-195) which was made from a portion of the sample prior to irradiation for ^{40}Ar–^{39}Ar measurements.

Table 2. 61156,31 Phase abundances, "average" phase compositions, and bulk-chemical composition.

	Plagioclase	Low-Ca pyroxene	Olivine	High-Ca pyroxene	K-rich interstitial material	Armalcolite	Ilmenite	Cr-spinel	Rutile	Fe-metal*	Apatite	Whitlockite	Troilite	Bulk composition	
vol.%	$62.1_2 \pm 1.7_7$	$20.6_0 \pm 1.4_2$	$10.2_0 \pm 0.7_2$	$5.1_3 \pm 0.5_1$	$0.6_0 \pm 0.1_7$		$0.5_4 \pm 0.1_7$			$0.3_5 \pm 0.1_3$		$0.3_0 \pm 0.1_2$	$0.1_4 \pm 0.0_9$	Calculated	LSPET
wt.%	55.4_9	23.0_9	12.9_2	5.6_3	0.5_7		0.8_6			0.9_1		0.3_1	0.22	1990 points	(1973)
						0.215^+	0.215^+	0.215^+	0.215^+		0.16^+	0.16^+			
SiO_2	45.08	52.24	37.17	50.82	65.98	0.35	0.36	0.91	0.31	0.05	0.71	0.59	0.11	45.12	44.65
Al_2O_3	35.37	1.48	0.14	2.82	19.73	1.12	0.14	8.63	0.09	n.a.	0.06	0.64	n.a.	20.28	22.94
Cr_2O_3	n.a.	0.46	0.15	0.77	n.a.	1.20	0.31	31.12	0.67	n.a.	n.a.	n.a.	n.a.	0.24	0.10
TiO_2	n.a.	0.74	0.05	2.10	0.32	71.73	55.55	22.38	94.88	n.a.	n.a.	n.a.	n.a.	0.82	0.64
MgO	0.14	26.17	38.82	16.81	0.01	9.91	9.29	8.94	0.07	0.01	0.25	6.12	n.a.	12.15	9.60
FeO	0.44	15.52	23.21	7.42	0.13	13.34	34.01	27.06	0.46	93.73	0.18	1.98	61.86	8.68	7.75
MnO	n.a.	0.26	0.17	0.19	n.a.	0.06	0.33	0.52	<0.01	n.a.	n.a.	n.a.	n.a.	0.09	0.12
CaO	18.74	3.38	0.24	19.53	2.93	n.a.	n.a.	n.a.	n.a.	0.01	53.56	38.03	0.13	12.47	13.34
Na_2O	0.65	0.06	n.a.	0.16	0.16	n.a.	n.a.	n.a.	n.a.	n.a.	0.01	0.39	n.a.	0.39	0.39
K_2O	0.13	n.a.	n.a.	n.a.	9.19	n.a.	n.a.	n.a.	n.a.	n.a.	n.a.	n.a.	n.a.	0.12	0.11
BaO	0.08	n.a.	n.a.	n.a.	0.40	n.a.	n.a.	n.a.	n.a.	n.a.	n.a.	n.a.	n.a.	0.05	0.02
P_2O_5	n.a.	n.a.	n.a.	n.a.	n.a.	n.a.	n.a.	n.a.	n.a.	0.02	39.52	40.90	0.01	0.13	0.22
ZrO_2	n.a.	n.a.	n.a.	n.a.	n.a.	2.12	0.04	0.02	1.34	n.a.	n.a.	n.a.	n.a.	0.01	0.03
V_2O_3	n.a.	n.a.	n.a.	n.a.	n.a.	0.12	0.02	0.33	0.02	n.a.	n.a.	n.a.	n.a.	<0.01	n.r.
Nb_2O_5	n.a.	n.a.	n.a.	n.a.	n.a.	n.a.	n.a.	n.a.	1.38	n.a.	n.a.	n.a.	n.a.	<0.01	<0.01
Ni	n.a.	n.a.	0.05	n.a.	n.a.	n.a.	n.a.	n.a.	n.a.	6.26	n.a.	n.a.	0.01	0.06	0.02
Co	n.a.	n.a.	n.a.	n.a.	n.a.	n.a.	n.a.	n.a.	n.a.	0.15	n.a.	n.a.	n.a.	<0.01	n.r.
F	n.a.	n.a.	n.a.	n.a.	n.a.	n.a.	n.a.	n.a.	n.a.	n.a.	3.10	0.01	n.a.	<0.01	n.r.
Cl	n.a.	n.a.	n.a.	n.a.	n.a.	n.a.	n.a.	n.a.	n.a.	—	0.74	0.01	n.a.	<0.01	n.r.
S	n.a.	n.a.	n.a.	n.a.	n.a.	n.a.	n.a.	n.a.	n.a.	<0.01	n.a.	n.a.	37.07	0.08	0.12
$\Sigma RE_2O_3+Y_2O_3$	n.a.	n.a.	n.a.	n.a.	n.a.	n.a.	n.a.	n.a.	n.a.	n.a.	2.55	5.93	—	0.01	n.r.
Total	100.63	100.31	100.00	100.62	98.85	99.95	100.05	99.91	99.22	100.21	100.68	94.60	99.19	100.70	100.05
	An 91	En 71	Fo 75	En 49											
	Ab 6	Fs 24	Fa 25	Fs 13											
	Or 1	Wo 5		Wo 38											
	Others 2														

*Elemental abundances.
n.a.=Not analyzed.
n.r.=Not reported.
$^+$=Values used for calculating bulk composition.

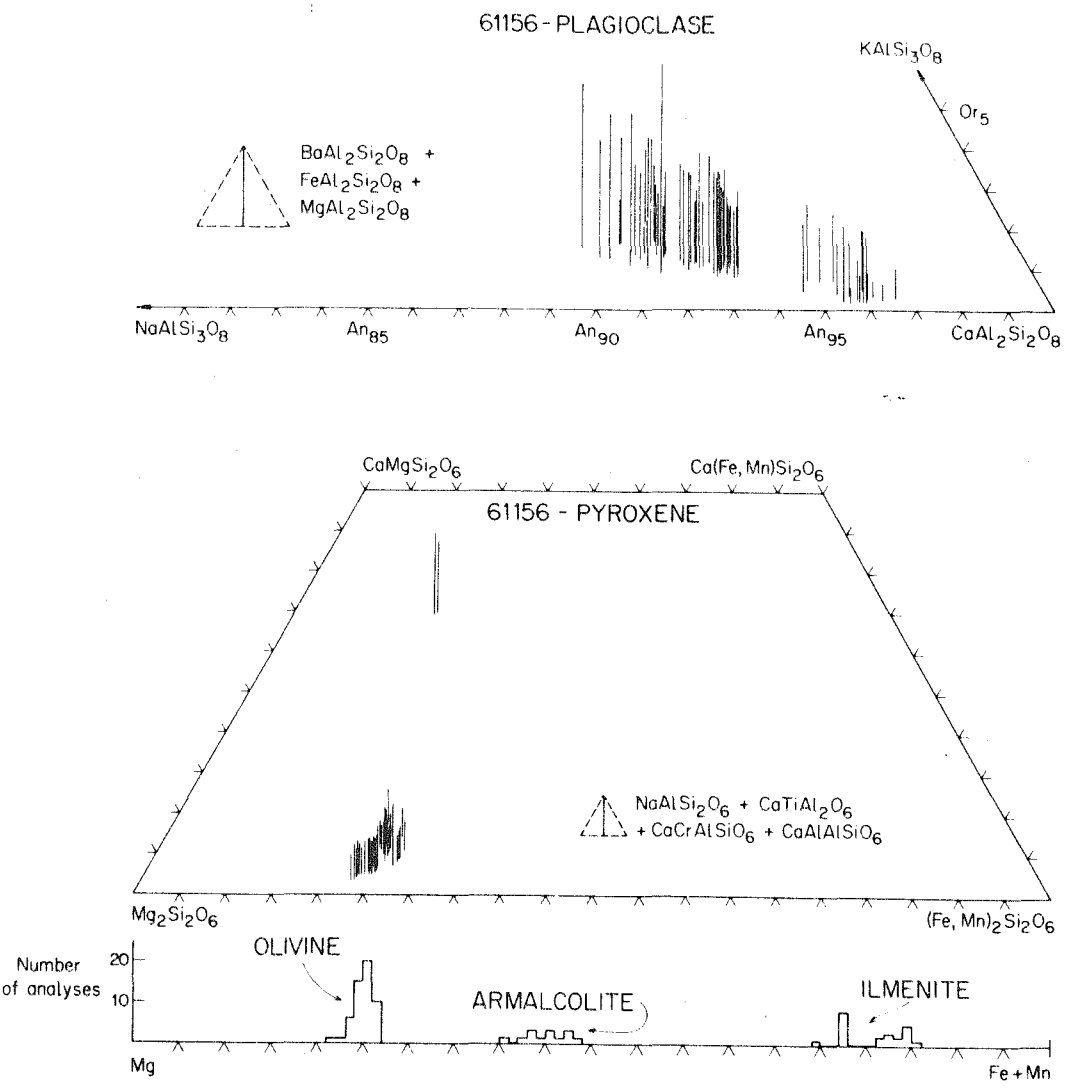

Fig. 7. Composition of the major mineral phases in Apollo 16 sample 61156.

The fragment is a fine-grained rock quite similar to 65015. An optical point-count (600 points) indicates that it is composed predominantly of plagioclase (59%), low-Ca pyroxene (27%) and olivine (12%) with minor ilmenite, Fe-metal, and troilite. About 10 percent of the rock consists of equant, 100–300 μm plagioclase grains, but most of the plagioclase is finer-grained (10–40 μm) and many of the smaller grains are lath shaped. No sharp break in grain size delineates the larger grains from the others. The larger grains are probably clasts, but they do not show well-developed reaction rims. No lithic clasts are present in this small thin section. Olivine occurs as equant grains (~ 50 μm) and ilmenite as laths about 60 μm in length. Low-Ca pyroxene forms irregular oikocrysts up to 350 μm, enclosing the smaller plagioclase and olivine grains and partially enclosing the larger plagioclase grains.

The major phases are quite homogeneous in composition (Fig. 8) and low-Ca pyroxene and olivine have nearly identical Fe/Mg values. Troilite and Fe-metal are more abundant than ilmenite. One ilmenite grain contains about 8.1 wt.% MgO and also includes abundant lamellae of Nb- and Zr-rich rutile, suggesting the possibility that it formed by recrystallization of armalcolite.

Sample 67483,15-2

Sample 67483,15-2 was a fragment from the 2–4 mm fraction of soil sample 67480 collected at Station 11 on the edge of North Ray Crater. A micro-thin section (FQM-197) was prepared from a portion of the fragment irradiated for ^{40}Ar–^{39}Ar measurements.

The thin section (area ~ 5 mm^2) is quite similar to Luna 20 sample 22007 and the extent of intergranular reaction in the matrix seems quite limited. Nearly half the sections consist of large plagioclase clasts, an anorthositic clast, and two globules of Fe-metal. No well-developed reaction rims occur on the clasts. The fine-grained metaclastic matrix consists predominantly of very fine-grained plagioclase and pyroxene, with sheaves of ilmenite and armalcolite and very fine opaque particles.

Sample 76055

Sample 76055 was a 6389 g, 23 × 13 × 13 cm loose block collected from the regolith surface at Station 6. Boulder tracks demonstrate that some of the larger boulders at this site rolled down from North Massif. Zap pits (0.3 to 3 mm) are absent on the inferred bottom of the block, but are abundant on other surfaces. The inferred top surface has a 1 cm circular glass splash.

As described in the catalogue, about 10 percent of the block consists of medium dark-gray, irregular, lens-like pods (10–35 mm in length) of fine-grained metaclastic rock. These are within a somewhat coarser-grained, greenish-gray matrix, which contains slit-like cavities (1–20 mm long) lined by crystals

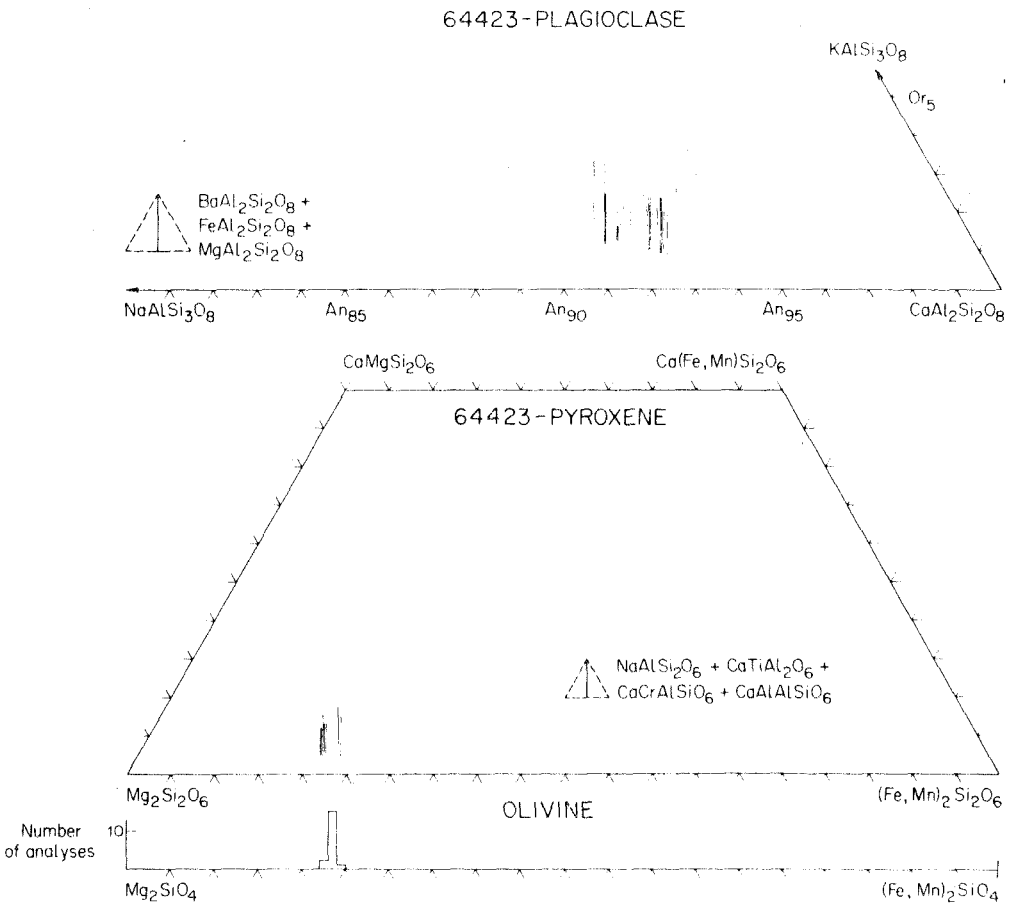

Fig. 8. Composition of the major mineral phases in Apollo 16 sample 64423,15-2.

of plagioclase, pyroxene, opaques, metal, and sulphide. The cavities form a foliation, which curves around the pods. About 5 percent of the matrix consists of mineral and lithic clasts (1–10 mm), including polycrystalline olivine(?), plagioclase, olivine, and aphanitic rock.

The sample was studied in polished thin section 76055,7 which has an area of about 350 mm^2. The thin section contains an ovoid area about 18×7 mm of a non-vesicular, poikilitic, metaclastic rock with the abundant elongate holes of the vesicular, non-poikilitic metaclastic rocks wrapping around the ovoid area (Fig. 1c). The two lithologies are distinctly different and are separated by a sharp boundary. It seems likely that the ovoid area of metaclastic rock is itself a clast. These two lithologies apparently correspond to those described in the original sample and will be described separately.

The non-vesicular pod is similar to sample 65015 described above. About 10 percent of the rock consists of subangular plagioclase and olivine clasts (50 to 500 μm) set in a finer-grained poikilitic metaclastic matrix. Lithic clasts are absent except for a few polygranular-plagioclase clasts. Many of the plagioclase clasts have overgrowths marked by a string of tiny olivine granules. The matrix consists of finer-grained plagioclase and olivine clasts and plagioclase laths (5–20 μm in length). These are poikilitically enclosed in a polygonal mosaic of low-Ca pyroxene oikocrysts (200–500 μm).

The non-poikilitic, vesicular portion of the thin section, excluding about 15 percent vugs, contains about 15 percent of mineral fragments (50–750 μm) and about 5 percent of rock fragments (50–1000 μm) set in a finer-grained, non-poikilitic metaclastic matrix. The mineral fragments are predominantly plagioclase, olivine, and high-Ca pyroxene. Lithic fragments include "spherulite" (11 fragments), intersertal feldspathic-basalt similar to 14310 (6) (Fig. 4a), poikilitic metaclasite (4), and anorthosite (2). Most of the "spherulite" clasts consist of radiating, acicular feldspar crystals (Fig. 4b) with the bulk composition (Table 4) of a K-rich calcic-plagioclase.

Tables 3 and 4 give the modes, "average" mineral compositions, and calculated bulk-chemical compositions for the poikilitic, non-vesicular portion and the non-poikilitic, vesicular portion of the thin section. Despite distinctive textural differences, the mineralogy, modal abundances, and bulk compositions of the two portions of the sample are quite similar. They differ mainly in the higher abundance of olivine and lower abundance of opaque minerals in the non-vesicular portion.

Mineral analyses from the two portions of the rock are illustrated in Figs. 9 and 10. Most of the analyses of matrix plagioclase in the non-vesicular portion have an An-content greater than 90 percent and the points with lower anorthite content are from an overgrown clast with a lower An-content core and a higher An-content rim. However, most of the analyses of matrix plagioclase in the vesicular portion have an An-content less than 90 percent and the points with higher anorthite content are from clasts. Low-Ca pyroxene, olivine, and armalcolite have rather similar compositions in both portions of the rock. High-Mg olivine points in the non-vesicular portion are from granules within a plagioclase clast at the contact of the higher-An rim. The more Fe-rich of the two high-Ca pyroxene analyses is from a clast whereas the other is from the matrix. The calculated bulk compositions (Tables 3 and 4) indicate that plagioclase contains about 80 percent of the K in the non-vesicular portion and about 70 percent in the vesicular portion with the remainder in the "spherulite" fragments.

Armalcolite occurs in complex intergrowths with ilmenite and rutile in the vesicular portion, but only minor armalcolite without ilmenite occurs in the non-vesicular portion. Fe-metal has a composition within the meteoritic range (Fig. 6) and has a considerable range in Co and Ni content. Schreibersite is associated with the Fe-metal and, as in 61156, Ca-phosphate is concentrated around the Fe-metal. Tiny wires of Fe-metal with high Ni and Co contents project into vesicles.

Samples 22006 and 22007

Samples 22006 and 22007 were very small metaclastic samples returned by the Luna 20 unmanned probe and described and figured previously (Podosek *et al.*, 1973; Laul and Schmitt, 1973). 22006 contains a few clasts of plagioclase and polygonal anorthosite set in a granular groundmass of 25–40 μm grains of plagioclase, pyroxene, olivine and anastomosing aggregates of ilmenite crystals. The limited compositional range of the major phases is illustrated in Fig. 11.

The difference in the Ca content between the low-Ca and high-Ca pyroxene in this sample is less than in any of the other metaclastic rocks described here. The assumption that the two pyroxene phases equilibrated would indicate that this rock was metamorphosed at the highest temperature of these samples.

Table 3. 76055,7 Non-vesicular breccia pod-phase abundances, "average" phase composition and bulk-chemical composition.

	Plagioclase	Olivine	Low-Ca Pyroxene	High-Ca Pyroxene	K-rich interstitial material	Armalcolite	Fe-metal*	Apatite	Whitlockite	Bulk Composition
vol.%	$48.3_4 \pm 1.7_4$	$24.2_3 \pm 1.2_3$	$21.9_7 \pm 1.1_7$	$4.2_1 \pm 0.5_1$	$0.7_5 \pm 0.2_2$	$0.3_1 \pm 0.1_4$	$0.1_3 \pm 0.0_9$	$0.0_6 \pm 0.0_6$		(1573 points)
wt.%	41.2_5	29.3_2	23.5_2	4.4_1	0.6_7	0.4_5	0.3_2	0.0_3	0.0_3	
SiO_2	44.51	39.17	54.49	50.69	46.36	0.28	0.08	0.46	0.35	45.2_1
Al_2O_3	35.11	0.12	1.74	2.57	33.19	1.01	n.a.	1.56	0.05	15.2_7
Cr_2O_3	n.a.	0.06	0.69	0.60	0.05	2.20	0.01	n.a.	n.a.	0.2_2
TiO_2	0.04	0.13	1.09	2.20	0.33	70.88	0.02	n.a.	n.a.	0.7_3
MgO	0.12	41.51	29.18	16.85	0.16	8.26	0.04	0.25	3.37	19.8_7
FeO	0.21	19.35	10.90	6.34	0.33	14.36	86.37	0.22	0.64	9.0_3
MnO	n.a.	0.15	0.14	0.14	<0.01	0.13	<0.01	n.a.	n.a.	0.0_8
CaO	19.31	0.24	2.60	20.06	17.29	n.a.	0.01	53.12	42.39	9.6_4
Na_2O	0.69	n.a.	0.02	0.13	0.83	n.a.	n.a.	0.04	0.61	0.3_0
K_2O	0.10	n.a.	n.a.	n.a.	1.35	n.a.	n.a.	n.a.	n.a.	0.0_5
BaO	0.01	n.a.	n.a.	n.a.	0.09	n.a.	n.a.	n.a.	n.a.	$<0.0_1$
P_2O_5	n.a.	n.a.	n.a.	n.a.	0.01	n.a.	0.06	40.15	42.66	0.0_3
ZrO_2	n.a.	n.a.	n.a.	n.a.	<0.01	1.78	n.a.	n.a.	n.a.	0.0_1
V_2O_3	n.a.	n.a.	n.a.	n.a.	n.a.	0.12	n.a.	n.a.	n.a.	$<0.0_1$
Ni	n.a.	0.03	n.a.	n.a.	n.a.	n.a.	11.97	n.a.	n.a.	0.0_5
Co	n.a.	n.a.	n.a.	n.a.	n.a.	n.a.	0.76	n.a.	n.a.	$<0.0_1$
F	n.a.	n.a.	n.a.	n.a.	n.a.	n.a.	n.a.	3.70	0.06	$< 0.0_1$
Cl	n.a.	n.a.	n.a.	n.a.	n.a.	n.a.	n.a.	0.09	0.02	$< 0.0_1$
$\Sigma RE_2O_3 + Y_2O_3$	n.a.	n.a.	n.a.	n.a.	n.a.	n.a.	n.a.	0.67	9.80	$<0.0_1$
Total	100.09	100.76	100.85	99.58	99.99	99.02	99.32	100.25	99.95	100.53
	An 92	Fo 79	En 80	En 50						
	Ab 6	Fa 21	Fs 17	Fs 11						
	Or 1		Wo 3	Wo 39						
	Others 1									

*Elemental abundances.
n.a. = Not analyzed.

Table 4. 76055,7 Vesicular breccia-phase abundances, "average" phase composition and bulk-chemical composition.

	Plagioclase	Low-Ca Pyroxene	Olivine	High-Ca Pyroxene	Spher-ulite	Armalcolite	Fe-metal*	Apatite	Whitlockite	Bulk composition Calculated	Bulk composition LSPET (1973)
vol.%	$48.5_1 \pm 1.6_5$	$24.0_0 \pm 1.1_6$	$18.1_0 \pm 1.0_1$	$5.8_5 \pm 0.5_7$	$2.0_8 \pm 0.3_4$	$0.8_4 \pm 0.2_2$	$0.3_4 \pm 0.1_4$	$0.2_8 \pm 0.1_3$		(1779 points)	
wt.%	41.6_7	25.8_6	22.0_5	6.1_8	1.8_8	1.2_3	0.8_5	0.1_4	0.1_4		
SiO_2	44.77	53.43	38.69	50.69	46.03	0.30	0.08	0.46	0.35	45.0_1	44.65
Al_2O_3	35.22	1.55	1.04	2.57	33.16	1.33	n.a.	1.56	0.05	16.1_1	16.47
Cr_2O_3	n.a.	0.53	0.19	0.60	0.17	1.90	0.01	n.a.	n.a.	0.2_4	n.a.
TiO_2	0.14	1.23	0.20	2.20	0.37	70.45	0.02	n.a.	n.a.	1.4_2	1.24
MgO	0.10	28.25	39.14	16.85	0.16	8.39	0.04	0.24	3.37	17.1_3	16.33
FeO	0.15	12.48	20.20	6.34	0.33	14.41	86.37	0.22	0.64	9.2_6	9.11
MnO	n.a.	0.29	0.19	0.14	n.a.	0.10	<0.01	n.a.	n.a.	0.1_3	0.11
CaO	19.00	2.36	0.44	20.06	16.85	n.a.	n.a.	53.12	42.39	10.3_1	9.93
Na_2O	0.83	0.04	n.a.	0.13	1.07	n.a.	n.a.	0.04	0.61	0.3_0	0.48
K_2O	0.14	n.a.	n.a.	n.a.	1.07	n.a.	n.a.	n.a.	n.a.	0.0_8	0.20
BaO	<0.01	n.a.	n.a.	n.a.	n.a.	n.a.	n.a.	n.a.	n.a.	$<0.0_1$	n.r.
P_2O_5	n.a.	n.a.	n.a.	n.a.	0.06	n.a.	0.06	40.15	42.66	0.1_2	0.19
ZrO_2	n.a.	n.a.	n.a.	n.a.	<0.01	2.25	n.a.	n.a.	n.a.	0.03_3	n.r.
V_2O_3	n.a.	n.a.	n.a.	n.a.	n.a.	0.04	n.a.	n.a.	n.a.	$<0.0_1$	n.r.
Ni	n.a.	n.a.	0.02	n.a.	n.a.	n.a.	11.97	n.a.	n.a.	0.1_1	n.r.
Co	n.a.	n.a.	n.a.	n.a.	n.a.	n.a.	0.76	n.a.	n.a.	0.1_1	n.r.
F	n.a.	n.a.	n.a.	n.a.	n.a.	n.a.	n.a.	3.70	0.06	0.0_1	n.r.
Cl	n.a.	n.a.	n.a.	n.a.	n.a.	n.a.	n.a.	0.09	0.02	$<0.0_1$	n.r.
$\Sigma RE_2O_3 + Y_2O_3$	n.a.	n.a.	n.a.	n.a.	n.a.	n.a.	n.a.	0.67	9.8	0.0_1	n.r.
Total	100.35	100.16	100.11	99.58	99.27	99.17	99.31	100.25	99.95	100.31	98.71
	An 91	En 77	Fo 77	En 50							
	Ab 7	Fs 20	Fa 23	Fs 11							
	Or 1	Wo 3		Wo 39							
	Others 1										

*Elemental abundances.
n.a.=Not analyzed.
n.r.=Not reported.

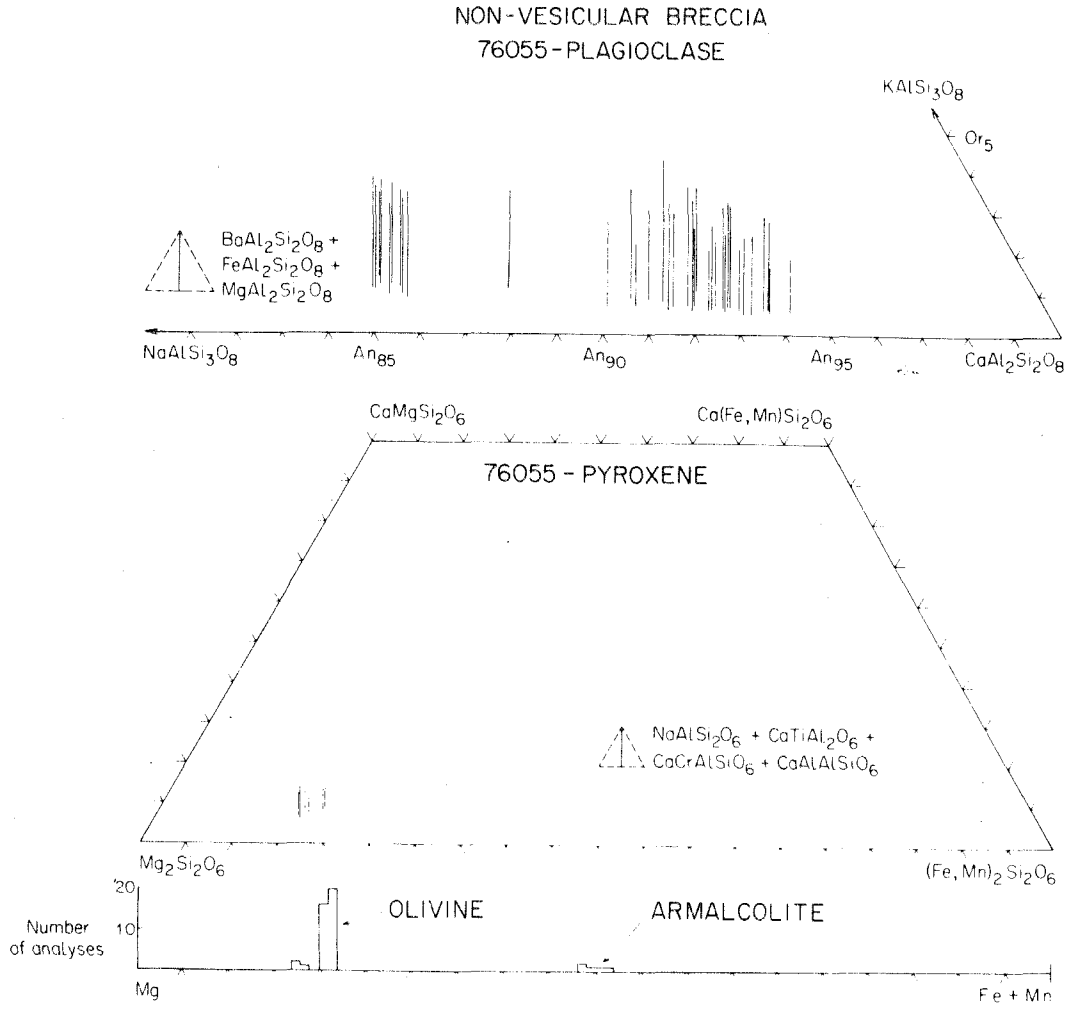

Fig. 9. Composition of the major mineral phases in non-vesicular, poikilitic portion of Apollo 17 sample 76055.

22007 is also a metaclastic rock, but it has a distinctly different texture. It contains subangular plagioclase clasts (to 200 μm) and rare anorthositic and troctolitic clasts set in a very fine-grained matrix. The semi-opaque matrix is composed of small laths of plagioclase surrounded by submicron-size particles of ferromagnesian silicate, and opaque minerals. Although intergranular reaction during metamorphism was apparently quite limited in this rock, the lath form of the groundmass plagioclase crystals indicates that they are recrystallization products rather than clasts.

Isotopic Evidence for the Time Nature and Extent of Metamorphism

The samples described in this paper include all those metaclastic rocks from the Apollo 16 and 17 and Luna 20 landing sites on which our colleagues have undertaken ^{40}Ar–^{39}Ar or Rb–Sr age measurements. It seems important that rocks from such different locations exhibit similar isotopic as well as petrologic and mineralogic characteristics. These are summarized in Table 5.

Table 5. Characteristics of dated metaclastic sample from Apollo 16 and 17 and Luna 20.

	61156	64423,14-2	65015	67483,15-2	76055 Vesicular	76055 Non-vesicular	22006 Luna 20	22007 Luna 20
^{40}Ar–^{39} = Time of metamorphism	?		3.94 ± 0.04 b.y.	3.93 ± 0.04 b.y.	3.98 ± 0.05 b.y.†	3.98 ± 0.05 b.y.†	3.90 ± 0.04 b.y.	3.91 ± 0.04 b.y.
Rb–Sr evidence for partial reequilibration	?		+	?	+	?	?	?
K content (ppm)*	1000		3000	1700	1650	?	1200	1800
Clast types								
Intersertal basalt	–	–	+	–	+	–	–	–
Anorthositic suite	+	–	+	+	+	–	+	+
Felsite	+	–	+	–	+	–	–	–
Mineral clasts	+	+	+	+	+	+	+	+
Texture								
Poikilitic low-Ca pyroxene	+	+	+	–	–	+	–	–
Extent of matrix recrystallization	very strong	extreme	extreme	weak	strong	extreme	strong	moderate
Relic cores in plagioclase	+	–	+	–	–	+	+	–
Complex oxide associations	+	+	+	–	+	–	–	–
Cavities	+	–	–	+	+	–	–	+
Ca-phosphate bordering Fe-metal	+	?	?	?	+	?	?	?
Mineralogy								
Pyroxene ●							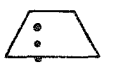	
Olivine ■								
Plagioclase	An_{87-96}	An_{88-93}	An_{88-96}	?	An_{83-94}	An_{83-94}	An_{86-95}	An_{89-95}
Ilmenite	+	+	+	+	–	–	+	+
Armalcolite	+	–	–	+	+	+	–	–
Fe-metal globules	+	–	+	+	+	+	–	–

*LSPET (1973); J. C. Huneke (oral communication, April, 1973)
†Turner *et al.* (1973).

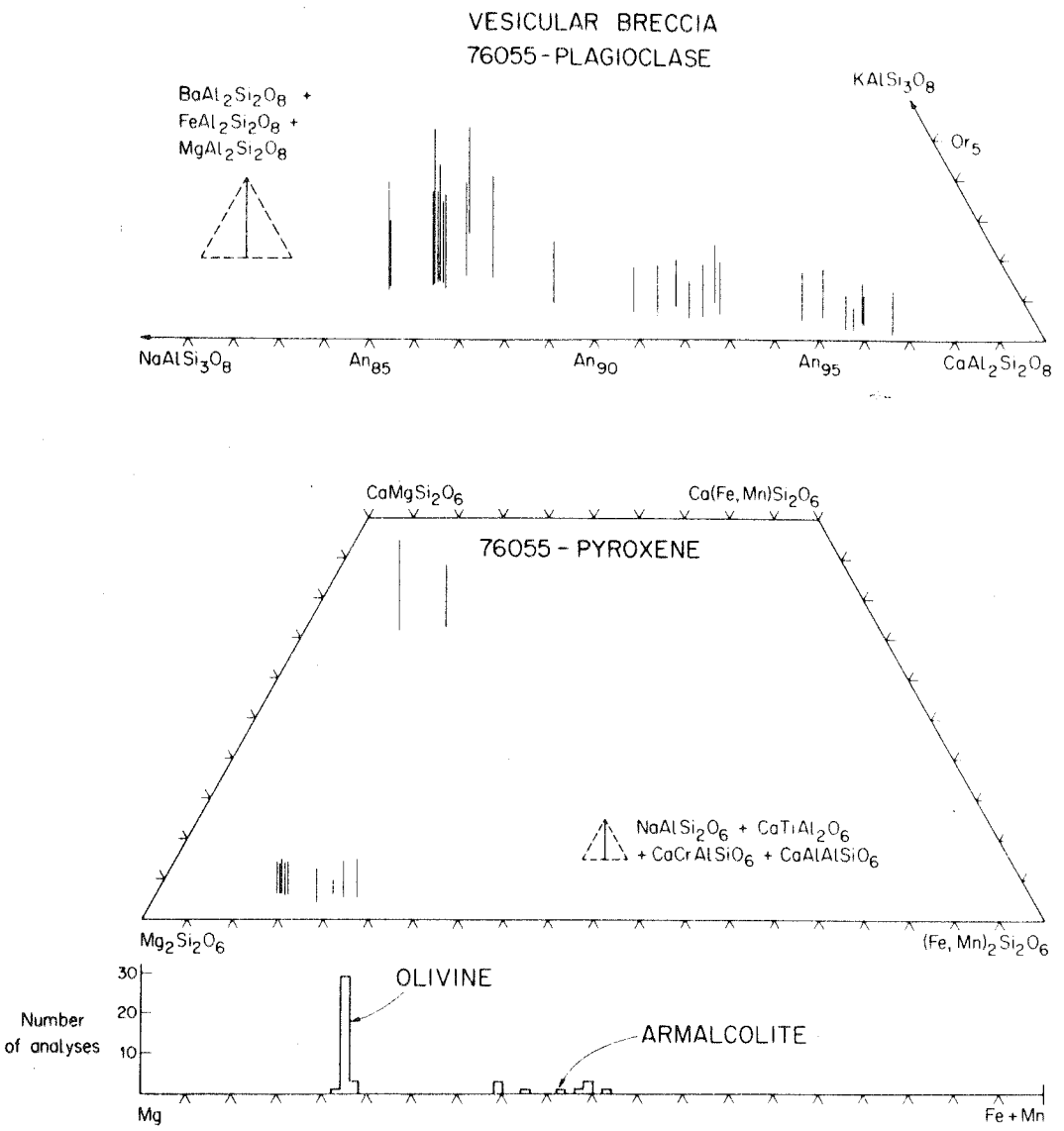

Fig. 10. Composition of the major mineral phases of vesicular, non-poikilitic portion of Apollo 17 sample 76055.

Stepwise heating ^{40}Ar–^{39}Ar measurements have been undertaken on all of these samples except 61156 and 64423,14–2 (Podosek *et al.*, 1973; Huneke *et al.*, 1973 a, b; Turner *et al.*, 1973; Huneke, personal communication, April, 1973). In general the release patterns are indicative of ages ranging from 3.90 b.y. to 3.98 b.y. (*see* Table 5), and do not exhibit well-defined older components. Since the evidence from the calculated bulk-chemical compositions shows that significant percentages (from about 10 to 80 percent) of the K resides in plagioclase, the lack of such older components in the release patterns suggests that during the metamorphism the rocks were extensively recrystallized or heated such that most

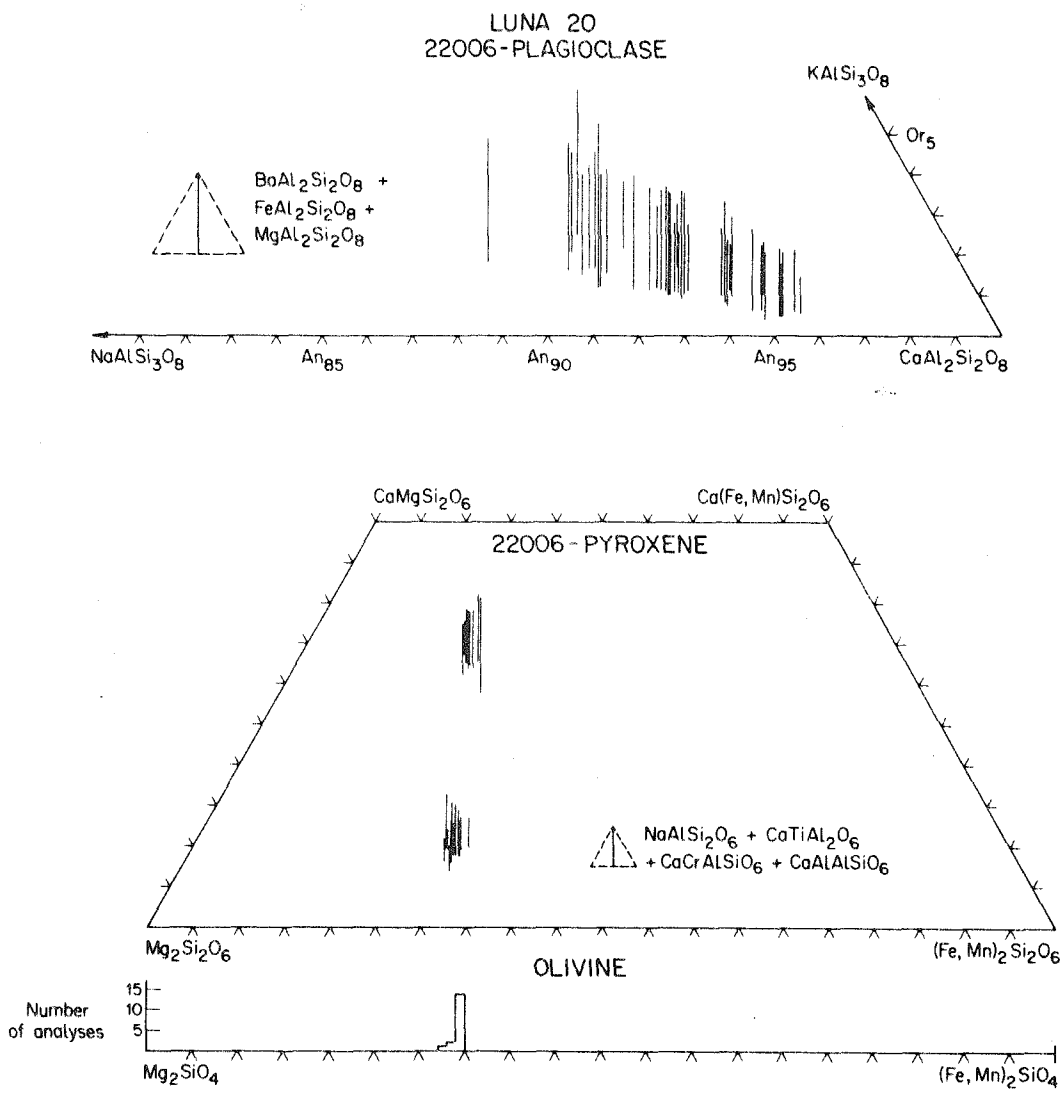

Fig. 11. Composition of the major mineral phases of Luna 20 sample 22006.

of the Ar was lost even from the apparently unrecrystallized cores of the larger plagioclase clasts. Alternatively relict Ar may be masked by Ar contributed from other phases.

Sample 65015 has been studied in detail by Rb–Sr isotopic techniques (Papanastassiou and Wasserburg, 1972; Tera *et al.*, 1973). ^{87}Rb–^{86}Sr and ^{87}Sr–^{86}Sr values for the total rock and mineral separates of pyroxene, pyroxene with 4 percent whitlockite, ilmenite, and K-rich separates form a linear array corresponding to an age of 3.92 b.y. and a $^{87}Sr/^{86}Sr$ intercept of 0.70003. This age is interpreted to represent the age of recrystallization and metamorphism. A plagioclase separate lies close to, but below this line, whereas a plagioclase, handpicked

to obtain the largest plagioclase clasts, lies much further below this line. These results indicate that the plagioclase clasts have not completely equilibrated with the matrix of the rock and agree with our petrographic observations. Similar, but less detailed results have been obtained on sample 76055 (D. A. Papanastassiou, oral communication, April, 1973) suggesting that only partial equilibration occurred and that it occurred at about 3.84 b.y. This age appears to differ from the ^{40}Ar–^{39}Ar age of 3.98 b.y., but each method requires various additional assumptions for partially re-equilibrated systems.

Sample 65015 has also been studied by U–Th–Pb isotopic techniques (Tera and Wasserburg, 1972). Based on plagioclase and total rock analyses, the data are interpreted to represent recrystallization and metamorphism at about 3.94 b.y.

Considering the errors and the assumptions involved in calculating ages from the isotopic data, the spread of isotopic ages could represent: (1) a single event occurring at about 3.95 b.y., (2) a single event marked by a range of possible cooling and recrystallization rates, or (3) a series of events within a rather short time span. Isotopic data, reported for a number of other Apollo 16 poikilitic metaclastic rocks, seem to indicate somewhat older ages (Husain and Schaeffer, 1973). However, a metaclastic rock with rather uniform-sized, small clasts containing relict Ar and with most of the K in plagioclase might contribute an older component over a wide temperature range yielding a relatively well-defined plateau and not show a well-defined, high-temperature, older component in the release pattern. Such results have been found in terrestrial rocks by Lanphere and Dalrymple (1971). This situation might also be responsible for the relatively old age (3.98 b.y.) for sample 76055.

DISCUSSION

Metaclastic rocks rich in low-Ca pyroxene and/or olivine, both poikilitic and non-poikilitic, are an important older lunar rock type and it will be necessary to understand the nature of both the protolith of such rocks and of the metamorphic processes which have affected them. The samples described here are from three landing sites—Apollo 16 and 17 and Luna 20—and numerous reports indicate that similar rocks are abundant at these sites (LSPET, 1973a,b; Cameron *et al.*, 1973; Kridelbaugh and Weill, 1973; Warner *et al.*, 1973; Bence *et al.*, 1973).

It is generally agreed that these rocks were polymict, clastic rocks that have undergone extensive, but not complete, intergranular reaction and recrystallization at high temperatures. Not generally agreed upon and without obvious answers are some important questions posed by these rocks:

(1) What was the exact nature of the clastic protolith, particularly the finer-grained, now completely-reacted, portion? Why are low-Ca pyroxene and olivine so abundant in these rocks?

(2) What was the nature of the metamorphism and the range of physical conditions?

(3) What fluid filled the cavities and vesicles? Was the presence of this fluid phase critical to intergranular reaction and oikocryst growth?

(4) How extensive was partial melting? Was the presence of a silicate melt critical to the intergranular reaction and oikocryst growth?

(5) Why are oikocrysts present in some samples and absent in others?

(6) Are these rocks related to KREEP-type rocks? If so, is it a parental or a derivative relationship?

(7) What was the cause of the metamorphism? How many events occurred? What was the total time span?

(8) What is the relation of these rocks to the highlands and to the early history of the moon?

Some of these questions will be discussed in the light of our observations, but it must be recognized that other similar rocks exhibit features not seen in the samples described in this paper (Bence *et al.*, 1973; Simonds *et al.*, 1973; oral communications with Bence and Warner, March, 1973).

Nature of the protolith

Despite extensive recrystallization the original nature of these rocks is clearly indicated by their texture—angular mineral and lithic clasts are set in a finer-grained matrix composed in part of smaller angular clasts. Most of the samples include such a variety of mineral and rock clasts that it is impossible to attribute the clastic texture simply to crushing of a homogeneous volcanic or plutonic rock. The most abundant lithic clasts are anorthositic rocks. Some of these are polygonal anorthosites, but many contain olivine or pyroxene as well as plagioclase. Samples 65015 and 76055 contain clasts of plagioclase-rich, intersertal basalt similar to 14310 and sample 76055 contains large pods, probably clasts, of poikilitic rock similar to 65015 in a non-poikilitic metaclastic matrix. Hence, each of the rock types included as clasts existed prior to the formation of the protolith and of its metamorphism.

Plagioclase is the dominant mineral clast. The grains are large and well-twinned and could be derived from the anorthositic rocks, but not from the basalts that occur as clasts. The olivine clasts could also be derived from anorthositic (troctolitic) rocks, but no source for the high-Ca pyroxene was observed as a lithic clast. Although some clasts show evidence of shock, a high degree of shock is not a general characteristic of the clasts. Glass clasts and balls, so abundant in many lunar breccias, are absent except possibly for a few "spherulite" clasts, which may be devitrified glass. However, they have a plagioclase-rich composition, atypical of glass fragments in most lunar clastic rocks. The Fe-globules and balls are larger than most of the grains and in some cases appear "corroded" or have a reaction border in the surrounding matrix suggesting that the globule form predates the metamorphism and that the globules are clastic in origin.

The fine-grained portion of the original clastic than is now a recrystallized aggregate of plagioclase, low-Ca pyroxene, and olivine, and its original mineralogy cannot be observed directly. It might be inferred that the matrix consisted of tiny fragments of these same minerals, but this seems unlikely since low-Ca pyroxene does not occur as large clasts or even as definite clasts at all. Many lunar clastic rocks or breccias contain abundant glass in the matrix to the clasts and it seems likely that the protolith of these rocks also contained glass, which has recrystallized during the metamorphism, producing the fine-grained, low-Ca pyroxene, plagioclase and olivine aggregates.

Nature of the metamorphism

The general similarity of the textures of these rocks to those of terrestrial granoblastic hornfels or metaclasites suggests that they have been thermally-metamorphosed, i.e., that they are like terrestrial rocks metamorphosed at high temperature without significant internal deformation. The oikocrysts of pyroxene are not unlike the porphyroblasts of cordierite and andalusite which commonly occur in terrestrial metaclasites. Similarly, (1) the overgrowths on the plagioclase clasts, (2) the corroded rims on olivine, high-Ca pyroxene, and Fe-metal clasts, (3) the depletion of pyroxene in plagioclase-rich zones bordering both Fe-metal globules and vesicles with low-Ca pyroxene crystals projecting into them, (4) the inferred general coarsening, and "cleaning-up" of the matrix—leading to a granoblastic texture, (5) the exclusion of K-rich material and ilmenite from the oikocryst and their concentration in the intervening matrix: all correspond to features seen in terrestrial metaclastics and are indicative of intergranular reaction and recrystallization without internal deformation.

The Ca contents of the coexisting pyroxene grains and the partition of Fe/Mg between low-Ca pyroxene and non-clastic recrystallized olivine indicate that temperatures were high and are compatible with the occurrence of partial melting. Slow cooling is suggested by subsolidus reactions of rutile and Cr-spinel with ilmenite, of rutile, ilmenite, and Cr-spinel with armalcolite, and of Ca-phosphate with Fe-metal. Bence *et al.* (1973) report exsolution in pyroxene in similar rocks.

In terrestrial rocks intergranular reaction is inferred to proceed in the presence of an intergranular film of volatile components and there is considerable doubt as to whether the textures in these rocks can form strictly by solid state reactions in a reasonable time scale—if at all. The abundant cavities and the crystals projecting into them suggest that some components of these rocks were volatile under the metamorphic conditions. The abundance of whitlockite and absence of apatite in 65015 suggest the possibility that F and Cl are lost by decomposition of apatite since most lunar rocks contain both phases. The possibility exists that other elements would then be lost as volatile halogen compounds. However, good evidence on the nature of the fluid phase forming the cavities and vesicles in lunar rocks is still lacking.

It also seems very likely that variable degrees of partial melting occurred

in these rocks. The presence of a fraction of a percent of intergranular melt can significantly increase the rate of intergranular reaction (Wong, 1972)—but it does raise the question of whether the process should be called metamorphism. Although not present in the samples described here, Bence *et al.* (1973) and Walker *et al.* (1973) described small pockets of diabasic-textured plagioclase–pyroxene material in poikilitic occurrence rocks and attributed them to the crystallization of small pockets of silicate melt. In these rocks the temperature may have been somewhat lower, but K-rich material, with a quartz-normative composition not corresponding to a phase, has concentrated in irregular interstitial areas in a number of these samples. In rock 12013, which is in many ways similar to these samples, such material has filled spherical vesicles (Lunatic Asylum, 1970). Such a composition could represent a very small degree of partial melting, the presence of which could greatly accelerate the rate of intergranular reaction.

Simonds *et al.* (1973) suggested that the euhedral nature of the fine-grained plagioclase laths and their common occurrence in the oikocrysts (*see* Fig. 4f) indicates growth in a melt. They also suggested that partial melting was very extensive, that the melting temperature of the oikocryst mineral was exceeded, and that the oikocrysts themselves grew in a melt. This explanation implies that the poikilitic metaclastic rocks were subjected to significantly higher temperatures than non-poikilitic metaclastic rocks of similar composition. Such poikilitic textures are typical of metamorphic rocks and a metamorphic origin for the lath-form of the plagioclase also seems possible. The degree of development of crystal faces depends upon the nature of both the crystal and its host and it is possible that plagioclase inclusions may develop crystal faces against pyroxene. In addition, the degree of development of crystal faces depends upon the nucleation and growth process and crystal faces would probably develop if the plagioclase nucleated prior to the growth of the pyroxene oikocryst.

In the samples described here the oikocrysts are predominantly low-Ca pyroxene with some high-Ca pyroxene, but most of the high-Ca pyroxene and olivine occurs as clasts or as grains not in optical continuity with one another. However, similar appearing oikocrysts of high-Ca pyroxene, olivine, or composite high-Ca, low-Ca pyroxene have been described in other samples (Bence *et al.*, 1973; Simonds *et al.*, 1973). Both poikilitic and non-poikilitic metaclastic rocks rich in low-Ca pyroxene appear to have quite similar compositions (*see* especially Tables 3 and 4 for sample 76055). Moreover, the fine-grained matrix of plagioclase and pyroxene appears quite similar regardless of whether the pyroxene grains are aligned in optical continuity. The development of oikocrysts could simply represent a greater response to the metamorphism, that is more time for, or more rapid, ordering or annealing of the independent grains, rather than different rock composition or metamorphic conditions. However, terrestrial porphyroblasts typically grow as the result of a reaction involving other phases rather than by recrystallization and reorientation of preexistent grains. Moreover, such an annealing process would be expected to be accompanied by the exclusion of the inclusions from the annealing porphyroblast.

The reasonable assumption that the original polymict breccia, like many lunar

breccia samples, contained a substantial amount of glass can explain many of the textural and chemical characteristics of these rocks. We would infer that the glass has a normative hypersthene–plagioclase–olivine composition and that its crystallization would yield the matrix of fine-grained plagioclase, pyroxene, and olivine. Euhedral plagioclase laths could nucleate and grow in the glass prior to the nucleation of low-Ca pyroxene, either as grains or oikocrysts. Partial melting would not be excluded. Indeed, a glass fragment of a particular composition, such as KREEP-type, could completely melt and phases crystallize from the melt in a small pocket like those described by Bence *et al.* (1973) while in the adjacent rock plagioclase laths could nucleate in a glass of slightly different composition followed by the growth of oikocrysts of low-Ca pyroxene. Slight differences in glass composition, glass distribution in the clastic rock or in kinetic factors could have determined whether oikocrysts grew or not and temperature differences could be quite unimportant. For example, the poikilitic "clast" in 76055 could be a glob of glass agglutinate metamorphosed within the metaclastic matrix rather than an actual clast.

The presence of a significant glass component in the protolith would significantly lower the required temperature below that required by the model of Simonds *et al.* (1973). Moreover, the contribution of heat of crystallization from the glass may be necessary to the attainment of extensive metamorphism and partial melting within an ejecta blanket.

Sample 65015 is high in K, U, Th (LSPET, 1973a), and Ba, REE, and P (Table 1) and has a composition similar to that of KREEP fragments (Meyer *et al.*, 1971). We have suggested (Albee *et al.*, 1973) that the most probable protolith of sample 65015 was a glassy agglutinate of mineral and lithic fragments cemented by KREEP glass. Subsequently it was extensively recrystallized with incipient melting of the interstitial K-rich material during sanidinite facies metamorphism at about 3.93 b.y. Such KREEP glass agglutinates are figured by Meyer *et al.* (1971) and glass agglutinates with various glass compositions have been returned from each landing site.

Many of the poikilitic metaclastic samples studied by Warner *et al.* (1973) and Simonds *et al.* (1973) have compositions relatively rich in K, P, and Ti, and they note that the composition of poikilitic rocks 60315 and 62235 (LSPET, 1973a) approach that of KREEP glass. As noted by Bence *et al.* (1973), *see also* Walker *et al.* (1972) partial melting of such a rock could lead to the production of KREEP liquids during the metamorphism. However, if our suggestion that these samples were KREEP-glass agglutinates is correct, then these rocks are peripheral to the major problem of the primary origin of KREEP-type rocks. However, partial melting during metamorphism could provide a means of "recycling" and distributing KREEP liquids during various metamorphic events.

CONCLUSIONS

Regardless of uncertainty about the extent of partial melting and about the exact origin of the poikilitic texture, this rock type clearly indicates the occur-

rence of some kind of metamorphic event or events at about 3.95 b.y. The metamorphism was clearly high temperature, may have involved a rather high degree of partial melting, and may be closely related to the formation of igneous rocks with the same age. The prevalence of this age, both in abundant metamorphic and igneous rocks at a number of sites and in limited samples from the other sites, and the apparent absence of significantly older rocks suggests that a wide area of the moon was either blanketed with material produced in an event at that time or that the near-surface rocks were extensively modified in place by the event (Podosek *et al.*, 1973).

The distribution, high temperature of metamorphism, slow cooling rate, and probability of extensive partial melting suggest that these rocks formed in thick, ejecta blankets from the Imbrium, Crisium, and possibly other events. Reid (in press) has discussed a mechanism involving tidal loss of satellites orbiting the moon which could result in multiple large events, nearly simultaneous, at about 3.95 b.y.

This veneer of metamorphic rocks has dominated the sampling at the highland landing sites and will interfere with the interpretation of chemical composition of the highlands from Orbiter data. Our understanding of earlier lunar history may have to be based in large part on petrologic and isotopic study of the clasts in these metaclastic rocks. Plagioclase-rich rocks dominate the clast population and it is evident that the anorthositic suite of rocks was widespread at the surface prior to the impact events producing the metamorphism. However, it is also notable that feldspathic, intersertal basalts occur as clasts.

Acknowledgments—We are indebted to our fellow inmates of the Lunatic Asylum for continued and invigorating discussions on the problems of these rocks. We are especially indebted to J. C. Huneke and F. A. Podosek for permission to include several ^{40}Ar–^{39}Ar ages in Table 5 in advance of publication. R. F. Dymek and D. S. Goldman provided valuable assistance in many aspects of the microprobe work. The manuscript was critically reviewed by R. F. Dymek, D. B. Stewart, and W. G. Melson. The research was supported by NASA contract NGL-05-002-188. The microprobe laboratory has been developed with the support of N.S.F., J.P.L., and The Union Pacific Foundation.

References

Albee A. L., Gancarz A. J., and Chodos A. A. (1973) Sanidinite facies metamorphism of Apollo 16 sample 65105 (abstract). In *Lunar Science—IV*, pp. 24–26. The Lunar Science Institute, Houston.

Bence A. E., Papike J. J., Sueno S., and Delano J. W. (1973) Pyroxene poikiloblastic rocks from Apollo 16 (abstract). In *Lunar Science—IV*, pp. 60–63. The Lunar Science Institute, Houston.

Cameron K. L., Papike J. J., Bence A. E., and Sueno S. (1973) Petrology of fine-grained rock fragments and petrologic implications of single crystals from the Luna 20 soil. *Geochim. Cosmochim. Acta* 37, 775–793.

Chodos A. A., Albee A. L., Gancarz A. J., and Laird J. (1973) Optimization of computer-controlled quantitative analysis of minerals. *Proc. Eight Annual Conference on Electron Probe Analysis.* In press.

Gancarz A. J. and Albee A. L. (1973). Microprobe analysis of the bulk composition of phase aggregates. *Proc. Eight Annual Conference on Electron Probe Analysis.* In press.

Goldstein J. I. and Yakowitz H. (1971). Metallic inclusions and metal particles in the Apollo 12 lunar

soil. *Proc. Second Lunar Sci. Conf. Geochim. Cosmochim. Acta*, Suppl. 2, Vol. 1, pp. 177–191. MIT Press.

Goldstein J. I., Axon H. J., and Yen C. F. (1972). Metallic particles in the Apollo 14 lunar soil. *Proc. Third Lunar Sci. Conf., Geochim. Cosmochim. Acta*, Suppl. 3, Vol. 1, pp. 1037–1064. MIT Press.

Haggerty S. E. (1972). Luna 16: An opaque mineral study and a systematic examination of compositional variations of spinels from Mare Fecunditatis. *Earth Planet. Sci. Lett.* **13**, 328–352.

Haggerty S. E. (1973) Armalcolite: compositional data and associated opaque oxides (abstract). In *Lunar Science—IV*, pp. 329–331. The Lunar Science Institute, Houston.

Huneke J. C., Podosek F. A., and Wasserburg G. J. (1973) An argon bouillabaisse including ages from the Luna 20 site (abstract). In *Lunar Science—IV*, pp. 403–405. The Lunar Science Institute, Houston.

Huneke J. C., Jessberger E. K., Podosek F. A., and Wasserburg G. J. (1973) ^{40}Ar–^{39}Ar chronology of metamorphic and volcanic activity in the Taurus-Littrow region. *Proc. Fourth Lunar Sci. Conf., Geochim. Cosmochim. Acta.* Volume 2.

Husain L. and Schaeffer O. A. (1973) ^{40}Ar–^{39}Ar crystallization ages and ^{38}Ar–^{37}Ar cosmic ray exposure ages of samples from the vicinity of the Apollo 16 landing site (abstract). In *Lunar Science—IV*, pp. 406–408. The Lunar Science Institute, Houston.

Kridelbaugh S. J. and Weill D. F. (1973) The mineralogy and petrology of the Luna 20 soil sample. *Geochim. Cosmochim. Acta* **37**, 915–926.

Lanphere M. A. and Dalrymple G. B. (1971) A test of the ^{40}Ar/^{39}Ar age spectrum technique on some terrestrial materials. *Earth Planet. Sci. Lett.* **12**, 359–372.

Laul J. C. and Schmitt R. A. (1973) Chemical composition of Luna 20 rocks and soil and Apollo 16 soils. *Geochim. Cosmochim. Acta* **37**, 927–942.

LSPET (Lunar Sample Preliminary Examination Team) (1973a) Preliminary examination of lunar samples from Apollo 16. *Science* **179**, 23–34.

LSPET (Lunar Sample Preliminary Examination Team) (1973b) Preliminary examination of lunar samples from Apollo 17. *Science*. In press.

Lunatic Asylum (1970) Mineralogic and isotopic investigation on lunar rock 12013. *Earth Planet. Sci. Lett.* **9**, 137–163.

Meyer C., Jr., Brett R., Hubbard N. J., Morrison D. A., McKay D. S., Aitken F. K., Takeda H., and Schonfeld E. (1971) Mineralogy chemistry, and origin of the KREEP component in soil samples from the Ocean of Storms. *Proc. Second Lunar Sci. Conf., Geochim. Cosmochim. Acta*, Suppl. 2, Vol. 1, pp. 393–411. MIT Press.

Papanastassiou D. A. and Wasserburg G. J. (1972) Rb–Sr systematics of Luna 20 and Apollo 16 samples. *Earth Planet. Sci. Lett.* **17**, 52–63.

Podosek F. A., Huneke J. C., Gancarz A. J., and Wasserburg G. J. (1973) The age and petrography of two Luna 20 fragments and inferences for widespread lunar metamorphism. *Geochim. Cosmochim. Acta* **37**, 887–904.

Reid M. J. The tidal loss of satellite-orbiting objects and its implications for the lunar surface. *Icarus*. In press.

Simonds C. H., Warner J. L., Phinney W. C., and Gooley R. (1973) Mineralogy and mode of formation of poikilitic rocks from Apollo 16 (abstract). In *Lunar Science—IV*, pp. 676–678. The Lunar Science Institute, Houston.

Smith J. V. (1971) Minor elements in Apollo 11 and 12 olivine and plagioclase. *Proc. Second Lunar Sci. Conf., Geochim. Cosmochim. Acta*, Suppl. 2, Vol. 1, pp. 143–153. MIT Press.

Tera F. and Wasserburg G. J. (1972) U–Th–Pb systematics in lunar highland samples from the Luna 20 and Apollo 16 missions. *Earth Planet. Sci. Lett.* **17**, 36–51.

Tera F., Papanastassiou D. A., and Wasserburg G. J. (1973) A lunar cataclysm at ~3.95 AE and the structure of the lunar crust (abstract). In *Lunar Science—IV*, pp. 723–725. The Lunar Science Institute, Houston.

Turner G., Cadogen P. H., and Yonge C. J. (1973) Apollo 17 age determinations. *Nature* **242**, pp. 513–515.

Walker D., Longhi J., and Hays J. F. (1972) Experimental petrology and origin of Fra Mauro rocks and soil (abstract). In *Lunar Science—III*, pp. 770–772. The Lunar Science Institute, Houston.

Walker D., Longhi J., and Hays J. F. (1973) Petrology of Apollo 16 metaigneous rocks (abstract). In *Lunar Science—IV*, pp. 752–754. The Lunar Science Institute, Houston.

Warner J., Phinney W. C., Simonds C. H., Gooley R., and Lofgren G. E. (1973) Petrology of rake samples from Apollo 16 Stations 1, 4 and 13 (abstract). In *Lunar Science—IV*, pp. 767–769. The Lunar Science Institute, Houston.

Wong B. (1972) Permeation of silicate liquids into sintered magnesia compacts. *Lawrence Berkeley Laboratory LBL-877*, p. 79.

DUNITE FROM THE LUNAR HIGHLANDS: PETROGRAPHY, DEFORMATIONAL HISTORY, Rb-Sr AGE
A.L.Albee,A.A.Chodos,R.F.Dymek,A.J.Gancarz,D.S.Goldman,D.A.Papanastassiou, and G.J.Wasserburg; Lunatic Asylum; Division of Geological and Planetary Sciences, California Institute of Technology, Pasadena, Ca. 91109, Contribution No. 2442

Five fragments of highly-crushed dunite (72415 to 72418) were collected at Apollo 17 Station 2 from a single 10x20cm clast in Boulder #2, which is a metaclastic blue-grey breccia (72435). It is logical to expect a lunar dunite to provide some insight into the composition of the lunar mantle, the origin of the ANT-rock suite, and possibly the character of primitive crustal-differentiation processes. Such insights are complicated by the complex history of deformation undergone by this sample. However, despite the complex history, Rb and Sr appear to have remained undisturbed and this rock is inferred to be a product of primary lunar differentiation.

Rounded clasts composed of large (to 10mm),single crystals of pale-green, translucent olivine are enclosed in a granular, white matrix composed predominantly of olivine. The matrix formed simply by crushing without recrystallization and has the same composition (Fo_{86-89}) as the olivine clasts. Other minerals, which include plagioclase, Cr-spinel, high- and low-Ca pyroxene, and Fe-metal, occur as clasts within the matrix and included within the olivine clasts. In both cases the habit of each of these minerals is similar.

Large, single olivine crystals have pronounced undulatory extinction and planar partings resulting in a mosaic of rhomb-shaped domains bounded by partings or strain-bands. Small ($\sim$50μm) oval or equant olivine grains, with relatively uniform extinction, are aligned along some of these strain-bands. Some of the planar partings appear to be decorated with minute beads, which are apparently Fe-metal, and some terminate in a string of Fe-metal beads. Most of the clasts are single olivine grains. However, zones of symplectic intergrowths, and rarely, aggregates of plagioclase laths associated with pyroxene granules, occur within the clasts. These zones are interpreted as relic grain boundaries and as primary crystallization features. Similar aggregates of plagioclase laths (An_{88-92}) and pyroxene granules also occur as broken fragments within the matrix. Olivine is dusted with tiny ($<1\mu$m) inclusions, which appear to be predominantly Fe-metal in some areas and predominantly spinel in other areas. Cr-spinel also occurs in olivine as discrete inclusions (up to 25 μm).

Symplectic intergrowths of Cr-spinel+high Ca pyroxene$\pm$low Ca pyroxene $\pm$ plagioclase $\pm$ Fe-metal occur as tiny, ovoid inclusions in olivine, along relic grain boundaries, and as broken fragments within the granulated matrix. Felty aggregates of shocked and recrystallized plagioclase (An_{94-97}) with minor pyroxene also occur as ovoid inclusions within the olivine clasts and as broken fragments in the matrix.

Table 1 gives the mode, "average" phase compositions, and calculated bulk-chemical composition of thin-sections 72415,11 and 72415,12. The phases are relatively uniform in composition, but plagioclase is slightly more sodic in the laths than in the felty aggregates and spinel is slightly more Cr-rich in inclusions than in the symplectic intergrowths. Olivine is low in Ca and Mn and exceptionally low in Cr. Rare grains of troilite and whitlockite associated with Fe-metal and of Zr-Cr armalcolite were identified. Fe-metal contains 1.3 to 2.2 wt. % Co and has an exceptionally high Ni content (24.5 to 31.8 wt. %), perhaps indicative of the primary origin of the metal and the primitive nature of the dunite.

Lunar Dunite

Albee, A. L., et al.

Table 1. 72415,11 and 72415,12 Phase abundances, "average" phase compositions and bulk-chemical composition

	Olivine	Plagioclase	Low-Ca pyroxene	High-Ca pyroxene	Fe-metal*	Spinel	Bulk composition
Vol.%	91.4±2.2	4.03±0.45	3.06±0.40	1.33±0.26	0.10±0.07	0.10±0.07	(1962 points)
Wt. %	91.85	3.55	3.08	1.34	0.24	0.14	
SiO_2	40.09	44.79	51.26	52.71	0.04	0.19	40.6_1
Al_2O_3	<0.01	35.00	1.07	2.73	n.a.	19.95	1.2_7
Cr_2O_3	<0.01	n.a.	0.84	0.85	0.36	48.28	0.1_1
TiO_2	<0.01	<0.01	0.31	0.54	<0.01	0.49	0.0_2
MgO	48.12	0.23	33.72	18.61	1.31	11.10	45.5_1
FeO	11.90	0.14	8.11	3.00	67.07	18.64	11.4_6
MnO	0.11	n.a.	0.11	0.13	0.06	0.75	0.1_1
CaO	0.13	19.25	5.55	21.28	<0.01	n.a.	1.2_2
Na_2O	n.a.	0.62	<0.01	0.05	n.a.	n.a.	0.0_2
K_2O	n.a.	0.09	n.a.	n.a.	n.a.	n.a.	$<0.0_1$
BaO	n.a.	0.04	n.a.	n.a.	n a.	n.a.	$<0.0_1$
ZrO_2	n.a.	n.a.	n.a.	n.a.	n.a.	0.08	$<0.0_1$
V_2O_3	n.a.	n.a.	n.a.	n.a	n.a.	0.35	$<0.0_1$
NiO	0.04	n.a.	n.a.	n.a.	29.67	n.a.	0.1_3
Co	n.a.	n.a.	n.a.	n.a.	1.46	n.a.	$<0.0_1$
Total	100.39	100.16	100.97	99.90	100.01	99.83	100.46
	Fo 88	An 92	En 81	En 54			$\bar{\beta}$ =3.30
	Fa 12	Ab 5	Fs 11	Fs 5			
		Or 1	Wo 8	Wo 41			
		Others 2					

*Element abundances: converted to oxides for bulk-composition calculation

n.a. = not analyzed

TABLE 2 : TRACE ELEMENT & ISOTOPIC DATA

	Sym.I[c]	TR chip[d]	TR[d]	L[e]
wt(g)	0.125	0.20	2.0	-
K(ppm)	29.1	7.30	21	.26
Ba(ppm)	5	1.2	4	.09
Rb[a]	0.0843	0.0830	0.088	.72
^{88}Sr[a]	15.08	2.712	11	.07
$^{87}Rb/^{86}Sr$[b]	1.304	7.14	-	-
$^{87}Sr/^{86}Sr$	.69985±5	.70370±6	-	-

a:10^{-8}mole/g; b: x10^2; c: Symplectic intergrowths; d: TR- Total rock; e: L- Fraction leached from total rock(col.4)

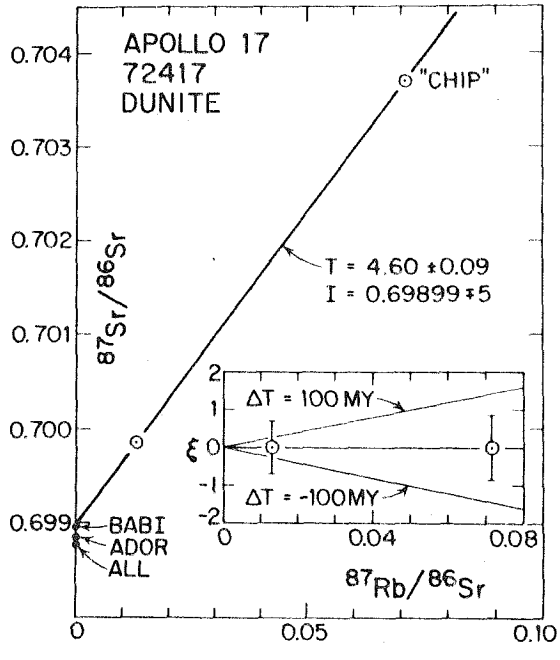

Figure: Rb-Sr evolution diagram for dunite 72417. Insert indicates the effect on age of uncertainties ξ (in parts in 10^4) of $^{87}Sr/^{86}Sr$. Sample enriched in symplectic intergrowths has the low Rb/Sr. Initial Sr is equal to BABI and distinctly higher than ADOR (Angra dos Reis) and ALL (Allende [2]).

Lunar Dunite

Albee, A. L. et al.

It is important, although difficult, to distinguish between the primary and the deformational features of this dunite breccia. We infer that the primary dunite consisted of about 95% coarse-grained (to at least 10 mm) olivine crystals containing spinel inclusions and melt inclusions, which probably had crystallized to plagioclase+pyroxene and spinel+plagioclase+pyroxene prior to the shock deformation. Interstitial to the coarse olivine grains were aggregates of spinel+pyroxene+plagioclase+Fe-metal, partly as symplectic intergrowths. The coarse grain-size, the symplectic intergrowths and the compositions of the phases suggest that this rock did not form as a near-surface cumulate. Subsequently, the dunite was excavated from depth by a cratering event and subjected to shock pressures in the range of 350 to 450 kb, resulting in the deformational and recrystallization features observed in the rounded olivine clasts. The rock was crushed at low shock-pressures, probably prior to its incorporation into the blue-grey matrix breccia as a clast, as there is no evident admixture of blue-grey matrix breccia material to the dunite.

Isotopic and trace element analyses were done on selected materials from sample 72417, which include a small "total rock chip", a 2g total rock, and hand-picked fragments rich in simplistic intergrowths (table 2). All samples were free of lunar exterior surfaces and were cleaned of adhering lunar soil. The differences in trace element concentrations between the total rock samples are due to biased sampling. There is considerable depletion of Sr in the small "chip" compared to the other samples. Leaching the total rock in HNO_3+ HCl showed that K and Rb are readily removed.

The figure shows the data points for the "chip" and the symplectic intergrowths, which define a remarkably straight line corresponding to an age of 4.60 AE and initial $^{87}Sr/^{86}Sr$, I=0.69899. Pb isotopic data on the leach of the total rock give a model age of 4.48 AE which is significantly younger [1]. If the Rb-Sr data represent a true internal isochron, then this dunite must be one of the earliest lunar differentiates. The value of I is low enough to be compatible with such an interpretation. A value greater than BABI would render this interpretation questionable. Because of the complex nature of this rock and the low trace element concentrations these results must be confirmed. The low laboratory blank levels have no significant effect on the Rb-Sr data. It is possible that the trace element concentrations, the isotopic compositions, and consequently the age result from the addition of extraneous lunar materials during the complex history of the dunite. Such materials include the matrix of the enclosing K-rich breccia (72435), clasts of anorthositic rocks, and lunar soil. However, the small "total rock chip", which critically controls the age, has K/Rb much less than any of these contaminants and less than mare basalts. Therefore, the possibility of contamination by these materials may be excluded. This is also true for the 2g total rock and the symplectic intergrowths, with regard to the high Rb/Sr contaminants. As there is no evidence for contamination from either petrographic or trace element data, we tentatively conclude that this rock must represent a very early differentiate, derived from the upper lunar mantle. This rock is so depleted in trace elements (including U and Th) that it cannot represent the source reservoirs from which younger basaltic magmas were derived. This rock must represent a cumulate formed during early lunar differentiation and associated differential gravitational settling.

[1] F. Tera et al., this volume.

[2] C. M. Gray et al., (1973) Icarus 20, 213

PRELIMINARY INVESTIGATION OF BOULDERS 2 and 3, APOLLO 17, STATION 2: PETROLOGY AND Rb-Sr MODEL AGES, A. L. Albee, A. A. Chodos, R. F. Dymek A. J. Gancarz, and D. S. Goldman, Division of Geological and Planetary Sciences, California Institute of Technology, Pasadena, California 91109. Contribution No. 2439.

Preliminary petrologic studies on samples from Station 2 indicate that the upper layered units of the South Massif are composed of metaclastic rocks. It can also be inferred from the clast assemblage that the formation of these units predates the extrusion of mare and feldspathic basalts. The clasts are predominantly members of the ANT-suite which, based on a Rb-Sr study of a dunite clast, apparently existed 4.6 b.y. ago [1].

The boulders at Station 2 are derived from the upper third of the South Massif and apparently include the two major lithologic units which comprise the South Massif. Samples of both matrix material and clasts were collected from a 2m tan-grey breccia boulder (#2) and a 0.5m blue-grey breccia boulder (#3). The matrix samples from both boulders are moderately-recrystallized metaclastic rocks not dissimilar to many metaclastic rock samples collected and described from the Apollo 16 site. Preliminary results on documented chips and thin-sections from these boulders are reported by members of the consortium elsewhere in this volume and include: field observations [2]; chemical data [3]; track and microcrater data and surface exposure ages [4]; petrologic and isotopic studies [1].

BOULDER #2 samples 72315 and 72335 were collected from an irregular 0.5m area which appeared to be a breccia clast and samples 72355, 72375, and 72395 were collected to represent the matrix of this boulder. Binocular microscope examination of these samples shows them to be similar-looking, sugary-textured, coherent, homogeneous metaclastic rocks. They contain only a few percent of clasts larger than 2-3mm. These are predominantly shocked plagioclase, but include anorthositic rock and single crystals of olivine and pyroxene. The largest such clast is 10mm across, but somewhat larger, highly-vesicular patches may be vestigial breccia inclusions. These patches are rich in irregularly-shaped vesicles and contain relatively coarse-grained plagioclase and pyroxene which are in the matrix and which also project into the vesicles. Sample 72395 contains a shallow, 10x14mm vesicle lined with pyroxene and plagioclase crystals. Irregular zones of slit vesicles and tiny spherical vesicles (<1mm) also occur in these samples.

The samples of both the clast and matrix from this boulder appear nearly identical in thin-section and contain about 20% megaclasts (0.1 to 2.5mm) set in a finer-grained, partially-recrystallized matrix. The clasts are mostly single crystals of plagioclase, but include some shocked grains and anhedral aggregates. Clasts of olivine, pyroxene, and pink spinel are much less abundant. Secondary overgrowths and reaction rims occur on numerous clasts.

The matrix consists of anhedral grains of plagioclase, pyroxene, and olivine. Portions of the matrix contain up to 10% K_2O. Plagioclase is not lath-shaped and pyroxene and olivine do not form oikocrysts as in many Apollo 16 metaclastic rocks. The compositions of these minerals are similar in the matrix and clasts in all five samples (fig. 1). Opaque minerals, which constitute several percent of the rock, include ilmenite, armalcolite, rutile,

APOLLO 17, STATION 2 BOULDERS

Albee, A. L., et al.

ulvöspinel, spinel, troilite, and Fe-metal.

The nature of the irregular patch, tentatively identified by Schmitt on the moon as a large clast, is not yet clear. Petrographically, both sets of samples are similar, but chemical data indicate that one sample from the clast (72315) differs from the other four [3]. Clast sample 72315 has had a much shorter exposure on the lunar surface than the matrix sample (72395) [4], suggesting that the irregular patch seen by Schmitt could be a spalled surface. Since no spalled fragments are present at the foot of the boulder, the time of spalling may predate the emplacement of the boulder in its present position.

Rb-Sr model ages (T_{BABI}) for chips from samples 72315, 72335, 72355, 72375, and 72395 are 4.54, 4.49, 4.38, 4.37 and 4.46 b.y., respectively [5]. Similar model ages have been obtained previously from other such metaclastic rocks, which yielded recrystallization ages of about 3.95 b.y. by $^{40}Ar/^{39}Ar$ stepwise heating or Rb-Sr internal isochrons.

BOULDER #3 samples 72415 to 72418 were collected from a single 10x20cm clast of crushed dunite and sample 72435 was collected to represent the matrix. Photographs indicate that, although the boulder contains a variety of 2-6cm clasts, the clast of dunite is the largest. Sample 72435 differs from the samples of boulder #2 in color (dark blue-grey), by a lesser abundance (by ~5%) and size (up to 15mm) of clasts, and by the presence of large (up to 8mm) smooth-walled vesicles. It contains zones of aligned, slit vesicles and minute spherical vesicles as in boulder #2, but not the crystalline-appearing, highly-vesicular patches. The large clasts include anorthosite, troctolite, dunite and individual crystals of olivine, pyroxene and shocked and unshocked plagioclase. No volcanic-textured clasts are present.

The thin section shows about 15% megaclasts set in a metaclastic groundmass which is finer-grained than the matrix of boulder #2. Most of the clasts are plagioclase, including shocked crystals which exhibit a felty, recrystallization texture. In addition, many plagioclase clasts have secondary overgrowths of plagioclase. Pyroxene and olivine, have a limited range of Mg/Fe which is similar to boulder #2, but some plagioclase is more sodic than in boulder #2 (fig. 1). One unique mineral is a 20μm grain of cordierite included in a spinel, which itself is part of a plagioclase-rich, lithic clast.

The clast of dunite, which exhibits a complex shock history and consists almost entirely of olivine (Fo_{86-89}), is discussed in a separate abstract [1]. Despite the complex shock history, isotopic data indicate an extremely old age (4.60±0.09 b.y.) for this rock [1].

DISCUSSION These preliminary data indicate that boulders #2 and #3 are metaclastic rocks, characterized by a great abundance of ANT-type material and by the general absence of both mare and feldspathic basalts. If these boulders are indeed from the upper portion of the South Massif, then the two units comprising the South Massif must be composed of metaclastic rock. From the abundance of ANT-type material and the absence of both mare and feldspathic basalts, it may be inferred that the formation of these units predates the extrusion of these basalts. Alternatively, the restricted clast population may just represent derivation from a limited source region. The

APOLLO 17, STATION 2 BOULDERS

Albee, A. L., et al.

occurrence of the 4.6 b.y. old dunite in a metaclastic unit, which contains clasts restricted to the ANT-suite, as well as the petrologic similarity of dunite to the ANT-suite of rocks, strongly suggest that the ANT-suite also formed at 4.60 b.y. even though most returned ANT samples have been extensively modified by later events. This corroborates the various hypotheses [6], which suggest that the lunar crust formed very early in the evolution of the moon by extensive melting with associated differential, gravitational separation of opaque oxides, olivine, pyroxene, plagioclase, and residual liquid.

REFERENCES

[1] A. L. Albee et al., this volume
[2] H. Schmitt, this volume
[3] J. C. Laul and R. Schmitt, this volume
[4] B. Price and F. Horz, this volume
[5] F. Tera, D. A. Papanastassiou and G. J. Wasserburg (1974) Earth Planet. Sci. Letters, in press.
[6] D. Walker, et al., (1973) Earth Planet. Sci. Letters, 20, 325.

FIGURE 1

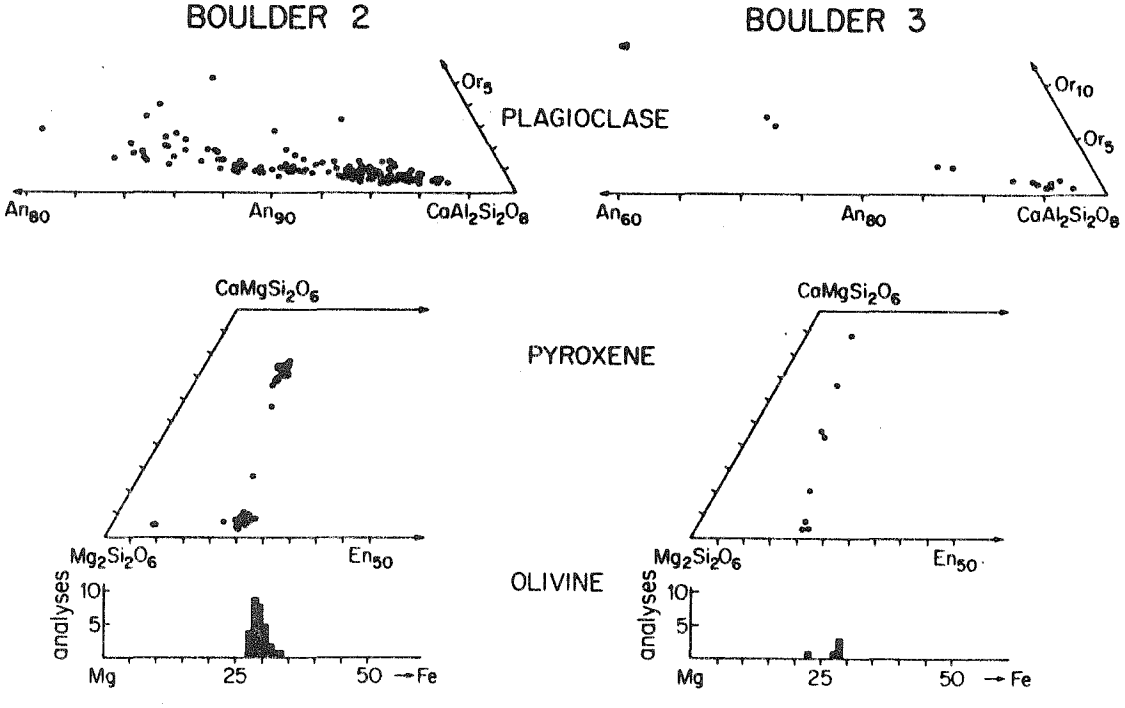

PETROGENESIS OF LUNAR ROCKS: Rb-Sr CONSTRAINTS AND LACK OF H_2O

Arden L. Albee and Alexander J. Gancarz

Division of Geological and Planetary Sciences*

California Institute of Technology

Pasadena, California 91125, U.S.A.

*Contribution No. 2474

ABSTRACT

Rb and Sr isotopic data and other chemical data indicate major lunar differentiation at about 4.6 AE and very limited subsequent differentiation. The constraints of limited differentiation post 4.6 AE and the apparent lack of H_2O on the moon, when applied to the derivation and petrogenesis of lunar samples, suggest the following: 1) soil samples, breccias, metaclastic rocks, and feldspathic basalts represent mixtures of repeatedly-modified clastic material, which was ultimately derived from materials formed during the $\sim$ 4.6 AE differentiation; 2) mare basalts crystallized from melts which formed by partial melting and, which developed without equilibration between the melt and crystalline residuum.

I. Introduction

Rb-Sr mineral isochrons currently provide the basic chronology of lunar evolution (Albee et al., 1970a, 1970b, 1974; Papanastassiou et al., 1970; Papanastassiou and Wasserburg, 1970, 1971a, 1971b, 1972a, 1972c, 1973; Tera et al., 1974a, 1974b, Wasserburg and Papanstassiou, 1971). Rb/Sr data also impose rigorous constraints on lunar petrogenetic models. This paper will discuss these constraints, emphasize the important role of large-scale differentiation which occurred at about 4.6 AE (AE $\equiv 10^9$ years) and show that only limited chemical fractionation occurred during the subsequent evolution of most lunar rocks. Regardless of other types of evidence, no petrogenetic theory for the origin of lunar rocks can invoke extensive fractionation later than about 4.6 AE as a dominant part of the theory. The lack of H_2O on the moon may be the critical physical-chemical factor limiting subsequent fractionation in many processes.

II. Rb-Sr systematics and fractionation factors

Measurements of the isotopic abundance of Rb and Sr in the various mineral phases of a rock provide information not only on the time of crystallization and equilibration (T_x), but also on the fractionation history of the rock prior to this most recent crystallization and equilibration. As illustrated on Figure 1, cogenetic systems, either consanguineous total-rocks or the various minerals in a single rock, attain identical values of $^{87}Sr/^{86}Sr$, but during equilibration at T_x

different values of $^{87}Rb/^{86}Sr$. On the Rb-Sr evolution diagram these different compositions subsequently evolve along straight line trajectories with a slope of -1. If the systems were closed to gain or loss of Rb and Sr since T_x, then the cogenetic systems measured at any time form a linear array on the Rb-Sr evolution diagram. An array based on minerals from a single rock is a mineral or internal isochron and one based on cogenetic rocks is a total-rock isochron. The isochron has a slope indicative of the time since equilibration (slope = $\exp(\lambda T_x - 1)$ and a $^{87}Sr/^{86}Sr$ intercept, $(^{87}Sr/^{86}Sr)_I$, equal to the Sr isotopic composition at time T_x (Lanphere et al., 1964).

The deviation of $(^{87}Sr/^{86}Sr)_I$ from that assumed to have existed at some time prior to T_x coupled with the $^{87}Rb/^{86}Sr$, provide an integrated measure of the Rb/Sr fractionation history of the rock. This fractionation history can be parametrized by a two-stage model as illustrated in Figure 1. The model assumes that a source material originated at reference time T_o = 4.6 AE with the "BABI" value of $^{87}Sr/^{86}Sr$ ($(^{87}Sr/^{86}Sr)_{BABI}$ = 0.69898) (Papanastassiou and Wasserburg, 1969). Fractionation at time T_x resulted in three fractions, one enriched in Rb relative to Sr, one unfractionated, and one depleted in Rb relative to Sr. Mineral isochrons on all three rocks would yield identical ages (T_x) and the same $(^{87}Sr/^{86}Sr)_I$. However, they would have different model ages, T_{BABI}, which is the time required for the $^{87}Sr/^{86}Sr$ of the total rock with its measured $^{87}Rb/^{86}Sr$ to evolve from $(^{87}Sr/^{86}Sr)_{BABI}$. The unfractionated rock will have T_{BABI} = 4.6 AE, the enriched rock will have $T_{BABI} < 4.6$ AE and the depleted rock will have $T_{BABI} > 4.6$ AE.

Thus, any deviation of T_{BABI} from 4.6 AE indicates a fractionation history prior to T_x.

The fractionation factor for this two-stage model is (Papanastassiou and Wasserburg, 1972c):

$$K_D \equiv \frac{(^{87}Rb/^{86}Sr)_2}{(^{87}Rb/^{86}Sr)_1} \cong \frac{T_o - T_x}{T_{BABI} - T_x}$$

This approximation is quite accurate since the decay constant for Rb is small. During the time interval from T_o to T_x numerous episodes of fractionation could have affected the rock as opposed to the simple two-stage model illustrated. However, $(^{87}Rb/^{86}Sr)_1$ is still the integrated $^{87}Rb/^{86}Sr$ in the interval from T_o to T_x.

As noted previously T_o = 4.6 AE and $(^{87}Sr/^{86}Sr)_{T_o}$ = 0.69898 are reference values, and the subsequent conclusions drawn in this paper are basically independent of their precise value. In fact, the time of major differentiation is probably not 4.6 AE, but may be as low as 4.5 AE or even 4.4 AE (Tera et al., 1974b).

III. Lunar rock groups

On the basis of petrologic characteristics seven different groups of lunar rocks are recognized. Each of these groups has a distinctive Rb-Sr isotopic pattern. The Rb-Sr data are summarized on Figure 2, which shows T_x, T_{BABI}, and K_D for representative members of each group.

Most of the type examples shown are those on which we have made detailed petrographic and electron probe studies in conjunction with the Rb-Sr isotopic studies of Papanastassiou and Wasserburg. Figure 2 indicates that six of these groups are characterized by T_{BABI} close to 4.6 and $K_D < 2$. The seven groups are as follows:

1) Soils with $T_{BABI} = 4.6 \pm 0.3$ AE

Clots from the soil samples and friable soil-breccia samples, as well as bulk soil samples, have model ages of about 4.6 AE. This group includes samples from all landing sites and has a wide range of Rb/Sr (Papanastassiou and Wasserburg, 1972c). To a large extent many of these model ages are dominated by a small fraction of very high Rb/Sr material with a model age of about 4.6 AE (Papanastassiou and Wasserburg, 1972c).

2) K-rich fragments with T_{BABI} = 4.3 to 4.6 AE

These fragments, the so-called "KREEP" rocks (Hubbard et al., 1971), include glass-rich agglutinates and metaclastic rocks, and have been found in the soils at all landing sites. Most are small fragments such as Luny Rock 1 (Albee and Chodos, 1970), and no internal isochrons have been measured on them. Nyquist et al. (1973), however, showed that by grouping such fragments by chemical composition and location, Rb and Sr data yield linear arrays, which, if interpreted as total-rock isochrons, indicate ages ranging from 4.1 to 4.4 AE. Sample 12013 is the only large sample which we would place in this group. It is a

heterogeneous metaclastic rock with K, Th, and U concentration a factor of forty greater than typical mare basalts and a factor of ten greater than Apollo 11 K-rich basalts (Anderson, 1970). Fragments of 12013 have a model age of 4.52 AE and a recrystallization age (T_x) of 4.01 AE (Albee et al., 1970b).

3) Metaclastic rocks with $T_x \approx 3.95$ AE and $T_{BABI} \approx 4.5$ AE

This group includes a large proportion of the Lunar Highlands samples and also constitutes a large proportion of the lithic fragments in soil samples from all landing sites. These clastic rocks, composed predominantly of plagioclase, have been extensively recrystallized by metamorphic and/or partial melting processes (Albee et al., 1973). Typical examples are 65015 and 76055, both of which display isotopic and petrologic evidence for extensive, but not complete equilibration at 3.95 AE (Albee et al., 1973; Papanastassiou and Wasserburg, 1972c; Tera et al., 1974b; Jessberger et al., 1974). Stepwise heating ^{40}Ar-^{39}Ar studies on 65015 suggest that the cores of the larger plagioclase clasts have an age greater than 4.46 AE (Jessberger et al., 1974). This is also suggested by Rb-Sr isotopic data (Papanastassiou and Wasserburg, 1972c).

4) Feldspathic basalts with $T_x \approx 3.85$ AE and $T_{BABI} \approx 4.3$ AE

This group includes a number of samples of intersertal, plagioclase-rich basalts from the Apollo 14 and 16 landing sites (e.g., 14310, 14276 and 68415). In addition to the high plagioclase

content (60 to 80%) they are characterized by high K, rare earth element, P, Ba, U and Th contents (Gancarz et al., 1972), and a high content of siderophile elements (Morgan et al., 1972). Even in these rocks, which almost certainly crystallized from a melt, plagioclase grains are present which, on the basis of electron probe data, have not completely equilibrated with the melt (Gancarz et al., 1972). ^{40}Ar-^{39}Ar studies also indicate older relict plagioclase and provide evidence for an older event (Huneke et al., 1972b, 1973).

5) Mare basalts with T_x = 3.16 to 3.95 AE and T_{BABI} = 4.1 to 5.0 AE

This group includes all of the mare basalts with the exception of those in Group 6. Samples from each landing site have similar T_x and T_{BABI}, but $(^{87}Sr/^{86}Sr)_I$ values and trace element concentrations differ for samples from an individual landing site (Papanastassiou and Wasserburg, 1971a, 1973; Tera et al., 1974a, 1974b; Schmitt and Laul, 1973). This suggests derivation of individual samples (and flows) from different sources (Schmitt and Laul, 1973) or differing degrees of assimilation of country rock (Papanastassiou and Wasserburg, 1971a). Typical well-characterized samples from the various landing sites include:

10044 (Agrell et al., 1970; Albee et al., 1970a; Turner, 1970),

12040 (French et al., 1972; Reid et al., 1973; Papanastassiou and Wasserburg, 1971a),

14053 (Gancarz et al., 1971; Papanastassiou and Wasserburg, 1971b; Turner et al., 1971),

15682 (Dowty et al., 1973; Papanastassiou and Wasserburg, 1973), 75055 (Albee et al., 1973; Tera et al., 1974b; Huneke et al., 1973), and Luna 16, B-1 (Albee et al., 1972; Papanastassiou and Wasserburg, 1972a; Huneke et al., 1972a).

6) Mare basalts with T_x = 3.65 AE and T_{BABI} = 3.85 AE

Although grossly similar to the Apollo 11 low-K basalts included in Group 5, these samples from the Apollo 11 landing site are higher in K and other incompatible elements, and have much younger model ages. A typical well-characterized example is 10017 (Adler et al., 1970; Albee et al., 1970a; Turner, 1970).

7) "ANT" rocks with T_{BABI} = 4.6 AE

The "ANT" rock suite includes the coarse-grained rocks of the anorthosite-norite-troctolite-dunite suite. In general they display magmatic cumulate textures, but are extensively modified by shock processes. Dunite sample 72417 has both an isochron age and a model age of about 4.6 AE (Albee et al., 1974). No mineral isochron ages have been measured on anorthosite samples such as 15415 (James, 1972; Turner, 1972) or on troctolite samples such as 76535 (Gooley et al., in press). However, low $^{87}Sr/^{86}Sr$ ratios indicate that these rocks cannot have equilibrated and resided in a higher Rb/Sr environment for any extended length of time (Wasserburg and Papanastassiou, 1971; Papanastassiou, personal communication).

IV. Nature of major differentiation at ∿ 4.6 AE

Many types of chemical, isotopic and physical evidence are consistent with the hypothesis of primitive, large-scale, crustal differentiation (Albee et al., 1970a; Ringwood and Essene, 1970; Smith et al., 1970; Wood et al., 1970). The presence of a "magic component" (Papanastassiou and Wasserburg, 1970) with T_{BABI} of 4.6 AE and a high $^{87}Rb/^{86}Sr$ which dominates the model age of many lunar soil samples indicates that this differentiation occurred at about 4.6 AE and produced rocks with very high Rb/Sr ratios. The existence of high Rb/Sr material with relatively old model ages was confirmed by the discovery of the K-rich rock 12013 (Albee et al., 1970b) and other fragments (Albee and Chodos, 1970; Hubbard et al., 1971). The existence of material complementary to the Rb/Sr-rich material is indicated by dunite sample 72417, which has crystallization and model ages of 4.6 AE (Albee et al., 1974).

Rb-Sr data also indicate that, only limited fractionation occurred, subsequent to the primitive differentiation, and furthermore suggest that most of the observed chemical characteristics were produced during the primitive differentiation. That most of the chemical differences observed in the lunar rocks are consistent with primitive differentiation at ∿ 4.6 AE rather than subsequent fractionation processes is illustrated in Figure 3. Sm/Eu, a parameter sensitive to fractionation, varies by a factor of ∿ 200, whereas K_D, a measure of fractionation after the differentiation at ∿ 4.6 AE, varies only by a factor of about 2. The strong fractionation indicated by Sm/Eu must have occurred

prior to the time of crystallization. Although neither K_D nor Sm/Eu are particularly sensitive to olivine or Ca-poor pyroxene fractionation, both are extremely sensitive to fractionation of plagioclase or of late stage K-rich material. The large range of Rb/Sr observed between samples, approximately a factor of 1000, is comparable to the range of Sm/Eu. Hence, we conclude that the Sm/Eu differences must have been a characteristic of the source from which the rocks were derived and that most chemical differences in lunar rocks are a result of primitive differentiation at about 4.6 AE.

Regardless of physical details, this primitive differentiation process resulted in a fraction rich in K, Rb, Ba, U, Th, trivalent rare earth elements, a Ca-Al-Si rich fraction (anorthosite and anorthositic gabbro), and a Mg-Fe rich fraction (dunite, troctolite, and norite). Samples of the Ca-Al-Si rich fraction and the Mg-Fe rich fraction have survived subsequent excavation by meteorite impact, but exhibit a wide range of modification. Less-modified samples suggest that these fractions cooled slowly enough to produce rocks with coarse-grained, homogeneous phases. The original nature of the K-rich fraction is not clear as no samples have been recognized which have not been extensively modified.

V. Possible petrogenetic processes involving limited fractionation

The Rb-Sr constraint on the amount of fractionation, as well as constraints imposed by many other kinds of data, are satisfied if we hypothesize that soils, glass-agglutinate fragments, friable breccias, and progenitors of metaclastic rocks and feldspathic basalts

(Groups 1-4) are all basically mixtures of clastic material, which have been subsequently modified by a variety of processes, including fragmentation, metamorphism, partial melting and complete melting. Rb and Sr would not be fractionated if the formation of the clastic mixture involved only fragmentation of preexistent rocks from one or many sources; even if fragmentation occurred repeatedly over a long period of time. Consequently, if the source regions of a clastic mixture are primary, unmodified materials formed during the primitive differentiation at $\sim$ 4.6 AE, or if they themselves are clastic mixtures repeatedly modified either by continued fragmentation and mixing, or by processes characterized below, then Rb and Sr will remain unfractionated and the model age of the mixture will still reflect the time of primitive differentiation.

Preservation of the old model age of such a mixture would be accomplished during subsequent modification by processes with the following characteristics, even if repeated many times:

1) Volatile loss of Rb was in general not significant.

2) Metamorphism, in the absence of H_2O, was strictly controlled by solid-state and grain-surface diffusion and resulted in lithification by sintering at grain boundaries with only short-range migration and limited segregation of elements.

3) Partial melting in the metaclastic rocks of Group 3 and in the K-rich fragments of Group 2, was characterized by extensive reaction between an interstitial melt and larger clastic grains. Lack of Rb-Sr fractionation dictates very limited mobility of the melt and only

short-range migration of elements within the melt. These characteristics can be partially attributed to the absence of H_2O and to the fine-scale homogeneity of the fragmental mixture. Local segregation of Rb-rich material and partial Sr equilibration is suggested by the Rb/Sr data of Nyquist et al. (1973) on small chemically-defined groups of samples from single sites. The Rb/Sr data on these samples have been interpreted as total-rock isochrons representing distinct events at times ranging from 4.1 AE to 4.4 AE. These may alternatively be interpreted as the result of local segregation of K-rich, Rb-rich material without total Sr equilibration at 3.95 AE.

4) Impact-produced melts, which formed by nearly total melting of soil, breccia, or metaclastic rocks, crystallized as the feldspathic basalts of Group 4. Such an origin would preserve the old model age of the source and would satisfy several other geochemical constraints on these rocks, such as the high content of siderophile elements. However, the Rb-Sr constraint could also be satisfied if these rocks formed by partial melting of plagioclase-rich source rocks with the additional restrictions described below for mare basalts.

The Rb-Sr restraint limiting fractionation is satisfied if the ultimate source of the clastic mixture formed during the large-scale differentiation at $\sim$ 4.6 AE. If the modification process or processes retain the characteristics described above, or if modification is a simple fragmentation process, then fractionation does not basically occur and old model ages are preserved. This is true regardless of either the order or the number of times this clastic mixture is modified.

Mare basalts with near 4.6 AE model ages (Group 5) must also have been derived without substantial fractionation of Rb and Sr, either during formation of the parent magma or during the ascent and crystallization. All other chemical parameters suggestive of a greater degree of fractionation must be a characteristic of the source region. The origin of the mare basalts is further restricted by the $(^{87}Sr/^{86}Sr)_I$ values, which suggest that rocks of the same age were derived from a number of different sources. A magma meeting these requirements could be produced by several mechanisms (Gancarz et al., 1972):

1) Total melting of a source rock which has a Rb-Sr model age of 4.6 AE and also meets all other chemical and isotopic constraints would form a rock satisfying the Rb-Sr constraints. Although total melting is generally regarded as an unlikely terrestrial event, it is possible that, in the absence of H_2O and tectonic activity, instability and separation of a melt from a source region would be delayed until complete melting occurs. Total melting could also occur as a result of impact processes.

2) Uniform contamination of relatively low Rb-Sr melts by assimilation of Rb-rich crustal material with a model age of 4.6 AE is the mechanism invoked by Papanastassiou and Wasserburg (1971a).

3) Our preferred hypothesis is that, in the absence of H_2O, partial melting occurs by incremental melting of integral volumes of solid phases with little or no equilibration between melt and crystalline residuum. Thus, the low-temperature phases rich in Rb and ^{87}Sr would melt totally and grains of higher-temperature phases would melt

peripherally, but the solid residuum would not equilibrate with the melt. As pointed out by Graham and Ringwood (1971), the resulting melt would have the same model age as the source region. Any crystallization and separation of Ca-rich pyroxene and/or plagioclase during the ascent of the melt to the surface would result in Rb-Sr fractionation. However, silicate melt curves typically have a positive slope ($\Delta P/\Delta T > 0$) in the absence of H_2O, and under these circumstances the melt may become superheated as it moves upward, effectively preventing crystallization and consequent Rb-Sr fractionation. Production of a superheated magma is also an important consideration in the contamination hypothesis, since it would facilitate assimilation and homogenization.

The Apollo 11 K-rich mare basalts (Group 6) could also form by this process, but the younger model ages require a greater degree of equilibration between the melt and residuum or of some fractional crystallization before extrusion onto the surface.

VI. Conclusion

An intriguing feature of these explanations for deriving lunar rocks without fractionation Rb and Sr is the linking of this special characteristic to another characteristic lunar feature--the apparent lack of indigenous H_2O. The hypotheses outlined here differ from other models of lunar petrogenesis in that many rock types would be derived by near-surface modification of rocks formed during primitive crustal differentiation. This can be accomplished with energy

partially derived from impacting bodies rather than totally from internal heat sources.

Acknowledgments

Most of the Rb-Sr patterns summarized here are based on mineral isochron data from G. J. Wasserburg and D. A. Papanastassiou. Furthermore, many of the arguments incorporated into these hypotheses have been expressed in their published papers and expressed even more vociferously in numerous discussions during the course of our cooperative work since July, 1969. Unpublished Sm and Eu data were provided by N. J. Hubbard and J. A. Philpotts. This paper has been supported by NASA grants NGL-05-002-188 and NGL-05-002-338.

References

Adler, I., Walter, L.S., Lowman, P.D., Glass, B.P., French, B.M., Philpotts, J. A., Heinrich, K.J.F., and Goldstein, J.I. (1970) Electron microprobe analysis of Apollo 11 lunar samples, Proceedings of the Apollo 11 Lunar Science Conference, Geochimica et Cosmochimica Acta, Supplement 1, V. 1, 87-92.

Agrell, S.O., Scoon, J.H., Muir, I.D., Long, J.V.P., McConnell, J.D.C. and Peckett, A. (1970) Observations on the chemistry, mineralogy, and petrology of some Apollo 11 lunar samples, Proceedings of the Apollo 11 Lunar Science Conference, Geochimica et Cosmochimica Acta, Supplement 1, V. 1, 93-128.

Albee, A.L. and Chodos, A.A. (1970) Microprobe investigations on Apollo 11 samples, Proceedings of the Apollo 11 Lunar Science Conference, Geochimica et Cosmochimica Acta, Supplement 1, V. 1, 135-157.

Albee, A.L., Burnett, D.S., Chodos, A.A., Eugster, O.J., Huneke, J.C., Papanastassiou, D.A., Podosek, F.A., Russ, G.P. III, Sanz, H.G., Tera, F. and Wasserburg, G.J. (1970a) Ages, irradiation history, and chemical composition of lunar rocks from the Sea of Tranquillity, Science, V. 167, 463-466.

Albee, A.L., Burnett, D.S., Chodos, A.A., Haines, E.L., Huneke, J.C., Papanastassiou, D.A., Podosek, F.A., Russ, G.P. III and Wasserburg, G.J. (1970b) Mineralogic and isotopic investigations on lunar rock 12013, Earth and Planetary Science Letters, V. 9, 137-163.

Albee, A.L., Chodos, A.A., Gancarz, A.J., Haines, E.L., Papanastassiou, D.A., Ray, L., Tera, F., Wasserburg, G.J. and Wen, T. (1972) Mineralogy, petrology, and chemistry of a Luna 16 basaltic fragment, sample B-1, Earth and Planetary Science Letters, V. 13, 353-367.

Albee, A.L., Gancarz, A.J. and Chodos, A.A. (1973) Metamorphism of Apollo 16 and 17 and Luna 20 metaclastic rocks at about 3.95 AE: Samples 61156, 64423,14-2, 65015, 67483,15-2, 76055, 22006, and 22007, Proceedings of the Fourth Lunar Science Conference, Geochimica et Cosmochimica Acta, Supplement 4, V. 1, 569-595.

Albee, A.L., Chodos, A.A., Dymek, R.F., Gancarz, A.J., Goldman, D.S., Papanastassiou, D.A. and Wasserburg, G.J. (1974) Dunite from the Lunar Highlands: Petrography, deformation history, Rb-Sr age, In: Lunar Science V, 3-5, The Lunar Science Institute, Houston, Texas.

Anderson, D.H. (1970) The preliminary examination and preparation of lunar sample 12013, Earth and Planetary Science Letters, V. 9, 94-102.

Brunfelt, A.O., Heier, K.S., Nilssen, B., Sundvoll, B. and Steinnes, E. (1972) Distribution of elements between different phases of Apollo 14 rocks and soils, Proceedings of the Third Lunar Science Conference, Geochimica et Cosmochimica Acta, Supplement 3, V. 2, 1133-1147.

Dowty, E., Prinz, M. and Keil, K. (1973) Composition, mineralogy, and petrology of 28 mare basalts from Apollo 15 rake samples, Proceedings of the Fourth Lunar Science Conference, Geochimica et Cosmochimica Acta, Supplement 4, V. 1, 423-444.

French, B.M., Walter, L.S., Heinrich, K.F.J., Lowman, P.D. Jr., Doan, A.S. Jr., and Adler, I. (1972) Compositions of major and minor minerals in five Apollo 12 crystalline rocks, National Aeronautics and Space Administration SP-306, 142 pp.

Gancarz, A.J., Albee, A.L. and Chodos, A.A. (1971) Petrologic and mineralogic investigation of some crystalline rocks returned by the Apollo 14 mission, Earth and Planetary Science Letters, V. 12, 1-18.

Gancarz, A.J., Albee, A.L. and Chodos, A.A. (1972) Comparative petrology of Apollo 16 sample 68415 and Apollo 14 samples 14276 and 14310, Earth and Planetary Science Letters, V. 16, 307-330.

Gast, P.W., Hubbard, N.J. and Wiesmann, H. (1970) Chemical composition and petrogenesis of basalts from Tranquillity Base, Proceedings of the Apollo 11 Lunar Science Conference, Geochimica et Cosmochimica Acta, Supplement 1, V. 2, 1143-1163.

Goles, G.G., Randle, K., Osawa, M., Lindstrom, D.J., Jérome, D.Y., Steinborn, T.L., Beyer, R.L., Martin, M.R. and McKay, S.M. (1970) Interpretations and speculations on elemental abundances in lunar samples, Proceedings of the Apollo 11 Lunar Science Conference, Geochimica et Cosmochimica Acta, Supplement 1, V. 2, 1177-1194.

Goles, G.G., Duncan, A.R., Lindstrom, D.J., Martin, M.R., Beyer, R.L., Osawa, M., Randle, K., Meek, L.T., Steinborn, T.L., and McKay, S.M. (1971) Analyses of Apollo 12 specimens: Compositional variations, differentiation processes, and lunar soil mixing models, Proceedings of the Second Lunar Science Conference, Geochimica et Cosmochimica Acta, Supplement 2, V. 2, 1063-1081.

Gooley, R., Brett, R., Warner, J. and Smyth, J.R., Sample 76535, a deep lunar crustal rock, Geochimica et Cosmochimica Acta, in press.

Graham, A.L. and Ringwood, A.E. (1971) Lunar basalt genesis: The origin of the Europium anomaly, Earth and Planetary Science Letters, V. 13, 105-115.

Haskin, L.A., Allen, R.O., Helmke, P.A., Paster, T.P., Anderson, M.R., Korotev, R.L. and Zweifel, K.A. (1970) Rare earths and other trace elements in Apollo 11 lunar samples, Proceedings of the Apollo 11 Lunar Science Conference, Geochimica et Cosmochimica Acta, Supplement 1, V. 2, 1213-1231.

Haskin, L.A., Helmke, P.A., Blanchard, D.P., Jacobs, J.W. and Telander, K. (1973) Major and trace element abundances in samples from the lunar highlands, Proceedings of the Fourth Lunar Science Conference, Geochimica et Cosmochimica Acta, Supplement 4, V. 2, 1275-1296.

Hubbard, N.J. and Gast, P.W. (1971) Chemical composition and origin of non-mare lunar basalts, Proceedings of the Second Lunar Science Conference, Geochimica et Cosmochimica Acta, Supplement 2, V. 2, 999-1020.

Hubbard, N.J., Meyer, C. Jr., Gast, P.W. and Wiesmann, H. (1971) The composition and derivation of Apollo 12 soils, Earth and Planetary Science Letters, V. 10, 341-350.

Hubbard, N.J., Gast, P.W. and Meyer, C. Jr. (1972a) Chemical composition of lunar anorthosites and their parent liquids, In: Lunar Science III, 404-406, The Lunar Science Institute, Houston, Texas.

Hubbard, N.J., Gast, P.W., Rhodes, J.M., Bansal, B.M., Wiesmann, H. and Church, S.E. (1972b) Nonmare basalts: Part II, Proceedings of the Third Lunar Science Conference, Geochimica et Cosmochimica Acta, Supplement 3, V. 2, 1161-1179.

Huneke, J.C., Podosek, F.A. and Wasserburg, G.J. (1972a) Gas retention and cosmic-ray exposure ages of a basalt fragment from Mare Fecunditatis, Earth and Planetary Science Letters, V. 13, 375-383.

Huneke, J.C., Podosek, F.A. and Wasserburg, G.J. (1972b) An argon bouillabaisse including ages from the Luna 20 site, In: Lunar Science IV, 403-405, The Lunar Science Institute, Houston, Texas.

Huneke, J.C., Jessberger, E.K., Podosek, F.A. and Wasserburg, G.J. (1973) $^{40}Ar/^{39}Ar$ measurements in Apollo 16 and 17 samples and the chronology of metamorphic and volcanic activity in the Taurus-Littrow region, Proceedings of the Fourth Lunar Science Conference, Geochimica et Cosmochimica Acta, Supplement 4, V. 2, 1725-1756.

James, O.B. (1972) Lunar anorthosite 15415: Texture, mineralogy, and metamorphic history, Science, V. 175, 434-438.

Jessberger, E.K., Huneke, J.C. and Wasserburg, G.J. (1974) Evidence for a ∿ 4.5 aeon age of plagioclase clasts in a lunar highland breccia, Nature, V. 248, 199-202.

Lanphere, M.A., Wasserburg, G.J.F., Albee, A.L. and Tilton, G.R. (1964) Redistribution of strontium and rubidium isotopes during metamorphism, World Beater Complex, Panamint Range, California, In: Isotopic and Cosmic Chemistry, eds, H. Craig, S.L. Miller and G.J. Wasserburg (North-Holland, Amsterdam, 1964) 553 pp.

Laul, J.C., Wakita, H., Showalter, D.L., Boynton, W.V. and Schmitt, R.A. (1972) Bulk, rare earth, and other trace elements in Apollo 14 and 15 and Luna 16 samples, Proceedings of the Third Lunar Science Conference, Geochimica et Cosmochimica Acta, Supplement 3, V. 2, 1181-1200.

Morgan, J.W., Laul, J.C., Krähenbühl, U., Ganapathy, R. and Anders, E. (1972) Major impacts on the moon: Characterization from trace elements in Apollo 12 and 14 samples, Proceedings of the Third Lunar Science Conference, Geochimica et Cosmochimica Acta, Supplement 3, V. 2, 1377-1395.

Morrison, G.H., Gerard, J.T., Potter, N.M., Gangadharam, E.V., Rothenberg, A.M. and Burdo R.A. (1971) Elemental abundances of lunar soil and rocks from Apollo 12, Proceedings of the Second Lunar Science Conference, Geochimica et Cosmochimica Acta, Supplement 2, V. 2, 1169-1185.

Nyquist, L.E., Hubbard, N.J., Gast, P.W., Bansal, B.M., Wiesmann, H. and Jahn, B. (1973) Rb-Sr systematics for chemically defined Apollo 15 and 16 materials, Proceedings of the Fourth Lunar Science Conference, Geochimica et Cosmochimica Acta, Supplement 4, V. 2, 1823-1846.

Papanastassiou, D.A. and Wasserburg, G.J. (1969) Initial strontium isotopic abundances and the resolution of small time differences in the formation of planetary objects, Earth and Planetary Science Letters, V. 5, 361-376.

Papanastassiou, D.A., Wasserburg, G.J. and Burnett, D.S. (1970) Rb-Sr ages of lunar rocks from the Sea of Tranquillity, Earth and Planetary Science Letters, V. 8, 1-19.

Papanastassiou, D.A. and Wasserburg, G.J. (1970) Rb-Sr ages from the Ocean of Storms, Earth and Planetary Science Letters, V. 8, 269-278.

Papanastassiou, D.A. and Wasserburg, G.J. (1971a) Lunar chronology and evolution from Rb-Sr studies of Apollo 11 and 12 samples, Earth and Planetary Science Letters, V. 11, 37-62.

Papanastassiou, D.A. and Wasserburg, G.J. (1971b) Rb-Sr ages of igneous rocks from the Apollo 14 mission and the age of the Fra Mauro Formation, Earth and Planetary Science Letters, V. 12, 36-48.

Papanastassiou, D.A. and Wasserburg, G.J. (1972a) Rb-Sr age of a Luna 16 basalt and the model age of lunar soils, Earth and Planetary Science Letters, V. 13, 368-374.

Papanastassiou, D.A. and Wasserburg, G.J. (1972b) The Rb-Sr age of a crystalline rock from Apollo 16, Earth and Planetary Science Letters, V. 16, 289-298.

Papanastassiou, D.A. and Wasserburg, G.J. (1972c) Rb-Sr systematics of Luna 20 and Apollo 16 samples, Earth and Planetary Science Letters, V. 17, 52-63.

Papanastassiou, D.A. and Wasserburg, G.J. (1973) Rb-Sr ages and initial strontium in basalts from Apollo 15, Earth and Planetary Science Letters, V. 17, 324-337.

Philpotts, J.A., Schnetzler, C.C., Nava, D.F., Schumann, S., Kouns, C.W., Lum, R.K.L. and Bickel, A.L. (1973) Apollo 16: Large ion lithophile trace element abundances in some fines, a basalt and an anorthosite, In: Lunar Science IV, 592-594, The Lunar Science Institute, Houston, Texas.

Reid, M.J., Gancarz, A.J. and Albee, A.L. (1973) Constrained least-squares analysis of petrologic problems with an application to lunar sample 12040, Earth and Planetary Science Letters, V. 17, 433-445.

Rhodes, J.M. and Hubbard, N.J. (1973) Chemistry, classification, and petrogenesis of Apollo 15 mare basalts, Proceedings of the Fourth Lunar Science Conference, Geochimica et Cosmochimica Acta, Supplement 4, V. 2, 1127-1148.

Ringwood, A.E. and Essene, E. (1970) Petrogenesis of Apollo 11 basalts, internal constitution and origin of the moon, Proceedings of the Apollo 11 Lunar Science Conference, Geochimica et Cosmochimica Acta, Supplement 1, V. 1, 769-799.

Schmitt, R.A. and Laul, J.C. (1973) A survey of the selenochemistry of major, minor and trace elements, The Moon, V. 8, 182-209.

Smith, J.V., Anderson, A.T., Newton, R.C., Olsen, E.J. and Wyllie, P.J. (1970) A petrologic model for the moon based on petrogenesis, experimental petrology, and physical properties, Journal of Geology, V. 78, 381-405.

Tera, F., Papanastassiou, D.A. and Wasserburg, G.J. (1974a) The lunar time scale and a summary of isotopic evidence for a terminal lunar cataclysm, In: Lunar Science V., 792-794, The Lunar Science Institute, Houston, Texas.

Tera, F., Papanastassiou, D.A. and Wasserburg, G.J. (1974b) Isotopic evidence for a terminal lunar cataclysm, Earth and Planetary Science Letters, V. 22, 1-21.

Turner, G. (1970) Argon-40/argon-39 dating of lunar rock samples, Proceedings of the Apollo 11 Lunar Science Conference, Geochimica et Cosmochimica Acta, Supplement 1, V. 2, 1665-1684.

Turner, G. (1972) ^{40}Ar-^{39}Ar age and cosmic ray irradiation history of the Apollo 15 anorthosite, 15415, Earth and Planetary Science Letters, V. 14, 169-175.

Turner, G., Huneke, J.C., Podosek, F.A. and Wasserburg, G.J. (1971) ^{40}Ar-^{39}Ar ages and cosmic ray exposure ages of Apollo 14 samples, Earth and Planetary Science Letters, V. 12, 19-35.

Vinogradov, A.P. (1971) Preliminary data on lunar ground brought to Earth by automatic probe "Luna-16", Proceedings of the Second Lunar Science Conference, Geochimica et Cosmochimica Acta, Supplement 2, V. 1, 1-16.

Wakita, H. and Schmitt, R.A. (1970) Elemental abundances in seven fragments from lunar rock 12013, Earth and Planetary Science Letters, V. 9, 169-176.

Wasserburg, G.J. and Papanastassiou, D.A. (1971) Age of an Apollo 15 mare basalt; Lunar crust and mantle evolution, Earth and Planetary Science Letters, V. 13, 97-104.

Wood, J.A., Dickey, J.S. Jr., Marvin, U.B. and Powell, B.N. (1970) Lunar anorthosites and a geophysical model of the Moon, Proceedings of the Apollo 11 Lunar Science Conference, Geochimica et Cosmochimica Acta, Supplement 1, V. 1, 965-988.

Figure 1. Rb-Sr evolution diagram. Material formed at T_o with $(^{87}Sr/^{86}Sr)$ equal to $(^{87}Sr/^{86}Sr)_{BABI}$ is represented by a square. Fractionation at time T_x results in a portion enriched and a portion depleted in Rb relative to Sr (circles) and an unfractionated portion (square), all of which lie along the T_x isochron. The unfractionated portion yields a model age, T_{BABI}, equal to T_o, whereas fractionated portions yield model ages different from T_o.

Figure 2. T_{BABI} versus T_x. Despite the variety of rock types represented, nearly all samples indicate less than a factor of 2 fractionation of Rb relative to Sr subsequent to T_o = 4.6 AE. Only the K-rich mare basalts indicate a greater degree of fractionation.

Figure 3. Sm/Eu versus K_D. The large range of Sm/Eu, indicative of extensive fractionation is not commensurate to the fractionation of Rb relative to Sr as indicated by the small range of K_D. This indicates that the fractionation of Sm and Eu occurred prior to T_x; and, from additional data, most likely occurred during the large-scale lunar differentiation at $\sim$ 4.6 AE. Sm and Eu data are from the following: Brunfelt et al. (1972), Gast et al. (1970), Goles et al. (1970,1971), Haskin et al. (1970,1973), Hubbard and Gast (1971), Hubbard et al. (1971,1972a,1972b), Laul et al. (1972), Morrison et al. (1971), Philpotts et al. (1973), Rhodes et al. (1973), Vinogradov et al. (1971) and Wakita et al. (1970).

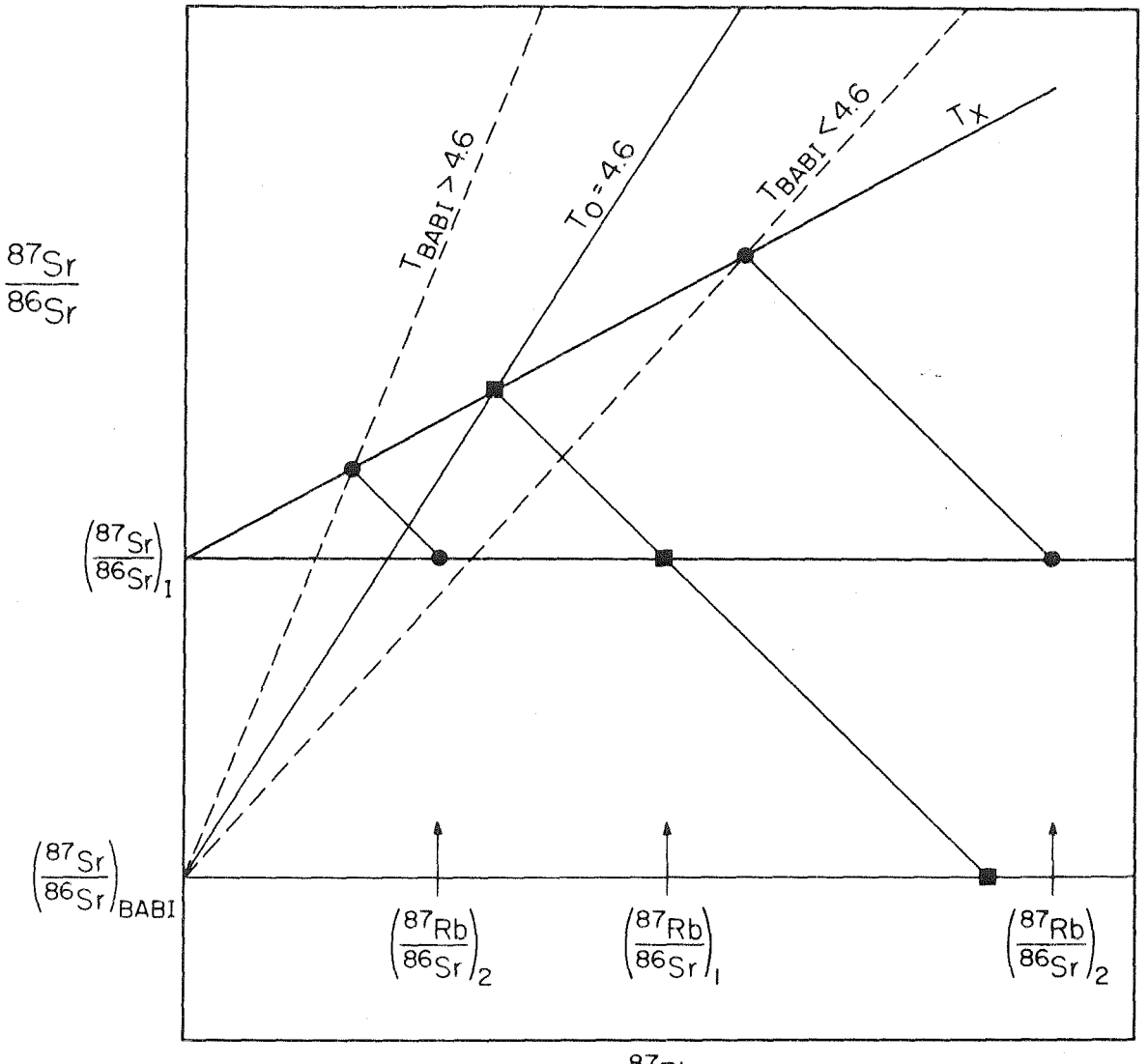

$$K_D \equiv \left(\frac{^{87}Rb}{^{86}Sr}\right)_2 \Big/ \left(\frac{^{87}Rb}{^{86}Sr}\right)_1 \cong \frac{T_0 - T_x}{T_{BABI} - T_x}$$

Figure 1

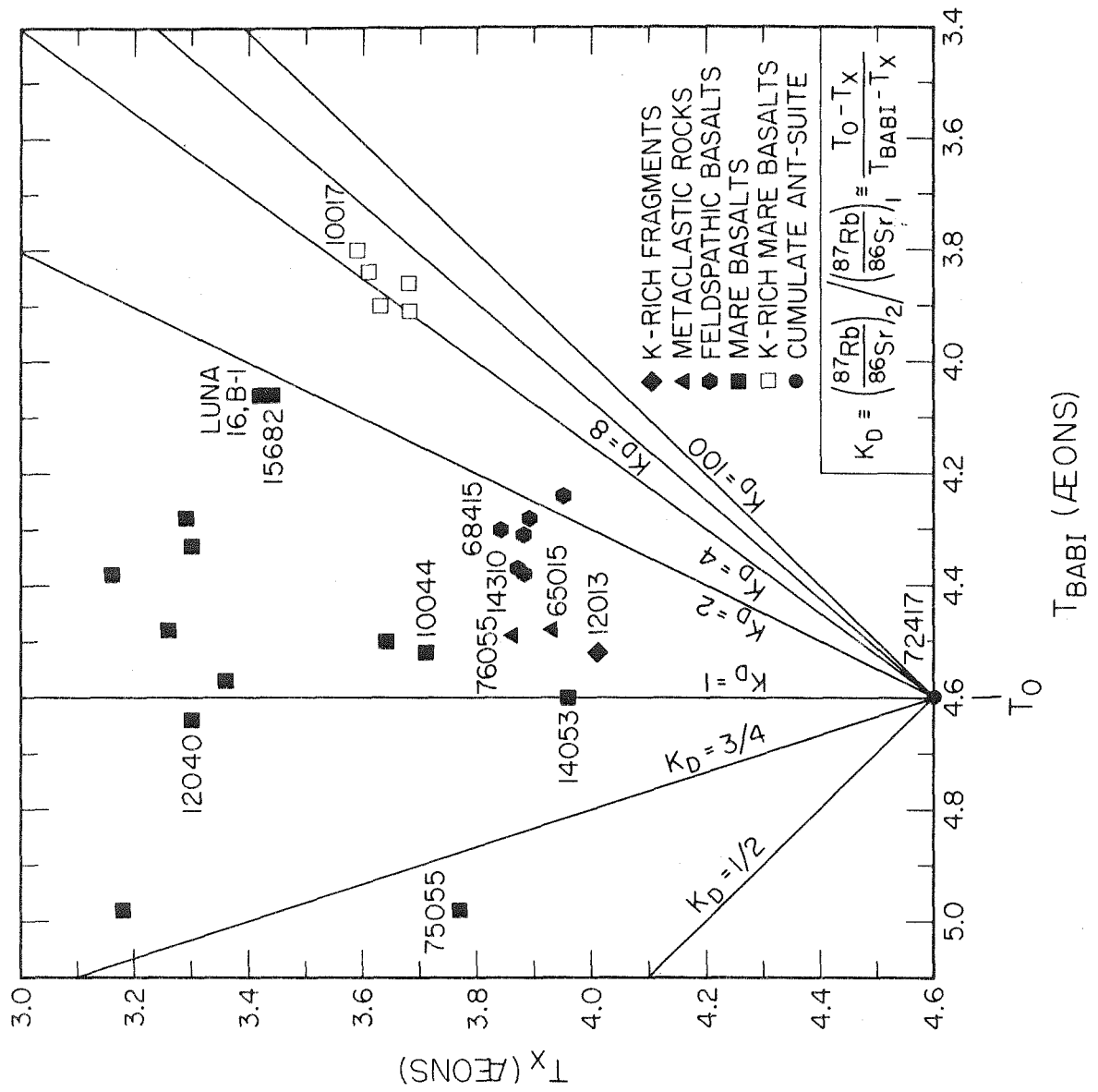
K-RICH FRAGMENTS
METACLASTIC ROCKS
FELDSPATHIC BASALTS
MARE BASALTS
K-RICH MARE BASALTS
CUMULATE ANT-SUITE
$K_D \equiv \left(\frac{^{87}Rb}{^{86}Sr}\right)_2 / \left(\frac{^{87}Rb}{^{86}Sr}\right)_1 \equiv \frac{T_O - T_X}{T_{BABI} - T_X}$
$K_D = 1/2$
$K_D = 3/4$
$K_D = 1$
$K_D = 2$
$K_D = 4$
$K_D = 8$
$K_D = 100$
LUNA 16, B-1
15682
12040
75055
14053
10017
10044
68415
14310
76055
65015
12013
72417
T_X (AEONS)
T_O
T_{BABI} (AEONS)
3.0
3.2
3.4
3.6
3.8
4.0
4.2
4.4
4.6
4.8
5.0

Figure 2

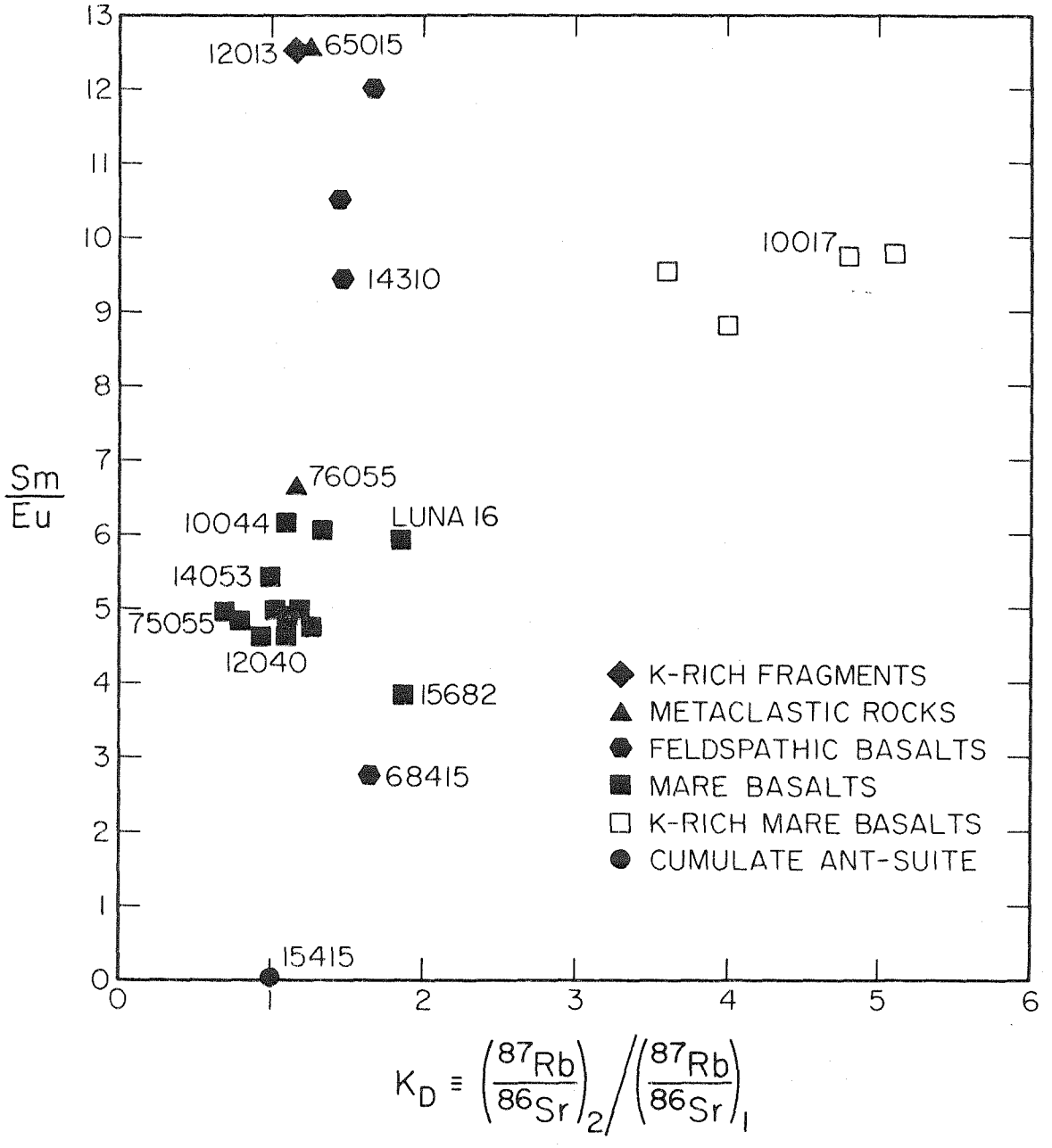
12013
65015
14310
10017
76055
10044
LUNA 16
14053
75055
12040
15682
68415
15415
K-RICH FRAGMENTS
METACLASTIC ROCKS
FELDSPATHIC BASALTS
MARE BASALTS
K-RICH MARE BASALTS
CUMULATE ANT-SUITE
Sm/Eu
$K_D \equiv \left(\frac{^{87}Rb}{^{86}Sr}\right)_2 \Big/ \left(\frac{^{87}Rb}{^{86}Sr}\right)_1$

Figure 3